DOE-DE-FC07-061D14781
Transmutation Research Program
Final Technical Report
July 1, 2006 to December 31, 2011

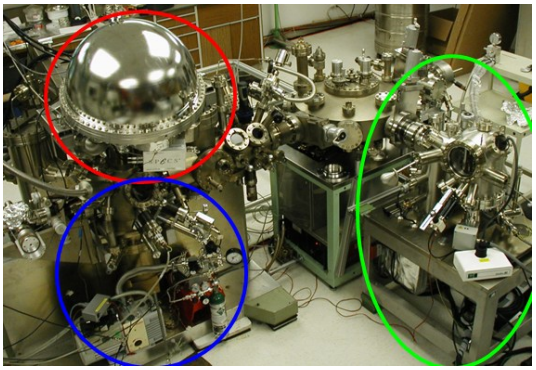

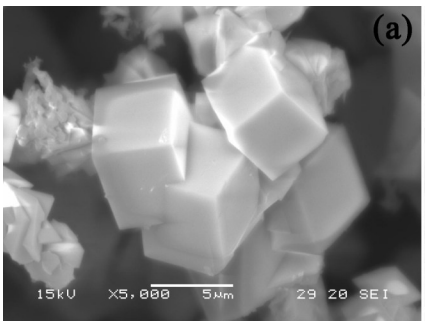

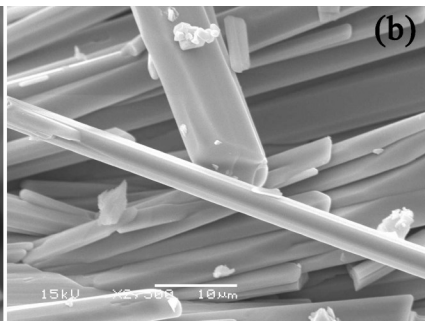

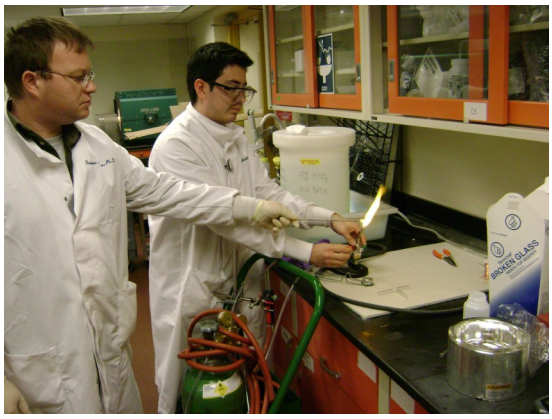

UNLV | HARRY REID CENTER

University of Nevada, Las Vegas Transmutation Research Program

Under Financial Assistance
DE-FC07-06ID14781

Final Technical Report
July 1, 2006 through December 31, 2011

Harry Reid Center
University of Nevada, Las Vegas
4505 Maryland Parkway, Box 454009
Las Vegas, NV 89154-4009

Paul Seidler
Principal Investigator
(702) 895-1457
(702) 895-2354 (FAX)
Paul.Seidler@unlv.edu

March 31, 2012

Table of Contents

Introduction
Transmutation Research Project, 2006-2011
University of Nevada, Las Vegas

Six years of research was conducted for the United States Department of Energy, Office of Nuclear Energy between the years of 2006 through 2011 at the University of Nevada, Las Vegas (UNLV). The results of this research are detailed in the narratives for tasks 1-45. The work performed spanned the range of experimental and modeling efforts. Radiochemistry (separations, waste separation, nuclear fuel, remote sensing, and waste forms) , material fabrication, material characterization, corrosion studies, nuclear criticality, sensors, and modeling comprise the major topics of study during these six years.

The academic accomplishments regarding student education spanned the areas of PhD, Masters, undergraduate, collaborations with other laboratories, and visiting scholars. The number of collaborators on these 45 projects was 235. Peer-reviewed publications numbered 256 among the UNLV academic collaborators. Ten scholars from foreign countries were involved in these research projects.

The following peer-reviewed publications were produced as a result of the six-year TRP program:

PhD Theses:	14
Masters Theses:	42
Journal Articles:	50
Conference Proceedings:	155

The following collaborators were involved with the research:

Tenured Professors at UNLV:	36
Graduate Students at UNLV:	120
Undergraduate Students at UNLV:	35
Visiting Scientist Collaborators:	64
Argonne NL	16
Los Alamos NL	19
Idaho NL	2
Idaho State University	9
Brookhaven NL	1
US Department of Energy	1
Khlopin Inst., Russia	5
Oak Ridge NL	4
Auburn University	1
Texas A&M University	1
University of Texas – Austin	1
University of Michigan	1
French Atomic Commission	1
RPI	1
University of New Mexico	1
Savannah River NL	1
Visiting Undergraduates:	5
Rhodes College	1
University of Puget Sound	1
Western Kentucky University	1
German Universities	2

Visiting Graduate Students:	10
Idaho State University	2
Georgia Tech	1
University of Florida	1
Francis Marion University	1
University of California, Berkeley	1
RPI	1
French Universities	3

Visiting Postdoctoral Researcher from Idaho State University

In addition, the design effort and equipment procurement for implementing the radiochemistry laboratory and for the augmentation of other researchers' laboratories totaled: $7.5M

Research Summary

Task 1 Design and Analysis of a Process for Melt Casting Metallic Fuel Pins Incorporating Volatile Actinides – Dr. Yitung Chen, Dr. Darrell Pepper, Dr. Randy Clarksean

Background:

Rapid vaporization of certain actinides, specifically Americium, during the fuel-pin fabrication process is problematic in that these actinides will not be incorporated into the transmutation fuel-pin matrix.

Research Objectives and Methods:

The goal of this project was to investigate the casting processes for metallic fuels to help design a process that minimizes the loss of the volatile actinide elements from the fuel. The research effort centered on the development of advanced numerical models to assess conditions that significantly impact the transport of volatile actinides during the melt casting process and represents a joint effort between researchers at UNLV and Argonne National Laboratory (ANL). Assessing critical equipment and process variables is required to build a successful system that will operate efficiently.

Research Accomplishments:

Modeling of induction-heating, casting, Americium transport, and a prototype furnace were completed. These results were used to determine which casting processes were best to produce fuel-pins so volatilization would be minimized, to explore how the Americium transported through the matrix, and to propose an optimal furnace design.

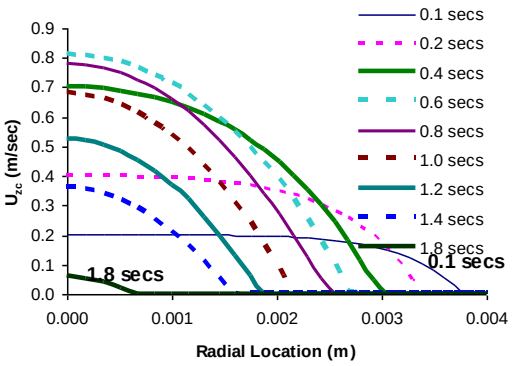

Axial velocity profile for constant inlet pressure of 20 kPa (Mold temperature = 400 ^{o}C, initial melt temperature = 1500 ^{o}C, interfacial heat transfer coefficient = 2,000 W/m^{2}-K).

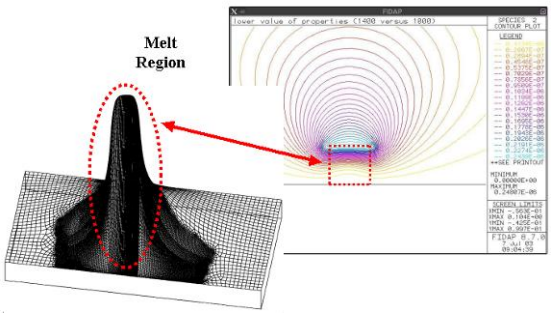

Contour plot and surface plot of field variable S in the induction field. Peak occurs near the top edge of the melt region.

Task 2 Modeling, Fabrication, and Optimization of Niobium Cavities – Dr. Robert Schill, Dr. Mohamed Trabia, and Dr. William Culbreth

Background, Research Objectives and Methods:

Niobium superconducting cavities show promise for increasing power through the minimization of electron multipacting (multiple impacting) or secondary electron emission. Computer models were used to design a one-of-a-kind secondary electron emission test stand. The resulting data was used to improve the existing ORNL codes.

Research Accomplishments:

The developed codes were used to design an experiment that employed LANL-provided niobium samples cleaned by electro-polishing and buffered chemical polishing. Secondary Electron Emission (SEE) measurements were made from the surface of a Faraday cup and the electron tracks were mapped. An improved niobium etching technique was evaluated and laminar flow with the absence of re-circulation pockets was evident within the cavities.

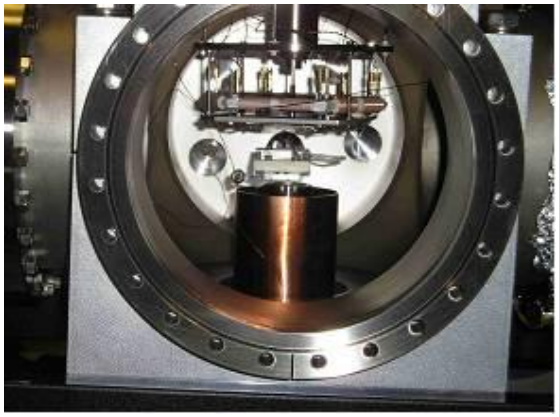

Side view of the secondary electron emission system. The components from top to bottom are: electron gun end, electron beam tube, particle position detector, micro-channel plate stack, business end of the manipulator arm, top of cryostat, and cryostat thermal guard

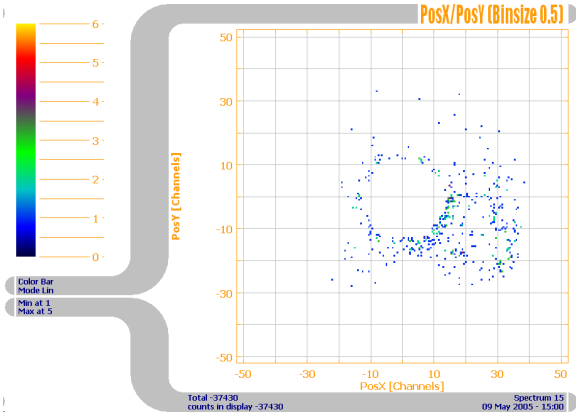

Typical secondary electron emission detected when a 100 ms pulse, 1 keV electron beam impinges on a 30 degree incline, virgin surface of niobium before in situ sample baking. Each pixel represents a spatial bin on the detector. The color of the pixel corresponds to the number of electrons detected at that position. The sample was buffered chemically polished. Single count events have been removed to enhance the scattering tendency.

Task 3 Corrosion of Steel by Lead Bismuth Eutectic – Dr. John Farley, Dr. Allen Johnson, Dr. Dale Perry (LBNL)

Background, Research Objectives and Methods:

Various steel compounds were evaluated for corrosion by Lead-Bismuth Eutectic (LBE) to determine the degree of corrosion reduction attainable with the addition of small (ppm) amounts of oxygen. Samples were analyzed with Scanning Electron Microscopes (SEMs), Energy Dispersive X-ray (EDAX) spectroscopy, X-ray Photoelectron Spectrometry (XPS), and laser Raman spectrometry. In addition, the samples were characterized, before and after exposure to LBE corrosion, using the Advanced Light Source (ALS) at Lawrence Berkeley National Laboratory and the Advanced Photon Source (APS) at Argonne National Laboratory.

Research Accomplishments:

For the 316/316L standard nuclear grade steel and HT9 steel showed that cold-rolled processing exhibited an order of magnitude less corrosion than an annealed sample. Oxide layer deposition was markedly different between the annealed sample (iron oxide over chromium/iron oxide mixtures tens of microns thick) and cold-rolled (chromium oxide layer approximately one micron thick). In the EP823 alloy (similar to HT9 but with added silicon), oxide layers were formed, but were not substantially protective because pockets of LBE migrated underneath the oxide layer potentially corroding the steel.

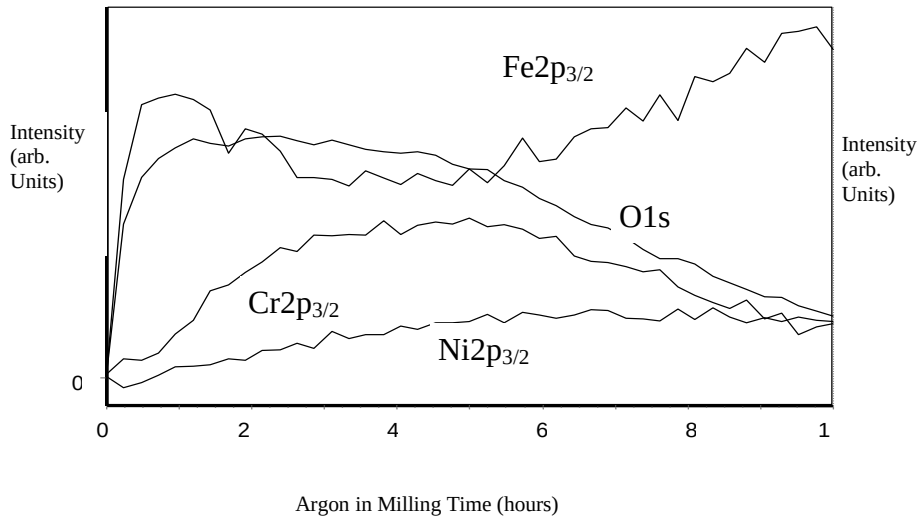

Sputter Depth Profile of annealed 316/316L stainless steel sample. Note iron oxide at the surface.

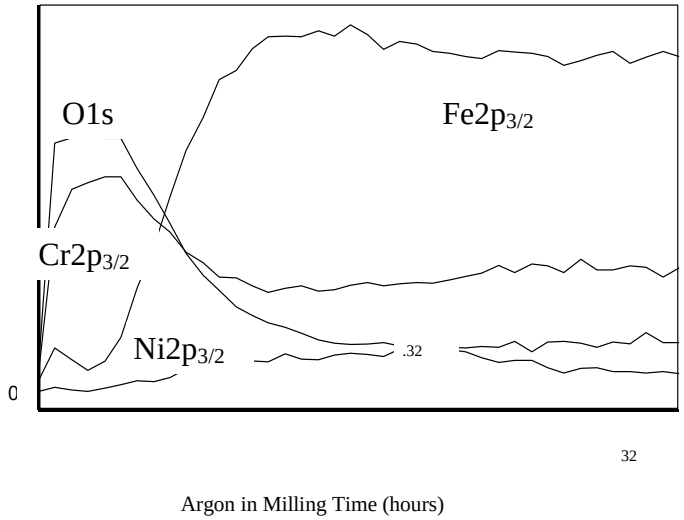

Sputter Depth Profile of cold-rolled 316/316L stainless steel sample. Note chromium oxide at the surface.

Task 4 Environment-Induced Degradation and Crack-Growth Studies of Candidate Target Materials – Dr. Ajit Roy

Background, Research Objectives and Methods:

Steel alloys HT-9, EP-823, and 422were studied to determine their degradation within spallation-neutron-target systems. The production of neutrons through proton bombardment of molten LBE systems can lead to induced degradations such as stress corrosion cracking (SCC), hydrogen embrittlement (HE), and localized (pitting and crevice) corrosion. As a precursor to evaluation of these alloys in molten LBE, aqueous solutions were employed to evaluate the corrosion behavior of these alloys. Constant-load (CL, slow-strain-rate (SSR), and cyclic potentiodynamic polarization (CPP) were employed to evaluate these corrosion phenomena. Optical microscopy and scanning electron microscopy (SEM) were used to analyze the metallurgical microstructures and fractography, respectively of the tested specimens.

Research Accomplishments:

The significant results derived from this task are summarized as follows:

- No failures were observed in smooth specimens of Alloys EP-823 and 422 in the neutral solution when tested at CL. However, Alloy HT-9 showed failure in the 90°C neutral solution at an applied stress (σ_a) of 112 ksi.
- All three alloys exhibited failure in the 90°C acidic solution at 95% of their YS values. Alloys HT-9 and 422 also showed failures at σ_a of 90 and 85% of their YS values, but no failure was observed with Alloy EP-823 at stresses below 0.95 YS.
- The magnitudes of the threshold stress (σ_{th}) for cracking for Alloys EP-823, HT-9 and 422 were 100, 95, and 98 ksi (689, 655, and 676 MPa), respectively based on CL testing in the 90°C acidic solution. The presence of a notch in the test specimen reduced the σ_{th} values in all three alloys.
- The results of SSR testing in the acidic solution involving smooth specimens showed gradual reduction in ductility parameters (percent elongation - %El and percent reduction in area-%RA), time-to-failure (TTF), and true failure stress (σ_f) with increasing temperature, indicating a synergistic effect of pH and temperature in enhancing the cracking susceptibility. The presence of a notch in the specimen produced enhanced SCC susceptibility due to the stress concentration.

However, the σ_f value was increased due to plastic constraint resulting from triaxial stress field at the notch.

- The magnitude of %El, %RA, TTF, and σ_f was reduced under an applied potential of -1,000 mV (Ag/AgCl) compared to those obtained without an applied potential.
- The failure mode at the primary fracture face of the specimen tested in the neutral solution, determined by SEM, was characterized by dimpled microstructure, indicating ductile failures. However, intergranular and/or transgranular brittle failures were observed in the acidic environment.
- Secondary cracks with branching were observed by optical microscopy on all three tested materials along the gage section of the specimens tested in the acidic solution.

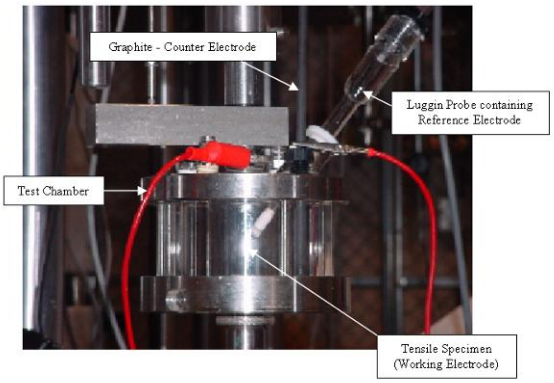

Controlled Potential Test Setup

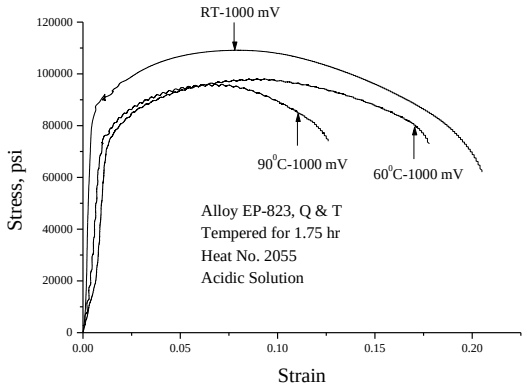

Stress vs Strain under Controlled Potential

Task 5 Modeling Corrosion in Oxygen Controlled LBE Systems with Coupling of Chem. Kinetics and Hydrodynamics – Dr. Samir Moujaes and Dr. Yitung Chen

Background:

Develop a model based on the Delta loop in LANL and a theoretical LBE accelerator target system.

Research Objectives and Methods:

Task one involved the variation of parameters such as average eutectic flow velocity, average mean bulk eutectic flow, inlet temperatures, and average inlet oxygen concentrations in three geometries: a straight flow section, an elbow bend, and a tee section. Corrosion concentration products were calculated, using STAR-CD software, at various axial locations close to the walls of several partial loop sections. These results acted as boundary conditions for the second task.

Task two varied parameters such as temperature, flow velocities, dissolved metal concentrations, oxygen potentials of the system, the kinetics of film formations in the presence of oxygen, and the kinetics of metal transport thorough the oxidized surface film to determine the kinetics of dissolution/deposition of corrosion precursors. Laminar and turbulent flow conditions were considered.

Comparisons between experimental results and modeling showed that the STAR-CD model was accurate. Concentration flux profiles were determined for both laminar and turbulent (k-ε model) profiles in a straight pipe and experiments were designed to study the corrosion in the LBE loop.

Research Accomplishments:

The location in the loop with the highest concentration occurred in the baffle cell which is adjacent to the iron surface while the area with lowest concentration occurs around the central line of the pipe. It can be inferred that after Fe_3O_4 is formed, it diffuses to the fluid area close to the central line of pipe. But, overall, the concentration value was very low.

Similar to the concentration gradient, the area with the highest temperature occurs in the baffle cell which is adjacent to iron surface while the area with lowest temperature occurs around the central line of the pipe. It is obvious, based on the model, that heat was transferred from inner wall to central area of the pipe due to the setting of constant heat flux boundary conditions in the baffle cells.

The chemical reaction model subroutine worked well and this simple CFD model roughly simulated the chemical reaction, diffusion, and heat transfer condition inside the LBE piping. Since the subroutine works well, it can be used in much more complex modeling.

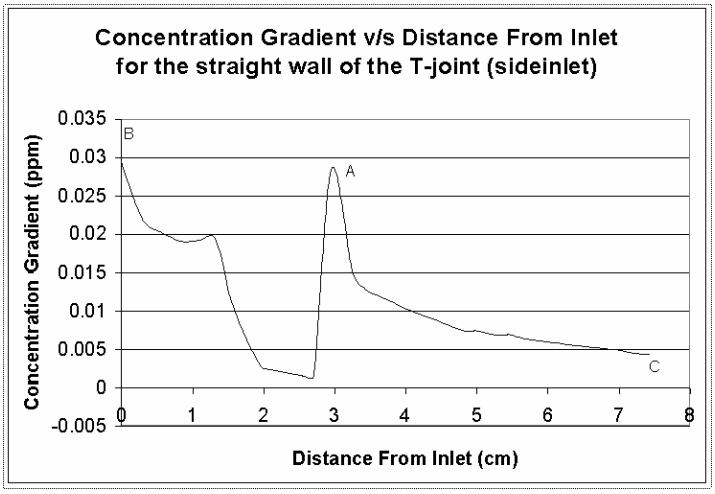

Concentration gradient versus distance from the inlet for the straight wall.

Task 6 Neutron Multiplicity Measurements of Target/Blanket Materials – Dr. Denis Beller

Background, Research Objectives and Methods:

For proper application of accelerator-driven transmutation of waste, neutron production systems using high-power accelerator systems and lead targets must be characterized for neutron multiplicity production. To test the model results, a 64-element ^{3}He Neutron Multiplicity Detector System (NDMS) array, with moderation material, was acquired from the Khlopin Radium Institute (KRI) in Russia.
Models developed by KRI (CONTROL) and UNLV (MCNPX) were used to describe: geometry of target-detector assemblies, neutron detection efficiency, a cylindrical target, system detection parameters (response times, collection efficiencies, and escape probabilities).
Background, Research Objectives and Methods:

Research Accomplishments:

Calibration of the NDMS was accomplished using a ^{252}Cf source. Efficiencies matched well with results acquired from KRI.

A major limitation of the system is the low number of neutrons that can be counted when considering the high amount of dead time in the system. Experiments were conducted at the Idaho Accelerator Center at Idaho State University and at the Remote Sensing Laboratory on Nellis AFB in Las Vegas. These

experiments agreed well with the models as long as the system was not saturated with neutrons. Calculations indicate that the system should handle 1000 n/s, but saturated at about 200 n/s. The reason was determined to be the outdated Russian hardware computing power. Plans are being made to acquire a modern computer hardware system which should substantially increase the performance of the system.

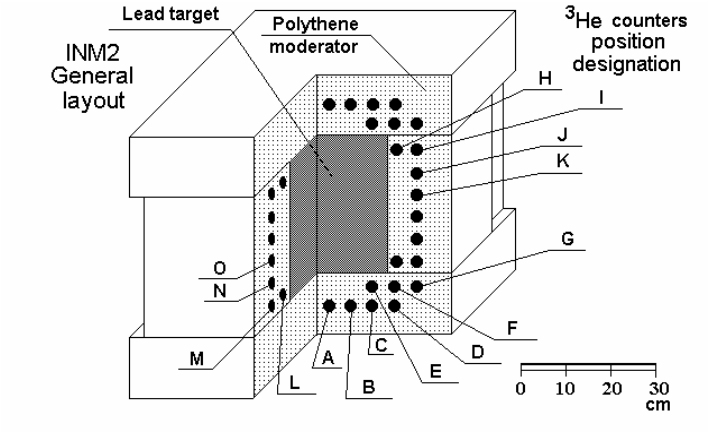

NMDS in the INM2 ("CUBE") geometry.

Task 7 Development of Dose Conversion Coefficients for Radionuclides Produced in Spallation Targets – Dr. Phillip Patton, Dr. Mark Rudin

Background, Research Objectives and Methods:

An important consideration when using spallation neutron targets is radiation safety related to target dose. Spallation experiments create up to 660 radioisotopes, many of which have no defined radiation safety standards. The Derived Air Concentrations (DACs) and Annual Limit of Intake (ALIs) for radionuclides not yet defined for appropriate dose conversion factors were studied in this effort. By reducing the radionuclides of concern only to those produced by a mercury target following an lengthy irradiation period, and for those radionuclides with half-lives more than one minute, the list of radionuclides of concern was narrowed to 81. These were divided into three groups based on half-life, available information, and other technical factors.

Research Accomplishments:

Dose coefficients were derived in accordance with FGR No. 11 using ENSDF and NUBASE. ALIs and DACs were determined for 20 of the radionuclides in a collaboration with other universities. These data were reported to the ICRP for consideration to be published in the next iteration of their metabolic models documents (30 and 66). In other cases, plans must be made to produce some of the isotopes in an accelerator facility and the Idaho Accelerator Center at Idaho State University has plans to do so in the future.

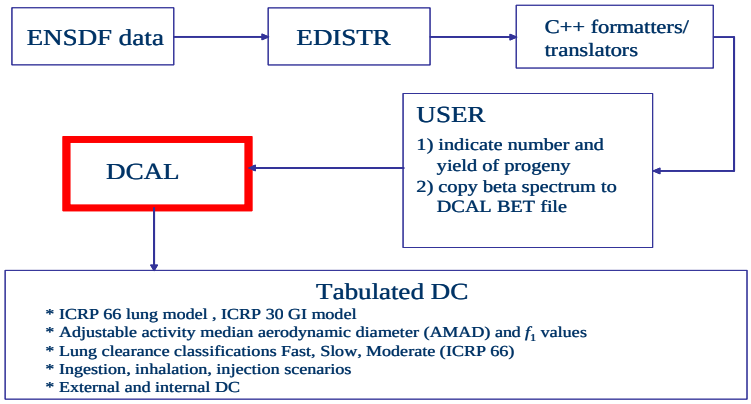

Dose Coefficient Working Group Methodology Flow Sheet. The ENSDF code is used to obtain nuclear physics data. The EDISTR code prepares the data for input into the dose calculation code DCAL

Task 8 Development of a Systems Engineering Model of the Chemical Separations Process – Dr. Yitung Chen, Dr. Darrell Pepper, Dr. Sean Hseih

Background, Research Objectives and Methods:

Complex chemical separation processes are critical to the transmutation of spent nuclear fuel into shorter-lived radionuclides. Systems analysis, or total systems modeling, is one of the strongest tools available to researchers for understanding and optimizing complex systems such as chemical separations processes. Systems analyses permit researchers to present decision-makers concise evaluations of system options and their characteristic features. The primary goal of this project was to develop a systems model that can be used to parameterize and optimize the chemical separations processes.

Research Accomplishments:

Integration with Argonne National Laboratory revealed some of the more pertinent steps in the process. The AMUSE code was used to organize the data into proper sequences and to capture necessary steps in the order they were required. A graphical user interface (GUI) was also developed.

This project developed software for a general-purpose systems engineering model named TRP System Engineering Model Program (TRPSEMPro) that will be used to improve productivity in the design process. The system model also includes various numerical optimization technologies and "Design of Experiments" study technologies.

Object-Oriented Analysis and Design was used for developing and implementing the TRPSEMPro system. A graphical notation, Unified Modeling Language, was employed to express object-oriented designs. Microsoft.Net architecture was used for system development and Visual Basic.NET was the major programming language behind the system. XML (Extensible Markup Language) was used widely to describe data and sets of elements and attributes that can be defined by researchers. XML Schema was used for describing the structure of the system engineering model. XML Database was used to store all the run-time data for the AMUSE module. Since significant experimental data will be generated and require systematic analysis, MS SQL Server 2000 database was selected for housing all run-time parameters and simulation results.

The model is combined with commercial software packages MATLAB OPTIMIZATION toolbox and SIMULINK module from Mathworks. The system model, TRPSEMPro, considers input simulation modules from multiple disciplines with inconsistent input/output handles. The package with the aid of

middleware can communicate with various simulation modules developed by other research groups and create an XML-based model description file. The critical components for the system engineering modeling include System Manager, Model Integration, Study Plan, and Solution Viewer.

The introduction of the middleware design provides flexibility to interface to other simulation modules without significant program modification. The demonstration code from AMUSE macros is kept intact during all system development stages. AMUSESimulator, is the middleware software package which was designed and implemented to serve as a bridge between the AMUSE code, and the systems engineering model, TRPSEMPro. Such an approach can reduce the time-consuming modification on the system model side and keep flexibility on the simulation modules development side.

Further system enhancement allowed the user to select various process types. An interface for conducting multiple runs was created. The GUI included a list of variables, a range for those variables, all of which provide an envelope of end results.

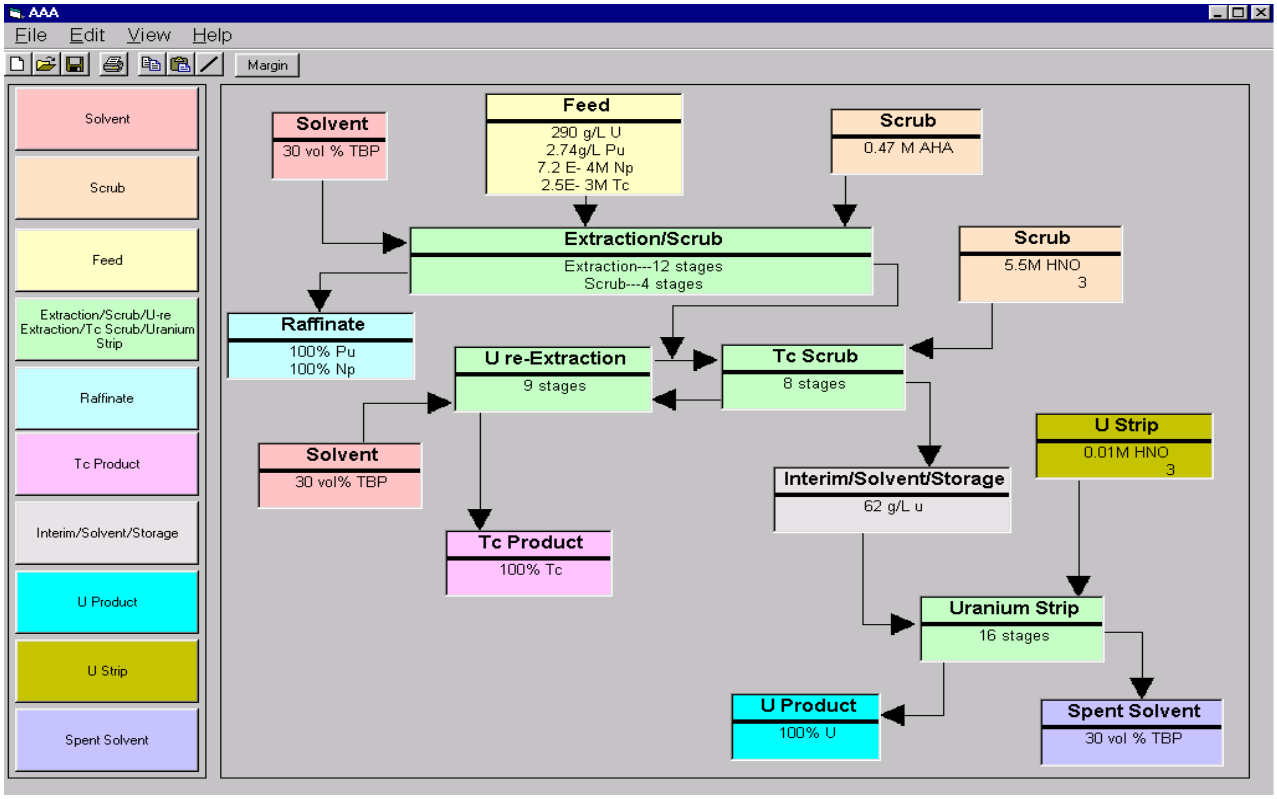

Figure 1. UREX demonstration flow sheet for glove box operations and uranium strip section.

Task 9 Design and Evaluation of Processes for Fuel Fabrication – Dr. George Mauer

Background:

Definition of processes required for a transmutation program must accommodate a wide range of requirements and be suited for remote operation in a hot cell. Complete life cycle processes must be considered, including design, operations and decommissioning. This project defined technical support to process designers for such operations.

Research Objectives and Methods:

Areas of consideration were categorized as follows:

Methods and processes
Simulations
Process and Equipment for Autonomous Manufacturing
Sensors, Controls, and Operational Safety
Cost, Feasibility, and Large Scale Deployment

Research Accomplishments:

A special simulation model with a Waelischmiller hot cell robot was developed and coupled with MatLab control software. Matlab provides the interface with the robot and is used to control the system. This renders a realistic simulation of the forces and torques present during robot motion. A 3-D manufacturing process simulation using CAD models and the Newtonian dynamics of the moving components was developed.

Results exist in the form of movies, data sets, and images. Simulations for several robot types were developed and their proper kinematic configuration was verified. The simulations permit the detailed analysis of forces and torques in any modeled part or component.

While the simulation process generally worked flawlessly, the simulation time rose considerably as more details were added to the simulation. The speed of the simulation has been increased about 100-fold by moving to fast dual-processor computers.

Efforts to develop a vision-based methodology for locating and identifying objects within the robot's workspace were conducted using the Artificial Intelligence (AI) algorithm for object identification.

Another accomplishment involved the development of algorithms for knowledge based pattern recognition using IF (a set of conditions is satisfied) THEN (a set of consequences can be executed) routines. Other simulation variables established included pattern matching using clustered indexing vectors containing information about an object and feature vector indexing, where a 3-D object is segmented into a set of simple geometric features. Each feature is stored with its vector segmentation and geometry information (magnitude, inner angle, etc.).

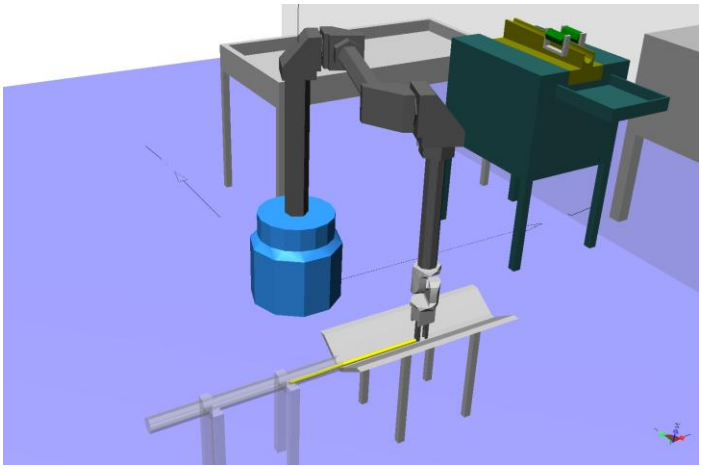

The Wäelischmiller robot inserts the fuel pins in the cladding tube

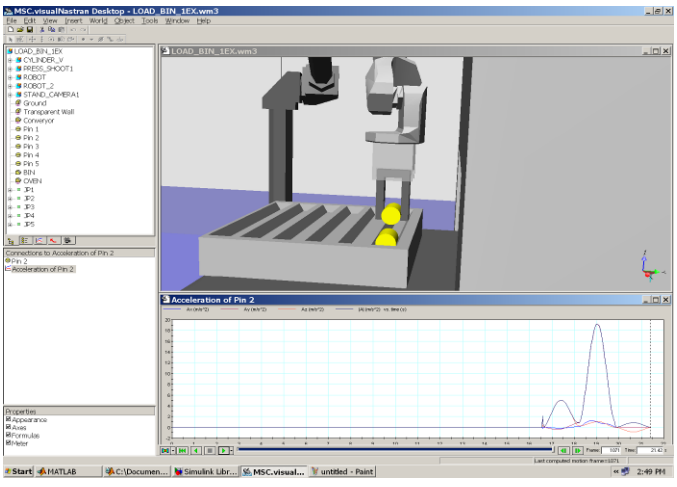

Visual Nastran Analysis of Pellet accelerations. The simulation verified that pellet's acceleration did not exceed a specified maximum of 20 m/s^2.

Task 10 Development of a Mechanistic Understanding of High-Temperature Deformation of Alloy EP-823 – Dr. Ajit Roy, Dr. Brendan O'Toole

Background, Research Objectives and Methods:

Deformation characteristics of steel alloys (EP-823, HT-9, and 422) in contact with molten Lead-Bismuth Eutectic (LBE) target material will be studied in properly heat-treated conditions at temperatures relevant to the operating conditions. The steel alloys were fabricated with tempering times of 1.25, 1.75, and 2.25 hours each. Tensile properties were determined at temperatures ranging from ambient to 600°C. At least two specimens of each alloy were tested under each of the three metallurgical conditions at the desired temperatures and the average values used for each experiment. Scanning Electron Microscope (SEM) images were used to determine the extent and morphology of failure. Results were recorded for percentage elongation (%El), percentage reduction in area (%RA), yield strength (YS), and ultimate tensile strength (UTS) as functions of testing temperature and thermal treatments.

Research Accomplishments:

The significant conclusions drawn from this investigation are summarized below:
• The hardness of all three austenitized and quenched alloys were significantly reduced due to tempering, showing a gradual reduction with increasing tempering time.
• The magnitude of the yield, ultimate and failure stress were gradually reduced with increasing temperature, showing significant reductions at temperatures above 400°C.
• The extent of ductility in terms of %El and %RA was reduced to some extent in the temperature regime of ambient to 300°C due to strain hardening. However, beyond 300°C, the magnitude of these parameters was enhanced due to increased plastic flow.
• The morphology of failure was characterized by increased plastic deformation at elevated temperatures. Reduced cracking and dimpled microstructures were observed on the fracture surfaces indicating improved ductility at higher temperatures.
• The tempering time did not influence the metallurgical microstructure and the resultant tensile properties to any great extent irrespective of the testing temperature.

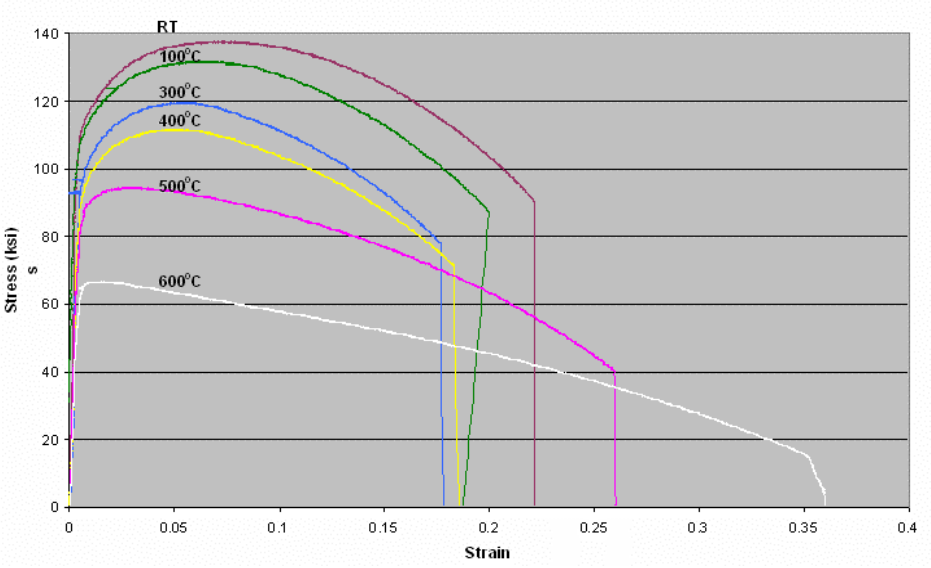

Stress-strain curves for Alloy HT-9 at different temperatures.

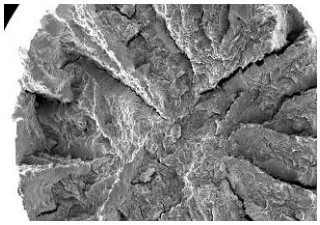

Room Temperature (RT)

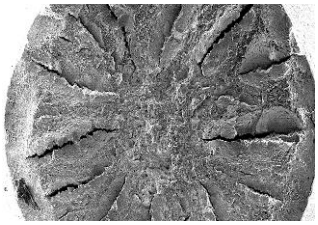

100°C

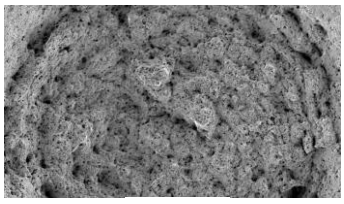

300°C

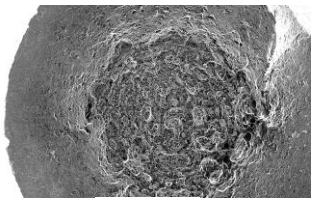

600°C

Scanning Electron Microscope micrographs of Alloy HT-9 at various temperatures (35X).

Task 11 Nuclear Criticality, Shielding, and Thermal Analyses of Separations Processes for the Transmutation Fuel Cycle – Dr. William Culbreth, Dr. Denis Beller

Background, Research Objectives and Methods:

Transmutation of used nuclear fuel requires separation techniques to isolate the radioisotopes of interest. This results in a highly radioactive waste stream, due to the fission product mix inherent in used nuclear fuel. Transuranic elements are also part of the separation stream. These have criticality implications (k_{eff}), as well as heat generation issues that have to be accommodated in the design process for transmutation research. UREX+ was used as the separation process for this study because it is currently the most promising candidate for transmutation separation chemistry. The goal of this program is to model configurations for the UREX+ process. Nuclear criticality calculations, as well as thermal properties of the Cs/Sr, Pu/Np, and Cm/Am waste streams are the focus of this effort.

Research Accomplishments:

Since Cm generates a substantial amount of decay heat, extensive criticality and thermal models were created for Cm. Analysis was also made for a container to house a homogenous mixture of TRU, process salt, and fission products. Ultimate temperature and k_{eff} studies were performed on other minor actinides, including plutonium and americium. SCALE 4.4 and MCNPX were used as the modeling software.

Cm Metal Cylinder		Criticality		Heat Transfer	
		rad (cm)	mass (kg)	rad (cm)	mass (kg)
	bare	4.6	82.52	1.1	1.129
	water	2.7	16.69	3.3	30.48
Cm_2O_3 Cylinder		Criticality		Heat Transfer	
		rad (cm)	mass (kg)	rad (cm)	mass (kg)
	bare	5.4	125.59	1.55	2.74
	water	3	21.53	2.25	8.37
Am_2O_3 Cylinder		Criticality		Heat Transfer	
		rad (cm)	mass (kg)	rad (cm)	mass (kg)
	bare	11.2	1032.28	1.6	3.01
	water	10.5	850.58	1.9	5.04
Am_2O_3+Cm_2O_3		Criticality		Heat Transfer	
Cylinder		rad (cm)	mass (kg)	rad (cm)	mass (kg)
	bare	10	737.9	1.4	2.02
	water	9.3	593.54	2	5.88

Recommendations for Cm and Am oxide inventories based on criticality and melting temperature

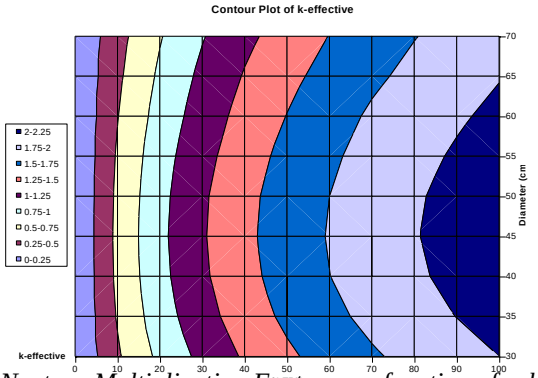

Contour Plot of the Effective Neutron Multiplication Factor as a function of cylinder diameter and % TRU in the mixture

Task 12 Radiation Transport Modeling using Parallel Computational Techniques – Dr. William Culbreth, Dr. Denis Beller

Background:

MCNPX nuclear transport code is used to model results of spallation neutron experiments conducted at the LANCE proton accelerator at LANL. UNLV researchers modeled these configurations and compared experimental data to validate the code. These data can also be used to alter the code as necessary and augment the nuclear data libraries. UNLV students were also involved in conducting experiments at LANL and in assisting researchers in designing new experiments.

Research Objectives and Methods:

This project involved modeling several aspects of the LANCSE
beam experiments:
• Modeling targets of varying diameter in air, in a vacuum, and in the presence of humid air;
• Modeling various proton beam profiles;
• Modeling the effects of off-axis proton beam impingement on the target;
• Modeling the asymmetry introduced by the steel table below the target;
• Modeling the effect of varying ratios of Pb to Bi and the effect of impurities; and

• Modeling the system, including other structures within the test room.

Research Accomplishments:

With the experience gained through modeling these systems, the UNLV researchers developed, with the assistance of their national laboratory collaborators, a benchmark program for the neutron leakage tests and other tests related to transmuter development. A comprehensive three-dimensional computer-aided design (CAD) image of the LANSCE experiments was prepared using ProEngineer to help benchmark the experiments and provide accurate geometric data for MCNPX modeling.

MCNPX models were used to benchmark data. These calculations were used to properly position foils and to determine the expected neutron flux from these foils. Solid Works CAD models of the Blue Room at LANSCE were also prepared. Slightly off-center proton beam strikes of the target and neutron spectra expected from time-of-flight neutron detectors were the subject of other modeling efforts.

Working with LANL scientists, these models were used to position detectors to measure leakage and provided for proton activation experiments in sodium coolant.

The Beowulf cluster accommodated parallel processing for MCNPX modeling and the Message Passing Interface (MPI) protocol was debugged and compiling problems were resolved. Benchmarking and optimization were completed and MCNPX simulation of experiments were performed. A graphical user interface (GUI) was developed in Virtual Basic and a user guide was published. The result is that MCNPX processing has been ported to a Beowulf cluster with between 32 and 50 processors and is optimized for running on this massively parallel system.

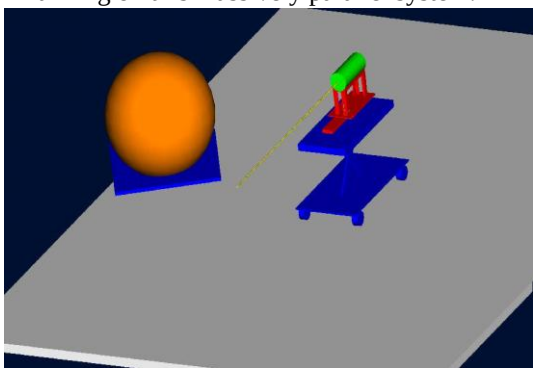

Schematic of the experimental facility at LANSCE used for modeling.

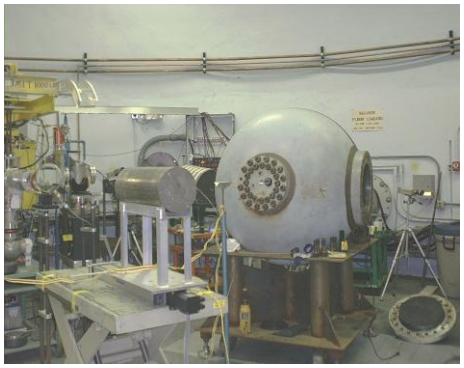

Experimental facility at LANSCE, Los Alamos, NM.

Task 13 Developing a Sensing System for the Measurement of Oxygen Concentration in Liquid Pb-Bi Eutectic – Dr. Yingtao Jiang, Dr. Bingmei Fu

Background:

Oxygen content within Lead-Bismuth Eutectic (LBE) is a critical factor in reducing corrosion in steel containment vessels. Measuring the level of oxygen in the LBE molten target is critical to controlling oxygen levels and minimizing corrosion. Yttria Stabilized Zirconia (YSZ) sensors have been used to measure oxygen in LBE. Performance has been modeled extensively and is well understood, however, real world performance of these sensors requires investigation.

Research Objectives and Methods:

The research objectives of this project were as follows:
• To generate calibration curves of voltage versus oxygen concentration for the YSZ oxygen sensor system under various temperatures in liquid LBE.
• To determine the sensor characteristics of the YSZ sensor system.
• To determine oxygen dissolving rates in LBE under different temperatures in vitro.

• To study the effects of unwanted electrical conductivity, contributed by the mobility of the electrons at high temperatures, for more accurate oxygen measurement.
• To study alternative and promising oxygen measuring methods.

Background, Research Objectives and Methods:

A new apparatus was developed to overcome some of the shortcomings of previous efforts:

• Instead of using a steel tube, this apparatus incorporates a cylindrical crucible made of Magnesia Stabilized Zirconia (MSZ), and the liquid LBE is contained in this MSZ crucible. MSZ was chosen because of its desirable material properties.
• The MSZ crucible sits on a stainless steel beaker. The beaker acts as a pressure boundary, and it can distribute the weight of the molten metal and crucible to the outer support. Back-up materials are used to fill the gap between the inner crucible and beaker.
• The crucible is tightly sealed with a metallic flange, with only a few openings left for gas inlets and outlets.
• A stirring unit is employed in order to mix the gases with the molten metal. The stirrer is made of Silicon Nitride (Si_3N_4) ceramic. Silicon Nitride has high temperature strength, creep resistance, oxidation resistance, and it is not wetted by any molten metal. On top of those, compared to many other ceramic materials, Si_3N_4 has good mechanical strength.

Sensor testing with the new apparatus reveals good agreement with models. Oxidation was a problem at high temperatures for tantalum. Sensitivity suffers and the sensors fail to report the proper oxygen levels. When introducing hydrogen and helium mixture into the system to clean excessive oxygen in the LBE container, it was found that Mo responds a little faster than Stainless Steel (SS). The level of Bi or Bi_2O_3 did not have any effect on sensor response. Smaller levels of oxygen than previously thought can cause Bi to be oxidized. Simulations with Finite Element Method (FEM) software, FEMLAB, showed that the oxygen concentration distributes evenly in the whole flow field due to the strong convection flow in LBE. These simulation results with the experimental measurements help to not only determine the oxygen dissolution rate and the diffusion coefficient under different temperatures, but also provide suggestions for better experimental design.

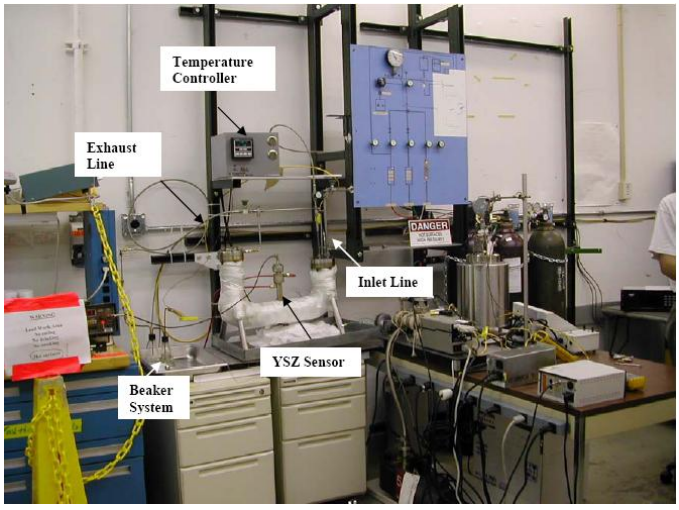

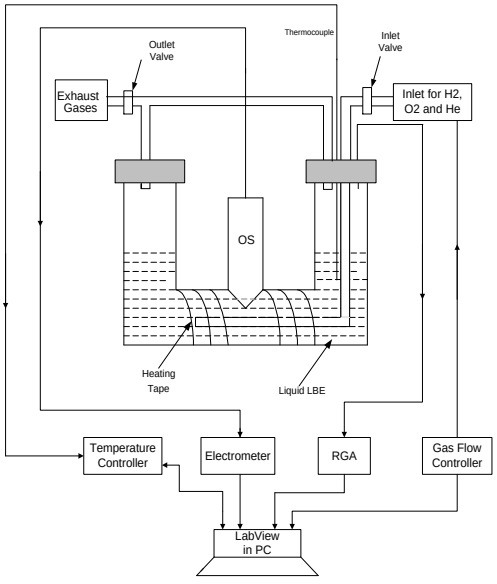

The first sensor calibration experimental setup.

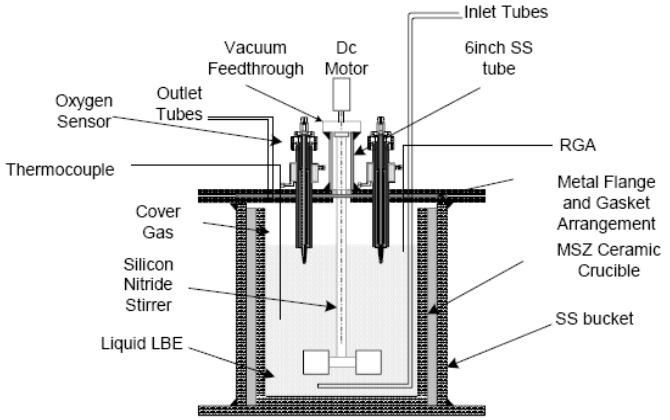

Schematic of the second sensor calibration

Task 14 Use of Positron Annihilation Spectroscopy for Stress-Strain Measurements – Dr. Ajit Roy

Background:

Residual stress in metals and alloys caused by tensile loading beyond a certain value produced because of defects and voids in the crystal lattice can be exacerbated by welding and plastic deformation. These types of operations can cause premature failures in structural materials unless these stresses are relieved by thermal treatments, which are commonly known as stress-relief operations.

Research Objectives and Methods:

Non-destructive characterization of residual stresses in such alloys may be conducted using positron annihilation spectroscopy (PAS). The focus of the study is using PAS on three leading steel alloys: type 304L stainless steel, and two Martensitic alloys: EP-823 and HT-9. The metallurgical microstructures and the nature of the defects were analyzed by optical microscopy and TEM, respectively.

Research Accomplishments:

The significant results obtained are summarized as follows:

- The residual stresses, characterized in all three tested materials in terms of the PAS line-shape parameters (S, W, and T) exhibited consistent patterns.
- The residual stresses in cylindrical calibration specimens under tensile loading were enhanced at increasing applied stresses, showing a gradual enhancement in the S-parameter.
- The extent of residual stress in terms of the W- and T- parameter was enhanced at higher applied stresses, showing a gradual reduction in both parameters.
- The overall data revealed that the residual stresses generated inside the cylindrical specimens of all tested materials were enhanced at higher applied loads, irrespective of the testing technique.
- The PAS data on the cold-reduced plates of alloy EP-823 showed reduced T-parameter value with an increasing level of cold deformation, indicating higher residual stresses.
- The TEM micrographs of the cold-reduced plates were characterized by the presence of dislocations and carbide precipitates, irrespective of the cold-reduction level.
- For welded specimens consisting of similar materials on both sides, the residual stress in terms of the S-, W-, and T-parameters was maximum at the FL. A gradual drop in residual stress was observed with these specimens at locations away from the FL.
- The extent of residual stress was higher in martensitic Alloy EP-823 compared to that of austenitic

Type 304L SS, irrespective of the weld configuration.

- Compressive residual stresses were observed in Alloy EP-823, when welded to Type 304L SS.
- The magnitude of dislocation density (ρ) was substantially higher at the HAZ compared to that of the base material of the welded specimens consisting of similar materials (Type 304L SS or Alloy EP-823) on both sides.
- In the case of the welded specimen of dissimilar materials (Type 304L SS and Alloy EP-823) on the opposite side, the concentration of dislocation in terms of ρ was greater at the HAZ on the Alloy EP-823 side of the weld.
- The enhanced value of ρ at the HAZ on the Alloy EP-823 side of the weld may be attributed to the faster rate of solidification of this alloy compared to that of the austenitic SS.
- The sizes of the HAZ on the Alloy EP-823 sides of the welded specimens were relatively larger, irrespective of the weld configuration.

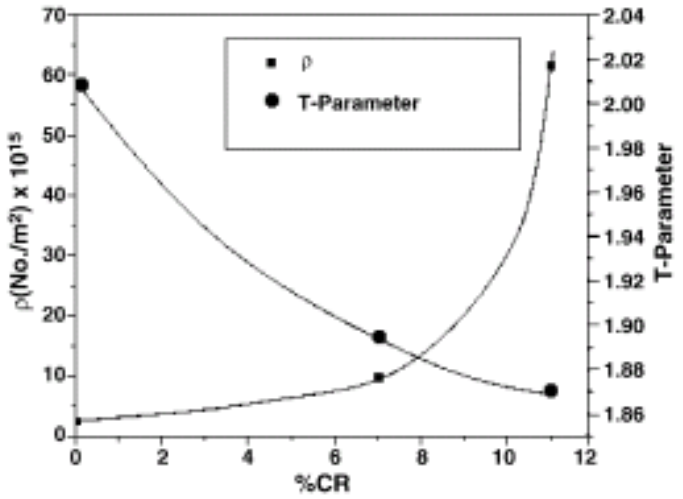

Variation of ρ and T-parameter with percent cold-reduction

Task 15 Immobilization of Fission Iodine by Reaction with a Fullerene Containing Carbon Compound and Insoluble Natural Matrix – Dr. Spencer Steinberg, Dr. Gary Cerefice, Dr. David Emerson

Background:

I-129 is a long-lived radioisotope of concern in used fuel reprocessing because it is volatile and, if inhaled or ingested, remains radioactive in the thyroid gland essentially forever. For this reason, recovery of iodine is important for implementing any nuclear transmutation strategy. Specialized filtration systems are used in an attempt to trap the iodine from this process. Fullerene Containing Carbon (FCC) compound or a Natural Organic Matter (NOM) matrix can immobilize iodine isotopes in a manner that is, according to the Khlopin Radium Institute (KRI) in Russia, useable as a transmutation target matrix when combined with ceramics.

The stability of the association of iodine with FCC and NOM products are the subject of this study. Product distributions for the various matrices under various reaction conditions were examined in order to maximize the binding of iodine. The recovery of the iodine from the sequestration matrices was also examined, along with the conversion of the iodine to matrices more suitable for geological storage and/or use as transmutation targets.

Research Objectives and Methods:

The following are the specific research objectives and goals:

- Develop bench-scale experimental set-up and procedures for simulating PUREX head-end vapor phase.
- Develop experimental procedures for evaluating iodine sequestering methods using bench-scale procedures.
- Develop FCC bearing material as potential iodine sequestration matrix.
- Determine binding of iodine to FCC and NOM.
- Examine alternate iodine sequestration matrices using techniques developed for FCC and NOM studies.
- Examine the effect of reaction conditions on binding.
- Elucidate the nature of the reaction products (volatile, hydrophobic, soluble, insoluble).
- Develop methodology and host matrix for converting sequestered iodine to solid matrix for evaluation as transmutation target and/or disposal matrix.
- Examine recovery of iodine from sequestration matrices.

Research Accomplishments:

The FCC compounds are developed and prepared by the KRI Research Industrial Enterprise (KIRSI). The KRI-KIRSI team researched the impacts of process parameters on sorption of iodine, and examined the material properties, such as how iodine attaches to the FCC compounds. The KRI-KIRSI team also examined the conversion of the iodine loaded FCC compound to a stabilized matrix (similar to ceramic) for potential use as a disposal form, acceptable transportation material, or potential target material.

Utilizing preparative gas chromatography, it was demonstrated that methyl iodide that was released by pyrolysis (of .05 to 0.5 grams of OM) could be purified and recovered.

Several methods for the conversion of methyl iodide to sodium iodide were explored. The Würst reaction was attempted and was not successful. Methyl iodide reacted rapidly with several nucleophiles including thiourea, mercapto ethanol. Methyl iodide could be easily reacted with GT-73 resin (mercaptan containing resin) in the sodium form. The result of this reaction was the release of sodium iodide that could be rinsed free of the resin.

The methyl pyridinium resin was prepared. Further experiments demonstrated that iodide could be recovered from aqueous solution and converted to methyl iodide by pyrolysis. Competitive effects from other aqueous anions were observed.

A number of potential reducing organic compounds as candidates for iodate reduction were examined. Lignin phenols and carbohydrates did not seem to be viable candidates. Hydroquinone however, rapidly reduces iodate to iodide. Furthermore, iodine (or HOI) was demonstrated to be an intermediate in this process and can be trapped as an organoiodine compound. For example a solution of hydroquinone and iodate can iodinate p-hydroxybenzoic acid or vanillic acid. It can be routinely observed that diphenolic moieties are produced during pyrolysis of lignin and other forms of NOM. Others have evoked this functionality to explain the redox properties of humic and fulvic acids.

It was demonstrated that iodide can be trapped in NOM in the presence of manganese dioxide (γ-MnO2). The oxidation of iodide to iodine (or I_3^-) can be observed at moderate pH (4-9). Also, it was demonstrated that at pH 7 iodide is incorporated into NOM in the presence of MnO_2. Observations indicate that the reaction occurs when microcrystalline MnO_2 (prepared by us) is utilized. Reagent grade MnO_2 does not appear to promote this reaction.

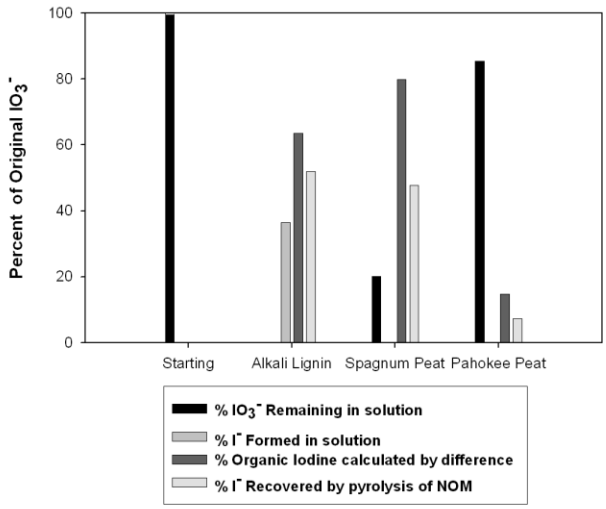

Distribution of iodine after iodate-NOM experiments at room temperature and pH 2.

A number of synthetic (nano-particle) manganese (III, IV) oxide preparations have been shown to be capable of oxidizing iodide to iodine (or IOH) at pH as high as 5. Various synthetic preparations of MnO_2 were examined. These various nano-particle manganese oxides have been characterized by transmission electron microscopy, scanning electron microscopy, and atomic force microscopy. In addition, surface areas, average manganese oxidation states and the kinetics of iodide oxidation by these materials have been measured. The rate of iodide oxidation by various manganese oxide preparations varies significantly. The oxidation rate appears to have some relationship to the average oxidation state of the manganese.

In another facet of this project, iodine distributions in salt impacted soils from the Virgin River, Nevada were examined. This study indicates that organic iodine was the most abundant form of iodine in the soil samples and that the content of organic iodine was correlated to total organic matter and to the lignin content (as measured by chemolysis) of the samples. These observations are consistent with the notion of the formation of organic iodine resulting from the cycling of iodine between iodide and iodate, with organic iodine resulting from the iodine or hypoiodic acid (I_2 and HIO) intermediate reacting with phenolic moeties in sedimentary and soil organic mater.

The formation of triiodide presumable involves the adsorption of iodide onto the MnO_2 surface (perhaps displacing a surface hydroxyl group). The

iodide should be subsequently oxidized and released back into solution as IOH or I_2, which rapidly forms I_3^-. The kinetic data has been modeled as a first order process. First order rate constants have been obtained for the formation of iodine in the presence of MnO_2. The increase in iodide oxidation rates with MnO_2 concentration is evident in the data. The reaction rate increases with iodide concentration although the dependence is not first order (an order of 1.4 appear to fit the data). The oxidation rate also increases with temperature and has an apparent activation energy of 16.2 kJ/mol.

The total yield of iodine form these materials was compared with the resulting Mn (II) concentration to estimate the oxygen to manganese ratio (MnO_x) for the starting material. This ratio (x) is a function of the average oxidation state of the material and is given by:

$$x = 1 + \frac{I_3^-}{Mn^{+2}}$$

The rate of iodide oxidation can be seen to vary significantly for the various preparations.

It is clear that some manganese oxide can oxidize iodide to iodine under mild pH and temperature conditions. By comparison, laboratory grade MnO_2 reacted sluggishly under these conditions. Because of

the wide distribution of this mineral in nature, it is believed that the oxidation of iodide by manganese oxide may result in the formation of organic iodine bonds in sedimentary and soil organic matter.

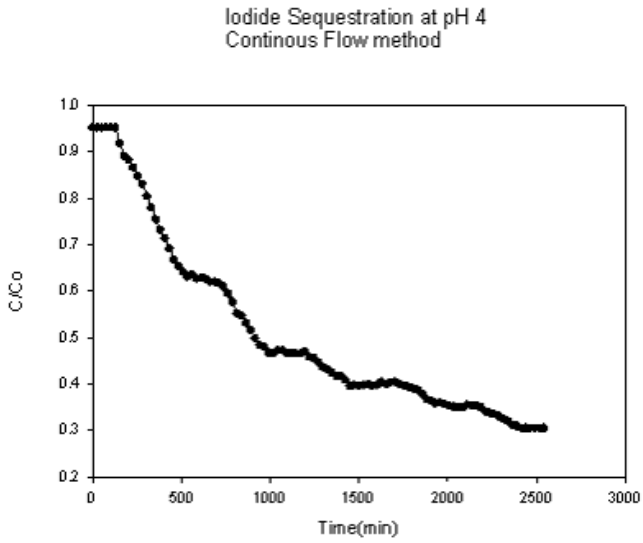

Sequestration of iodide (10^{-4}M) in the presence of sphagnum peat and MnO_2. The solution was circulated through a column at 5 mL/min.

Task 16 Evaluation of Fluorapatite as a Waste-Form Material – Dr. Dennis Lindle, Dr. Oliver Hemmers, Dr. Dale Perry

Background:

TRISO-coated fuel (a silicon-carbide and pyrocarbon composite coating) is being studied as a candidate for fuel used in High-Temperature Gas Cooled Reactors (HTGRs). The Fluoride Extraction (FLEX) process is a method developed by Argonne National Laboratory to reprocess used TRISO-coated fuels. Since the waste stream consists of fission products in a zirconium fluoride salt, it is not a candidate for conversion to borosilicate glass and an alternate, suitable disposal form must be found.

Research Objectives and Methods:

The following were the specific research objectives:

- To develop a waste matrix for the disposal of the fission product waste stream from the FLEX process;
- To develop a process to make synthetic fluorapatite that incorporates the FP-bearing ZrF_4 salt;
- To develop a fundamental understanding of the chemistry of this new waste form in order to better predict its long term behavior in a repository environment; and,
- To develop a fundamental understanding of natural, fluoride-bearing mineral phases to use as natural analogs to bound the predicted behavior of the FLEX fission product waste stream.

The research effort was divided along two parallel paths: the *Fabrication Path*, led by collaborators at the Khlopin Radium Institute (KRI) in St. Petersburg, Russia; and the *Characterization Path*, led by researchers from UNLV.

The Fabrication Path focused on examining and evaluating various techniques for fabricating synthetic fluorapatite; synthesizing synthetic fluorapatite; and examining the impacts of waste loading and other fabrication process factors on the performance of the synthetic fluorapatite as a potential waste form.

The Characterization Path focused on adapting and refining the X-ray spectroscopy techniques currently used to characterize borosilicate glass for use in examining the fluorapatite system. This path also encompassed the examination of the ceramic and synthetic mineral waste forms created at KRI, with subsequent examination of these techniques to develop a molecular-level understanding of natural fluorapatite and other fluorine-bearing natural phases as natural analogs for the waste form. These techniques were also be used to examine the changes in surface chemistry caused by environmental degradation of these materials.

Experiments were conducted to examine various Ca surrogates (Zn, Sr, Yt, Cs, Cu, Ni, and Zr) and different weight ratios. Characterization of the results were conducted with x-ray spectroscopy, Fourier Transform Infrared Spectrometry (FTIR), SEM, XRD, TEM, and Raman Spectroscopy.

Research Accomplishments:

Significant results are as follows:

Microscopy Techniques:

The microstructure of as-synthesized fluorapatite samples were characterized by transmission electron microscopy (TEM). The phase purity and crystallographic structure of these samples were first verified by X-ray powder diffraction with the help of Rietveld analysis.

Different methods (solution-drop and microtome cutting) were used to make the samples for TEM analysis. The solution-drop method was suitable to analyze the crystallographic structure of the fluorapatite by high resolution TEM. Furthermore, the solution-drop method was successfully used to study the particle morphology of fluorapatite.

The microtome cutting method allowed studying both particle shape and cross-sectional morphology of fluorapatite crystals. Microtome cutting, however, introduced periodical fringe artifacts in high resolution TEM imaging due to deformation effects on the material. Therefore, in order to completely characterize the microstructure and morphology of fluorapatite-type particles a combination of both sample preparation techniques was necessary.

Calcium Substitution by Zinc:

Substitution of calcium in fluorapatite by zinc is possible and was demonstrated to be concentration dependent. The phase purity of fluorapatite in the samples decreases with the increase in zinc substitution.

A 25 mol % of zinc substitution leads to a single-phased fluorapatite, but the formation of a secondary phase was identified when the zinc level increased to 50 mol %. A fluorapatite phase could not be identified in samples with 75 mol % and 100 mol % zinc substitution.

The two samples synthesized using 25 mol % and 50 mol % of zinc showed some similar morphological and micro-structural properties to that of phase-pure fluorapatite. However, the closest similarities to pure fluorapatite were identified in the 25 mol % sample.

The 50 mol % sample shows a lower thermal stability that decreases with increasing zinc level. The low thermal stability of the 50 mol % sample is most likely due to the identified secondary chemical phase.

The sintering properties of the 25 mol % sample are similar to pure fluorapatite. However, complete decomposition of the zinc-incorporated fluorapatite chemical phase in the calcined 25 mol % sample results in lower thermal stability than for phase-pure fluorapatite.

Calcium Substitution by Strontium:

The synthesis of foreign cation-incorporated fluorapatite, in this case strontium ions, was achieved successfully. XRD powder patterns of fluorapatite and Sr-fluorapatite showed identical peaks except for slight peak shifts and peak merging.

Increasing strontium content showed a linear relationship with unit cell dimensions, the relationship of which can allow one to measure unknown percentages of strontium in fluorapatite.

It has been shown that Sr occupies only Ca sites and not P or O sites.

Scanning electron microscope images of strontium-incorporated fluorapatite showed the formation of hexagonal crystals on the surfaces of most samples. Formation of fluorapatite crystals has not been observed in the same samples before annealing at 1200 °C.

Re-synthesis of apatite using natural fluorapatite as a starting material was achieved. The final product contained fluorapatite, chloroapatite and hydroxyapatite phases and it is inconclusive as to which was the major component.

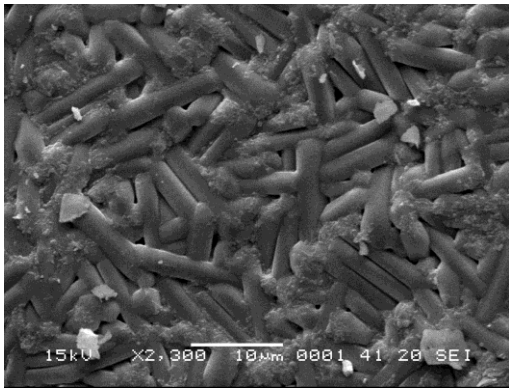

SEM micrograph of Ca_4SrFap (annealed sample).

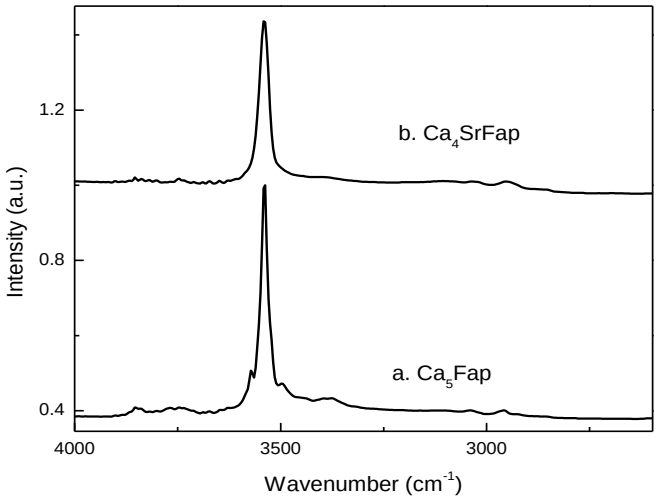

IR spectra of Ca_5Fap and Ca_4SrFap after annealing.

Task 17 Interaction between Metal Fission Products and TRISO Coating Materials: A Study of Chemical Bonding and Interdiffusion – Dr. Clemens Heske

Background:

TRISO-coated fuel fission product mix forms metal fission products with the coating material. The project studies the interface formation of Pd, Cs, and Ag with SiC and pyrolytic carbon. Using SiC single crystals and highly-ordered pyrolytic carbon (HOPG) as substrates, interfaces are prepared under controlled conditions in an ultra-high vacuum environment and are studied with a combination of experimental methods, including Photoelectron Spectroscopy, Auger Electron Spectroscopy, X-ray Emission Spectroscopy, and X-ray Absorption Spectroscopy. Furthermore, microscopic techniques (in particular Atomic Force Microscopy) are being employed.

Research Objectives and Methods:

Research methods focused on failure mechanisms for TRISO-coated fuel as it relates to fission product transport. Interface properties were investigated to optimize their effectiveness for long-term chemical stability. The ORNL Advanced Fuel Cycle Initiative (AFCI) was supported through irradiation testing and post-irradiation examinations. UNLV employed its ultra-high vacuum system and the SXF end station at beamline 8.0 at the Advanced Light Source at Lawrence Berkeley National Laboratory (LBNL). The ultra-high vacuum system analysis chamber is equipped with a state-of-the-art electron analyzer, an X-ray source, an ultraviolet (UV) source, and an inverse photoemission setup consisting of a low-energy high-flux electron gun and a UV detector. The preparation chamber is used for cleaning samples with an ion source and for the deposition of metal films with an evaporator. Using SiC single crystals, ZrC pellets and thin films, and highly-ordered pyrolytic carbon (HOPG) as substrates, interfaces are prepared under controlled conditions in an ultra-high vacuum environment and are studied with a combination of experimental methods, including Photoelectron Spectroscopy, Auger Electron Spectroscopy, X-ray Emission Spectroscopy, and X-ray Absorption Spectroscopy. Furthermore, microscopic techniques (in particular Atomic Force Microscopy) are being employed.

Research Accomplishments:

Combining all spectral regions (in XPS and UPS), a detailed picture of the Pd/SiC interface formation can be painted, in particular when taking additional soft X-ray emission and absorption data into account, which was taken in the experimental campaigns at the Advanced Light Source. Emphasis was then placed on a detailed analysis and description of the Cs/SiC interface formation process. Different thicknesses of Cs on the SiC substrate were fabricated. These were characterized with XPS spectra and UV photoemission to determine the valence electron configuration. The Advanced Light Source at LBNL was used to examine the Si L2,3 and C K edges using x-ray emission spectroscopy. Hithly-ordered Apyrolitic Carbon (HOPG) substrate material was introduced into the study. Different thicknesses of Cs were fabricated and x-ray photoemission was used to create an image after the samples were cleaved in a nitrogen atmosphere resulting in a very clean and nearly adsorbate-free surface. The results of this experimentation were that: a) that Cs grows in a cluster-like fashion on HOPG (at room temperature), and (b) that the presence of Cs clusters on the surface of pyrolytic graphite can lead to the formation of crater- and crack-like diffusion pathways during annealing at 600 °C, while the annealing of pyrolytic graphite only leads to the formation of cracks, but not craters. Focus then turned toward the interaction of Pd with ZrC. The ultra-high vacuum system was completed and moved to the Science and Engineering Building from the Chemistry building at UNLV. A sample storage chamber was designed and installed. Experiments at the Advanced Light Source at LBNL to investigate the Pd/ZrC interface formation. Finally, X-ray emission (XES) and X-ray absorption (XAS) spectroscopy data from a ZrC sample was analyzed from samples prepared at UNLV using the optimized surface cleaning procedure.

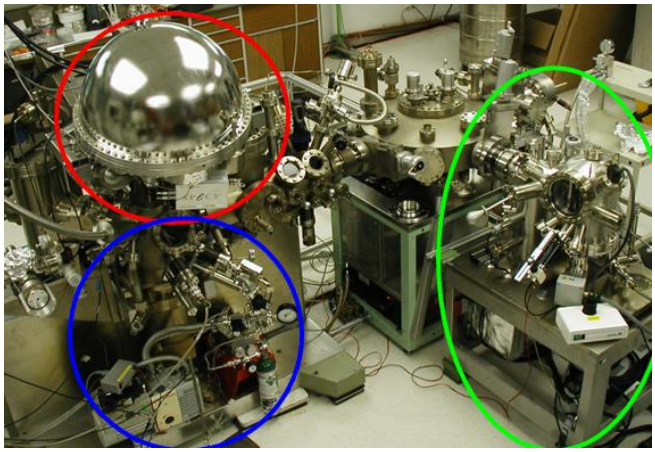

Bird's eye view of the modified multi-chamber ultra-high vacuum apparatus. Red: replacement electron analyzer; blue: inverse photoemission setup, green: scanning probe microscope.

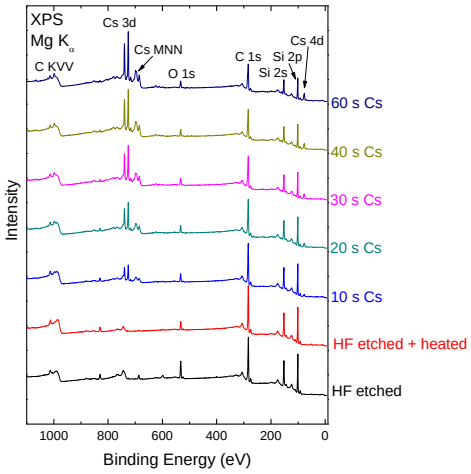

XPS survey spectra of an HF-etched SiC single crystal surface, after heat treatment at approximately 400°C, and after various deposition steps of Cs (given is the deposition time in seconds).

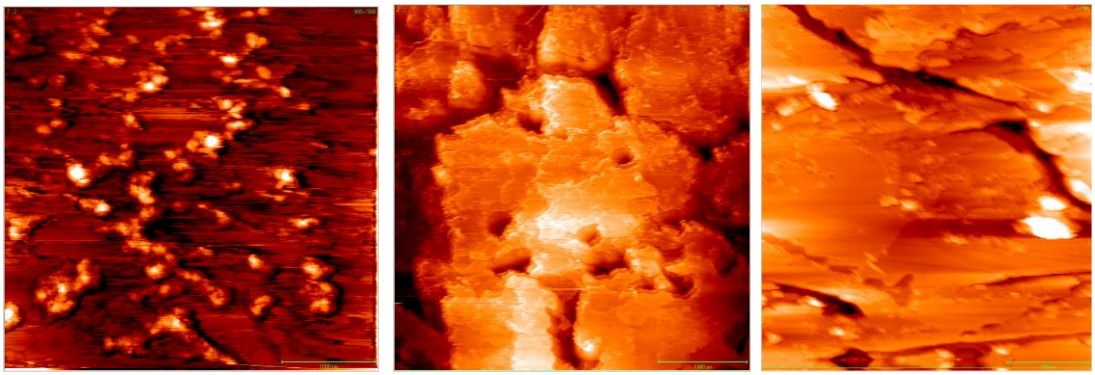

Left: Atomic force microscope picture of a highly-ordered pyrolytic graphite (HOPG) substrate after deposition of Cs for 300 seconds. Center: Atomic force microscope picture Cs/HOPG substrate after annealing at 600 ℃ for 60 minutes in a furnace. Right: Atomic force microscope picture of HOPG without cesium deposition, annealed at 600 ℃ for 60 minutes in a furnace. All image scales are 4 x 4 μm^2.

Task 18 Fundamental and Applied Experimental Investigations of Corrosion of Steel by LBE under Controlled Conditions: Kinetics, Chemistry, Morphology, and Surface Preparation - Dr. John Farley, Dr. Allen Johnson

Background:

Continued work from Task 3, "Steel Alloy Corrosion Experiments by Lead-Bismuth Eutectic (LBE)". Structural materials used for fast neutron transmutation operations must be stable (non-corroding) in the presence of non-moderating coolants such as LBE (used here as the corroding agent) and sodium. LBE corrodes stainless steel, so more resistant alloys and/or compounds must be explored. Oxide layers have been found by the Russians (more than 80 reactor-years of experience) to significantly reduce corrosion in LBE systems. However, the fundamental understanding of the role of oxygen in passivating oxide layers is incomplete.

Samples of steel exposed to LBE were examined using various types of surface microscopy: Scanning Electron Microscopy (SEM), Energy Dispersive X-ray Spectroscopy (EDAX), Wavelength Dispersed X-ray, X-ray Diffraction (XRD), X-ray Photoelectron Spectrometry (XPS) with sputter depth profiling (SDP), and Laser Raman Spectroscopy. The objectives are (1) to examine the morphology and composition of the oxide layer, its elemental and chemical composition, and its relation to the bulk material, (2) to probe the formation, nature, composition, breakdown, passivation, and healing of oxide layers on steel exposed to LBE, and (3) thereby gain some insight into the fundamentals of corrosion of steel by LBE.

Research Objectives and Methods:

The following 8 activities were conducted:

- The UNLV group has continued collaborations with the LANL group, which has an LBE loop ("DELTA" loop). Samples of steel that were exposed to LBE at the DELTA loop at LANL were analyzed.
- Silicon has been proposed as a component to improve the corrosion resistance of steel in LBE systems. Si-containing steel that was exposed to LBE by Eric Loewen at INL was examined.
- A bay in the chemistry building, CHE 112C, was converted into the High Temperature Materials Experimental Facility (HTMEF).
- An experimental apparatus, the Liquid Metal Corrosion Experiment (LMCE) is being built.
- Gas phase experiments in which steel samples were oxidized in glass capsules at elevated temperatures in a tube furnace at UNLV.
- An existing ion beam apparatus will be restarted to produce mass-selected ion beams. These will be used for isotopic labeling experiments for studying diffusion rates of iron, oxygen,

nickel, and chromium atoms in steel matrices at elevated temperatures. Detection will be accomplished using the SIMS-TOF experiment at the EMSL laboratory at PNNL.
- A laser Raman experiment was designed to examine the chemical species present in oxide films produced in steel/LBE corrosion experiments.
- Corrosion of D-9 steel, which is a proprietary surface treatment, was studied.
- Compare current results with results from Russian studies conducted at the Institute for Physics and Power Engineering in Obninsk, Russia.

Research Accomplishments:

Approximately 250 DELTA loop samples were analyzed using SEM and EDAX. This was important to the LANL research group, which was having some issues controlling the crucial oxygen level in their DELTA loop.

A model was developed and presented at the AFCI materials working group March 2006 in Santa Fe. This model and supporting experimental results indicate that the conversion of the oxide layer on the austenitic steels from an initial compact thin layer to a porous thick multilayer occurs at localized failures of the thin oxide, with the formation of diffusion channels in the thick oxide. At the May 2007 Heavy Liquid Metals (HLM) Workshop in Rome, Italy, other researchers supported this model. (2006-2007)

The silicon-containing steel samples at INL were examined using SEM, XPS, and SDP. Samples with four different concentrations of silicon were examined. Silicon was found in the form of elemental silicon (in the metal), in the form of silica (SiO_2) at the bottom of the oxide layer, and silicates in the oxide. A layer of silica formed between the oxide and the bulk metal. The details were written up and published in the peer-reviewed *Journal of Nuclear Materials*.

Facility development

Renovation of room CHE 112C into The High Temperature Materials Exposure Facility (HTMEF) was completed. This included renovating the floor, walls, air conditioning, and utilities. The Liquid Metal Corrosion Experiment (LMCE) was placed in the HTMEF.

Gas phase experimental results

The first results using the gas-phase experiment were obtained, using a quartz tube in a tube furnace, containing a steel sample and a copper/copper oxide pellet to determine the oxygen level. Steel samples were corroded by contact with controlled amounts of oxygen at elevated temperatures.

The Raman experiment obtained its first results. The Raman technique allows determination of the chemical species (e.g., Fe_2O_3 or Fe_3O_4) while other techniques (XPS, EDAX) can only yield elemental composition (e.g., Fe and O are present but not what chemical species). Graduate student Brian Hosterman used the Raman experiment to demonstrate that the iron oxide in a sample exposed by the Russian collaborators was Fe_3O_4 and not Fe_2O_3.

The gas phase oxidation of steels has been examined at oxygen concentrations approximating those in LBE. This study determines the unique aspects of oxidation in LBE. For example, in the gas phase experiments on these steels, tin was sometimes observed at the surface. Tin has been implicated in temper embrittlement. In LBE, tin does not accumulate due to the solubility of tin in LBE. Conversely, nickel is depleted from the oxide layer that forms on the austenitic steels. In LBE, this nickel can dissolve. In the gas phase, Ni depletion was also observed, indicating that nickel must dissolve into the bulk metal in this case.

After 100 h of oxidation up to 10 microns of oxide is formed, which indicates a flux of oxygen onto the metal surface that is much higher than the oxygen control mechanism (CuO/Cu couple) would allow, suggesting that some other oxygen containing species is active. Of course water is a likely suspect, and experiments have been initiated to determine the role of water as an oxygen containing/transport agent in

LBE. In summary, gas phase experiments have directed the project towards studies expected to give insight into the mechanisms of LBE corrosion of steel. The laser Raman microscope can easily distinguish between the two oxides of iron, hematite (Fe_2O_3) and magnetite (Fe_3O_4).

Measurements have been made of the gas-phase oxidation of steel, using the tube furnace in the High Temperature Materials Exposure Facility in the UNLV Chemistry building. The goal is to clarify the differences between gas phase corrosion and corrosion by LBE. Oxidation of metal surfaces is carried out by the residual gas, which was characterized using a residual gas analyzer. The residual gas was determined to consists of much water vapor but little oxygen or hydrogen. The role of water as an oxygen carrier may be an underestimated factor in corrosion.

In other experiments, investigations were performed to determine whether alloys undergoing sputtering are chemically altered by the sputtering process. Such an artifact would reveal itself as a change from stoichiometric to non-stoichiometric composition during the sputtering process. Chromia (Cr_2O_3) was found to be affected minimally if at all, but hematite (Fe_3O_4) was significantly affected.

Characterization of samples

Oxide layers were studied using high-resolution XPS with sputter depth profiling, revealing the extent of oxidation as a function of position within the oxide layer.

A new capability in microRaman spectroscopy was built by physics graduate student Brian Hosterman in order to examine the Raman spectra of compounds relevant to corrosion. Raman studies can distinguish between different chemical species by their characteristic vibrational spectra. For example, Fe_2O_3 can be distinguished from Fe_3O_4 by its Raman spectrum. The Raman microscope gives a lateral spatial resolution of the order of a few microns.

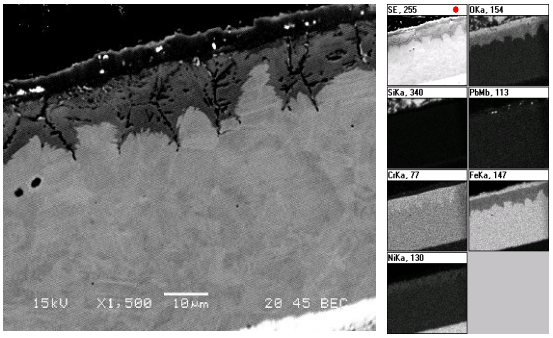

Back Scattered Image *Elemental Map*

Transverse section of D9, a 316 class stainless steel. Note the large anisotropy in the growth of the thick inner oxide layer, showing obvious pathways for migration of oxidation reactants affecting the growth rate and morphology of the oxide layer.

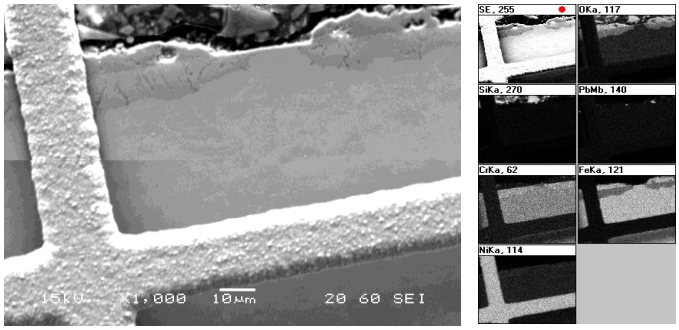

Back Scattered Image *Elemental Map*

D-9 shows failure of the thin oxide and formation of duplex oxide in localized patches. The iron moves outside the original metal surface to form Fe_3O_4 (as shown by Raman Spectroscopy) and the chromium stays in place to form an iron/chromium oxide which undercuts the thin oxide

Synthesis of standards

Chemical characterization of the species involved in corrosion can be revealed by microRaman studies, in which the spectrum of an unknown compound is matched to a library of spectra of standards. Standards have been purchased when possible, but some standards have been synthesized in the laboratory. Spinels (compounds with formula XY_2O_4) are of special interest because they are believed to form part of the metal oxides under investigation. Spectra of standards have been measured, and are in good agreement with literature values. The crystal structure of the oxide layers can be determined by X-ray diffraction. The XRD spectrum of $FeCr_2O_4$ is illustrated (below). The lattice spacings derived from analysis of this spectrum agree with literature values.

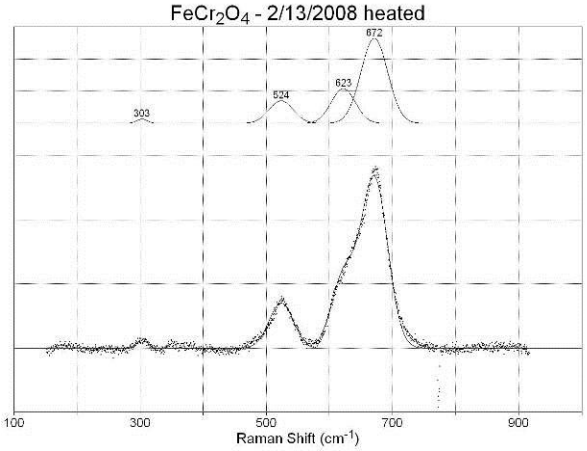

Raman Spectrum of $FeCr_2O_4$

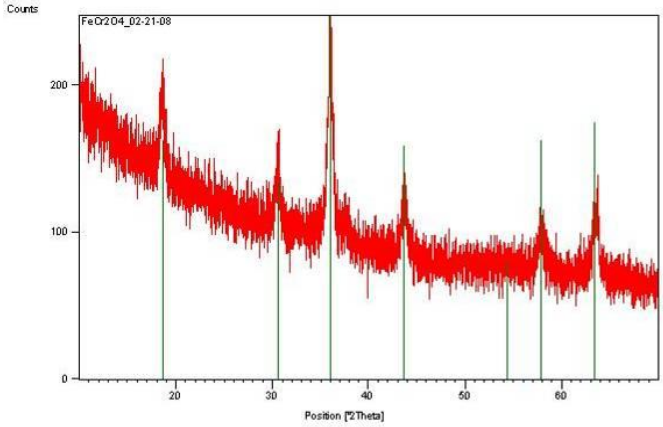

X-ray diffraction spectrum of $FeCr_2O_4$.

Technical Summary

Investigations of steels samples exposed to LBE in a Russian test loop, as well as samples from other sources, are continuing.

It was found that very similar steels can show very different corrosion behavior in concert with different protective oxide morphology: slow corroding steels have a thin, high chromium surface layer similar to the initial oxide, while the faster corroding steels have a duplex oxide, magnetite above an iron-chromium oxide which is ~10x thicker than the thin protective oxide.

Inhibition of the conversion from protective thin oxide to less protective duplex oxide may lead to improved service life. Recently, an investigation of D9 steel, which has intermediate corrosion resistance, was finished. It was found that the oxide was primarily thin, with patches of duplex oxide.

The conversion from protective thin oxide to less protective duplex oxide seems to occur at localized sites. Further, the boundary between the chromium free magnetite layer and the chromium containing iron-chromium oxide is the same as the original metal surface – i.e. the chromium does not move nearly as rapidly as the iron does.

This means that the failure sites of the thin oxide in D9 are not healing to form thin oxide, in contrast with previous work on cold rolled 316 steel which did show healing to reform thin oxide. Control of the localized failure mode and understanding the healing mechanism may lead to improved corrosion resistance.

The migration channels for oxygen into and iron out of the iron-chromium oxide layer can be observed. Anisotropic etching of the underlying metal grains by the oxygen diffusing into the duplex oxide were noted, indicating some crystal planes seem to be more subject to oxidation than other planes. This opens another possible mechanism for improvement of oxidation resistance: If metal grains at the surface are

oriented by shear between the underlying metal and the surface (by cold rolling, for example), the steel may become more resistant to formation of the thicker, non-resistant oxides.

A model of the LBE corrosion process is emerging, incorporating theoretical and experimental results from UNLV laboratory results and elsewhere. Several of the presentations at the May 2007 Heavy Liquid Metals Workshop in Rome, Italy were based on the new insights. UNLV has contributed the observation that localized failure in the initial oxide layer leads to formation of duplex/complex oxide structures. Scientific collaboration with Los Alamos National Laboratory has continued. Steel samples exposed to LBE at LANL have been analyzed by the UNLV group.

Task 19 Dissolution, Reactor, and Environmental Behavior of ZrO_2-MgO Inert Fuel Matrix – Dr. Ken Czerwinski

Background

There has been a recent resurgence of interest in different oxide fuel types (e.g., Th, inert matrix, and Pu fuels) as potential advanced fuels that can be operated to relatively high burnups at lower costs than current UO_2 fuels. These fuels can also be formed to incorporate transuranics elements in the matrix. Inert fuel matrices have the advantage of burning Pu and other transuranic elements from the fuel cycle without the production of other actinide elements. Of the possible materials for use in an inert matrix, ZrO_2 has been examined. The inclusion of ZrO_2 is expected to increase chemical stability and radiation resistance. The natural analogue of zirconia, baddeleyite ($(Zr,M)O_2$), where M is a tetravalent ion such as hafnium), contains up to 3000 ppm U or Th. This supports the durability of inert matrix fuels using ZrO_2 in reactor conditions and repository conditions. However, fuels appropriate for the advanced fuel cycle applications should have desirable reprocessing properties, namely ease of dissolution for separations. An additional oxide which is somewhat soluble may need to be added to the ZrO_2 matrix to achieve desirable reprocessing properties. A candidate oxide is MgO.

Research Objectives and Methods:

This project will examine inert fuels containing ZrO_2 and MgO as the inert matrix. Ceramics with this inert matrix, Ce, U and eventually Pu will be synthesized and examined. While the Advanced Fuel Cycle Initiative focus is on inert fuels with Pu as the fissile component, this task will perform initial laboratory experiments with Ce and U. The initial work with Ce will be performed early in the project with results used as a basis for U studies. Reactor physics calculations will be used to examine suitable quantities of burnable poisons from the candidate elements Gd, Er, or Hf. Most fuels use Gd or Er, but the chemical properties of Hf lend themselves to formation of solid solutions with Zr and the tetravalent actinides and will therefore be investigated. This project will provide the necessary data for evaluating the performance, reprocessing, and waste behavior of the MgO-ZrO_2 fuels from a quantified, chemical perspective.

Reactor physics calculations are used to examine suitable quantities of burnable poisons from the candidate elements Gd, Er, or Hf. The solubility of the fuel ceramics, in reactor conditions, reprocessing conditions, and repository conditions, are investigated in a manner to provide thermodynamic data necessary for modeling.

The research objectives of this project are as follows:

- To examine the neutronic behavior of MgO-ZrO_2 inert fuels. Variation of MgO and ZrO_2 composition ranges from 30% to 70% MgO in ZrO_2. Analysis of Gd, Er, and Hf for reactivity control ranging from 5-10% lanthanides. Analysis of reactor grade Pu as fissile component ranging from 5-10% Pu. Results will be used as parameters for fuel composition.
- To synthesize and characterize MgO-ZrO_2 ceramics containing burnable poison and fissile composition. Synthesis is based on a precipitation method. Range of MgO in ZrO_2, fissile component concentration, and burnable poison concentration based on results of neutronic calculations. Characterization of ceramics will include density, X-ray diffraction (XRD), surface

area analysis, X-ray absorption fine structure, and chemical composition. Results will be applied to behavior in high temperature water, acid, and environmental conditions.

- To describe the chemical behavior of synthesized ceramics. Chemical thermodynamic and kinetic analysis will use equilibrium data, kinetic data, and surface area normalized dissolution. Different conditions will include reactor conditions (high temperature and high pressure water) and reprocessing conditions (nitric acid and elevated temperature). Environmental conditions will be near neutral solution conditions.
- To utilize project data in kinetic and thermodynamic modeling codes to evaluate the speciation of the elements in the ceramics under reactor, reprocessing, and repository conditions.

Soxhlet apparatus to compare corrosion resistance and to determine long-term behavior.

Research Accomplishments:

Development of X-ray fluorescence characterization method

A reliable method for X-ray fluorescence (XRF) was developed involving ashing the individual oxides, then preparing standards through the dry synthesis route. It was believed that the samples that showed heterogeneous Ce distribution were due to insufficient sintering times. Therefore, one such sample was removed from resin, resintered, and elemental mapping was performed a second time. This second mapping showed a homogenous distribution of cerium demonstrating the suitability of the method.

Synthesis and characterization of U-containing ceramics

Ceramics were synthesized using MgO-ZrO_2 as the inert matrix and Er_2O_3 as a burnable poison as in previous studies; however, UO_2 is now being used as a more accurate PuO_2 analog than the previous CeO_2 containing ceramics.

A soxhlet experiment was initiated to determine the corrosion resistance of the ceramics. The results demonstrated the corrosion resistance enhancement from the inclusion of ZrO_2. A thermogravimetry and differential scanning calorimetry scan was performed on the precipitated material to examine calcining and sintering behavior. The material appears to change from the oxy-hydroxide precipitate to the oxide at the same temperature as the Ce-containing ceramics (260°C). The phase change also starts at the same temperature (510°C), but it does not proceed as quickly and therefore shows a broader peak.

XRD patterns were taken of all samples under investigation to qualitatively determine the phases present within the sintered sample. With no MgO present the UO_2 and Er_2O_3 only partially stabilizes the ZrO_2 resulting in a mixture of monoclinic and tetragonal Zr oxide phases. With as little as 5% wt/wt MgO, the material fully stabilizes to form a pure cubic zirconium phase. Over 10% MgO results in a MgO phase, in addition to the cubic zirconia. This pure MgO phase increases with total MgO content. When there is no longer ZrO_2 in the sample a MgO phase dominates, while there is a minor cubic uranium erbium oxide phase. Quantitative analysis will be performed once TOPAZ software is obtained.

Scanning Electron Microscopy and optical microscopy were used to image the material and identify the nature of the phase mixing within the sample. The MgO phase appears darker than the ZrO_2 phase due to lower mass number. The color images show large areas of various colors, but higher magnification in greyscale shows a high degree of mixing the two phases. Microprobe was also used to sweep large areas of the sample to determine where each element is concentrated. This shows that Zr, Er, and U are all within the same area (phase), while Mg is contained within its own phase. This compliments the XRD findings well. In the U and Er map the brightness and contrast were enhanced because of the low concentrations of those elements.

Dissolution studies with nitric acid have shown a linear dissolution rate for U; however, improvements are needed for consistent kinetic constants. Also, U leaching in nitric acid is only possible at high Mg concentrations. This is due to the greater surface area of the exposed zirconia phase once the magnesia is dissolved, and the higher U concentration within the zirconia phase in these samples. Dissolution in supercritical water was extended to 3 weeks with the same results. Only Mg is found in solution.

Oxide waste forms based on project results

UY_6O_{12} pellets were synthesized for Los Alamos National Laboratory for initial waste form studies complementary to the inert fuel research. Composition was confirmed to be delta

Other progress

The Soxhlet has concluded with samples ($Zr_{0.885}Mg_{0.05}U_{0.05}Er_{0.025}O_{1.96}$, $Zr_{0.725}Mg_{0.2}U_{0.05}Er_{0.025}O_{1.79}$, and $Mg_{0.925}U_{0.05}Er_{0.025}O_{1.06}$). The data has been analyzed and compared with previous experiments.

Pure water, silicate water, and brine solutions were used to test fluoride leachability in polytetrafluoroethylene (PTFE) vessels for environmental dissolution studies.

Environmental dissolution study was conducted with $Zr_{0.625}Mg_{0.3}U_{0.05}Er_{0.025}O_{1.6875}$, $Zr_{0.475}Mg_{0.45}U_{0.05}Er_{0.025}O_{1.5375}$, and $Zr_{0.325}Mg_{0.6}U_{0.05}Er_{0.025}O_{1.3875}$ in water, silicate water, and brine each in triplicate.

Scanning Electron Microscopy images were taken of corrosion damage from Soxhlet study.
UY_6O_{12} was synthesized for the LANL group. Delta phase was confirmed by XRD. UY_6O_{12} pellets were characterized by SEM, microprobe, XRD, optical microscopy, and TEM.

HNO_3 dissolution studies were conducted, residue was analyzed by XRD.

Sample #	Zr %	Mg %	U %	Er %
1	92.5	0	5	2.5
2	87.5	5	5	2.5
3	82.5	10	5	2.5
4	77.5	15	5	2.5
5	72.5	20	5	2.5
6	62.5	30	5	2.5
7	47.5	45	5	2.5
8	32.5	60	5	2.5
9	17.5	75	5	2.5
10	0	92.5	5	2.5

Metal Concentrations for Uranium Containing Ceramics

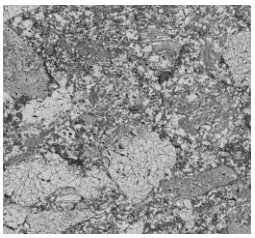

Sample 6 (3 x 3 mm U map)

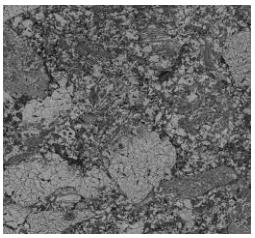

Sample 6 (3 x 3 mm Er map)

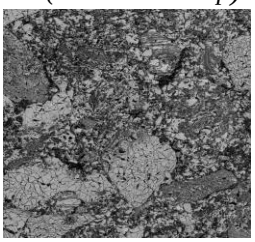

Sample 6 (3 x 3 mm Zr map)

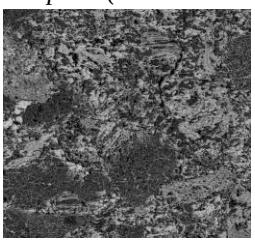

Sample 6 (3 x 3 mm Mg map)

Elemental Scanning by Microprobe

Task 20 Effect of Silicon Content on the Corrosion Resistance and Radiation-Induced Embrittlement of Materials for Advanced Heavy Liquid Metal Nuclear Systems – Dr. Ajit Roy

Background

This task is focused on the evaluation of the effects of silicon content on both the corrosion behavior and radiation-induced-embrittlement of martensitic stainless steels having compositions similar to that of modified 9Cr-1Mo steel, also known as T91 grade steel. T91 grade steel was selected to be a candidate structural material to contain molten lead-bismuth eutectic (LBE), which can act both as a target material and a coolant during the spallation process. The operating temperature during this process may range from 420-550 °C. Thus, moderate tensile strength of the containment material (T91) is a major requirement.

The beneficial effects of Si on both the metallurgical and corrosion properties of chromium-molybdenum (Cr-Mo) steels have previously been demonstrated at UNLV. Therefore, additions of Si ranging from 0.5-2.0 weight percent (wt%) was attempted in this investigation to explore Si effect on both the high temperature tensile properties and corrosion behavior of T91 grade steel. Corrosion studies in the presence of molten LBE could not be performed due to a lack of proper experimental facilities at UNLV. Therefore, detailed corrosion studies involving Si-containing T91 grade steels were performed in an aggressive aqueous solution of acidic pH. Further, significant efforts have been made to determine both the impact and fracture toughness of the tested materials as a function of Si content.

Research Objectives and Methods:

Four different experimental heats of ASTM A213 Type T91-grade alloy steels (similar to Mod9Cr-1Mo) with different Si content (0.48, 1.02, 1.55 and 1.88 weight percent) have been melted by a vacuum-induction-melting (VIM) practice at the Timken Research Laboratory. An additional four heats containing higher Si content were also melted by the VIM practice, which are also being studied for detailed metallurgical and corrosion characterization. All eight heats were subsequently processed into rectangular and square bars by forging and hot-rolling. These bars were then austenitized, oil-quenched, and tempered to achieve fine-grained and fully-tempered martensitic microstructure.

Tensile testing of T91 grade steels having Si content ranging between 0.48 and 1.88 weight percent were completed, as a function of temperature relevant to the transmutation process. The role of strain rate on the tensile properties is also under investigation. The tensile properties are being interpreted in terms of the yield strength (YS), ultimate tensile strength (UTS), percent elongation (%El), and percent reduction in area (%RA). The morphology of failure at the primary fracture surface is being investigated by SEM as a function of the testing temperature.

In order to better understand the plastic deformation of all four heats, TEM is being employed to characterize the nature of imperfections such as dislocations. Simultaneously, the microstructural variations are being investigated by using both TEM and optical microscopy (OM).

The susceptibility of the test materials to SCC has been investigated in the presence of molten LBE using self-loaded specimens (C-Ring/U-Bend) at LANL. Simultaneously, SCC testing involving all four heats is in progress at UNLV in the presence of an acidic aqueous solution at temperatures ranging between ambient and 90ºC.

The localized corrosion susceptibility of these materials has also been investigated by cyclic potentiodynamic polarization (CPP) technique. The CPP testing has enabled the development of an understanding on localized corrosion behavior in terms of the corrosion potential (E_{corr}) and the critical pitting potential (E_{pit}).

SEM has been used to analyze the extent and morphology of failure at the primary fracture surface of the specimens tested under a slow-strain-rate (SSR) condition. The cracking susceptibility has been expressed in terms of the true failure stress, time to failure and ductility parameters (%El and %RA).

Research Accomplishments:

- The tensile data indicates that the magnitudes of both YS and UTS were gradually reduced with increasing temperature, as anticipated. However, there was a gradual drop in the failure strain in the temperature regime of ambient to 400ºC. Also indicated is that the magnitude of failure strain (e_f) was gradually reduced with increasing temperature within a susceptible temperature range, irrespective of the Si content. This is attributable to a metallurgical phenomenon known as Dynamic Strain Aging (DSA). Simultaneously, serrations were also noted in the engineering stress vs. strain diagrams.
- The gradual reduction in failure strain in the susceptible temperature regime has often been cited to be the result of work hardening resulting from the diffusion of interstitial solute elements onto the dislocations near the grain boundaries. This is DSA and is also a function of strain rate used during plastic deformation under tensile loading.
- At 550ºC, there was an increase in ductility in terms of failure strain, possibly due to enhanced plastic flow even under an identical strain rate of $5x10^{-4}$ s^{-1}.
- In view of the minimum failure strain noted at 400ºC within the susceptible temperature regime (ambient to 400ºC) for all four alloys, testing was performed under three additional strain rates of 10^{-2}, 10^{-3} and 10^{-4} s^{-1} at this temperature. The resultant data indicate that the maximum failure strain at this temperature was observed at a strain rate of 10^{-4} s^{-1}, suggesting that this could be the critical strain rate at or below which the concept of DSA may not be prevalent.
- The results of SSR testing in an acidic solution (pH~2.2) suggest that the cracking susceptibility was enhanced at 90ºC in terms of the reduced time to failure and failure strain.
- SEM study on self-loaded C-Ring specimens revealed a separation of grains possibly due to the decohesion of surface layers resulting from their interaction with the molten metal (LBE). Intergranular brittle crack was seen on the convex .
- The gradual reduction in failure strain in the susceptible temperature regime has often been cited to be the result of work hardening resulting from the diffusion of interstitial solute elements onto the dislocations near the grain boundaries. This phenomenon, known as dynamic strain ageing, is also a function of strain rate used during plastic deformation under tensile loading.

- At 550ºC, there was an increase in ductility in terms of failure strain, possibly due to enhanced plastic flow even under an identical strain rate of $5x10^{-4}$ s^{-1}.
- In view of the minimum failure strain noted at 400ºC within the susceptible temperature regime (ambient to 400ºC) for all four alloys, testing was performed under three additional strain rates of 10^{-2}, 10^{-3} and 10^{-4} s^{-1} at this temperature. The resultant data indicate that the maximum failure strain at this temperature was observed at a strain rate of 10^{-4} s^{-1}, suggesting that this could be the critical strain rate at or below which the concept of DSA may not be prevalent.
- The results of SSR testing in an acidic solution (pH~2.2) suggest that the cracking susceptibility was enhanced at 90ºC in terms of the reduced time to failure and failure strain.
- SEM study on self-loaded C-Ring specimens revealed a separation of grains possibly due to the decohesion of surface layers resulting from their interaction with the molten metal (LBE). Intergranular brittle crack was seen on the convex side of this specimen, which also revealed the presence of lead, as observed by energy dispersive spectroscopy (EDS).

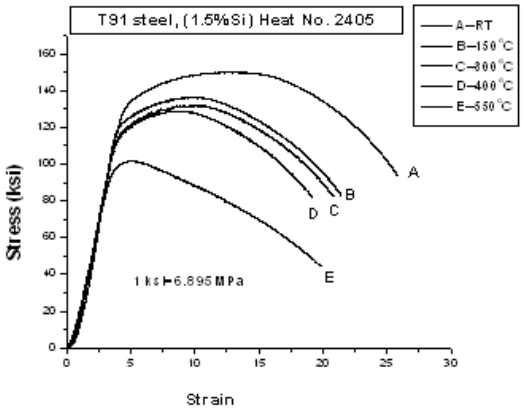

Stress-Strain Diagrams of T91 Steel with 1.5 wt% Si

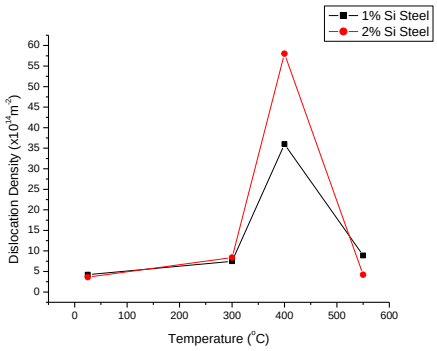

Dislocation Density vs. Temperature (°C)

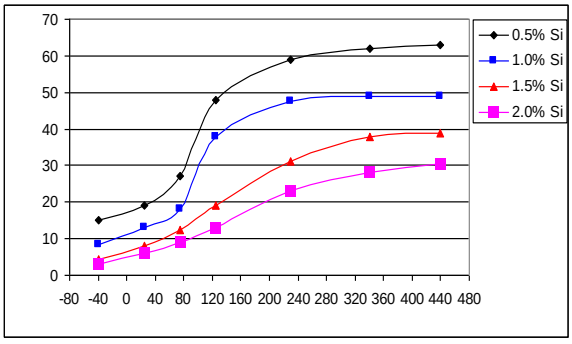

Impact Energy (ft-lb) vs. Temperature (°C)

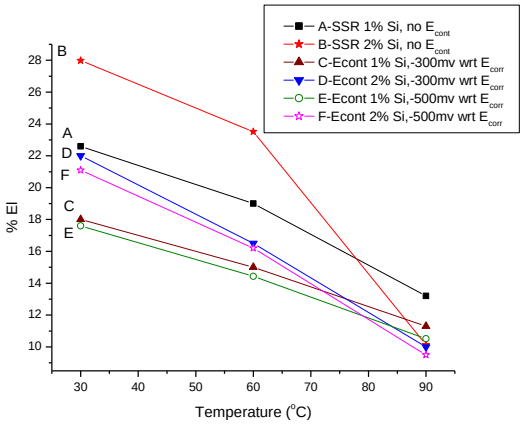

Variation of %El with temperature for steels (1 and 2 wt% Si), with and without cathodic E_{cont}

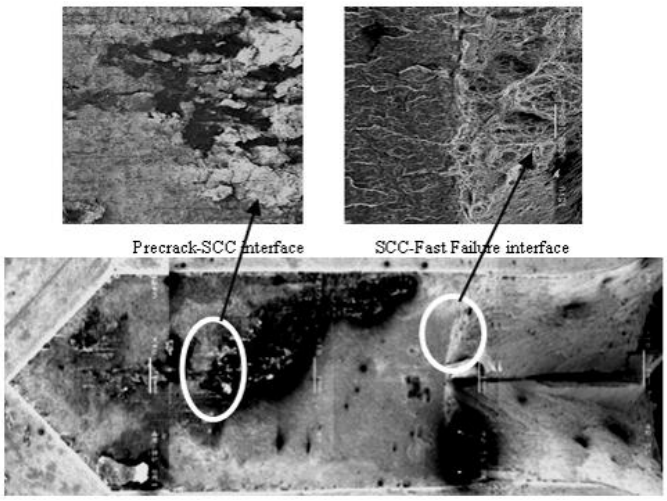

Scanning electron microscope micrographs of double-cantilever beam specimens with 0.5 wt% Si subjected to SCC testing at 100°C in acidic solution for 30 days.

Task 21 Theoretical Modeling of Protective Oxide Layer Growth in Non-isothermal Lead-Alloys Coolant Systems – Dr. Yitung Chen, Dr. Jichun Li

Background

In advanced nuclear energy systems, lead alloys emerge as strong candidates for transmutation and advanced reactor systems as nuclear coolants and spallation neutron targets. However, it is widely recognized that corrosion of materials caused by lead alloys presents a critical barrier to their industrial use. A few experimental research and development projects have been set up by different groups such as at Los Alamos National Laboratory to study the corrosion phenomena in their test facilities and to develop mitigation techniques and materials. One of the central or main techniques under development is to use active control of oxygen thermodynamic activity (OTA) to provide protective oxide layers.

Setting OTA in flowing lead alloys makes corrosion highly dependent upon the oxygen concentration and the oxidation processes at materials surfaces. The active oxygen control technique exploits the fact that lead and bismuth are chemically less active than the major components of steels, such as Fe, Ni, and Cr. By carefully controlling the oxygen concentration in lead-bismuth eutectic (LBE), it is possible to maintain an iron- and chrome- based oxide film on the surfaces of structural steels, while keeping lead and bismuth from excessive oxidization that can lead to precipitation contamination. Thermal analysis has given an ideal oxygen level range in a non-isothermal lead alloy coolant system. However, in a practical coolant loop, the proper oxygen level depends not only on thermal factors but also on hydraulic factors (system operating temperature, temperature profile, flow velocity, etc.). In addition, the oxygen distribution in a non-isothermal lead alloy coolant system is still unclear. The optimal oxygen levels still need to be investigated.

Research Objectives and Methods:

The goals of this research project are to provide a basic understanding of protective oxide layer behaviors and to develop oxide layer growth models of steels in non-isothermal lead alloys coolant systems, in particular:

- To elucidate the mechanism of the protective oxide layer growth of steels in static, non-isothermal

flowing lead alloy coolant systems with oxygen concentration level control.

- To elucidate the mechanism of mass transport of oxygen and corrosion products in the multi-phase system.
- To develop oxidation growth models of steels in lead alloy coolant systems.
- To clarify the dependence of the oxidation process on the hydraulic factors and the oxygen concentration distribution and level.
- To clarify the optimal oxygen concentration levels in practical coolant system scales.
- To interpret the experimental results from test loops and to apply them to the design of practical nuclear coolant systems.

Research Accomplishments:

Numerical analysis on oxygen transport in LBE system
The Lattice Boltzmann simulations of oxygen transfer in the liquid lead alloy system were performed to investigate the enhancement of the oxygen transport by force convection. To mix the oxygen uniformly and quickly, the forced convection is proposed to enhance the oxygen transport with a cover gas scheme. The oxygen control technique with cover gas scheme is formulated. To optimize efficient mixing of the oxygen, three different forced convection flow patterns on the oxygen transport are investigated.

Stochastic modeling on morphology of oxide layer growth.A cellular automaton model, which combines the surface growth and internal oxidation, was created to explain the oxidation mechanism of steels in liquid lead-alloys. Based on Rebertson's theory, the morphology of steel under the mechanism of corrosion and oxidation under lead-alloy environment is modeled by a cellular automaton method, which uses the simple mathematical model to investigate self-organization in statistical mechanics, and especially suitable for complex systems. A global random walk method is included to characterize the diffusion process of iron. Working on the mesoscopic level, three main processes, which include the corrosion of the substrate, the diffusion of iron species across the oxide layer and precipitation of iron on the oxide layer, are included. In contact with liquid lead alloy, a piece of steel (mainly Fe and Cr) is corroded. The oxide layer is formed by one part of the corroded steel at the local place where corrosion occurs. Meanwhile, the remaining part of iron starts to diffuse across the oxide layer till they reach the layer boundary where they precipitate as new oxide product.

Numerical modeling on the oxygen-diffusion controlled oxide layer growth model
The numerical modeling of the oxygen-diffusion controlled oxide layer growth model was developed. This moving boundary problem was solved by finite difference method with transformation of the dependent variables and the coordinates. Also, the numerical code was benchmarked with available publication results.

Theoretical modeling on oxidation with scale removal in LBE system
An oxidation model with scale removal in LBE system was developed. The common kinetics of the oxide layer thickness and weight change per unit area depend on the pre-oxide thickness and the critical spallation thickness of the oxide. The steady state thickness was found to be a function of the operation conditions, such the materials, oxygen concentration, the flow velocity and the temperature.

Cellular automata modeling of oxide layer growth with scale removal: To simulate the scale removal effect on oxide layer growth, the previous cellular automata model of oxide layer growth has been improved to consider the scale removal effect. In this model, the scale removal rate was taken to be linear. It is assumed that the oxide layer sites which are close to the oxidant site have a probability to move away. The global random walker model is still used to simulate the solid state diffusion of the ionic metal site in the oxide layer. The phenomena of oxide growth which obeyed Tedmon theory was found.

Stochastic modeling with cellular automata method on the surface growth and internal oxidation: The quantitative cellular automata model on the inward oxidation mechanism was developed. The stochastic rule to the population of particles is based on the exclusion principle. Considering the exclusion principle, which permits at most one particle per site, a particle moves to its targeted site if this site is free and simply does not move if the site it targeted was already occupied. To avoid the confliction between particles

competing for a single free site, the following rule was adopted. When more than one particle attempts to move to a single open site, only one of the competing particles, which will be chosen randomly from among them, is allowed to move to this open site and the others do not move. A benchmark with the theoretical solution was made, and a good agreement was obtained.

Numerical modeling on the diffusion controlling oxidation model with scale removal: A numerical diffusion-controlling oxidation model with scale removal was developed in oxygen-containing liquid flow. Scale removal effect was considered and the formation mechanism of duplex oxide layer structure was analyzed and employed in the model. The volume expansion effect caused by density difference during the oxidation is coupled with the consideration of increasing weight of reacted oxygen. To solve the diffusion equations with an advection term caused by the moving boundaries, a coordinate transform technique was employed. The governing equations were analogized with the Stefan problem in heat transfer with phase change in the enthalpy formulation and then solved numerically by finite difference method.

Cellular automaton model on the oxide growth coupled with inward oxygen diffusion: To simulate the oxide layer growth of steel in liquid lead alloy environment, a cellular automaton model was developed that considered inward oxygen diffusion. In this model, the lattice sites are occupied by metal, oxide, or lead alloy, while the interstitial sites are route ways for oxygen to occupy and diffuse. The benchmark of cellular automata model for pure oxygen diffusion has been made and a good agreement has been obtained.

Boundary conditions study of the self-coded cellular automata (CA) oxidation model coupled with inward oxygen diffusion

In a previous study of the CA model, the oxide layer growth of steel in a liquid lead alloy environment was studied considering the inward oxygen diffusion. The boundary condition of the oxygen concentration at the far away conditions was set as a Dirichlet boundary condition. The oxygen sites were simply eliminated whenever they diffused to the far boundary. This, however, is not a proper physics model. The code of the improved CA oxide layer growth model has been modified with a Neumann boundary condition of oxygen concentration at the far end of the specimen (at y=0). The self-coded CA model considers eight Moore neighborhood lattice sites and oxygen diffuses along the boundary of the lattices. The result shows that the oxygen concentration at the far end satisfies the Dirichlet boundary condition as well if the oxygen diffusion rates in the oxide layer and the metal are relatively small compared to the reaction rate. This is true in most of the real cases and the specimen is usually relatively large compared to the oxide layer thickness.

A simple scale removal model based on the improved CA oxidation model

A stochastic CA oxidation model was developed to consider the scale removal effect. In the simple scale removal model, it is assumed that the oxide layer sites which are close to oxidant sites have a probability to move away. An average removing probability of a lattice oxide cell was assumed, if the oxide cell is contacting with the LBE flow. The simulation results show that the oxide layer growth following the parabolic law, with a thinner thickness than the case without scale removal.

A new scale removal model considering the hydraulic effect (the flow direction)

In the new scale removal model, the scale removing probability considers the influence of more neighboring cells (the eastern, western, northern, northeastern, and northwestern sites) which surround the objective oxide layer site. The effect of the neighboring cells on the objective oxide cell is based on the estimation of the hydraulic effect (the flow direction). The proposed scale removal model can lay a basis for a future study coupling with alloy components added in the stainless steel.

For example, if the flow direction is assumed to be from left flowing to right, more solid sites at the left hand side will make the objective oxide cell more difficult to be removed. Basically, the scale removing probability averaged from the total possible cases should equal to as in the simple model. However, the advantage is that the new model may predict a different roughness on the oxide surface, especially when alloy components are considered, for each cell,

$$P_{Kr}^{i} = f_i \overline{P_{kr}}$$

Where f_i is a factor reflects the difficulty by which the objective oxide cell will be removed. The more

difficult a cell will be to remove, the lower the factor value will be. Thus,

$$\frac{1}{M}\sum_{i}^{M} f_i = 1$$

where M is the total number of the possible cases. The scale removal effect on the oxide layer growth has been studied extensively using the self coded CA model. The oxide layer growth was found to obey Tedmon's theory.

Optimization approach in variable charge potential for metal/metal oxide systems in the molecular dynamics (MD) simulations

A new direct approach for finding charge distributions among ions has been proposed in the MD study. Earlier attempts on minimizing the total system energy of metal/metal oxide systems with given charge constraints appear to be indirect and unnecessarily complicated. The energy minimization problem is in fact an optimization problem and hence can be solved by an optimization method. The approach is based on an optimization algorithm, called the Generalized Reduced Gradient (GRG) method. This efficient approach can be readily employed in molecular dynamic simulations for metal/metal oxide systems.

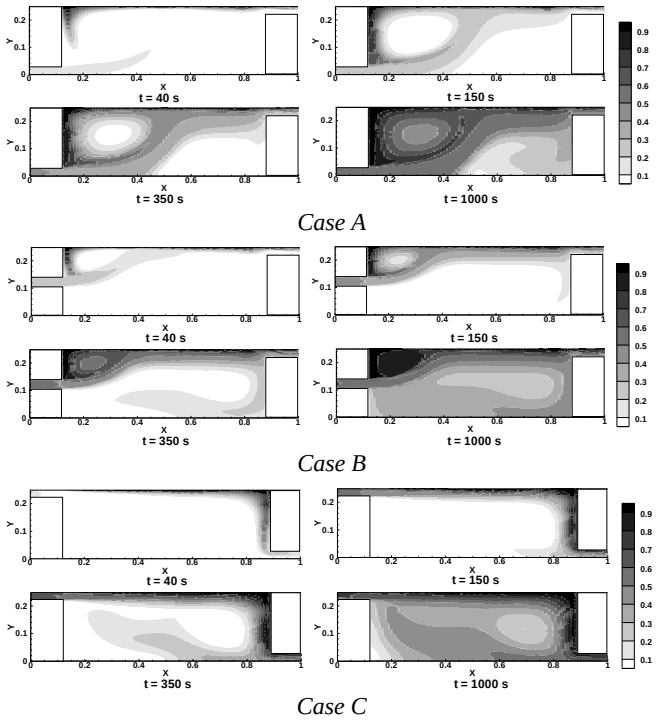

Oxygen concentration contours at different times (t = 40, 150, 350 and 1000 s) for different convection mode. Re = 1143 and Sc = 5 for all cases.

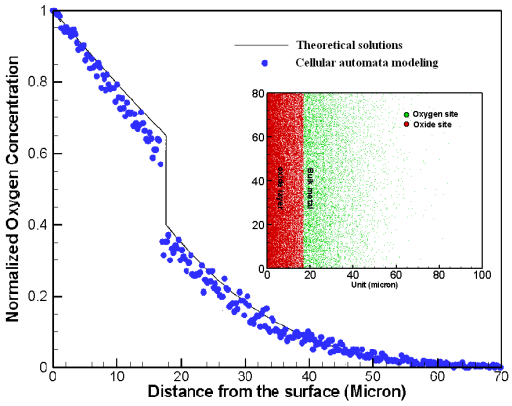

Distribution of oxygen concentration at 0.5 hour. Application of quantitative cellular automata modeling of oxidation in metal matrix composite

Task 22 Design Concepts and Process Analysis for Transmutation Fuel Manufacturing – Dr. George Mauer

Background

The safe and effective manufacturing of actinide-bearing fuels for any transmutation strategy requires that the entire manufacturing process be contained within a shielded hot cell environment. To ensure that the fabrication process is feasible, the entire process must be designed for remote operation. The equipment must be reliable enough to perform over several decades, and also easy to maintain or repair remotely. The facility must also be designed to facilitate its own decontamination and decommissioning. In addition to these design factors, the potential viability of any fuel fabrication process will also be impacted by a number of variables, such as the current state of technology, potential problem areas, deployment scaling,

facility safety, and cost.

Research Objectives and Methods:

The goal of this project was to provide technical support to process designers working on the development of the fuel cycles for transmutation applications. Detailed process models were developed to better define the impact of fuel choice on the transmuter fuel cycle, including relative process losses, waste generation, and plant capital cost. These process models provide insight regarding required plant size and the number of plants needed to mesh with the fuel recycling line. They also determine requirements for automation.

Manufacturing models for large-scale production in a hot cell environment were also developed. Combined, these two models allow the assessment of plant layout, and provide the framework for estimation of plant capital and operating cost estimates, and for feasibility in general. The operations of robotic equipment and the sensor technology required for safe ad reliable robot control have been evaluated through simulations in three-dimensional space. The manufacturing technology developed for hot cell applications is also applicable to other, more general uses, where occupational hazards prevent human presence near processes.

Simulations: This task modeled manufacturing processes to generate a realistic assessment of plant layout, size, feasibility, and technology development required for large-scale remote fabrication of fuel. Modeling of the candidate fuel manufacturing processes was performed using the MSC.visualNastran and ProEngineer simulation software tools. The modeling of dispersion and TRISO fuels were completed.

Cost, Feasibility, and Large Scale Deployment: This task developed the database necessary to provide cost estimates and differential cost for various fuel manufacturing options. Cost estimates regarding projected capital cost, reliability, and plant life were developed and should be refined as additional knowledge is developed.

Automated Vision-Based Image Acquisition and Robot Control: This task explored and demonstrated strategies for the reliable and flexible control of the material handling robots inside the hot cell by means of automated vision systems. Since the cameras can be positioned outside the hot cell, such systems would have significant advantages over sensors inside the hot cell, resulting in potentially reduced system maintenance and increased system reliability.

Research Accomplishments:

A 3-D manufacturing process simulation with several Waelischmiller robots in a hot cell using Mathlab CAD models and the Newtonian dynamics of the moving components was developed.

Analysis of Fabrication Plant Reliability

A fabrication plant for transuranic elements of spent fuel to be transmuted was designed using work cell layouts with redundant robots. Methods for the assessment of plant reliability and optimization strategies for optimizing the work cell layout with redundant robots were investigated. The performance of various selected layouts was simulated in order to verify the overall plant performance and to study conceivable accident scenarios. Both powder and metallic processing methods were considered. A redundant system using four robots was used. A cost model was implemented as an interactive simulation in Matlab Simulink that permits the evaluation of multiple alternative scenarios.

Automated Vision-Based Image Acquisition and Robot Control

A remote-controlled surveillance camera (Sony EVI-D30) is operated from a computer. Image acquisition is performed by a frame grabber in the computer. The camera functions (pan, tilt, zoom, and focus) are controlled through a serial connection between camera and PC. The frame grabber transmits the image to Matlab for processing.

Object recognition is performed by identifying the object's contour, and by then matching the detected contour to those of known objects.

Recognition of Cylindrical Fuel Pellets by the Charge-Coupled Device (CCD) Camera: The images of cylinders that are captured by the camera have properties which make the recognition of the cylinder more difficult. The real time cylinder pictures contain shadows as well as reflections (specularity) caused by lighting conditions. This project seeks to detect the cylinders' contours in order to identify and classify it correctly. Changes of lighting conditions can make the correct identification difficult at times.

Camera Calibration and Dimensional Measurements using the CCD Camera

Calibration objects: Calibrating a camera requires several corresponding 3D and 2D points. Calibration objects are mostly planes or cubes (two or three orthogonal planes) with special markings. Here, those markings are chess board patterns with equidistant corners distributed accurately over the object surface. The corners define the known points in the world coordinate system and can be easily identified in the image from edge detection algorithms. This step provides the opportunity to estimate the projection matrix. Another method of calibrating is self-calibration. This technique obtains correspondences from the camera movement in a static scene using image information alone.

Estimation of the projection matrix: The camera calibration algorithm was programmed in Matlab. The regions of interest were defined for every single image by selecting the 4 outmost corners of the chess pattern. The Matlab software identifies and saves the positions of the individual black square's corners for processing. The optimization method of Levenberg-Marquardt is applied which also includes the adaptive correction of the lens distortion.

Two-View Triangulation: Triangulation is the process of finding the position of a point in space given its position in a stereo image pair. This task is essential for vision-based robot pick and place operations. The Linear-Eigenmethod is the simple triangulation method that is used for extracting the 3D points.

Optimal Triangulation: Suppose there are two point correspondences x and x' from two images, and the goal is to reconstruct the 3D point X. If the correspondences are accurate (which cannot usually be expected) the rays of x and x' will lie in the same plane and thus will intersect in X. In the presence of noise, accurate point coordinates cannot be expected. It follows that x and x' may not lie in a plane, which means that there is no intersection. A method for correcting the existing point correspondences such that the corresponding rays will lie in the same plane consists in finding a global minimum of a cost function. For this approach, it is assumed that the fundamental matrix is well defined.

Recognizing calibration cubes: Until now a disadvantage of the calibration process has been the need to determine the point correspondences of the calibration object and a given 3D model manually. A desirable feature would be the automatic mapping from calibration cube points to the 3D locations of a 3 plane model. This would allow estimating the projective matrix automatically. For the experimental validation, several calibration objects were arranged on a paper grid in order to cover multiple points in the 3D space.

For the tests, 50 points were used to estimate the fundamental matrix. The same points have been reapplied as control points. The triangulation error was around 0.2 inches at a distance to the calibration points of 10 inches. In the proximity of the calibration points the error was below 0.1 inch. The errors are attributed by the following effects:

- Quality deficiencies of the camera device
- Inaccurate calibration objects (perpendicularity)
- Linearity of the algorithm

Hot Cell robot control: Visual servoing was demonstrated. For this purpose, the stereo vision system was set up in a laboratory next to a Fanuc M-16iB industrial robot.

Sensor-Robot Integration: Driver software was written, tested and implemented for the transmission of sensor data, i.e., the target object's position and orientation, to the Fanuc robot controller.

Accelerated Object Extraction: The contour extraction algorithm can require long durations during image feature extraction (Canny Edge Detection, up to one second per image). Since the cylindrical targets each cover only a portion of the image, there is no need to apply the feature extraction to the whole image. By fragmenting each image into sub-images containing the desired objects, the duration of the feature extraction can be significantly reduced.

Targets are found by under sampling the image and testing the neighborhood of the respective pixels for their color. In application, black pellets were used for black pixels in the neighborhood. By merging all black neighboring locations, the rectangular boundaries of the pellets can be determined by ascertaining their respective contours.

To avoid the issue that corners of targets in certain angles are not collected by the sampling, and possibly eliminated, the search algorithm doubles the number of search points at each of the four sides. The duration of the edge detection process depends on the number of objects in the scene, but is usually a fraction of the amount a complete detailed search.

Steering and Rotation of the Robot End Effecter, Gripping Operations: For gripping horizontal cylindrical targets, the orientation of the cylinder is required. The orientation can easily be computed as the angle between the two extracted surface points and the x axis. To align the gripper with the target's orientation, the last joint of the robot has to be rotated. For this purpose, the orientation of the cylinder in the bin (in world coordinates) is transformed to robot-specific joint coordinates

After accomplishing the process of picking up targets with a given position and orientation, the first autonomous tests were conducted. In these tests, a single target was randomly placed in the scene, picked up by the robot, and dropped in a box. In later test scenarios, the robot placed the target at randomly generated positions and picked it up again. This procedure was tested iteratively.

Multiple Objects: To extract multiple objects, the existing algorithm, which so far extracted only the coordinates of one object, was extended. The extended algorithm returns a list of points representing the two cylinder surface points for each identified target in the corresponding image. When these lists are created for each of the stereo image pairs, the correspondence matching between targets in both lists is performed using epipolar geometry.

To organize the search for correspondences uniquely, additional information may have to be included. These could be the locations of the image edges, for example, the bottom of the first image matches with the top of the second image.

Upright and Horizontal Targets: In general, there is no need to differentiate between upright and horizontal objects during the target extraction phase. The objects' orientations have no bearing on the appearance of the cylinder in the image (usually the mantle and one end surface). The determination of a cylinder's orientation is made after the two surface end points of each detected object have been triangulated. If the resulting 3D points are located at the same vertical elevation, the object is horizontal. Otherwise a standing object is assumed.

Graphical User Interface: After the completion of the basic operations for cylinder grasping, a demonstration application was developed. The program offers a graphical map of the scene contents (such as position and orientation of the objects), and tracks the manipulation of single objects. To perform picking and placing of targets, the user selects a specific target by mouse click in order to have the robot execute a set of user-defined operations.

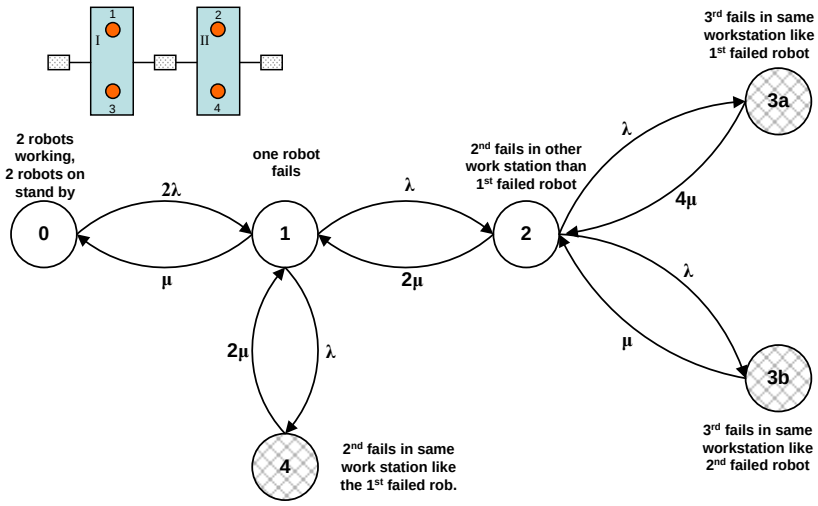

Markov Model of Hot Cell Layout with two redundant robots

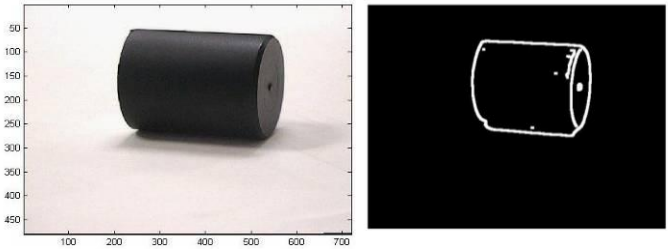

CCD image (left), and Contour (right) of a cylinder

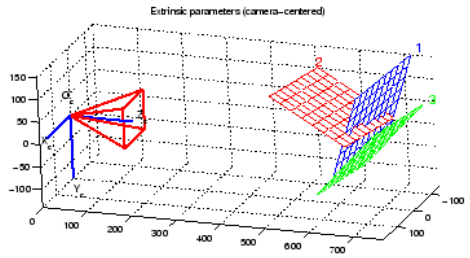

Estimated 3D Structure of a calibration plane

Robot grasping a cylindrical pellet

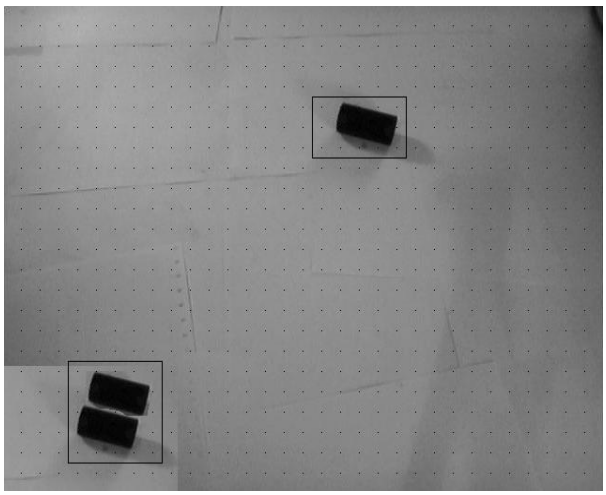

Finding the regions containing the targets by undersampling: The black spots represent the sample points, the black rectanales are associated with the

Task 23 Development of Nanostructure based Corrosion-Barrier Coatings on Steel for Transmutation 50 Applications – Dr. BJ Das

Background

Advanced transmutation systems require structural materials that are able to withstand high neutron fluxes, high thermal cycling, and high resistance to chemical corrosion. The current candidate materials for such structures are ferritic and ferritic-martensitic steels due to their strong resistance to swelling, good microstructural stability under irradiation, and the retention of adequate ductility at typical reactor operating temperatures.

In parallel, lead-bismuth eutectic (LBE) has emerged as a potential spallation target material for efficient production of neutrons, as well as a coolant in the accelerator system. While LBE has excellent properties as a nuclear coolant, it is also highly corrosive to stainless steel. The corrosion is due to relatively high solubilities of the base and major alloying components of steel, such as Ni, Fe, Cr, etc. in LBE at elevated temperatures. Without some protection, the steel structures rapidly corrode in LBE through dissolution and leaching of these materials.

Thus, for long term reliability of the structures, it is necessary to provide some protection of the steel surface from corrosion, without affecting the bulk properties of the steel. One such technique that has been well investigated is the use of oxygen control at the surface of the steel, which maintains a coating of oxide layer that protects the steel surface. The protective layer forms due to the higher affinities of the steel alloying components to oxygen compared to lead and bismuth. However, once a continuous film of oxide is formed, a competing process takes place; the oxide layer interacts with the LBE causing reduction of the oxide layer at higher temperatures. It is thus critical to maintain an optimum flow of oxygen at the LBE/steel interface, which is made challenging by the non-uniform temperature distribution in the transmutation systems. In addition, while the oxygen control technique works effectively at lower temperatures, it is not appropriate for higher operational temperatures (500-600 °C), which is becoming increasingly important. Thus, it is necessary to develop alternative techniques for corrosion protection of steel that will perform reliably at elevated temperatures and under thermal cycling in LBE.

Research Objectives and Methods:

The objective of this project is to develop a novel nanostructure based coating technology that will provide significantly improved corrosion resistance for steel in LBE at elevated temperatures (500-600 °C), as well as provide long-term reliability under thermal cycling. The nanostructure based coatings will consist of a layer of nanoporous alumina with the pores filled with an oxidizing metal such as Cr, followed by a capping layer of alumina. Alumina, which is a robust anti-corrosion material, provides corrosion resistance at elevated temperatures. The Cr serves two purposes: (1) it acts as a solid filler material for the pores in the alumina, enhancing its mechanical and chemical integrity, and (2) it acts as a second layer of defense against corrosion by providing a replenishable source of Cr (for the formation of a chromium oxide protective layer) in case the alumina layer is compromised. The innovation of this project is the use of a nanoporous alumina layer for the coating, which is mechanically flexible and can expand and contract with the underneath steel surface. As a result, the mechanical integrity of the coating is preserved under thermal cycling. In addition to their usefulness at higher temperatures, the proposed coatings can also provide increased reliability at lower temperatures by complementing the oxygen control technique. The nanostructure based coatings developed in this project will significantly enhance the long-term reliability of steel structures in LBE at elevated temperatures and under thermal cycling.

Working with the national laboratory collaborator, the stainless steel alloys HT-9 and EP-823 were chosen as the candidate materials for investigation at this time. The above project objective will be achieved in three phases; each phase will be carried out over a one-year period.

Phase I will develop the fabrication technology for the coatings on steel, and study their structural integrity at elevated temperatures and under thermal cycling.

Phase II will perform corrosion studies of the structures in LBE at elevated temperatures.

Phase III will use the data from Phases I and II to develop an optimized coating technology for improved structural integrity under thermal cycling, and improved corrosion resistance in LBE at elevated temperatures. If necessary, multiple layers of such coating structures will be used for increased resistance to corrosion.

Research Accomplishments:

A significant problem was encountered with the synthesis of Cr nanowires inside the alumina pores, the uniformity of coverage was very poor. As a result, alternative metals to form nanowires were looked into and nickel was selected primarily due to its established electrochemical synthesis procedure.

Alternative metals were looked at to form the nanowires. The purpose of the metal nanowires is to provide structural integrity to the nanoporous alumina, as well as a second defense mechanism against corrosion by oxidizing in case the top alumina layer is compromised. Nickel was selected due to its established electrochemical synthesis procedure and deposition of Ni nanowires was achieved.

A number of recipes were investigated for their suitability for synthesis inside nanoscale pores, and the process parameters were experimentally optimized for the synthesis of nanowires. The deposition of the Ni nanowire was performed in a two-electrode arrangement with a mixture of $NiSO_4 \bullet_6 H_2O$, $NiCl_2 \bullet_6 H_2O$ and H_3BO_3 as the source of Ni. The wires were deposited at a potential difference of 1 V between the anode and the cathode and at ambient temperatures. The Ni nanowire samples were characterized by Field Emission Scanning Electron Microscopy (SEM), which showed excellent uniformity and coverage. However, while Ni can provide very good structural integrity to the porous alumina, one potential problem is its higher dissolution rate in LBE.

In addition, it was noted that the heights of the Ni nanowires were limited, and even with extended deposition times, the heights were limited to a few tenths of a micron. This limited height was believed to be arising due to the dynamics of fluid flow inside the nanoporous alumina.

To address the above issues, two different approaches were taken, A systematic study was continued during the past year to improve the deposition uniformity of the Cr nanowires, and some improvement was achieved. The uniformity of coverage showed improvement and experimental optimization of process parameters was continued for further improvement of the coverage uniformity. In addition, a new and promising approach was initiated for the deposition of metal nanowires inside the nanoporous alumina as described below.

A new technique was initiated and investigated for the deposition of metal nanowires inside the nanoporous alumina. This technique involves the electro-phoretic deposition of nanoparticles inside the pores followed by recrystallization into nanowires. The major advantage of this technique is that the chemistry of nanoparticle synthesis is separated from the formation of nanowires, as a result it has the potential to eliminate the limitations encountered in nanowire synthesis. Nanowire deposition inside the alumina pores is made challenging by the nanoscale fluid flow and chemical reactions inside the nanoscale volume of nanoporous alumina pores. In this new technique, nanoparticles of the desired metal are first synthesized by an established technique in an emulsion form, which are then incorporated inside the nanoporous alumina pores. Since nanoparticles are relatively less complex to incorporate inside pores, it provides an excellent means for the synthesis of nanowires of good uniformity and desired heights. The nanoparticles can be synthesized using an established technique such as sol gel technique. The nanoparticles can be then annealed to form the nanowires or sonication can be used during electro-phoretic incorporation to form the nanowires.

Deposition of Cr nanowires on steel substrates will be achieved by using the following procedure. A new batch of steel samples will be coated with metallic aluminum which will be anodized using constant current anodization. Since it is not possible to obtain cross-sectional images of the structures on steel samples, the voltage-time characteristics will be measured to monitor the quality of the anodized alumina structures. A typical voltage-time characteristic obtained during the anodization of aluminum on steel samples, when compared to data from silicon samples, confirms the good quality of the nanoporous alumina. Cr nanoparticles will be synthesized using the sol-gel technique and will be then electro-phoretically incorporated inside the nanoporous alumina. Sonication will be used during deposition to fuse the nanoparticles to form nanowires. A sonication apparatus was obtained for this purpose. This will be followed by the deposition of a thick film of dense alumina, the process technology for which has already been developed during the previous phase of the research.

The thick layer of dense alumina on top of the Ni nanowires provides the first layer of defense against corrosion for the steel substrates. After investigating the various techniques to deposit alumina, sputter deposition was identified as the appropriate technique for depositing thick layers of insulators. However, the insulating nature of alumina makes it a difficult task to deposit by sputtering technique. To address this problem, a pulsed DC sputtering technique was used, which is a relatively new technique for the deposition of insulators. An alumina sputter target of the appropriate dimensions was obtained for this purpose and an extensive preliminary testing was carried out to optimize the deposition process. Such preliminary experiments were carried out on silicon substrates since it allows cross-sectional imaging of the samples. The deposition rate for alumina was determined from a series of such cross-sectional images. The experimentally obtained deposition rate was used to deposit a 3 micron layer thick dense alumina layer on top of the Ni nanowires. The samples are currently being tested for thermal recycling. Effort is also continuing to deposit thicker layers of alumina, preferably up to 10 microns.

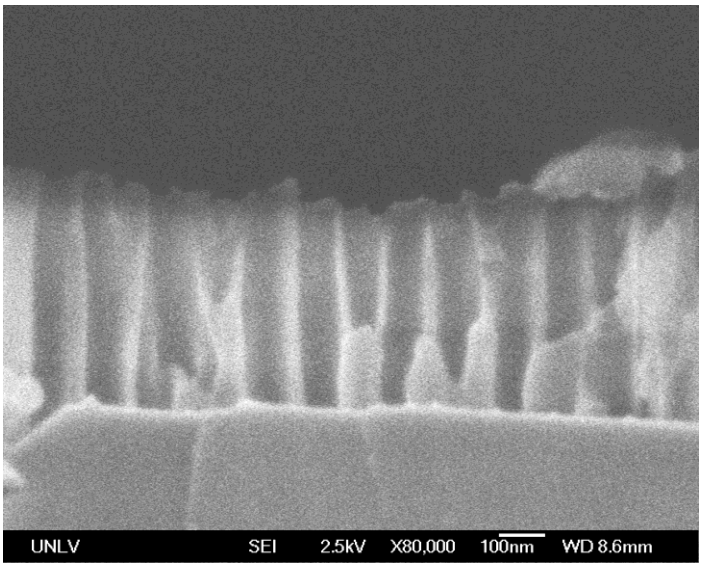

Cross-sectional FESEM image of Cr nanowires inside a porous alumina template showing non-uniform distribution of nanowires

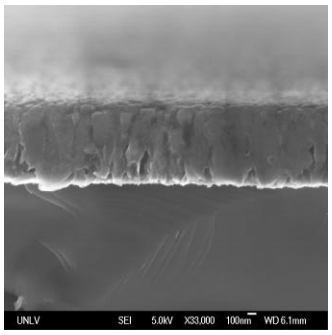

A typical cross-sectional image of dense alumina deposited on a silicon substrate by pulsed DC sputtering. Charging of the insulator prevented from getting SEM images of thicker alumina layers

Task 24 Development of Integrated Process Simulation System Model for Spent Fuel Treatment Facility Design – Dr. Yitung Chen, Dr. Sean Hseih

Background

Integrating and enhancing the Argonne Model for Universal Solvent Extraction (AMUSE) code, which contains a great deal of chemical separations processing, was part of TRP Task 8, "Development of a

Systems Engineering Model of the Chemical Separations Process". Simulating the Light Water Reactor (LWR) Spent Fuel Treatment Facility (SFTF) processes is the major focus for this project. This approach combines commercial process simulation software (ASPEN-Plus) with the chemical separation calculation from the AMUSE code. Based on the current Integrated System Optimization Program, ISOPro (developed by UNLV), this project aims to create a system framework that interacts with both programs and provides analyzed results useful for a SFTF design that provides the functionality of receiving, temporarily storing, and preparing spent nuclear fuel for leaching.

A spent fuel treatment facility has many individual processes that make up the overall separation. Each block in the overall process flow sheet represents a unique process that carries out an individual chemical separation, and each block contains numerous operations that are responsible for the chemical separation.

The Uranium Extraction Process (UREX) is often the first removal process in the overall scheme of spent fuel recycling. After extracting U and Tc from the spent fuel, the washed and rinsed effluents (Cs/Sr raffinate) move on to the next separation process.

A key concept in the SFTF plant design is the recycling of nitric acid. The purpose of the nitric acid recycling system is to concentrate the spent nitric acid to a desired molarity which, in turn, can be recycled back into the process. The spent nitric acid streams from many processes are collected and sent to a distillation column where it is separated from the impurities collected in the various separation processes.

Research Objectives and Methods:

The major objectives will lead to the creation of a framework that combines all the strengths of AMUSE's complicated calculations, well-established commercial system process package, and ISOPro's flexible parameter optimization modules. Development of the process simulation code can be done using the solvent extraction process at Argonne National Laboratory in collaboration with the research team from the Mechanical Engineering Department at UNLV. The objectives are as follows:

- To develop a framework for simulating the Spent Fuel Treatment Facility process using the AMUSE code, ASPEN-Plus commercial process package and ISOPro system engineering model.
- To develop middleware interfaces that can communicate between the AMUSE code and ASPEN-Plus packages.
- To extend the existing system engineering model for the optimization process that includes process simulation results.
- To include a scenario-based database system that efficiently reports required information as chart output using web-based programming, and Microsoft Visual Basic (MS VB).

Research Accomplishments:

- Completed the feasibility study of the nitric acid recycle process using the ASPEN-Plus system process package.
- Completed the "skeletal backbone" study of the NPEX process using the ASPEN-Plus system process package.
- Integrated the ASPEN-Plus process model with the TRPSEMPro system engineering modeling package, developed by the UNLV team.
- Integrated the ASPEN-Plus process model with the ISOPro system engineering modeling package, developed by the UNLV team.
- Tested the simplified system process integration using the ISOPro package.
- Generated complete version of the ISOPro package user manual and tutorial.
- Made an interface to interact with ASPEN-Plus through the ISOPRO Package
- Completed final version of the ISOPro User Manual associated with summarized ISOPro source codes.
- Redesigned and completed use case and design class diagrams (DCD) of the ISOPro package using ArgoUML.

- Improved ISOPro system and AMSUE data flow and re-coding on VB.NET and ActiveX Data Objects (ADO) with improved data reading function.

Process Simulation of Nitric Acid

ANL is interested in understanding the feasibility of applying tower separation for nitric acid, acetic acid and water separation, with nitric acid leaving as bottoms product with a higher concentration of 4.5M from 0.6M. The purpose of the simulation is to validate the feasibility of using tower design. An arbitrarily assigned molar flow rate was chosen in an effort to test the hypothesis. Two parametric studies were conducted for this distillation simulation. The first parametric study was to observe the effects of varying the reflux ratio on the outlet flow rates while the second one examined the effect of varying the number of stages on outlet flow rate.

With the temperature, pressure, feed concentration, distillate rate and number of stages held constant it was desired to study how changing the reflux ratio in the column affects product flow rates. Increasing of reflux ratio gives an overall decrease of nitric acid flow rate and increase of acetic acid and water flow rate in the bottom streams. In the second parametric study, molar flow rate of nitric acid from the bottom streams continuously decreases along with the increasing of the number of stages and is gradually stabilized after number of stages larger than 6.

While the studies performed have shown that the manipulation of both reflux ratio and number of stages affects the separation of feed components, the changes are minimal and can be considered negligible. The simulation showed that it is not feasible to design a tower that removes nitric acid as a bottoms product from a feed of nitric acid, acetic acid and water. If it is desired to separate and obtain a high purity nitric acid stream; having the nitric acid leave the column as distillate is an option. Under such a circumstance, it is no longer necessary to have a rigorous separation model. ASPEN Plus can calculate the number of stages and reflux ratio based on the engineer's desired separation efficiency.

The new ASPEN Plus flow sheet for this second separation simulation will concentrate a 0.6M feed of nitric acid (in water) to a 4.5 M solution (in the tops stream). The ASPEN Plus simulation data indicates a possible optimized number of stages is around 15 with the reflux ratio of 0.60.

Process Simulation of NPEX Process

The NPEX process is used by ANL scientists to remove plutonium and neptunium from spent fuel. The work conducted in this project is the simulation of the process following the removal of the plutonium/neptunium strip product. The simulation is intended to construct a "skeletal backbone" of the plutonium metal production process due to the difficulty of acquiring the plutonium metal production process simulation parameters.

Interface to ASPEN-Plus through the TRPSEMPro Package

To generate the middleware interface between TRPSEMPro and ASPEN Plus, element types of "Streams" and "Blocks" from ASPEN-Plus package need to be clearly identified. Streams can be further divided into input and output parts while blocks store system-related information. The currently developed interface shows the essential functions of file selection, data processing and file storage. The major role of the developed TRPSEMPro package is to perform the optimization process using both ASPEN-Plus system process engineering and chemical separation process. The data communication and result presentation from these two programs can be valuable for the SFTF design. Since the AMUSE code has been integrated with the TRPSEMPro package, the current internal database is integrated with those results generated from the ASPEN-Plus simulation. While the development of the data communication and processing tool is the major focus, optimization criteria development will be provided or developed by researchers from the ANL.

To interact with both the AMUSE and ISOPro packages, the middleware interface based on the ISOPro should provide the capability of interacting with external programs, converting input and output data and managing process results. The major task for the year was to complete the interface to the ASPEN-Plus

program through the developed ISOPro package. The data communication and result presentation from these two programs are valuable for the SFTF's process design task. The internal MS Access database was developed for storing intermediate and final simulation results from both programs. However, input and output data files originally generated from each individual program are kept intact and are used to populate the initial data sheet within each middleware interface. Although the program integration was completed, the final SFTF's system optimization work is not included in this report due the export control nature of the AMUSE code. The optimization can be completed by the ANL research team by plugging the full AMUSE program into the ISOPro package. The accomplishments for the year are summarized as follows:

- The framework design was revised to improve the performance of the system. It defines the data flow from ASPEN-plus to AMUSE with the data set "parser module" in the middle. Based on the discussion with ANL staff, the UREX+1a process simulation flow chart was updated based on the input and output natures defined in the database storage.
- The middleware for the ASPEN-Plus interacts with the ASPEN-Plus and populates data into a user friendly, tabulated format. It displays the information from streams and its elements. The user can modify the input values and directly run the simulation through the interface. There are sets of standard menu items listed to provide faster access. A "Tree" view of the streams is organized into "Input" and "Output" based on the "Blocks" definition retrieved from the Aspen "bkp" file. After each simulation run from the ASPEN-plus, input/output information is updated into the interface. The selected programming algorithm can significantly impact the read/write efficiency of the code, especially loading a large and complicated "bkp" file. A "nested hash" programming technique was used. To accelerate data access, ASPEN-Plus information was stored in two hashes, one for Input streams and one for Output streams.

To better maintain and improve the ISOPro system engineering package, construction of Unified Modeling Language (UML) diagrams was initiated. Unlike the general user manual or tutorial, the UML diagrams are specifically designed for communication among programmers and software engineers with standardized terminology and module definition. The creation of such diagrams provides high flexibility on version control, code comparison and module modification. They can be distributed to different development identities (institutes) in the future for coordinating software improvement and modification efforts. Three major components were developed. They are Use Cases for ISOPro package, Class Diagram for AMUSE middleware interface, and Class Diagram for ASPEN-Plus middleware interface.

Use Case Model

Use cases are about defining requirements needed for the package development. For example, 15 user goals were determined in the current ISOPro system. The user initially decides to execute either the AMUSE or ASPEN-Plus package. Once the package is selected, sequential actions are followed. Each block (goal) is associated with a checklist that guides the code development. Use cases summarize both functional and non–functional requirements. To improve the package in the future, developers can easily identity existing functional blocks from use cases and effectively modify this package.

Design Class Diagram

Design class diagrams are used to identify the specification for the software classes after determining use cases. Information related to classes, associations and attributes, interfaces, methods, and dependencies was included in the DCD. There are seven classes associated with ExprotFilePaser class. No method was developed under these classes.

Initial design of the ISOPro interface read in a large amount of ASPEN-plus parameters into the system (or database), which slows down the system dramatically. The identified solution was to rewrite the program to read in all parameter fields into database sequentially and flag null parameter fields during reading. An optimized "search" algorithm was implemented to exclude those null data fields during data from the database into the interface. The improvement was completed. UML diagrams were used to evaluate data flow and efficiency for the ISOPro system. The ISOPro interaction with the AMUSE macros was identified as the bottleneck. The proposed UML diagram solution is to change the existing VB programming into a

VB.NET architecture, which provides better data access module and easier coding style. The Improvement was started by changing AMUSE data flow and re-coding ADO for better extendibility and maintainability. Methods and attributes from complicate classes such as TreeView, Flowsheet, and FlowsheetProperty have been identified. The development of the diagram makes maintenance and modification more effective. Programs or modules from the ASPEN-Plus simulation can be attached into the current diagram effectively.

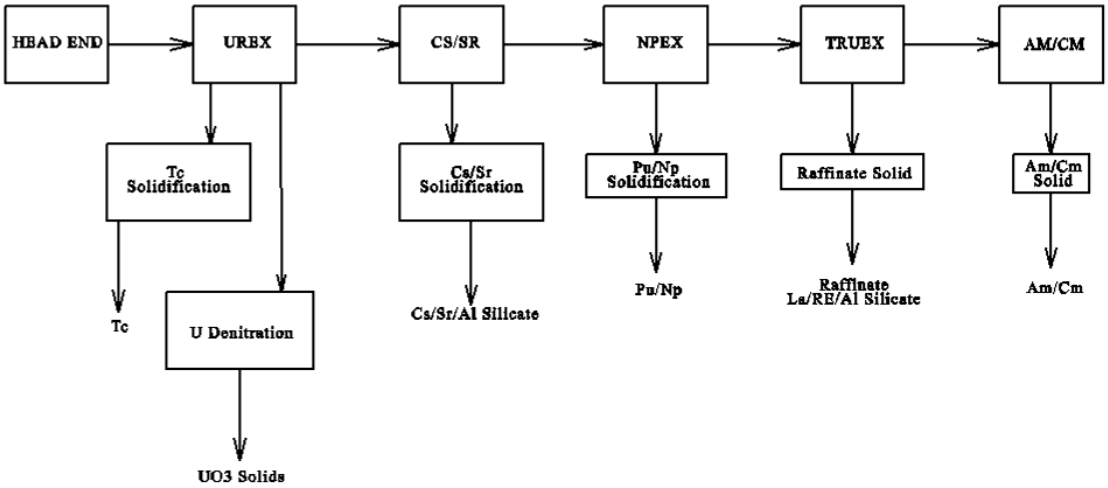

Overall process flow sheet.

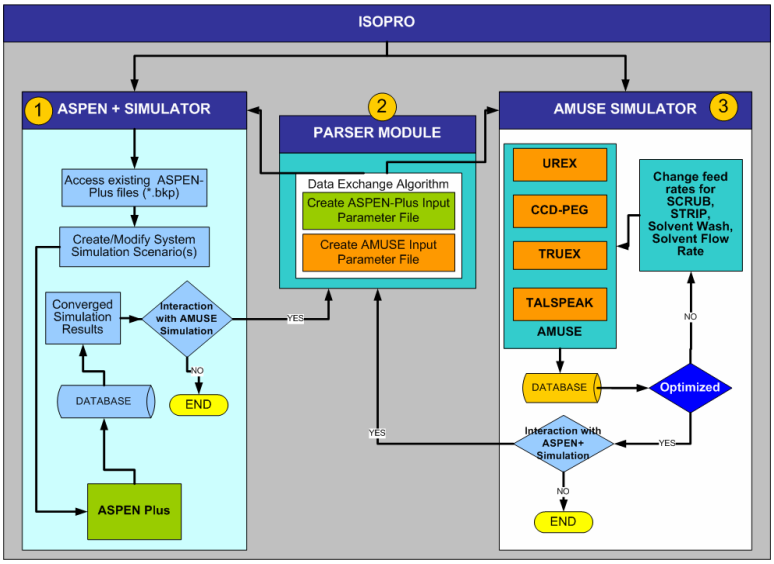

Modified TRPSEMPro system architecture

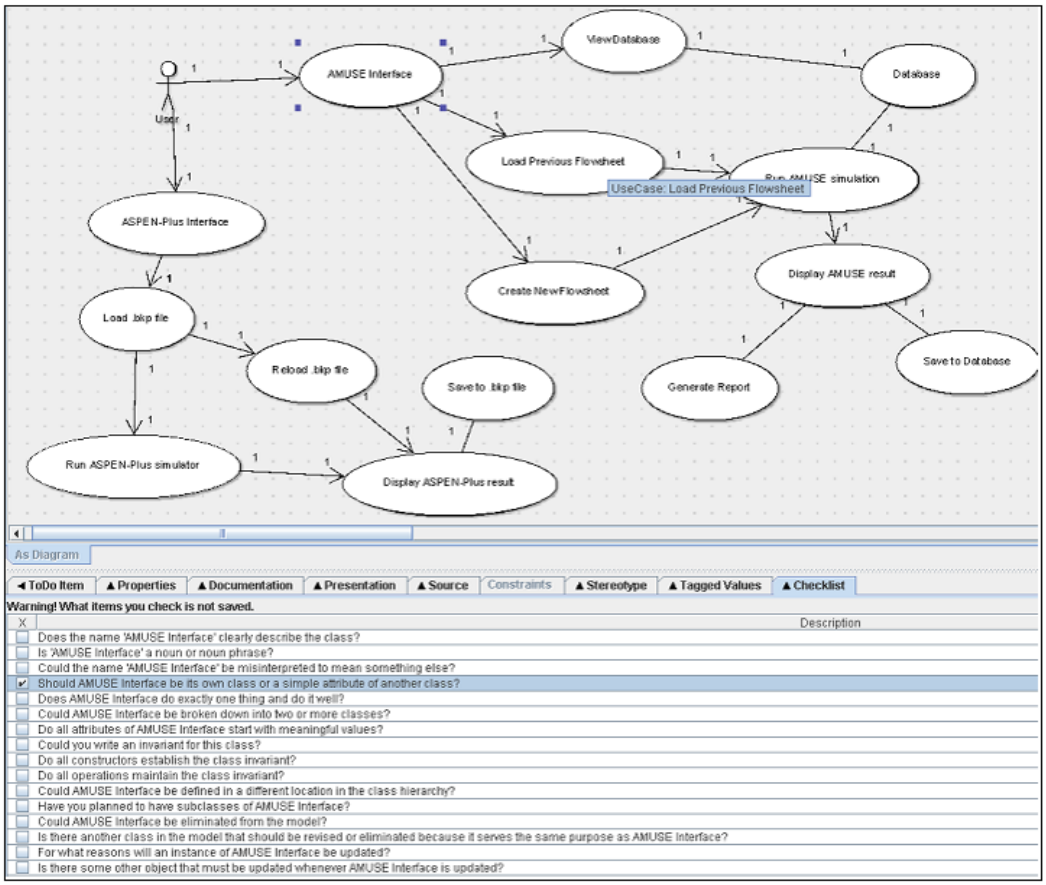

Example case for the updated Integrated System Optimization Program package.

Task 25 Electrochemical Separation of Curium and Americium – Dr. David Hatchett, Dr. Ken Czerwinski

Background

In the Transmutation Research Program the separation of the trivalent actinides Am and Cm from the trivalent lanthanides, and even each other, has been identified as an area of particular interest. The removal of lanthanides from trivalent actinides is necessitated for the neutron economy of a fuel containing Am and Cm. Furthermore, a fuel containing only Am would ease the demands on a reactor for transmutation. The destruction rate of Cm isotopes in a reactor is comparable to their decay rate. Separation and storage of the Cm, and reintroduction into the fuel of the Pu daughters, is a transmutation option that can be explored if a suitable method for the separation of Cm from Am is obtained. Furthermore, removal of Cm would reduce difficulties in fuel fabrication.

Electrochemical methods can be used to effectively separate actinide and lanthanide species from complex mixtures. This is based on the unique electrochemical properties of each specific target species. In studies it has been found that with the exception of Ce, aqueous solutions provide unsuitable electrochemical windows to effectively evaluate the thermodynamic properties that are useful for chemical separation. Therefore a more novel approach was examined which eliminated the aqueous solution with a Room Temperature Ionic Liquid (RTIL) solution. RTIL solutions do not suffer from the side reactions that are prominent in aqueous environments. In addition the potential window is much larger for the RTIL solutions. The RTIL solutions are a new starting point for the electrochemical separation of individual

species from a mixture.

RTIL solutions do not suffer from the side reactions that are prominent in aqueous environments. In addition, the potential window is much larger for the RTIL solutions. The RTIL solutions are a new starting point for the electrochemical separation of individual species from a mixture.

Research Objectives and Methods:

The objective was to use electrochemical techniques to develop a thermodynamic understanding of actinide and lanthanide species in RTIL solutions, and use this data to effectively separate species with very similar chemical properties.

In consultation with a DOE collaborator, electrochemical methods and materials were evaluated and used to exploit the thermodynamic differences between similar chemical species enhancing the ability to selectively target and sequester individual species from mixtures. This project, in its third year, successfully completed phases 1, 2. Phase 3 was partially completed. The project expanded to include phase 4.

Phase 1

Evaluated thermodynamic oxidation/reduction properties of Ce using electrochemical methods.

Phase 2

Evaluated the thermodynamic properties of chelated Ce, Sm, and Eu at carbon, platinum and gold electrodes.

Phase 3

Examined the use of conductive polymer membranes for the uptake and expulsion of complexed and uncomplexed actinide and lanthanide species. The uptake and selective adsorption and separation of individual actinide and lanthanide species, including the isolation of Cm from Am, still needs to be examined using conductive polymer/metal composite membranes containing bound chelates. Follow-on work was conducted under a new TRP project (Task 38).

Phase 4

Prepare and characterize RTIL solutions. Examine the electrochemical window and evaluate the electrochemical properties of lanthanide and actinide species in the non-aqueous ionic environment (also see Task 38).

- The following were specific goals for 2007-2008:
- To prepare RTIL solutions.
- To evaluate the potential window of RTIL solutions.
- To develop a fundamental understanding of the thermodynamic properties of actinide and lanthanide species such as Cm, Am, Ce, Nd, Eu, and Sm in RTIL solutions.

Research Accomplishments:

Phase 1

The thermodynamic characterization of Ce^{3+}/Ce^{4+} redox couple and other lanthanide species has been completed in various supporting electrolytes (0.3 M $NaNO_3$, 0.5 M HNO_3, and H_2SO_4 at concentrations of 0.1 M, 1.0 M, 2.0 M, and 4.0 M). The results show that the Ce^{3+}/Ce^{4+} redox couple can be successfully resolved in aqueous environments. While the potential range was suitable for the resolution of the Ce^{3+}/Ce^{4+} redox couple it was insufficient for others. Species such as Eu and Sm were not resolved within the potential limitation of the aqueous system.

The success of shifting the redox potentials for Ce bound to species such as EDTA and citrate ion suggest that species that were not resolved when unbound may be resolved after chelation. For example, the figure above shows the voltammetric response of Eu which was not resolved when unbound, after chelation with EDTA. The redox chemistry has been shifted such that the oxidation and reduction Eu/EDTA can be resolved at very negative potentials. This

species should precipitate as a hydroxide at the pH values presented in this figure. However, EDTA stabilizes the species at higher pH values allowing the electrochemistry to be resolved. The voltammetry at pH = 6 is more fully resolved than at the other pH values. However, the oxidation and reduction can be resolved at all three pH values. The redox chemistry of the Sm/EDTA species has also been successfully observed.

It was apparent from the initial studies that the ability to examine lanthanide and actinide species was limited in aqueous solution. However, there was success in resolving the Ce redox couple in aqueous solution. In addition, complexation with ethylene diamine tetraacetate (EDTA) provided increased stability of the Ce redox couple at pH values that would typically lead to the precipitation of $Ce(OH)_x$ (x = 2 or 3). The voltammetric response of the Ce redox couple before and after EDTA complex formation is illustrated (see opposite page).

The advantage to eliminating aqueous side reactions and expanding the potential window is that previously inaccessible electrochemical reactions may be observed. These systems provide a huge potential window for the observation of oxidation and reduction of lanthanides and actinides.

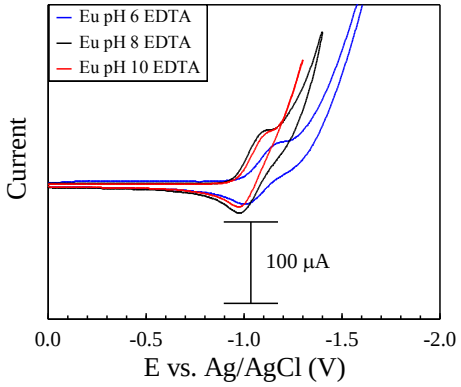

Electrochemistry of Eu/EDTA chelated species as a function of pH

Phase 2

To expand the ability to resolve the electrochemical response of other species besides the Ce^{3+}/Ce^{4+} redox couple the chelation properties of ligands such as EDTA, NTA, and Citrate were utilized. The Ce^{3+}/Ce^{4+} redox couple was examined first due to the fact that the electrochemistry of the unbound species has been fully characterized.

These studies were expanded to include other chelating species with similar results including citrate. The difference in redox potentials for Ce bound by EDTA and Citrate indicate that chelation can be used effectively to separate species in solution. It is also apparent that the pH dramatically influences the voltammetry in citrate solutions. This is not the case for EDTA with stable redox chemistry over a pH range from 2 to 12.

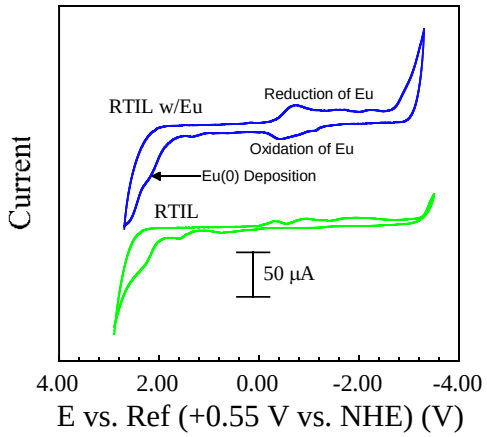

Electrochemistry of Eu at a Pt electrode in RTIL ([$MeBu_3N$][NTf_2]).

Phase 3

The last phase of this research is based on the electrochemical separation of americium and curium. The proof of principal for the electrochemical separation of americium and curium involves the doping of polyaniline (PANI) followed by the second doping after the uptake and reduction of Au particles in the polymer membrane. These particles will be used to affix the chelating ligand and then the applied potential will be used to facilitate complexation and speciation. To test the ability of the Au particles interaction with thiol molecules a simple five carbon thiol with a ferrocene tail was allowed to interact with the PANI/Au membrane. The oxidation and reduction of ferrocene thiol is clearly visible in the polymer indicating the gold particles are electroactive and can act in potential mediated chemical reactions. The ultimate goal is to use this in separation reactions using an EDTA/thiol ligand that was synthesized in the lab.

The advantage to eliminating aqueous side reactions and expanding the potential window is that previously inaccessible electrochemical reactions may be observed. These systems provide a huge potential window for the observation of oxidation and reduction of lanthanides and actinides. In addition, the potential mediated deposition of f-elements is possible - indicating that the controlled separation of chemical species is thermodynamically feasible. For example, the reduction of Pu^{3+}, Am^{2+}, Am^{3+},Cm^{3+}, and U^{3+} all occur before E = -1.90 V vs. Ag/AgCl, well within the negative potential limit for the RTIL at platinum (-2.6 V vs. Ag/AgCl), gold (-2.2 V vs. Ag/AgCl), and glassy carbon electrode (-3.4 V vs. Ag/AgCl) in the RTIL solutions.

In addition, the potential mediated deposition of f-elements is possible indicating the controlled separation of chemical species is thermodynamically feasible. For example, the reduction of Pu^{3+}, Am^{2+}, Am^{3+},Cm^{3+}, and U^{3+} all occur before E = -1.90 V vs. Ag/AgCl, well within the negative potential limit for the RTIL at platinum (-2.6 V vs. Ag/AgCl), gold (-2.2 V vs. Ag/AgCl), and glassy carbon electrode (-3.4 V vs. Ag/AgCl).

The formation of lanthanide and actinide complexes are based on the principal that the neutral species must be extracted to minimize crossover contamination. The complex would be extracted into the RTIL directly without TBP. This process may enhance the extraction of the f-element relative to the TBP/n-dodecane system based on incorporation of the common ion into the complex and diluent. The complexes can also be formed directly in RTIL. We have successfully prepared the UO2(TFSI)2, Sm(TFSI)3, U(TFSI)3,

and the U(TFSI)4 complexes using the methods defined in Scheme 1. The individual complexes have also been extracted and directly dissolved into RTIL ([MeBu3N+][TFSI-]). The electrochemical properties of UO2(TFSI)2 have been evaluated and the potentialdependent deposition of UO2(s) has been achieved, Figure 1. The SEM image of the electrodeposited UO2 is shown. These studies demonstrate that RTIL solutions can be used to effectively probe the oxidation/reduction of f-element species and complexes. In addition the potential mediated deposition of f-elements is demonstrated indicating the controlled separation of chemical species is thermodynamically feasible. The deposition of UO2(s) is initiated at ~-2.0 V vs.Ag/AgCl in the RTIL solution. The reduction of UO2(s) to U(s) should occur at -2.443V in aqueous solution. The initial reduction occurs at more thermodynamically favorable potentials (~0.44 V). However, the deposit composition is complicated because the sample was exposed to air before SEM measurement with a final product of UO2(s) obtained based on EDX verification. Additional studies are required in inert environments to ensure the deposit is not influenced by air exposure. The electrochemical deposition of common lanthanides and actinides from RTIL solution can also be envisioned based on the following reduction potentials: Pu3+ (-2.228 V), Am2+ (-2.097 V), Am3+ (-2.245 V), Cm3+ (-2.237 V), and U3+ (-1.997 V). The reduction of any of these species would occur well within the negative potential limit for the RTIL at platinum (-2.8 V), gold (-2.4 V), and glassy carbon electrode (-3.6 V vs. Ag/AgCl) in the RTIL ([MeBu3N+][TFSI]) solution.

The electrodeposition of Sm and U metal have also been achieved from RTIL solutions using the $Sm(TFSI)_3$, $U(TFSI)_3$, and $U(TFSI)_4$ complexes prepared using the synthesis described in scheme1. The deposition of U at room temperature from ionic liquid had not been achieved previously. However we successfully deposited U metal on Au electrodes using $U(TFSI)_3$ and $U(TFSI)_4$ prepared using the defined synthetic methods from scheme 1. To date we have not examined the selective deposition of Lanthanides followed by Actinides as a method of separation. However, now that deposition potential are know for the RTIL solutions it is a logical progression to try to selectively electrodeposit the lanthanides in one step followed by U deposition provides the voltammetric response of an Au electrode for the deposition of U from RTIL and an SEM image of U deposits for clarity.

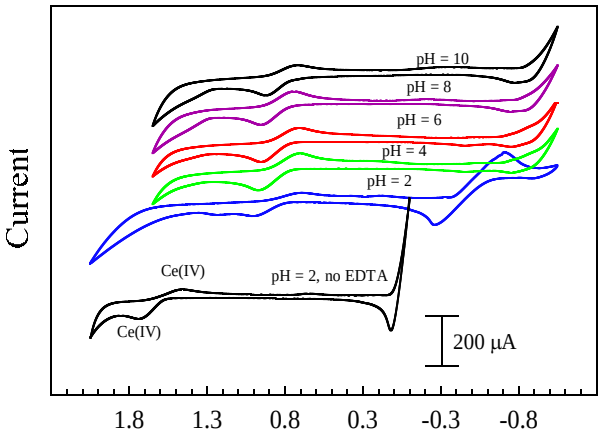

Electrochemistry of the Ce(III)/Ce(IV) redox couple at a Platinum electrode uncomplexed and complexed with ethylene diamine tetraacetate (EDTA) as a function of pH. [EDTA] = 12 mM [Ce(III)] = 6 mM, v = 100 mV/s. Free [Ce(III)] = 6 mM is shown on the bottom of the figure for comparison.

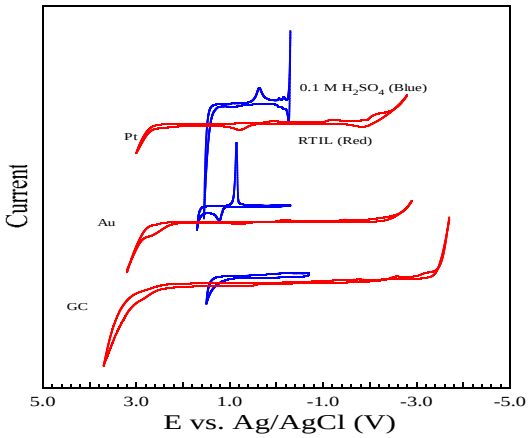

Electrochemistry of Gc, Au, and Pt electrodes in room temperature ionic liquid (RTIL) ([MeBu$_3$N][NTf$_2$]), (Red) and 1.0 M H_2SO_4, (Blue). Electrochemistry of Gc, Au, and Pt electrodes in room temperature ionic liquid (RTIL) ([MeBu$_3$N][NTf$_2$]), (Red) and 1.0 M H_2SO_4, (Blue).

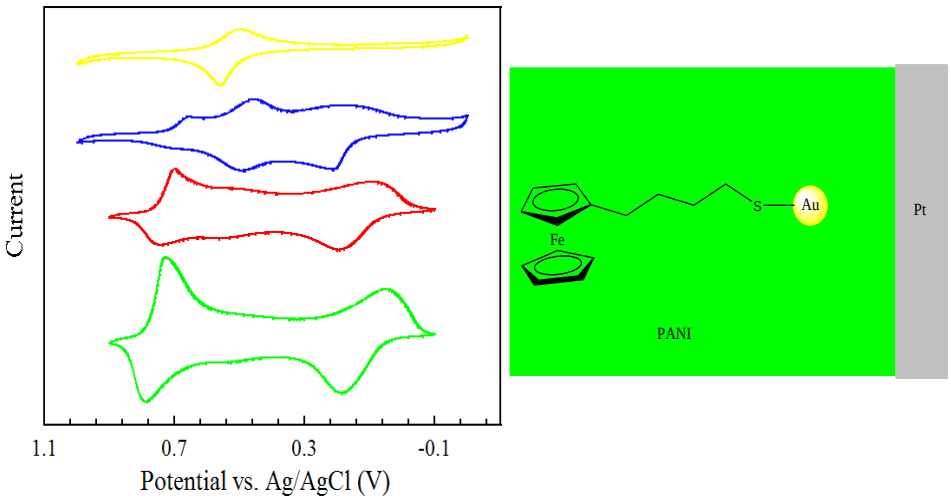

Acid doping of PANI in $HClO_4$ before uptake of Au (green) and after (red). Redox properties of a PANI/Au/FcThiol membrane in $HClO_4$ (blue) and Au/FcThiol (yellow). A schematic of the PANI/Au/FcThiol is provided to the right for clarity.

Electrochemistry of Lanthanides in RTIL solutions:

- The direct dissolution of Ce, Sm, and Eu was achieved into RTIL consistent with methods currently used for aqueous dissolution processes.
- The influence of temperature on the electrochemical response of lanthanide, Ce, and Ferrocene in [Me_3NBu][TFSI] was evaluated as a function of scan rate.
- The electrochemistry of Ce in RTIL was examined as a function of increasing temperature to determine if kinetically limited electrochemical processes can be resolved.
- A temperature study examining the electrochemical reduction of $Ce(TFSI)_3$ and deposition of Ce metal from RTIL was conducted at elevated temperatures (24, 45, 60, 75, 90 °C).
- UV-Vis was performed on the 10 mM direct dissolution $Ce(TFSI)_3$ into $Me_3NBuTFSI$ (from $Ce_2(CO_3)_3$ with HTFSI) sample along with comparison samples of $Me_3NBuTFSI$, HTFSI in $Me_3NBuTFSI$ background, similar concentration of $Ce_2(CO_3)_3$ with HTFSI in water, HTFSI in water background, and water.
- UV-Vis was performed on the 4.05 mM direct dissolution $Sm(TFSI)_3$ into $Me_3NBuTFSI$ from the $Sm_2(CO_3)_3$ with HTFSI sample along with comparison samples of $Me_3NBuTFSI$, HTFSI in $Me_3NBuTFSI$ background, similar concentration of $Sm_2(CO_3)_3$ with HTFSI in water, HTFSI in water background, and water. Previous $Sm(TFSI)_3$ that was first synthesized in water and crystallized then added to $Me_3NBuTFSI$, and two samples of $Sm(TFSI)_3$ in water were also examined.

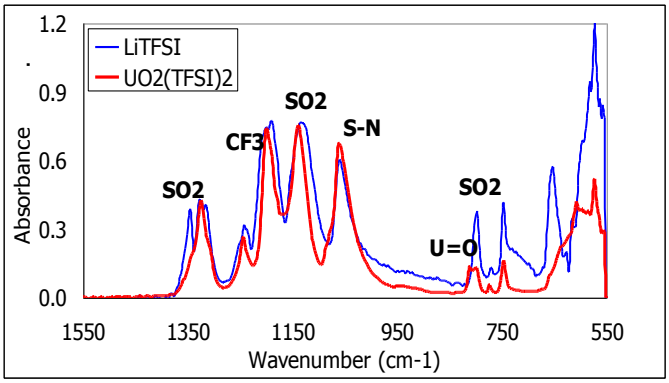

The IR spectra show the typical RTIL anion Li(TFSI) (blue), and UO_2 complexed to TFSI (red). The shift of the SO_2 peak at 1350cm^{-1} indicates TFSI complexation, and the peak around 810cm^{-1} indicates the presence of a U=O bond.

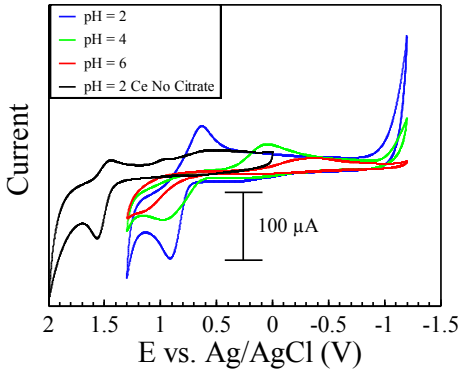

Electrochemistry of Ce and Ce/Citrate chelated species as a function of pH. The unbound Ce (black) and Ce/EDTA (blue) at pH = 2 are shown with Ce/EDTA at pH = 4 and pH = 6.

Direct Dissolution and Electrochemistry of UO_2CO_3 and U_3O_8

- $UO_2(TFSI)_2$ synthesis and characterization was initiated in an attempt to isolate crystals of the species for further analysis
- U_3O_8 Dissolution into RTIL was conducted using minimum concentrations of acid and ozone. Two additional measurements were conducted for verification of the processes.
- The U_3O_8 dissolution was verified spectroscopically with the characteristic uranyl peaks observed between 400-450 nm.
- The synthesis of $UO_2(TFSI)_2$ has continued and the crystallization was initiated using the pH of the solution to mediate the process.
- UV-Vis characterization of the $UO_2(TFSI)_2$ was completed with broad absorbance between 400 and 500 with lower definition of intrinsic peaks observed for aqueous uranyl carbonate.
- $U(TFSI)_3$ dissolution and cyclic voltammetry is being conducted. Specifically $U(TFSI)_3$ (0.0177 g) was transferred into a new cell with RTIL and cyclic voltammetry was then performed on the sample (1.9 to -2.8 V) using an Au disc working electrode and Pt counter electrode for 200, 100, 50, 25, and 10 mV/s so scan rate dependence could be investigated
- U_3O_8 synthesis was conducted. Uranyl nitrate was dissolved in water and precipitated out with ammonium hydroxide, removed from the centrifuge tube, placed into a ceramic vessel and heated in an oven at 100°C for 19 hours with U_3O_8 confirmed using the C2mm phase by TOPAS.
- The original U_3O_8 RTIL dissolution solution (2.01 mM U_3O_8 dissolved into $Me_3NBuTFSI$) was used in the newly designed e-chem cell for electro-depositing and electrochemical deposition was initiated.
- Dissolution was started with a control sample: 0.0338 g U_3O_8 (w/^{223}U) was placed in 20 mL of $Me_3NBuTFSI$. No HTFSI was added. Ozonation without acid produced only a 9% dissolution concentration. Increases were achieved with the addition of HTFSI.

- Deposition of UO_2(s) on stainless steel and Au electrodes was achieved used the direct dissolution of U_3O_8 in RTIL.

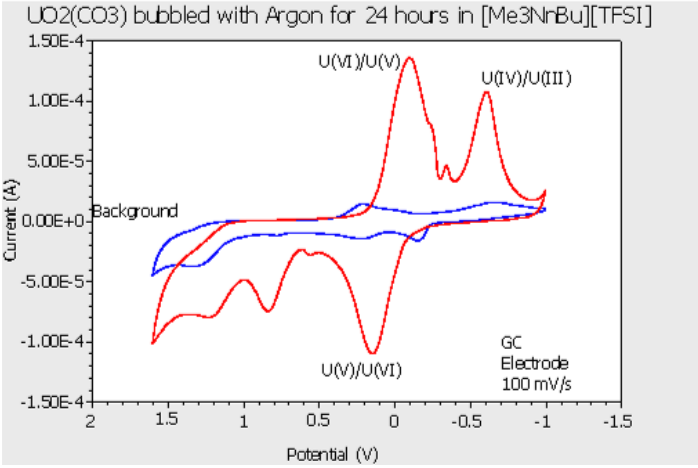

CV of UO_2-TFSI complex formed by added $UO_2(CO_3)$ directly to the RTIL and using Argon to remove the carbonate from the system

Phase 4

The electrochemical window for RTIL systems is based primarily on the reduction of the cation and oxidation of the anion used to make the solution. The potential window is significantly larger for RTILs ranging from approximately 4.5 to 6 V when compared to aqueous environments. The figure illustrates the potential windows obtained in aqueous solutions of 0.1 M H_2SO_4 (blue line) and the RTIL, tri-n-butylmethylammonium bis(trifluoromethylsulfonyl)imide ([$MeBu_3N$][NTf_2], red line) at GC, Au, and Pt electrodes. For each electrode the positive and negative potential limits provide an absolute potential window of approximately 4.5 V for Pt, 5.0 V for Au, and 6.0 V for GC.

Through using infrared (IR) and ultraviolet-visible spectra, it was observed that the uranyl did complex to the anion of the RTIL. However, a more interesting way to complex the uranyl to the RTIL is by adding uranyl carbonate directly to the RTIL and then using Argon gas to remove the carbonate. The results yielded a soluble UO_2-bis(trifluoromethylsulfonyl)amide (TFSI) complex that produced reversible electrochemical reactions with Uranium including the U(VI)/U(V) couple. The Cyclic Voltammogram (CV) also yielded the U(IV)/U(III) couple. This method could prove to be very useful in observing the electrochemistry of any metal-carbonate species.

Another advantage is the increased solubility of lanthanide and actinide species in the RTIL. RTIL solutions have been utilized in the waste cycle for extraction of species. These solutions could be useful in the potential dependent separations of lanthanide and actinide species. The preliminary evaluation of RTIL solutions relative to normal aqueous conditions is also illustrated.

- Karl-Fischer titrations were performed on a RTIL samples the water content was determined for pristine RTIL and RTIL/HTFSI solutions.

- Karl-Fischer titrations were performed on RTIL samples after the direct dissolution of lanthanides and U_3O_8.

- The redox properties of ferrocene were examined to determine the working reference electrode potential relative to more common reference electrodes including NHE and Ag/AgCl.

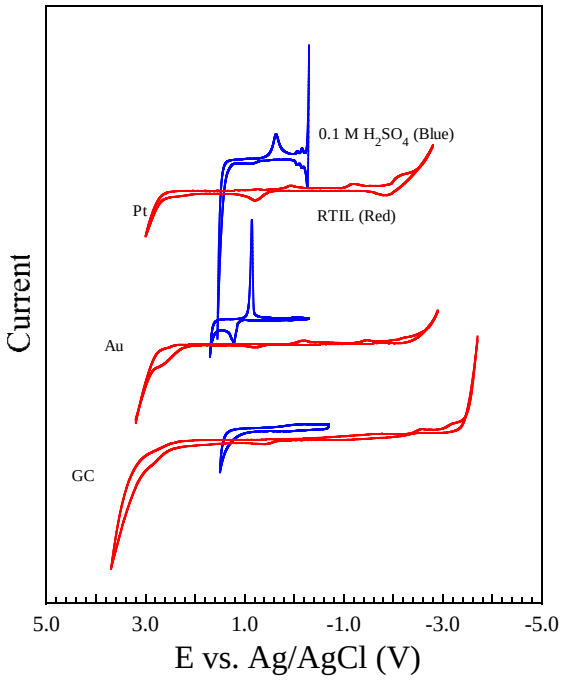

Electrochemistry of GC, Au, and Pt electrodes in RTIL ([$MeBu_3N$][NTf_2]) (red) and 0.1 M H_2SO_4 (blue).

Task 26 Fundamental Chemistry of Uranium and Plutonium in the TBP - Dodecane - Nitric Acid System – Dr. Ken Czerwinski

Background

The extraction of tetravalent Pu and hexavalent uranyl in nitric acid solution by tributylphosphate (TBP), based on the formation of organic phase neutral complexes such as $Pu(NO_3)_4$•2TBP and $UO_2(NO_3)_2$•2TBP, has been the foundation of actinide purification for a number of decades. Upon reduction of Pu(IV), Pu(III) is back extracted into an aqueous phase. However, the data needed for detailed modeling of Pu extraction is not available for all conditions of concern to the Advanced Fuel Cycle Research and Development program. This proposal was developed with Dr. George Vandegrift of Argonne National Laboratory to obtain the necessary data for Pu extraction modeling.

Understanding the role of nitrate in actinide speciation is important for determining the necessary data for extraction modeling. Difficulties in modeling Pu extraction under some nitrate conditions may be due to ill-defined constants of formation for the dinitrate and trinitrate species of U and Pu. The influence of pertechnetate on the speciation of U and Pu in the TBP-dodecane-nitric acid system is still poorly understood. Since pertechnetate is capable of reoxidizing reduced Pu species, it may have a profound impact on the extraction of Pu.

In the uranium extraction process, acetohydroxamic acid (AHA) is expected to be used. AHA can complex and reduce Pu, decreasing its extraction into the organic phase; the effect of uranyl-AHA on U extraction has not been quantified. AHA can reduce pertechnetate as well, initiating a redox cycle with both U and Pu. In a solvent extraction system using AHA, it is necessary to determine the complexation kinetics, redox reactions, and thermodynamics of AHA interactions with these elements.

Research Objectives and Methods:

The research objective is to experimentally evaluate the fundamental speciation of Pu and U in the TBP-dodecane-nitric acid-AHA system and the effect of pertechnetate, specifically:

- To determine the influence of nitrate on the speciation of U and Pu in the TBP-dodecane-nitric acid system. The aqueous and organic speciation of U and Pu are examined as a function of the nitric acid concentration, nitrate concentration, actinide ion concentration, temperature, and time.
- To determine the speciation of U and Pu with AHA in the presence and absence of TBP-dodecane organic phase. The aqueous and organic speciation of U and Pu are evaluated as a function of AHA concentration, metal ion concentration, metal ion redox state, pH, and temperature.
- To determine the interaction of AHA with pertechnetate, and the effect on the interaction of AHA and pertechnetate with U and Pu.
- To incorporate thermodynamic and kinetic data into existing modeling codes.

All of the initial experiments were performed with uranyl, UO_2^{2+}. The results obtained from U are the basis for further experiments with Pu. In extraction experiments, the aqueous and organic phases are contacted in equal volumes from 0.3 to 5.0 mL.

Research Accomplishments:

Uranyl Nitrate.

Efforts focused on methods for the determination of nitrate concentration in the experimental system. Ion Chromatography (IC) was examined as a method for nitrate determination and was found to be suitable.

The complexation of uranyl (0.01 to 0.1 M) with nitrate was studied at 1 M HNO_3 with excess nitrate (from $LiNO_3$)varied from 0 to 10 M. It was found that at higher nitrate concentrations, more uranyl was present in the organic phase, and, in the absence of uranyl, more HNO_3 extracted.

Extraction studies on samples containing two different uranium concentrations were performed. The organic phase of each sample consisted of a pre-equilibrated solution of 30% TBP (tributylphosphate) in dodecane. The aqueous phase consisted of nitric acid (0-12M), lithium nitrate (0-12M), uranyl nitrate (0.1 and 0.05M) and water. After contact the phases were separated and analyzed for nitrate and uranium concentrations by IC (ion chromatography) and LSC (liquid scintillation counting), respectively. The amount of nitrate extracted into the organic phase was surveyed. The data shows a slightly increasing trend as nitric acid and total nitrate increase though, generally the amount of nitrate extracted stays between 0.5 M and 1.5 M regardless of the varying initial nitrate, acid or uranium concentrations. The distribution ratio for uranium has shown a general decrease with increasing acid concentration and an increasing trend with increasing nitrate concentration. Both of these effects seem to level of around a K_d value of 10 which occurs around 10 M acid and nitrate.

The acid concentrations of the samples were determined by titration in order to have more complete information about the phases. Also UV-Vis spectroscopy was done on the organic phases of the samples.

The organic phases of the samples were examined with UV-Visible spectroscopy. There are not noticeable peak shifts as the nitrate increases, but the relative peak heights do change. The peak around 403nm gets larger while the peak at 425nm gets smaller. The trends in this spectrum are very similar to the other spectra taken when holding acid concentration constant. Similar effects are not seen when holding total nitrate concentration constant. This suggests that as nitrate concentration increases there may be a difference in the bonding around uranium with a chance in speciation to the nitrate form.

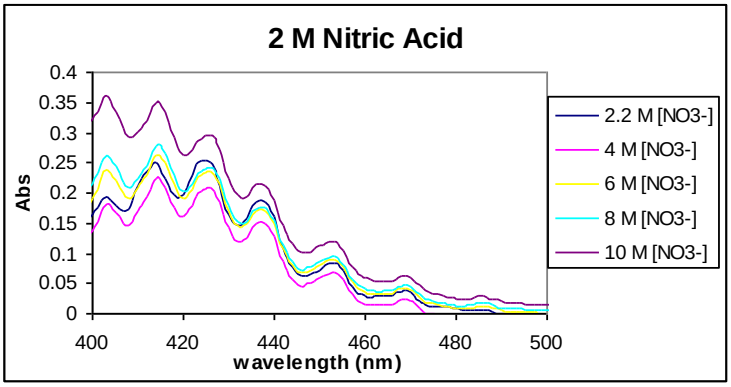

Uranium absorbance with varied nitrate.

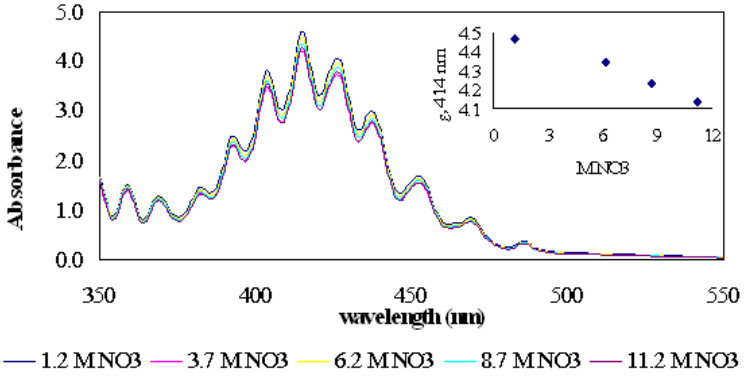

The UV-Vis spectrum of uranyl nitrate in 30% TBP varies with nitrate concentration.

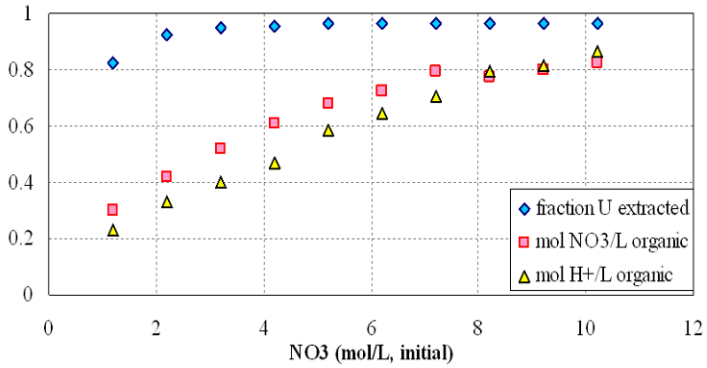

The measured concentrations of uranyl, nitrate, and acid in the organic phase extracted from 0.02 M U, 1.0 M HNO_3, and varied initial nitrate.

Uranyl-AHA.

Analysis of XAFS data was used to verify the models. Different hypotheses were proposed in the literature concerning the nature of the U species in the heavy organic phase examined:

i) formation of the compound $HUO_2(NO_3)_3.xTBP$
ii) formation of U(VI) polymer
iii) modification of nitrate bounding and formation of hydrogen bond with water or acid nitric present in the third phase

According to EXAFS result obtained in this study the following was found for the different theories. Hypothesis (i) was rejected since the formation of an eventual $HUO_2(NO_3)_3.xTBP$ will lead 6 O(N) atom at 2.50 Å, and this was not found. Hypothesis (ii) cannot be completely rejected, and it might be possible that $[UO_2(NO_3)_2.2TBP]_2$ and $UO_2(NO_3)_2.2TBP$ are simultaneously extracted in the heavy third phase. Hypothesis (iii) corroborates the observation from 15 M HNO_3 media but is not verified in 8M and 12 M HNO_3 media.

The interaction of uranium with AHA was reinvestigated. The ionic strength was held constant at 1.003 M using $NaClO_4$ with a constant 4:1 ratio AHA to uranium and the pH varied from approximately 0 to 10. There was a noticeable optical variation with pH and an accompanying change in absorbance. Further experiments were performed at pH 5 with a constant uranium concentration and the AHA varied. Kinetic experiments were also performed and showed rapid complexation of uranium to AHA.

The complexation of uranyl with AHA and its effect on U extraction into TBP-dodecane was studied via ultraviolet visible spectroscopy (UV-Vis), nuclear magnetic resonance (NMR), and Inductively Coupled Plasma-Atomic Emission Spectroscopy in perchlorate and nitrate media. The concentrations of uranyl (0.1 to 10 mM) and AHA (1 to 700 mM) and the pH (1 to 10) were systematically varied. It was determined via NMR that there are at least two species of uranyl-AHA, that the species formed is pH-dependent, and that there is little hydrolysis at 25times or higher molar excess AHA. The low-pH species extracts from perchlorate media as well as free uranyl, and the high-pH species remains in aqueous solution. In nitrate media, the nitrate competes with and oxidizes the AHA under acidic conditions; the exact interactions remain to be explored.

In addition, methods for synthesis of the uranyl-AHA solid were developed; the solid was characterized by UV-Vis, Fourier Transform Infrared spectroscopy, NMR, laser fluorescence, melting point, and X-ray Absorption Fine-structure Spectroscopy (XAFS),and a crystal structure was obtained. The uranyl-AHA is present as a highly symmetrical polymer, in which each equatorial atom is exactly 180° from its opposite and the ligand planes are twisted within and between unit cells.

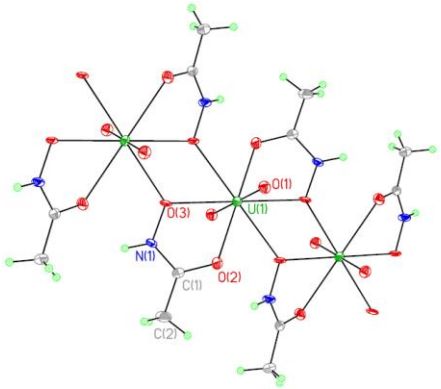

Crystal Structure of Uranyl-AHA

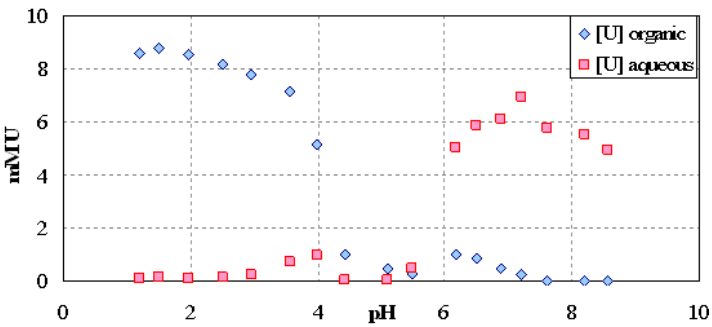

The measured concentrations in the organic and aqueous phases of 10 mM uranyl, 100 mM AHA extracted with TBP.

Technetium-AHA. Previous work failed to observe pertechnetate reduction by AHA; however, in the presence of catalytic acid (0.5 to 4 M HNO_3 or $HClO_4$) and a large excess of AHA (0.5 to 4 M), pertechnetate (0.1 - 20 mM) will be reduced to the $Tc^{II}NO(AHA)_2$ species in aqueous media. This species is highly water soluble and does not extract into 30% TBP. The presence of uranyl has no effect on the formation or extraction of this species, and up to hundredfold excess UO_2^{2+} does not affect the rate of formation. There is significant evidence that the reaction is instantaneous and the change in the Tc-AHA UV-Vis spectrum is due to the increasing pH as AHA hydrolyzes to acetic acid. However, the mechanism of formation is yet to be elucidated.

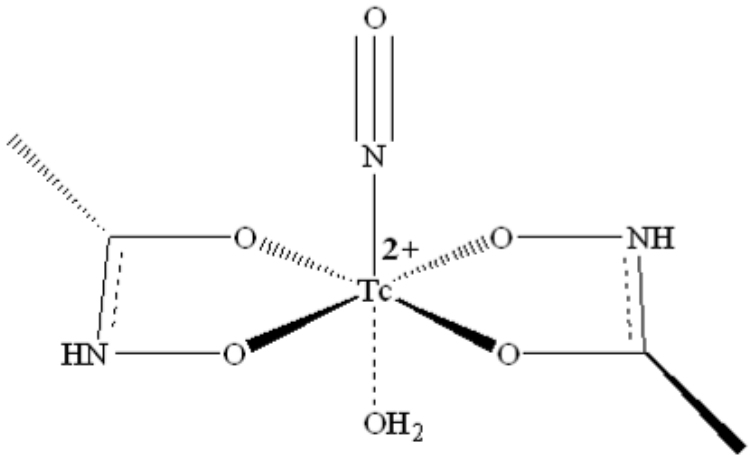

XAFS Structure of Technetium(II)-nitrosyl-AHA.

Task 27 Reactor Physics Studies for the AFCI Reactor-Accelerator Coupling Experiments Project – Dr. Denis Beller

Background

In the Reactor-Accelerator Coupling Experiments (RACE) Project of the U.S. Advanced Fuel Cycle Initiative (AFCI), a series of accelerator-driven subcritical systems (ADSS) experiments have been conducted at the Idaho State University's Idaho Accelerator Center (ISU-IAC) and at the University of Texas (UT) at Austin. In these experiments, electron accelerators are used to induce Bremsstrahlung photon-neutron reactions in heavy-metal targets. They produce a neutron source of 0.8 to 1.0 x 10^{12} n/s per kW of electron beam, which will then initiate fission reactions in the subcritical systems. These subcritical systems include a compact, transportable assembly at ISU and a TRIGA reactor at UT-Austin. A variety of fuel and assembly geometries are being studied: at ISU 150 flat plates of 20%-enriched uranium-aluminum alloy plated with aluminum are used; and at UT-Austin 20%-enriched UZr-H fuel are used. A third phase at Texas A&M using 70%-enriched UZr-H "FLIP" fuel has been put on hold. The use of compact accelerators and a small target allow the target to be placed in various positions in or adjacent to these subcritical assemblies to "map" the coupling of driven neutron sources; measuring core coupling and mapping adjoint flux.

The RACE Project is an important intermediate step between the recent European program MUSE and a future near full-scale demo. For MUSE, which was conducted by the CEA at Cadarache, France, the driving neutron source was produced by D-D or D-T reactions which produced a nearly mono-energetic source of 2.45 or 14.1 MeV and a maximum strength of ~10^{10} n/s. For design of full scale ADSS, a complete knowledge of the effects of the driving neutron source is essential. This will ultimately require spectral, temporal, directional, and intensity fidelity in prototype experiments. In the absence of this fidelity,

simulated sources should match some of the characteristics of projected driving sources to build confidence in the predicting performance of these systems, and codes and methods must be validated. The RACE Project will provide experience in a higher energy range (above 14.1 MeV) and with a stronger and more isotropic source than the MUSE experiments. In addition, a high-power RACE phase could provide valuable information on thermal feedback effects in TRIGA reactors. This combination of attributes of the RACE Project will provide highly valuable information in advance of the prototype or demonstration programs.

Research Objectives and Methods:

The specific research objective of this three-year project is to design and conduct accelerator driven experiments, which will help demonstrate in the U.S. the ability to design, compute, and conduct ADSS experiments and to predict and measure source importance, coupling efficiency, sub-critical reactor kinetics and source-driven transients. In addition, databases will be created for both steady state and transient ADSS experiments for the nuclear community to develop and test new computational codes and methods, and the importance of a driving neutron source in various regions of different subcritical assemblies will be mapped. Experiments will be conducted and compared to calculations with radiation transport and thermal-hydraulics codes such as MCNPX and RELAP.

Research Accomplishments:

Modeling for Texas RACE

UNLV examined the thermal performance of the accelerator target for experiments to be conducted at UT-Austin with their TRIGA reactor. A MCNPX (LANL radiation transport code) model was developed to produce energy deposition data for thermal analysis of the Texas RACE target. FLUENT, a computational fluid dynamics code, was then used to predict the thermal performance of the target.

In the early phases of the RACE project, modeling studies were also conducted at both the University of Michigan and Texas A&M University. Texas A&M examined different experiments: (1) use of the TAMU Nuclear Science Center (NSC) TRIGA, which is fueled with 70%-enriched "FLIP" fuel, and has a capability to be pulsed to 1000 MW_{th}; and, (2) assembly of an existing used-fuel, 20%-enriched core around the accelerator target in a different part of the NSC pool (the Texas Transmutation System). The University of Michigan supported the RACE project with computational reactor physics studies of the kinetics of subcritical systems. They studied dynamic response and optimized the ERANOS transport theory model for a RACE configuration by using several different energy group structures and orders of polynomial expansion for the neutron flux. In addition, they worked to resolve difficulties encountered with the time-dependent VARIANT transport theory solution.

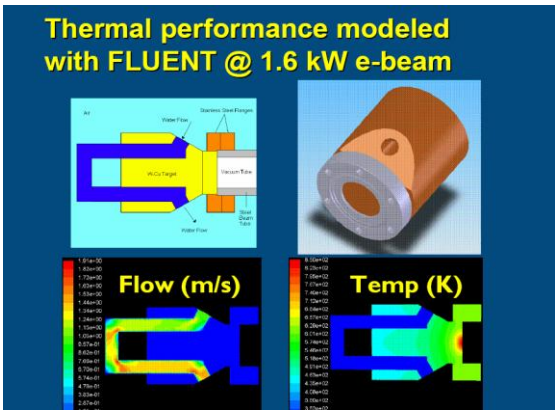

Modeling of the Texas RACE target with FLUENT computational fluid dynamics code

ISU RACE Experiments: UNLV collaborated with ISU and CEA in a series of ADSS experiments at the Idaho Accelerator Center. This series of ADSS experiments was conducted with a low-power, 20-MeV electron accelerator coupled to the Subcritical Assembly (SCA) with a tungsten-copper neutron generating target. Dozens of individual experiments were conducted to measure a variety of parameters and ADSS responses, including breakpoint frequency, flux stability, a long-duration reference pulsed-neutron-source experiment, a beam trip experiment, and a variable criticality experiment, which was conducted by observing the neutron response while water was drained from the SCA. The last series of these experiments were completed in October, 2006.

Since the conclusion of the ISU RACE Project experiments, results were compared from ISU RACE experiments conducted at ISU in October with Monte Carlo radiation transport modeling to analyze effective delayed neutron fraction (β_{eff}) in these far-subcritical, under-moderated systems using MCNP. The simplest approach based on 2 k-eigenvalue predictions with and without accounting for delayed neutrons gave unsatisfactory results due to the lack of convergence. Calculations have been completed with and without a plutonium-beryllium neutron source, which, although it was small, did affect the results. Two more-suitable techniques based on different weighting functions are currently under investigation.

The statistical behavior of calculated effective delayed neutron fraction based on two independent calculations (with and without delayed neutrons) for a critical system was more stable than for the subcritical case. Again, calculations have been completed with and without a plutonium-beryllium neutron source. Two more-suitable techniques based on different weighting functions are currently under investigation. The importance function is being used as an approximation of an adjoint weighting of the space- and velocity-dependent neutron population to calculate the effective neutron lifetime. Use of the value of a particle leaving a collision is being compared to that of a particle entering an event. Another computational approach that is based on a power iterations method (KCODE) to directly assess the efficiency of delayed neutrons is under development. The shape function for the steady-state problem, which will be used as a weighting function, was calculated and the relative efficiency of neutrons causing fission was determined.

A low-power phase of the RACE project was conducted in collaboration with the European Community (EC) at ISU with the participation of a member of the EC, ISU, and UNLV. Participants investigated the potential to increase neutron generation by one to two orders of magnitude, which would allow for high-average-power experiments with significant, and easily measured, thermal feedback. In a separate effort, ISU investigated connecting a high-power modulator and klystrons to existing 20 and 25-MeV linacs. This new configuration would provide 20 to 30 kW of electron current, compared to 1 to 2 kW with the existing ISU and Texas accelerators. In addition, incorporating depleted or natural uranium into existing heavy metal targets was investigated to increase the photon-neutron yield. A high-power RACE target was designed and constructed at UNLV and tested for thermal and neutron generation performance at ISU. Simultaneously, an EC Target Working Group examined several alternate high-power target designs. The combination of these two enhancements, if successful, would generate 5 x 10^{13} to 10^{14} n/s in the center of one of the Texas reactors.

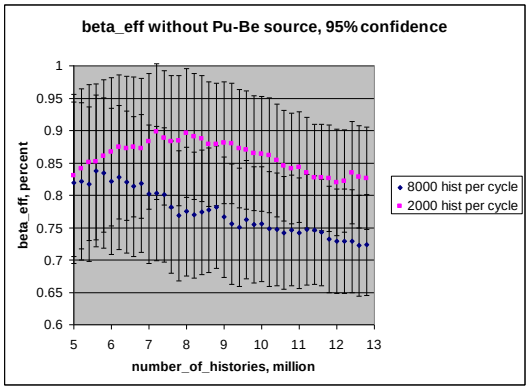

Calculated effective delayed neutron fraction for a subcritical (left side) versus a critical (right side); without a PuBe source.

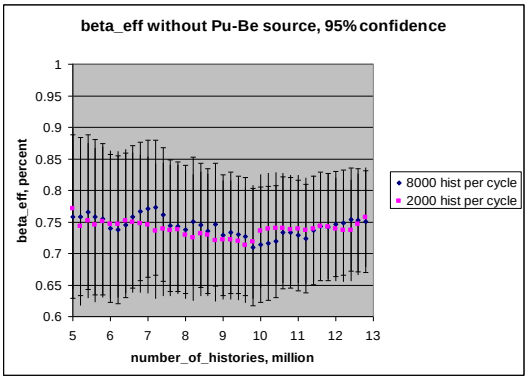

RACE Project Management: In his role as national RACE Project Director, the PI began to conclude the RACE Project with several universities and several European organizations. These organizations have contributed to several aspects of the RACE Project, including target design and analysis for High-Power RACE. Contracts supporting RACE Project work at the University of Michigan, Texas A&M University, and University of Texas at Austin ended during the summer, the Idaho participation was terminated in December, and the UNLV portion of the RACE Project will end summer 2007. EUROTRANS participants may continue to evaluate experimental data.

UNLV hosted, and students and faculty attended, an Advanced MCNPX Workshop at UNLV. As a result, the group was able to greatly improve statistical results of calculations of electron-photon-neutron transport.

High-power Target Design

A new high-power, uranium-containing water-cooled target for the RACE Project was designed, constructed and tested. The design included a tungsten electron-photon converter, an aluminum cooling shroud, and aluminum-clad natural uranium photon-neutron converter. After analyzing and constructing a prototype of a compact version of the Cooled Electron Target — Optimized for Neutron production (CETON), it was determined that a design change was needed. The new design includes a multiple plate tungsten electron-photon converter, an aluminum cooling shroud, and a cavity for inserting an aluminum-clad natural uranium photon-neutron converter. The CETON was assembled in Nevada and successfully leak tested with high-pressure water. The finished High-Power RACE (CETON) Target was then assembled and tested at the Idaho Accelerator Center with lead beads substituted for the uranium rod. Thermal and neutron production performance with an electron linac were measured.

As a result of their design, acquisition, fabrication, and construction, the students won the UNLV Mechanical Engineering Senior Design Competition for their design of the High-Power RACE Target.

The High-power RACE Target was transported to ISU's IAC in August 2006 for further tests to measure neutron generation and heat transfer while coupled to an electron linac. An accelerator-driven neutron production experiment was conducted and temperatures were recorded at several points. Since completing the experiments, experimental results are being evaluated. The Target is being modeled using Gambit and the CFD code FLUENT for comparison with experiments. During this reporting period, the potential complexity of the CFD modeling was upgraded with a parallel processing system. Refinement was continued of the MCNPX transport model to reduce statistical uncertainty and to perform parametric studies to study impacts of accelerator performance and characteristics, such as beam spread in energy or position.

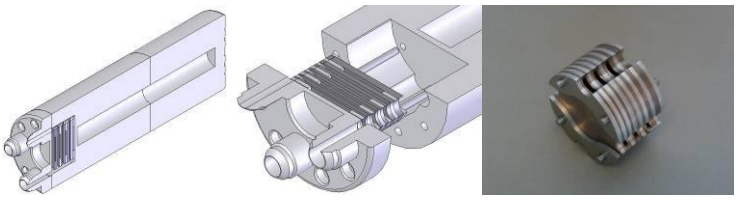

High-power RACE Target. The left is a cutaway drawing of the full assembly as assembled showing the target, water cooling channels, and electron-to-photon converter plates. The middle picture is a close-up of the plate assembly and water cooling channels. At the right is a photograph of tungsten-copper converter plates and spacer assembly with alignment pins.

Reactor Physics Studies

A variety of code systems for modeling neutron generation and transport and thermal feedback effects in accelerator-driven TRIGA as well as other reactors were evaluated. Code systems considered were ERANOS, RELAP, PARCS, and APOLLO. Modeling with MCNPX was initiated in support of subcritical experiments at the Idaho Accelerator Center and of target design studies for Texas RACE. Electron beam/target interactions were studied for maximizing and characterizing photoneutron production from high-energy electrons.

Experiments

UNLV collaborated with ISU and CEA in a series of accelerator-driven subcritical (ADS) experiments at the Idaho Accelerator Center. A fuel loading/criticality measurement experiment was conducted in the ISU RACE Subcritical Assembly (SCA). This measurement was followed by a series of ADS experiments using a low-power, 20-MeV electron accelerator coupled to the SCA with a tungsten-copper neutron generating target. Results are being analyzed.

Full-core ADS experiments were conducted at ISU in a compact, subcritical assembly that was constructed at the ISU and fueled with a modular core. Accelerator-coupled experiments with the TRIGA reactor at the UT-Austin were also conducted beginning summer 2005, and were completed in March 2006. The most extensive experimental program was conducted at ISU, where accelerators were assembled, the beam-target neutron generators were developed, a subcritical assembly was licensed and constructed, and RACE tests were conducted for more than two years. These experiments are described in a wide array of papers.

An accelerator was constructed at ISU, shipped to Texas, and installed in the summer of 2005. It was assembled in a cave at the floor level of the UT Nuclear Engineering Teaching Laboratory (NETL), adjacent to the NETL TRIGA reactor. This reactor can operate at 1 MW_{th}, and can produce pulses up to 1000 MW_{th}. The accelerator target was placed immediately adjacent to one side of the core, centered on that side.

The first UT experiments were conducted with the reactor completely shut down with a criticality of about 0.92, similar to the criticality at ISU experiments. Follow-on experiments were conducted with k_{eff} between 0.92 and 0.95 to possibly 0.97, 0.98, or even critical. Measurements were made with flux wires, fission chambers, and other detectors. In addition, beam diagnostics and monitoring techniques were developed at UT to improve the performance of the linac/target system.

Components of the CETON (Cooled Electron Target — Optimized for Neutron production) excluding tungsten-copper disks for converting electrons to photons. The W-Cu disks fit in the cavity at the upper left. In addition, the body is bored to accept a 10" aluminum-clad uranium photo-neutron generator.

Task 28 Impact of the Synthesis Process on Structure Properties for AFC Fuel Candidates – Dr. Ken Czerwinski

Background

Advanced Fuel Cycle Initiative research on transmutation fuels includes mono-nitride ceramic fuel forms, and consists of closely coordinated "hot" actinide and "cold" inert and surrogate fuels work. Matrix and surrogate materials work involves three major components: (1) fuel matrix synthesis and fabrication, (2) fuel performance, and (3) fuel materials modeling. The synthesis and fabrication component supports basic material studies, as well as actinide fuel fabrication work through fuel fabrication process development. Fuel performance studies are examining the tolerance of nitride-type fuel to heavy irradiation damage. The fuel materials simulation work involves both atomistic and continuum scale modeling employing first principles, molecular dynamics, and thermo-chemical calculations. This modeling work is closely integrated with fuel design and experimental work where it provides prediction of phase transformation and stability, reaction kinetics, radiation damage mechanism and tolerance, and fission product retention. Results for fuel fabrication and radiation tolerance studies based on the proposed ZrN fuel matrix material will be reviewed as well as experimental surrogate studies for volatilization and phase stability. The actinide fuel effort at LANL emphasizes synthesis and fabrication of actinide-bearing nitride fuel pellets. These pellets are designed to be inserted into the Advanced Test Reactor and contain varying amounts of Pu, Am, Cm, and Np.

Presently, fuel materials simulation work which involves atomistic and continuum scale modeling, molecular dynamics, and thermo-chemical calculations are based on a theoretical understanding of crystal structure and microstructure of inert matrix fuels. This task's contribution is to provide real structural data on surrogate and radioactive fuels. Crystallographic properties are being determined and nano structures of oxide-based and nitride-based fuels, as considered for next generation reactor fuels, are being imaged after applying different synthesis routes. The chemical behavior of the ceramics under repository, reprocessing, and reactor conditions will be examined. Two fully equipped sample preparation laboratories can be taken advantage of, one for the preparation of surrogate fuel, and one for the preparation of radioactive fuel specimens.

Synthesis of actinium mononitrides using carbothermic reduction of the corresponding oxides has a few outstanding issues, including the formation of secondary phases such as oxides and carbides and low densities of the final product. Furthermore the requirement of a high process temperature at 1700°C, for more than 12 hours is also a drawback particularly for Americium-bearing samples. Therefore, it is important to explore the use of other possible routes to synthesize actinide mononitrides.

A low temperature process is used in this research to produce actinide mononitrides using a fluoride route in which the first step is to mix the actinide oxide with NH_4HF_2. The second step involves the heat-treatment of the resulting ammonium actinide fluoride salts in ammonia atmosphere. Using different analytical techniques available, the experimental conditions can be studied and optimized to synthesize the required materials with high phase purity. Such available techniques are X-ray Powder Diffraction (XRD), Thermogravimetry and Differential Scanning Calorimetry (TG/DSC), and microscopic techniques such as Scanning Electron Microscopy (SEM) and Transmission Electron Microscopy (TEM). Once the experimental conditions are studied and optimized, a number of actinide nitride systems (uranium, thorium, and neptunium) will be synthesized and characterized to provide knowledge on the chemistry of the systems. Characterization of these nitride systems will include chemical phase identification, lattice parameter refinements, morphological studies, microstructural verifications, thermal behavior, reaction mechanism, and reaction kinetics.

Research Objectives and Methods:

- Installation of sample preparation equipment for radioactive fuel samples to allow the manufacture of high quality polished microscopy samples and electron transparent TEM specimens.
- Literature research on Inert Fuel Matrix (IMF) fuels.
- Optimized synthesis of oxide fuels in the system ZrO2 – Er2O3 – UO2.
- Synthesis of nitride fuels in the system ZrN-ErN-UN by carbothermic reduction / nitridization.
- To explore a low-temperature fluoride route to synthesize actinide nitrides.
- To characterize actinide nitrides structurally and thermally.
- To use high resolution TEM techniques to explore the microstructure of the radioactive samples.

Research Accomplishments:

Oxide fuels have been successfully synthesized in the system ZrO_2-UO_2-$ErO_{1.5}$ as phase-pure solid-solution phases of $Zr_{1-(x+y)}U_xEr_yO_{2-(y/2)}$ for $0.3<(x+y)<0.45$. The oxide phase $Zr_{1-(x+y)}U_xEr_yO_{2-(y/2)}$ is showing a linear increase in the lattice parameter as the substitution of U+Er for Zr progresses and the lattice parameter *a* increases from 5.2070(3) Å for (x+y)=0.3 to 5.2507(3) Å for (x+y)=0.45.

Prototype Zirconia-based ceramic fuel in the System ZrO_2-$ErO_{1.5}$-UO_2 was produced through dry chemical processing. The synthesis was completed after annealing at 1700°C for 24 hrs to 48 hrs in inert/reducing atmosphere.

Ceramic Nitride Fuel in the System ZrN-ErN-UN

The synthesis of radioactive nitride fuel in the system ZrN-ErN-UN through carbothermic reduction/nitridization led to the formation of a ZrN-based solid solution phase and UN_2-based solid solution phase, indicating different affinities of zirconium and uranium to nitrogen. An electron-transparent TEM specimen was prepared and the structure of the ceramics could be imaged with highest resolution. Ceramic ZrN surrogate fuel samples (provided by LANL) were analyzed by TGA/DSC thermal analysis in the temperature range of 25°C to 1400°C in N_2 atmosphere, and changes in phase constitution and crystal structure were analyzed by XRD-Rietveld analysis and by TEM. One of three ZrN samples exhibited an exothermal reaction at about 1169°C while all samples gain about 1% in weight associated with the formation of Zr_2ON_2 and increased cubic zirconia contents.

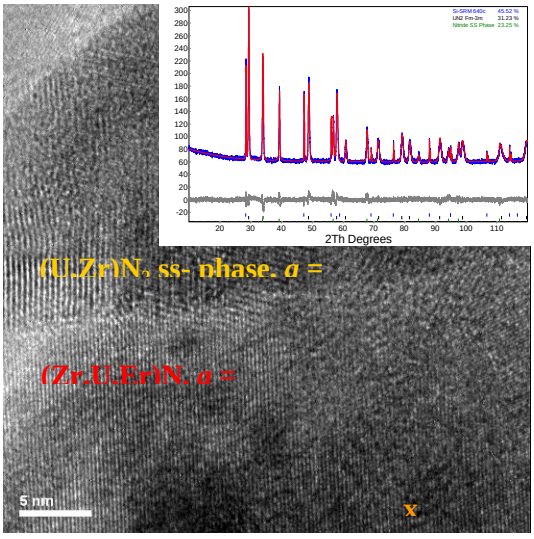

High resolution image of Zr-Er-U-N ceramic nitride fuel after carbothermic reduction/nitridization of an oxide solid solution. An interface between two solid solution phases can be observed. The radioactive ceramic TEM sample was prepared using an ultra-microtome. The phase constitution was confirmed by XRD/Rietveld Analysis and the crystallographic parameter refined. The image is 1,000,000 times magnified.

Ceramic Nitride Fuel in the System ZrN-ErN

The carbothermic reduction / nitridization of $Zr_{0.7}Er_{0.3}O_{1.85}$ lead to the formation of $Zr_{1-x}Er_xN$ (lattice parameter a = 4.6085(3) Å) and $(Zr_{1-x}Er_x)_2(N,O)_3$ (lattice parameter a = 10.940(1) Å). As a result, the solubility e.g. of rare earth elements in nitrides is significantly lower than in the precursor oxide system, which can result in phase separation while applying carbothermic reduction / nitridization. In order to closer study and to quantify these phenomena focus was placed on solubility limits of erbium (a designated neutron poison) in zirconium nitrides. The solubility limit of erbium in zirconium-mononitride surrogate fuel at 1700°C was determined. Therefore a mono-phase $Zr_{0.7}Er_{0.3}O_{1.85}$ precursor oxide-solid solution was synthesized and treated at 1700°C for 20h in purified nitrogen atmosphere. The phase constitution and the phase compositions of the equilibrium phases were determined quantitatively using XRD/Rietveld analysis and especially electron microprobe analysis. The impact of erbium solubility on the crystallographic parameter of ZrO_2 and ZrN was determined. Four samples of the solid-solution phase $Zr_{1-x}Er_xO_{2-x/2}$ for $0.02<x<0.12$ were synthesized and their lattice parameter were determined by XRD/Rietveld analysis. The solid solution phases in the system $Zr_{1-x}Er_xO_{2-x/2}$ were treated by carbothermic reduction/nitridization to further determine the impact of erbium solubility on the crystallographic parameter in ZrN-based mononitrides. The phase constitution of the mononitride system $Zr_{1-x}Er_xN$ was determined. The solubility limit for erbium in the system $Zr_{1-x}Er_xN$ was measured to be $0.07<x<0.10$.

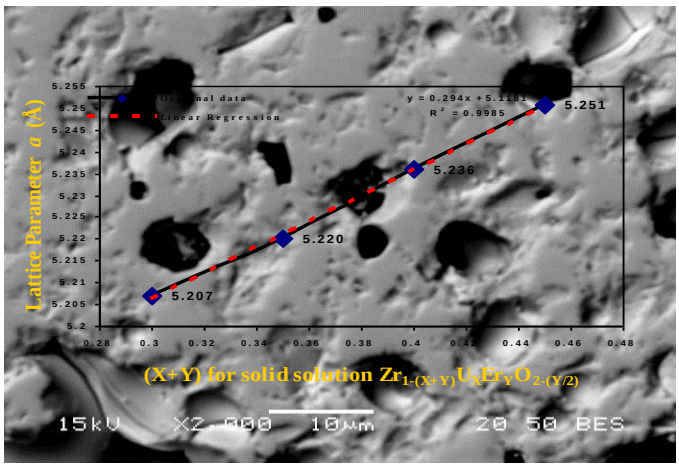

Oxide fuel sample in the system Zr-U-Er-O by Scanning Electron Microscopy, BES, 2,000 times magnified. The oxide fuels do not contain domains or impurities. The lattice parameter a in the solid-solution phases $Zr_{1-(X+Y)}U_XEr_YO_{2-(Y/2)}$ increases linearly with the substitution of uranium and erbium for zirconium.

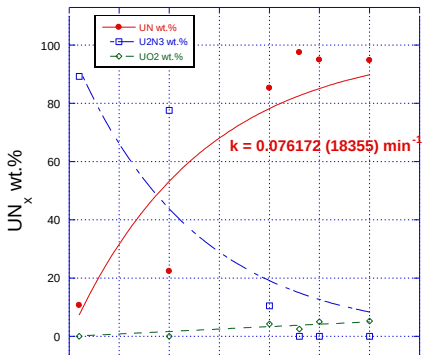

Pseudo-first-order kinetics of UN_2 denitriding at 1100°C.

Production of TRISO-type fuel kernels by Sol-Gel Method

The first spherical precursors for the potential production of TRISO-type kernels could be produced and - after calcination - kernel sizes between 400 mm and 320 mm were measured. For now the spheres show poor isotropy. Some kernels are hollow and the overall kernel quality has to be improved much further.

Uranium based nitride synthesis and characterization

The fluoride route was successfully used to synthesize three uranium nitride samples with different stoichiometry (UN_2, U_2N_3, and UN). Experimental conditions were optimized to synthesize high phase purity UN (97 wt.%). Thermal decomposition of UN_2 under different atmospheric conditions was also studied, and ultra high purity argon could successfully be used to reduce the sample completely to UN at 1100°C, see graph on the opposite page. UN_2 and U_2N_3 decomposition kinetics into UN were studied under argon at three different temperatures (1000, 1050, and 1100°C).

Optical microscopy and SEM were used to explore the morphology of uranium nitride samples. Bright Field Transmission Electron Microscopy was also used to confirm the morphological observations. Microstructural studies of the samples were carried out using high resolution (HR) TEM with the help of selected area diffraction (SAD) patterns. X-ray energy dispersive spectrometry of TEM was utilized to characterize the elemental distribution and to verify the phase purity of the samples. Powder XRD patterns of the as-synthesized uranium nitrides, UN_2, U_2N_3, and UN were collected and analyzed. Optical microscopic studies showed that the particle sizes of these uranium nitride samples range from 100 to 5000 nm. The microstructure of the UN sample shows the presence of UO_2 as a secondary phase on the surface of the sample. In this region, the lattice fringes correspond to the (222) interplanar *d*-spacing of UO_2. X-ray Energy Dispersive Spectrometry (XEDS) demonstrated that U was prominent, but it is difficult to identify the presence of N due to overlaps with peaks from O and C. However, the magnified XEDS spectra verifies the presence of N in samples, and this figure also displays the presence of O only in the UN sample. Thus, the XEDS verifies the phase purity of the synthesized sample.

Thorium based nitride synthesis and characterization

Use of the fluoride route was successful only up to the formation of ThNF. The removal of fluorine, which should have lead to the formation of thorium nitrides was unsuccessful at different experimental conditions. However, the characterization of ammonium thorium fluoride and ThNF was done using the above mentioned techniques.

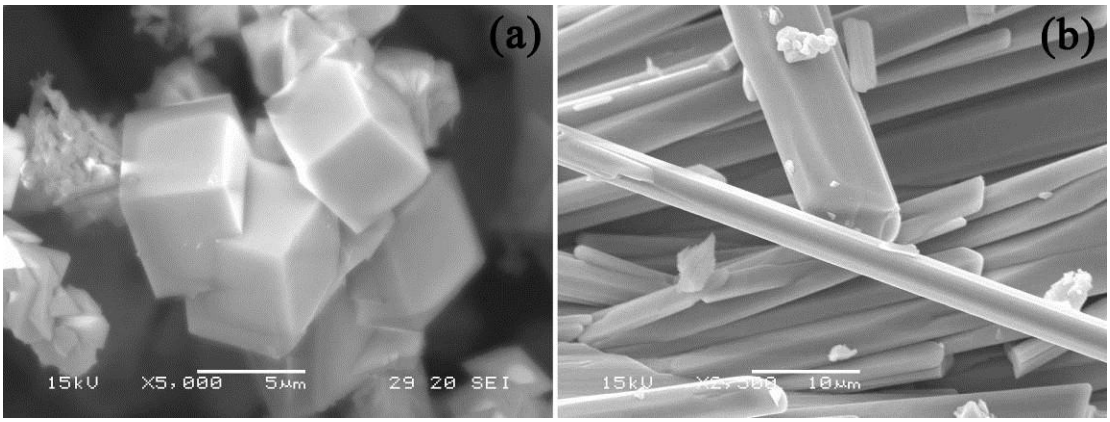

Scanning Electron Microscopic images of the (a)$7NH_4F.6UF_4$ and (b) $(NH_4)_4ThF_8$ samples. (a) $7NH_4F.6UF_4$ particles are well-crystallized (hexagonal unit cell with a rhomb-centered, a (b) = 15.40 Å and c = 10.49 Å and UN_2 is cubic (fcc) with a = 5.310 Å) (b) Well-crystallized $(NH_4)_4ThF_8$ acicular-shaped particles (triclinic unit cell with lattice parameters a = 8.477, b = 8.364, and c = 7.308 Å).

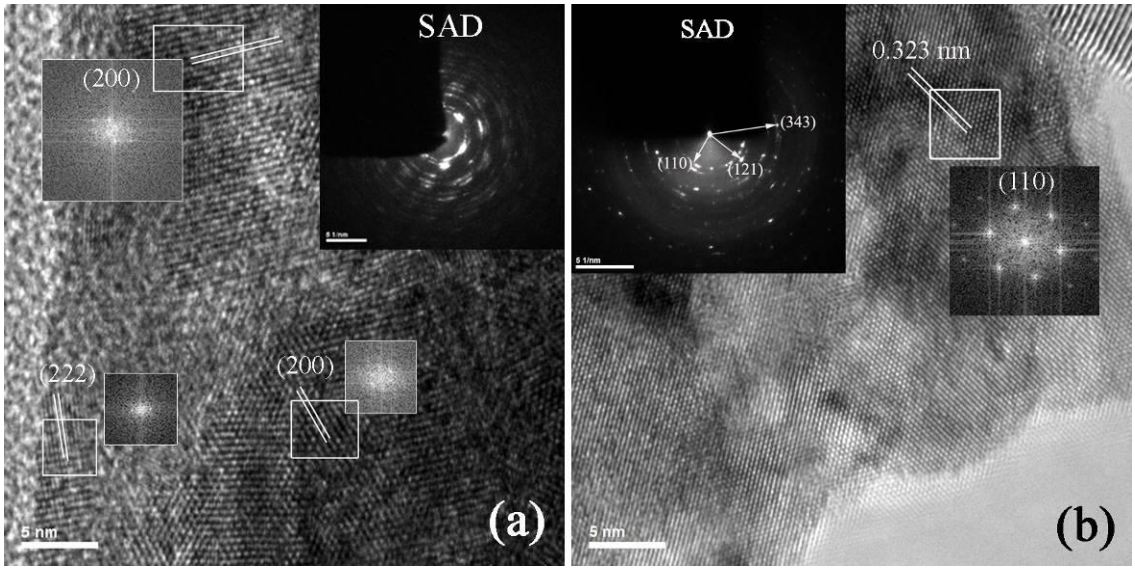

High resolution TEM images of (a) UN and (b) ThNF samples. (a) Crystallography of UN was confirmed using the lattice fringes of HRTEM image, and the secondary oxide phase was only identified at the surface of the particle edge. (b) ThNF crystal structure which is determined using XRD was confirmed by the HRTEM and SAD pattern.

Task 29 Investigation of Optical Spectroscopy Techniques for On-Line Materials Accountability in the Solvent Extraction Process – Dr. Gary Cerefice, Dr. Ken Czerwinski

Background

Increasing the proliferation resistance of the nuclear fuel cycle is one of the stated goals for the Global Nuclear Energy Partnership program. From a proliferation aspect, the greatest challenge to closing the nuclear fuel cycle is ensuring that nuclear material is not diverted during the recycling processes. As part of the safeguards-by-design concept, new separations facilities will incorporate integral systems capable of providing materials accountability for the actinide elements to minimize the potential for undetected diversion of material. The goal of this project is to evaluate technologies to meet this need. Optical spectroscopic techniques, such as Ultraviolet-Visible Spectroscopy (UV/Vis) and Laser Fluorescence Spectroscopy (LFS), are quantitative analytical techniques that have been used for measuring the concentration of the actinides under laboratory conditions.

In UV/Vis spectroscopy, the sample is illuminated by a continuous spectrum (from the UV through the Visible wavelengths). The transmitted light is measured, allowing the determination of the absorbance of the light as a function of wavelength. The wavelength of the absorbance is dependant on the electronic structure of the absorbing atom, and is proportional to the concentration of the absorbing element in the sample. For LFS, the sample is illuminated at a single wavelength, which is absorbed by the target atoms in the sample. The energy absorbed is re-emitted through fluorescence. The wavelength of the absorbance,

and the fluorescence-response, is again dependant on the electronic structure of the absorbing atom, and is proportional to the concentration of the absorbing element in the sample.

Both techniques are strongly dependent on the chemical speciation of the elements to be measured, providing a tool for not only the determination of material concentrations for mass balances, but also providing inspectors and plant operators with a tool to examine the process chemistry itself. As optical techniques, both of these methods can be adapted for fiber optics, allowing the instrumentation to be placed in shielded areas of the plant to minimize the impact of the radiation fields on the detectors and increase the accessibility of the systems for maintenance and inspection.

Research Objectives and Methods:

The goal of this project is to evaluate the application of these analytical techniques to the on-line, real-time measurement of the actinide elements in the process streams of a solvent extraction process, with particular attention to the UREX+ and PUREX processes. Based on the experience gained through this effort, engineers will have the information necessary to decide if these technologies should be advanced to the prototype stage and tested at the pilot plant level. Through the experimental work planned as part of this effort, researchers will also develop a better understanding of the chemical interactions of the actinide elements, providing additional data for the development of first-principles based models of the solvent extraction process. The information gathered through these experiments will also add to the database on the UREX+ solvent extraction process, particularly in the off-normal operating regimes.

The research objectives are:

- To evaluate the potential for utilizing UV-Visible and laser fluorescence spectroscopy to determine actinide concentrations under process conditions, including the spectroscopic impact of acid concentration, solvent vs. aqueous product streams, ligand concentrations (TBP, AHA), and chromophoric agents (e.g. iron) from fission products or corrosion/degradation products.
- To examine what process chemistry information can be extracted from the spectroscopic signals along with the actinide metal concentrations.
- To examine the fundamental chemistry underlying the spectroscopic behavior under process conditions in support of process chemistry modeling activities.

Research Accomplishments:

To evaluate the potential application of UV/Visible spectroscopy for the determination of uranium in the aqueous process streams of the UREX process the impact of process chemical conditions on the absorbance behavior of the uranyl ion was examined. The process streams of interest are distinguished by three main variables concentration, and ligand concentration (NO_3^-, AHA). General trends were observed in the molar absorptivity constants as conditions were varied. The most noticeable changes occurred as the nitrate concentration was increased. The figure on the opposite page shows the effect of increasing nitrate concentration at constant metal and acid concentrations. There is a large change in the molar absorptivity constant as the concentration of the free uranyl ion is decreased and two or more uranyl nitrate solution complexes become dominant. An accompanying shift in the uranium spectrum, as well as a wavelength shift at the peak intensity was observed as the nitrate concentration was increased from 2 M to 8 M.

The UREX feed stream and uranium product will both have molar quantities of uranium present. The concentration of uranium in these streams is expected to exceed the linear range of detection for a 1 cm path length cell, which will require either the reduction of the path length or the dilution of the feed prior to analysis. In designing the equipment train for the recycling plant, a slip stream could be extracted from the feed or uranium product streams for analysis. This slip stream could easily be mixed in a controlled mass ratio with a diluent stream of nitric acid or passed through a reduced diameter section to provide a significant reduction in path length.

The raffinate and technetium streams are expected to have significantly lower concentrations of uranium. The primary differences in these streams are the nitric acid concentrations and the presence of AHA in the

raffinate stream. In these streams, the expected concentrations will likely fall below the detection limits observed for a 1 cm optical path.

In addition to the potential applications for direct, on-line concentration measurements, UV/Visible spectroscopy may also provide analysts with the ability to directly observe process chemistry. From a proliferation resistance point-of-view, two observations show immediate promise. By examining the absorbance spectrum, it should be possible to detect the conversion of a recycling plant from the UREX process, which does not separate plutonium, to the PUREX process, which does result in a purified plutonium product due to the associated increase in molar absorptivity along with a change in peak shape. The spectrum loses individual peaks and is replaced by one broad, flat peak. This change in process chemistry could also be detected in the raffinate stream. The presence, or absence, of AHA in the raffinate stream becomes significantly more pronounced as the pH of the analyzed stream is increased. By titrating a slip stream from the raffinate product stream to higher pH, and comparing the observed spectrum to one from a second, unaltered slip stream, the presence of AHA in the raffinate can be confirmed.

To evaluate the potential application of optical spectroscopy techniques for the determination of uranium in the aqueous process streams of the UREX process, the impact of process chemistry on the absorbance and fluorescence behavior of the uranyl ion was examined. For the UREX flowsheet, the potential areas for deployment of these techniques was divided into four categories, based on the chemical environment, each represented by a feed or product stream: the process feed, the raffinate (actinide/fission product) stream, the technetium product stream, and the uranium product stream. These process ranges also allowed researchers to examine the potential application of these technologies to a PUREX-based flow sheet as well.

UV/Vis Spectroscopy

The UREX feed stream and uranium product will both have molar quantities of uranium present. The concentration of uranium in these streams is expected to exceed the linear range of detection for a 1 cm path length cell. To measure these high concentration streams by UV/Vis, plant designers would need to either insert a reduced path-length slip stream or add the capability for a fixed mass dilution in the slip stream. Either of these options, or more realistically the combination of the two, could reduce the absorbance in the system back to within the linear response range of the technique.

The raffinate and technetium streams are expected to have significantly lower concentrations of uranium. For the UREX process, the raffinate stream will also contain the AHA from the process. Based on the measured molar extinction coefficients for uranium under the chemical environments expected for these streams, the expected uranium concentrations will likely fall below the detection limits observed for a 1 cm optical path. While the limits of detection may be able to be extended with a longer path length, scattering and other phenomena would likely only limit this to an order of magnitude reduction in the detection limit. Even with these limitations, the technique could still be used to establish a threshold value for uranium, which may be useful in detecting changes in process chemistry. UV/Vis spectroscopy, combined with titration by a fixed mass of a caustic stream, can also be used to probe for the presence of AHA in the raffinate stream, allowing for independent confirmation that the plant is running the UREX flowsheet and has not switched to a plutonium extraction process (such as PUREX).

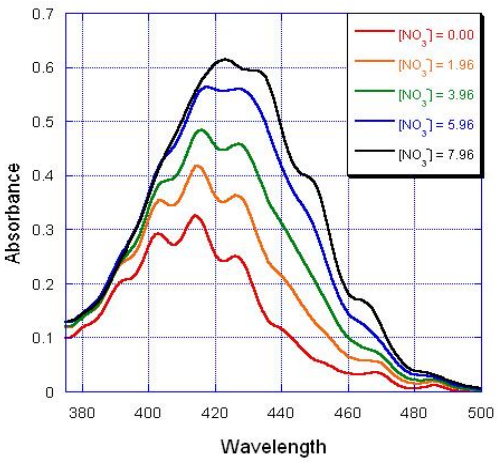

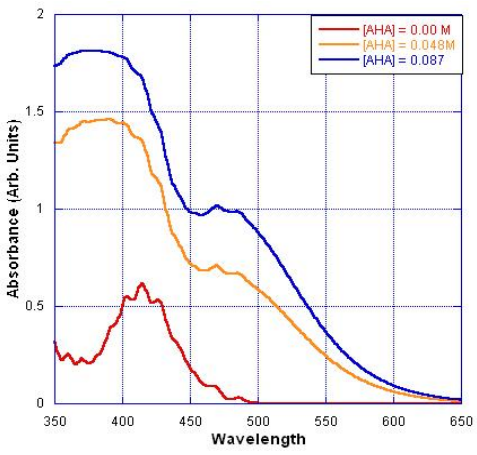

Effect of increasing nitrate concentration on uranyl spectra. $[UO_2^{2+}]$ = 0.047 M, $[H^+]$ = 2.0 M

Effect of increasing AHA concentration on uranyl spectra at pH=2. $[UO_2^{2+}]$ = 0.094 M, $[NO_3^+]$ = 1.2 M

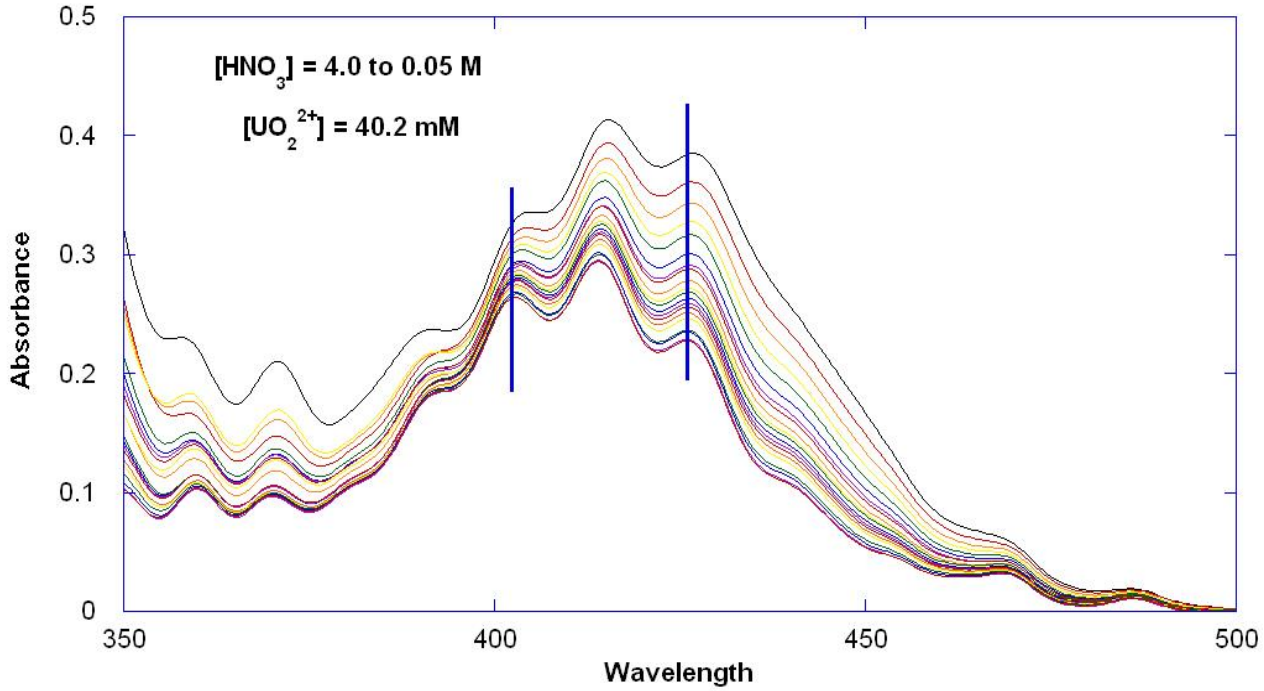

Impact of process conditions on uranium absorbance spectrum. Blue lines indicate peaks used for determining nitrate for the Peak Ratio Methodology.

Laser Fluorescence Spectroscopy

The primary focus of the year two work on the project was the evaluation of Time Resolved Laser-induced Fluorescence Spectroscopy (TRLFS) techniques for the determination of uranium under process conditions. The impact of process chemistry on the observed lifetime and fluorescence yield of uranium in the aqueous process streams was investigated. TRLFS was determined to be significantly more sensitive for the detection of uranium, so much so that the signals in the feed and uranium product streams would easily saturate the detection systems. This sensitivity, however, may make the technique ideal for observing streams where the uranium concentration is expected to be very low, such as the technetium product stream and the raffinate stream. The detection limits and linear response regimes for both these process streams have been examined.

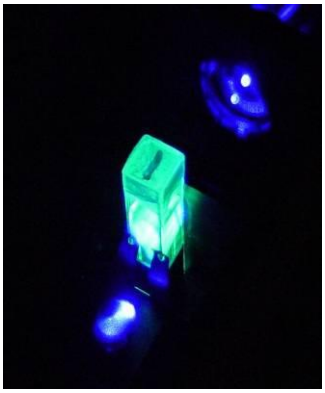

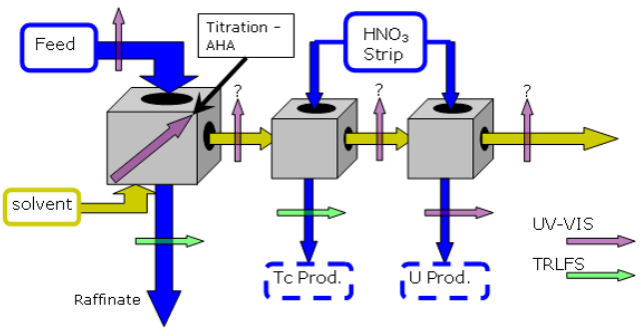

Laser induced fluorescence of a uranium sample in nitric acid

Potential Application Locations for Optical Spectroscopy in the UREX Flowsheet

Data Analysis

Deviations in nitrate concentration from the expected process chemistry result in an increase in uncertainty in the measured uranium concentration. Not only do these deviations in process chemistry increase measurement uncertainty, but they also reveal a systemic bias on the measurement that could be exploitable in a potential diversion scenario. Further efforts have focused on reducing measurement uncertainty in the determination of uranium concentrations under process conditions and on measuring the nitrate concentration spectroscopically for process monitoring applications.

To address this concern, the research team developed a new analytical method, the Peak Ratio Method (PRM) to simultaneously determine the nitrate concentration and uranium concentration in the system. Taking advantage of modern solid-state detectors to measure the full uranium absorption spectrum (instead of a single wavelength), the PRM utilizes the ratio of two secondary absorbance peaks to determine the nitrate concentration, which is then used to correct the uranium concentration measurement determined from the primary absorbance peak. By simultaneously determining the nitrate concentration and uranium concentration in the process stream, the systemic bias introduced into the uranium determination by deviations in process chemistry is eliminated and the uncertainty in the measurement itself is reduced.

Through the evaluation of the PRM as process conditions varied, it was observed that the uranium absorbance spectrum was unexpectedly dependant on acid concentration. As proposed chemical models for uranyl ion speciation in nitric acid systems do not include any acid dependant species, this observation further elucidates the need to better understand the fundamental chemistry underlying the solvent extraction processes. While the root cause of this effect still needs to be determined, an empirical relationship has been developed to correct the nitrate concentrations determined by the peak ratio method. Using this correction to the PRM, the bias introduced by acid concentration in the process stream can be greatly reduced. However, it does require the use of some other technique to determine acid concentration in parallel to the UV-Vis system.

Task 30 Combined Radiation Detection Methods for Assay of Higher Actinides in Separation Processes – Dr. Denis Beller, Dr. Charlotta Sanders, Dr. Warnick Kernan (Remote Sensing Lab)

Background

Monitoring of higher actinides (HA, includes neptunium, plutonium, americium, and curium) during the separation of used nuclear fuel has been identified as a critical research area in the Advanced Fuel Cycle Initiative. Recycling of used fuel by chemically separating it into uranium, fission products, and HA would be the first step in this new fuel cycle. Material Protection, Accounting, and Control (MPAC) is necessary for materials accounting, criticality monitoring, and assurance of proliferation resistance. The objective of this MPAC project is to develop technology to detect and accurately measure quantities of higher actinides in used fuel assemblies and processing systems without taking frequent samples. Process systems may include separations batches, pipelines, storage tanks, and fuel fabrication equipment. A variety of measurements may be combined to calculate flow rates of actinide elements with a to-be-determined precision.

In this MPAC project, faculty and students will investigate the potential to use combined neutron and gamma-ray detector systems to measure quantities and isotopic constituents contained during separations and intermediate storage. This will require knowledge of the nuclear and decay characteristics of materials

during processing, the development of conceptual designs of monitoring systems, radiation transport studies to develop an understanding of operational regimes, and experiments to confirm performance. In addition, both passive and active concepts will be investigated, including collaborations with the Idaho Accelerator Center (IAC) at Idaho State University (ISU) to use electron linear accelerators for producing photoneutrons in situ, for photon activation of HA, or for stimulating emissions processes (e.g. x-ray fluorescence).

Research Objectives and Methods:

In the MPAC project, faculty and students are investigating the potential to use combined neutron and gamma-ray detector systems to measure quantities and isotopic constituents contained during separations and intermediate storage. This will require knowledge of the nuclear and decay characteristics of materials during processing, the development of conceptual designs of monitoring systems, radiation transport studies to develop an understanding of operational regimes, and experiments to confirm performance. In addition, both passive and active concepts will be investigated, including collaborations with the Idaho Accelerator Center at Idaho State University (ISU) to use electron linear accelerators for producing photoneutrons in situ, for photon activation of HA, or for stimulating emissions processes (e.g., X-ray fluorescence).

Radiation transport and scoping studies will be conducted to investigate combined gamma-ray, neutron, and active and passive detection techniques to measure quantities and isotopic constituents contained during separations and intermediate storage. Scoping and design studies will first be performed using validated data sets (decay properties and reaction cross sections) and the radiation transport code MCNPX. Basic measurements will then be performed and compared to predictions. Planned experiments have not been conducted.

Research Accomplishments:

To initiate the AFCI MPAC Project, a kick-off meeting was held that included representatives and technical staff from the DOE, LANL, INL, ANL, PNNL, UNLV, ISU, and others. A collaboration with Los Alamos, which supplied safeguards monitoring equipment for the Rokkasho reprocessing plant in Japan, was initiated. UNLV faculty met with group leaders and technical staff at LANL in conjunction with the MPAC PI and others from Idaho State University to develop collaborations for monitoring systems development. They also met with N-1 Safeguards Science & Technology Group and N-2 Advanced Nuclear Technology Group. In addition, technical staff from N-1, N-2, and N-4 Safeguards Systems Group visited UNLV to discuss ongoing and potential MPAC projects, to tour labs, and to meet with students.

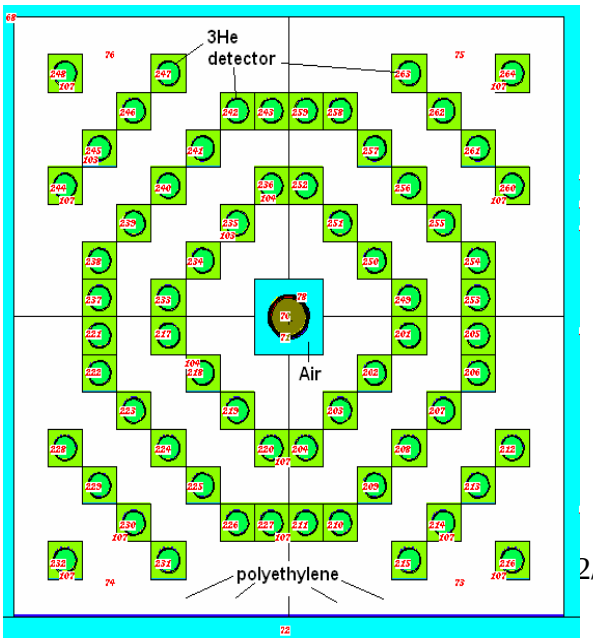

Cross section of NMDS surrounding a steel pipe

Lead and Carbon-based Slowing Down Spectrometers

Neutron slowing down spectrometers (SDSs) were modeled and plans were developed to conduct experiments at ISU with their carbon-based SDS. This work will be used to investigate technology for assaying fuel rods and/or complete assemblies. In preparation for these experiments, MCNPX was used to model neutron transport characteristics in lead and carbon-based SDSs. The energy of neutrons measured in a neutron detector with an SDS can be characterized by the equation $E = K/(t+t_0)^2$, where E is the energy of the neutron when it was created at the source (not its energy when detected), t is the time of the radiation detection (count) after a source event, and K and t_0 are characteristics of the particular SDS. Thus, if an accelerator pulse is used to generate neutrons which then initiate fission, the time history of the spectrum can be de-convolved to yield the energy spectrum. In addition, the neutron multiplicity can simultaneously be measured by the NMDS.

However, the detector system must be able to resolve the time dependence of the neutron signal. Because ^{3}He detectors, such as those contained in the NMDS, have a slow response, the SDS configurations must be studied before conducting experiments. Those studies are currently ongoing, beginning with benchmarking computational methods. A Los Alamos lead SDS was modeled to benchmark computational methods for determining energy-time correlation constants, and energy-time correlation constants are now close to those obtained in LANL experiments. The next step will be to use the MCNPX code to design an experiment using the ISU carbon-based SDS and electron linac, followed by experiments conducted at ISU in the next year. During this period, plans were developed to conduct experiments at ISU with the carbon-based SDS to develop technology for assaying fuel rods and/or assemblies.

In preparation for future experiments, MCNPX was used to model neutron transport characteristics in the Lead Slowing Down Spectrometer (LSDS) and the Carbon Slowing Down Spectrometer (CSDS). However, the detector system must be able to resolve the time dependence of the neutron signal. Because ^{3}He detectors, such as those contained in the NMDS, have a slow response, SDS configurations must be studied before conducting experiments. A Los Alamos National Laboratory (LANL) LSDS was modeled to benchmark computational methods for determining energy-time correlation constants. The benchmark exercise was completed and published. Multiplicity measurements for spontaneous fission and spontaneous-fission induced fission for isotopes of U, Pu, and Cf were verified within Monte Carlo statistical uncertainty limits. Simulations were conducted for other isotopes (Am, Np, and others) for multiplicity measurement experiments using a subset of the NMDS detectors.

In future work, the MCNPX code will be used to design an experiment using the ISU CSDS and electron linac, followed by experiments conducted at ISU. During this period, plans will be developed to conduct experiments at ISU with the CSDS to develop technology for assaying fuel rods and/or assemblies.

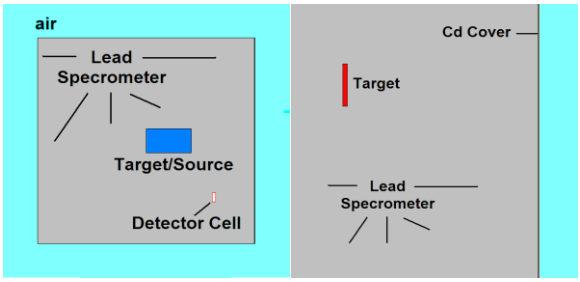

Cross sections of the UNLV benchmark of the LANL lead SDS taken from MXNPX models. (Left) The overall geometry, (Right) A close-up of a cross section of the thin target. The response to neutrons of various energies (time constants) is influenced by the position and isotopic composition of the detector

MPAC for UREX+ Processes

Another application of NMDS to MPAC might utilize the measurement of both passive and active neutron multiplicity in very dilute concentrations of higher actinides, such as in a non-actinide waste stream. This is being investigated since it may be more feasible to monitor where actinides are not supposed to be than where they are. The NMDS will be used to assay actinides in pipes, tanks, etc. in a UREX+ fuel separations plant to measure quantities and isotopic constituents in such a stream. Sources and configurations were investigated to simulate a waste pipe that contains residual higher actinides from UREX-plus for use in upcoming experiments.

Neutron Multiplicity Detector System

One technique that has been used in a variety of MPAC applications is neutron multiplicity measurement. This is the coincidence measurement of multiple neutrons that are emitted in individual fission events. A Neutron Multiplicity Detector System (NMDS) was previously built in collaboration with the V. G. Khlopin Radium Institute (KRI) in St. Petersburg, Russia (see Task 6). The system has since been extensively tested at UNLV and ISU. The NMDS is a modular system consisting of 64 ^{3}He detectors (tubes), electronics, and lead and polyethylene bricks. The modular nature of the system allows it to be used in a variety of configurations and for a variety of purposes. Examples are measurement of neutron multiplicity from high-power, high-energy spallation targets, detection of fissile materials in cargo systems or luggage, and assay of actinides in fuel or storage containers. Count rate and data acquisition capabilities of the NMDS were expanded in TRP Task 6, "Neutron Multiplicity Measurements for the AFCI Program." As part of Task 30, a new connector board was acquired to interface the remaining 32 detectors to the field programmable gate array (FPGA) board, such that the entire NMDS can now be operated with either the Russian DAQ or the new high-rate UNLV DAQ. Comparison testing was ongoing to the end of the project.

Several programming and maintenance issues with the NMDS that were revealed during testing in December were repaired or resolved. New detector wiring that was installed on one detector group of NMDS significantly reduced background count rates (noise). As a result, all of the standard cables were replaced with coaxial cables. In addition, as a result of differences in detector response between the original Russian data acquisition system and the new LabView-based system, detector response is being re-mapped with the data collection and analysis software. These improvements are expected to significantly improve the performance of the NMDS.

Modeling efforts were expanded to include the UNLV ^{3}He Neutron Multiplicity Detector System (NMDS, which was developed as part of Task 6) with multiple neutron detectors in up to four layers surrounding used nuclear fuel rods or assemblies. Modeling also included simulation of decay gamma rays for coincidence counting investigations.

Collaboration with the V.G. Khlopin Radium Institute (KRI) was developed for an upgrade to and maintenance on the Neutron Multiplicity Detector System. KRI completed design studies for a coincidence/anti-coincidence using a multi-plate plastic scintillator system to reduce background and provide greater neutron-muon discrimination. KRI procured components for the upgrade, installed them and coupled outputs to their NMDS channels, and began measurements in St. Petersburg, Russia.

In preparation for the KRI visit, the NMDS was reconnected to the original Russian data acquisition system and several neutron multiplicity counts were conducted to confirm its performance. The data files were

transmitted to KRI where they were evaluated. All detectors appear to be operating as they were when the system was initially delivered and set up at UNLV several years ago. Two specialists from KRI visited UNLV in November to service the NMDS; they cleaned and secured connections, replaced some parts, and adjusted bias voltages on some detectors.

A commercial control program was installed to automate the collection and storage of data on the 60-channel NMDS. It will automatically take data and has operated reliably since this upgrade.

Neutron Multiplicity Detector System configured in a cubic geometry for background and source counting.

Isotope	Resonance energy (eV)	K (keV*μsec²) LANL	K (keV*μsec²) UNLV
In-115	1.5	164	
Ta-181	4.3	161	148
Au-197	4.9	158	194
Ag-109	5.2	161.5	191
Ta-181	10.4	162	153
Ag-107	16.3	162.5	166
Cd-111	27.5	163	167
Au-197	59	159	174

Comparison of UNLV MCNPX computed time constants versus LANL's values for the LANL LSDS benchmark

Modeling

Data required for studying detection concepts includes elemental and isotopic constituents of discharged reactor fuel rods or assemblies, separations processes, storage systems, and fuel and waste-form fabrication systems. The RADDB code system, which is a user-friendly SCALE/ORIGEN-based code, was initially used to generate isotopic fractions for the higher actinides for initial scoping studies, in which the MCNPX radiation transport code system was used with the latest data libraries to model the NMDS. Elemental constituents of process flows and flow rates were later obtained from a detailed UREX+ flow sheet from ANL for use in designing conceptual detector systems. This information was then used in MCNP modeling. In one of these studies, the system was configured to surround a separations processing pipe to measure mixed transuranics. In addition, the effects of isotopic concentration on neutron multiplicity counting was studied. The NMDS model in MCNPX was reconfigured to surround a 2-inch process pipe containing actinides in solution (see the figure on the opposite page. Physical models were also assembled to ensure that there would be sufficient materials (e.g. polyethylene).

In addition to the NMDS, modeling of a germanium detector with MCNPX was initiated based on a report of similar work from Sandia National Laboratories. In addition, concepts for combined neutron-gamma and passive-active interrogation systems using the NMDS were developed.

Rensselaer Polytechnic Institute collaboration

Rensselaer Polytechnic Institute (RPI) collaborators investigated neutron slowing down spectroscopy for quantitative analysis of ^{239}Pu, ^{235}U and possibly ^{241}Pu in used fuel assemblies or rods. Several fuels, configurations, and parametric studies were modeled.

RPI completed various parametric studies to compare computed response to measurements in the LSDS. First order calculations were conducted with one fuel pin based on data from an AP1000 reactor. A detector was placed in the assay channel of the lead and the tally was convoluted with the ^{235}U fission cross section. This data was compared to experimental fission data for ^{235}U collected in the LSDS in 2007. Differences between calculated and experimental data are due to the broadening of the neutron energy resolution at lower neutron energies. Also, the reaction rate decreases as the slowing-down time increases, so that background becomes a larger factor as the neutron energy decreases.

Other RPI results:

- Simulation of ^{235}U fission chamber response was compared to measured data indicating that hydrogen content and impurities in the lead must be included to accurately simulate the measured response.
- Simulation of a single SPERT fuel pin and a ^{238}U assay detector were performed.
- Analysis of optimization and biasing methods for LSDS calculations demonstrated that, due to the nature of the LSDS, all areas of the lead as well as all neutron energies are critical to the problem and that even biasing the source will affect the resulting spectrum in the ^{238}U detectors.
- A model of an AP1000 fuel assembly was completed to study effects of self shielding within the assembly. These studies demonstrated that MCNP can produce results that agree with measurements of time-dependent fission rates in the LSDS; however, great effort must continue to be made to optimize the calculations. Particular effort must be made to increase efficiency to allow for smaller statistical error with a minimum of calculation time.

Rensselaer Polytechnic Institute's lead slowing down spectrometer (left), and a cross section at x = -37.5 cm showing the assay channel and fuel pin (the x axis is positive along the beam line).

Task 31 Decoupling and Disturbance Rejection Control for Target Circulation – Dr. Jian Ma, Dr. Joon Soo Lee, Dr. Woosoon Yim

Background

The Target Complex loop TC-1 was originally conceived as part of an accelerator-driven system (ADS) pilot plant that was designed and developed by the Institute of Physics and Power Engineering (IPPE) and Experimental and Development Organization (EDO) "Gidropress" in Obninsk, Russia, under the International Science and Technology Center Project #559 in 1998. It was to be used as the target in a 1 MW_{th} ADS experiment run off of the LANSCE proton accelerator at Los Alamos National Laboratory (LANL). When the U.S. transmutation program changed priorities from accelerator-driven systems towards nuclear fission reactors, the TC-1 loop was brought to UNLV to be developed as an academic research tool.

Liquid lead-bismuth eutectic (LBE) is employed as a spallation target, as well as a heat transfer fluid or coolant, in the TC-1 loop. The TC-1 loop can play a role as a testing facility in the U.S. to support research in heavy liquid metal coolant for the nuclear industry. During a thermal and engineering test of the TC-1 loop in 2005 at UNLV, it was observed that the existing control algorithm led to a very slow convergence to the target temperature setting, and also showed unstable oscillatory behavior. The existing algorithm was not robust enough to handle the complicated heating system of the TC-1 loop, where nine heating

zones or elements are compacted in one tight container. This interaction and coupling between each heating zone, as well as a heat disturbance from a low efficiency electromagnetic (EM) pump, caused the overall temperature control system to be complex and nonlinear.

Research Objectives and Methods:

The primary objective of this task was to study and modify the coupling effect between heating zones and the existing control algorithm to achieve precise temperature control in the TC-1 loop system. Safety concerns, the alarm system, and a user-friendly design became the secondary objective.

The TC-1 loop system has more than a single input and a single output, and it exhibits a nonlinear interactive property between the heater inputs and temperature outputs. For effective temperature control in multiple locations of the TC-1 loop, these nonlinear interaction terms must be eliminated (decoupled) in the control loop. Eliminating these interaction terms requires the identification of these interacting (coupling) terms. After successful elimination of the coupling terms, a closed loop control algorithm was designed which achieved the precise tracking of the temperature on multiple locations of the TC-1 loop under external temperature disturbance from an electromagnetic pump. One example of such an algorithm is a Proportional-Integral-Derivative (PID) control law. This law can easily be implemented within the existing LabView codes of the Monitoring, Controlling, and Scram Protection System (MCSPS).

In addition, the electromagnetic pump, used for molten lead circulation, becomes a large heat source. This, in particular, is due to its low efficiency. A "disturbance observer"-based control method was used to compensate modeling uncertainties as well as external disturbance. The disturbance observer regards the difference between the actual output and the output of the nominal model as an equivalent disturbance applied to the nominal model. The disturbance observer based control algorithm achieves a precise tracking of set temperatures despite the highly coupled thermal disturbance existing in the loop. Finally, the alarm system and a 24-hour monitoring and dial-out system was designed.

Research Accomplishments:

The performance of the TC-1 loop in 2001 at Obninsk, Russia and 2005 at UNLV was evaluated using available raw data. The processes of heating-up, cooling-down, non-circulation and circulation while running the EM pump were studied. The temperatures of different zones were not regulated well at the desired levels. The temperature of all zones should be controlled within the range of 190-200°C, however the temperature difference for all heating zones was approximately 80°C. This exceeds the safety range and has a high risk to cause thermal inhomogeneity.

The interacting terms between heater inputs and target temperature outputs in each zone were identified experimentally. These identified terms were then expressed in a discrete transfer function matrix. The system identification was carried out by heating up one zone from room temperature to 50 °C, while keeping others off. 50 °C was selected to avoid large temperature differences between zones. The transfer functions, which are used to describe dynamic response between individual inputs and outputs, were identified. One non-interacting (decoupling) control algorithm, based on the identified model, was developed to reduce the influences from each zone.

Significant improvement in the controller performance was achieved by upgrading the existing controlling algorithm. The heaters of all heating zones were well controlled to maintain the temperature of all zones within the desired range. The difference between maximum and minimum was only about 5 °C. In the previous algorithm, the temperatures of different zones were not regulated well at the desired levels. It is desired that the temperature of all zones should be controlled within a range of 190 to 200 °C. However, the temperature difference between all heating zones was about 80 °C. This exceeds the safety range and has a high risk to cause thermal inhomogeneity.

Wired to the main program, the 24-hour monitor device can automatically dial out when a TC-1 loop temperature is too high or there is abnormal current passing through EM pump. In addition, if the communication between computer and watch-dog is not connected, the alert signal will be sent out. The current transformers were assembled to detect actual heater on/off status. Signals from these current transformers were regulated and recorded by the data acquisition system for investigation.

TC-1 loop. The monitoring system for cooling fluid flow rate, temperature, and pressure was coded in the main program to make this main system sophisticated. The improved program will help to find the optimized parameter for the pump to continuously operate the TC-1 loop for extended periods of time.

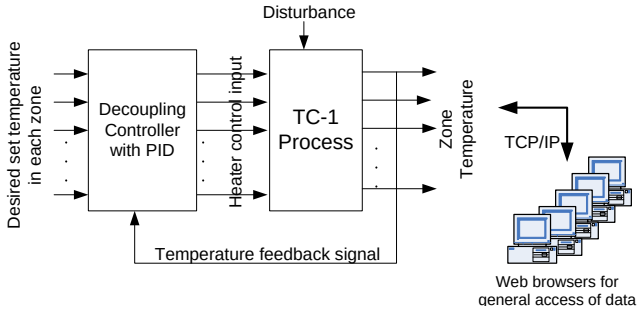

Overall control block diagram of the TC-1 system.

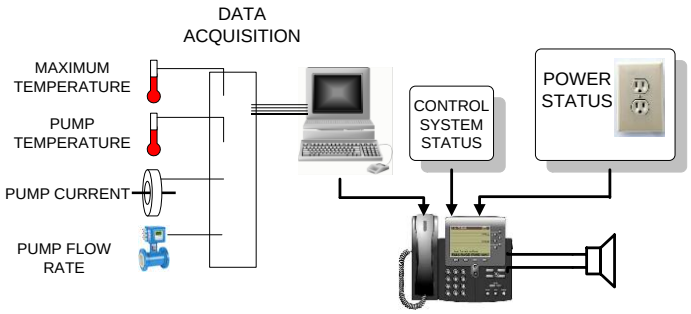

Diagram of the alarm and dial-out system.

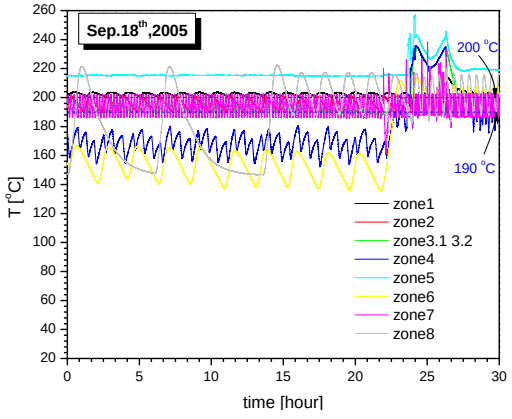

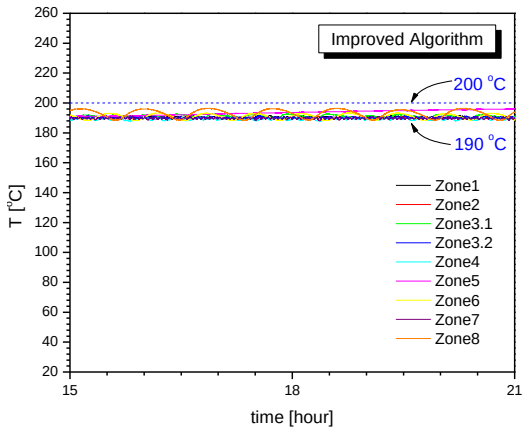

Temperature profiles of nine heating zones before algorithm improvement

Temperature response of nine heating zones obtained by the new algorithm

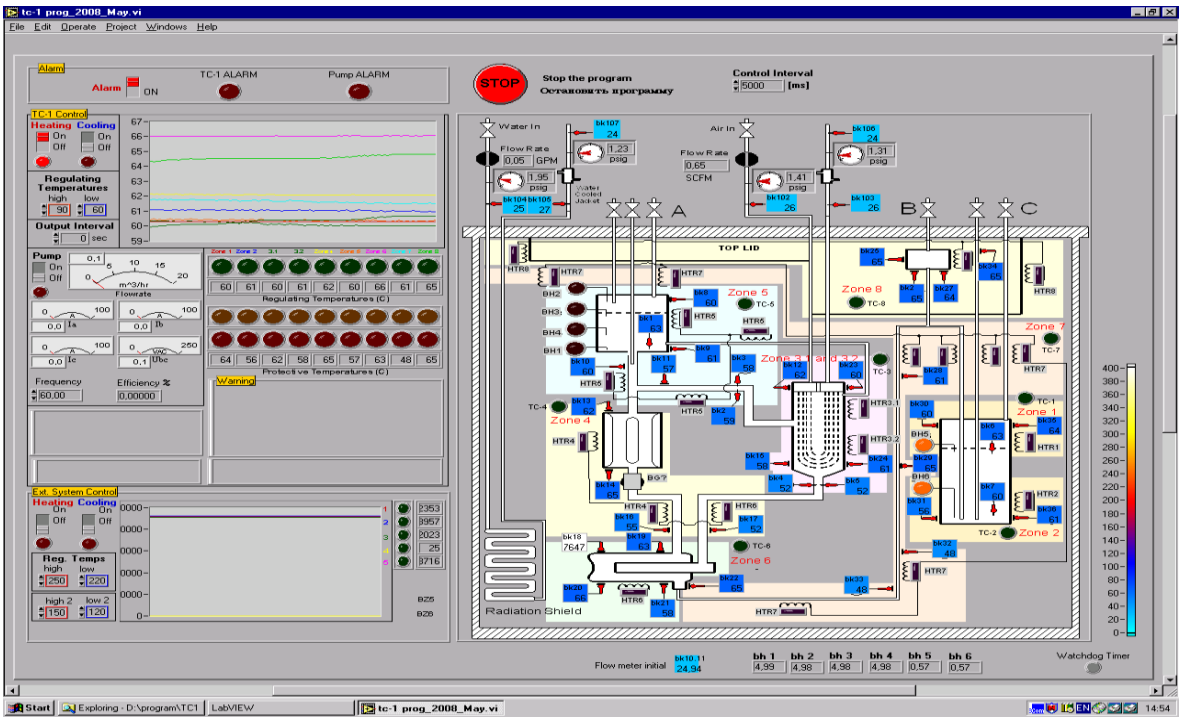

Interface of Control System for TC-1.

Task 32 Modeling and Design Algorithms for Electromagnetic Pumps – Dr. Dan Cook, Dr. Yitung Chen, Dr. Jian Ma

Background

Electromagnetic (EM) induction pumps are used in a number of nuclear energy related applications, such as circulation of molten lead-bismuth eutectic alloys in neutron targets, and circulation of liquid sodium metal in Gen IV Sodium-cooled Fast Reactors (SFR). Because EM pumps have no moving parts which can fail, they are considerably more reliable than conventional mechanical pumps for molten metal usage, and thus EM pumps are favored over mechanical pumps even though their pumping efficiency is lower and their initial cost is higher when compared to mechanical pumps of similar flow rates.

The figure below shows a cut-away picture of an annular, linear induction pump (ALIP), such as has been used in prototype SFRs and the Target Complex 1 (TC-1) loop at UNLV. These ALIPs consist of three main parts:

- an inner cylindrical core fabricated from a ferromagnetic material,
- an annular channel through which the liquid sodium flows, and
- an outer ferromagnetic core in which a set of inductor coils are embedded.

During operation, a 3-phase, alternating current travels through the inductor coils. This current produces a magnetic field which, in turn, induces a current in the liquid sodium in the pump annulus and inner core. Pumping forces develop in the liquid sodium due to the interaction of the magnetic field and the induced current, causing the liquid sodium to flow down the length of the annulus. The magnitude of these pumping forces, and hence the operational efficiency of the pump, is dependent on a large number of design parameters, including coil current and position, material selection for the inner and outer cores, and size of the annular gap.

Research on the design of EM pumps has been conducted by a number of researchers in Korea, Germany, Japan and Russia. No major papers on the topic have been published by researchers in the U.S. in the past 10 years. If the U.S. is to continue to maintain a research presence in nuclear power research and development, it is imperative that a solid foundation in EM pump design be developed by researchers within this country. The development of this foundation is the primary aim of this research task.

Research Objectives and Methods:

- A literature review of topics pertinent to EM pump design. These topics include the equations governing the physical phenomena occurring in EM pumps and mathematical algorithms used in modeling these physical phenomena, different EM pump configurations, and the effects of materials properties on pump performance.
- Development of computational models of the TC-1 loop at UNLV.
- Evaluation of the computational models through comparison with experimental data taken on the TC-1 loop.
- A parametric study of the TC-1 loop investigating the pumping efficiency as a function of operating conditions, materials properties, and geometric parameters.

Research Accomplishments:

<u>On-line EM pump literature database</u>

The on-line literature database has been available for over a year and now contains over 140 entries. New entries are added on a regular basis by the various researchers working on the project. Currently, this database can be found at:

http://nstg.nevada.edu/mmrg/research/LitSurvey/EMP-Literature.html.

<u>Computational Modeling</u>

Several preliminary models of EM pumps have been developed. The results published to date from this task have focused on the calculation of the EM phenomena (current density, magnetic field, and electromagnetic body forces) in the pump. The first of these EM models was an analytic formulation of Maxwell's equations, in which the magnetic vector potential was the primary solution variable. Use of the method of separation of variables and Fourier transforms allowed the expression of the magnetic vector potential to be expressed in an integral form that could then be solved numerically.

The second model was developed using Comsol, a MATLAB-based platform, and relies on the finite element method to discretize and solve the partial differential equations. The software can run the finite

element analysis together with adaptive meshing and error control according to a variety of iterative numerical solvers. The figures above and bottom right show a comparison of the radial and axial components of the magnetic flux density calculated in the pump from the analytic and numeric model. It should be noted that, in these calculations, the velocity of the liquid metal, which can have a significant effect on the magnetic field, was specified, not calculated via solution of the Navier-Stokes equations.

An analytic model of the EM phenomena in a generic ALIP has been developed using the method of separation of variables and Fourier transforms applied to the magnetic vector potential form of the induction equation. The model is written in Fortran and consists of a library of functions that calculate the various EM phenomena (magnetic vector potential, magnetic field components, Lorentz forces, induced current density distribution, etc.).

While working through these results, some of the earlier results from this project were revisited, in particular, the calculated values for the TC-1 pump efficiency. There are several ways to calculate the efficiency for an EM pump. One way, often referred to as the energy efficiency of the pump, is to divide the energy of the flowing fluid, i.e., pressure times flow-rate, by the energy it takes to run the pump, i.e., voltage times current. A second way to calculate the efficiency of an EM pump, often termed the effective real efficiency, basically relates the speed of the fluid to the speed of the traveling magnetic field. Both of these types of efficiency are illustrated below as a function of mass flow rate through the TC-1 loop. It should be noted that previously calculated efficiencies were always less than 1%, whereas the new calculations are all significantly above 1%. This discrepancy needs to be explored further and clarified.

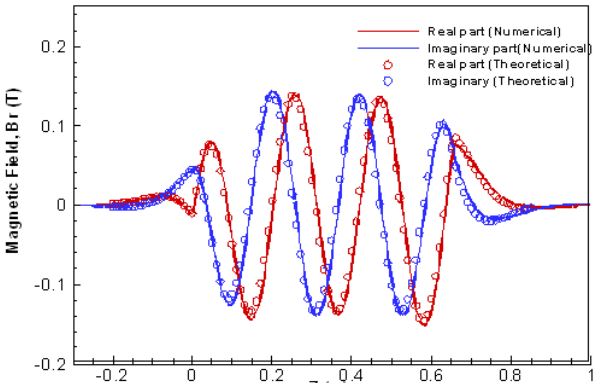

Comparison of the analytic and numeric calculations of the radial component of the magnetic flux density in the TC-1 pump along the pump axis.

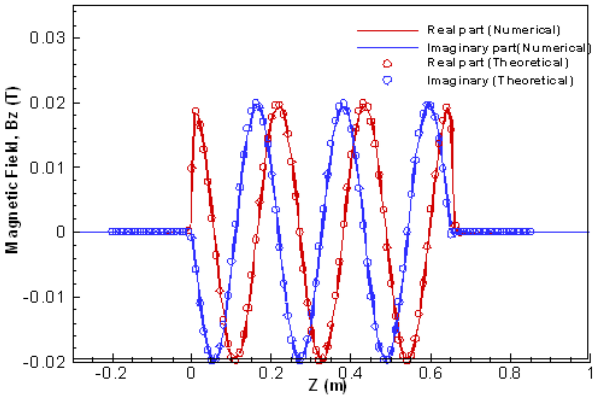

Comparison of the analytic and numeric calculations of the axial component of the magnetic flux density in the TC-1 pump along the pump axis.

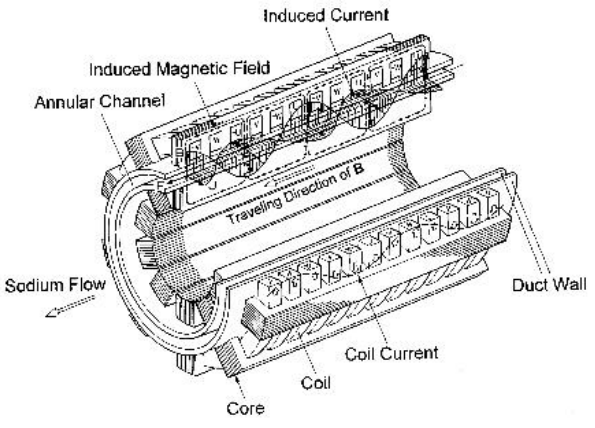

Cut-away picture of an annular, linear induction pump (ALIP)

TC-1 Loop laboratory located at UNLV.

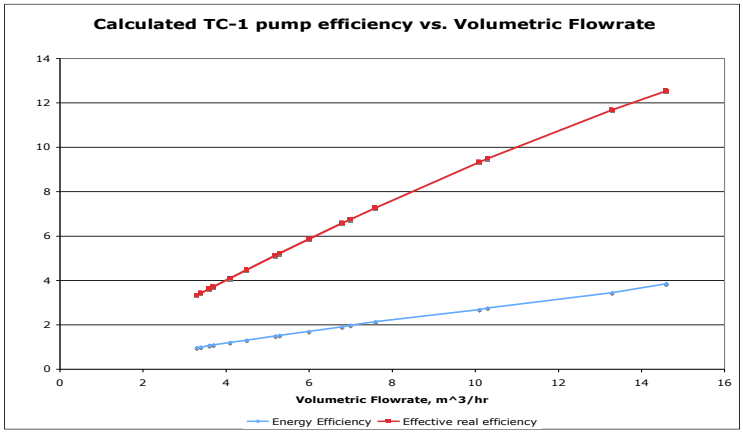

Calculated efficiencies for TC-1 loop pump.

Task 33 Separation of Technetium from Uranium and Waste Form Synthesis – Dr. Ken Czerwinski

Background

&D) activities, the uranium extraction (UREX+1) process is proposed as one of the most promising technique to separate transuranic elements (TRU) from light water reactor spent nuclear fuel in the years to come. The isotope ^{99}Tc will be separated together with U within the first process steps. After the separation of U, Tc must be immobilized by their incorporation in a suitable storage and waste form.

A candidate process to immobilize ^{99}Tc is to alloy metallic Tc with excess metallic zirconium. This material has potential advantages in terms of the future reuse of ^{99}Tc and its potential transmutation. Providing a Tc storage/waste form strongly promotes the AFC R&D and the separation of TRU elements using the UREX+1 process. However, little thermodynamic data in the binary technetium–zirconium metal system exist, and only few data are available on the synthesis of Tc-Zr alloys and on their potential performance under temporary or geological storage conditions.

In this project, systematic investigations on the Tc-Zr binary metal system will be evaluated for the first time. The synthesis of metallic Tc as well as its alloys with Zr will be evaluated. In order to provide valuable data to AFC R&D, the thermodynamic equilibrium phases, as well as their performance under repository conditions, will be examined.

Research Objectives and Methods:

- Evaluate anion exchange methods for achieving the separation of Tc from U.
- Synthesize metallic Tc from the separated product.
- Synthesize and characterize Tc alloys.
- Investigate Tc-corrosion and Tc-leaching of binary Tc-Zr phases under a range of conditions.

The following experimental techniques are used in the evaluation of the solutions and solids from the experiments: ultraviolet-visible spectroscopy, time-resolved laser fluorescence spectroscopy, X-ray Absorption Fine-Structure Spectroscopy (XAFS), and microscopy.

Research Accomplishments:

<u>Separations</u>

Static and dynamic experiments were performed to investigate the interaction of technetium with selected anion exchange resins. The kinetic static experiments showed Reillex resin had superior Tc sorption kinetics and was selected for further study. Reillex treated by nitric acid (Resin 6) was also used in the studies.

Dynamics experiments were performed on simulated UREX solution in order to determine the separation factor for uranium and technetium and to study the possibility of a Tc elution from the resin. The one column experimental set-up consisted of a reservoir of 250 mL, linked to a peristaltic pump, with a constant flux which can be between 1.2 to 8.4 mL/min. It is connected to a small column (length = 5 cm and diameter = 1 cm) and contained 1 g of resin (Reillex HP or Resin 6).

The process is divided into 3 steps: absorption, washing, and elution. For absorption, 150 mL of the UREX solution were placed in the reservoir and pumped with a peristaltic pump through the column at a constant flow rate (2, 4 or 8 mL/min). Samples were collected into centrifugation tubes (45 m ± 0.5 mL for the first two and 10 mL ± 0.2 mL for the others). For each sample, 10 µL of solution were removed and mixed with 10 mL of liquid scintillation fluid in a plastic vial, and ^{99}Tc was counted by liquid scintillation. The samples were eluted with a 50 mL solution of NH_4OH (1M or 2 M) and were introduced in the reservoir and poured through the column with the same constant flow rate.

Samples were collected into centrifugation tubes of 10 mL ± 0.2 mL with 10 µL of samples were removed and mixed with 10 mL of liquid scintillation fluid for ^{99}Tc analysis. For samples containing a high amount of technetium, a dilution (1/100) was necessary for the liquid scintillation analysis in order to be able to use the calibration curve. To optimize U/Tc separation, treated and untreated resin were combined. The set-up is composed as before by a reservoir, a pump and two columns.

The absorption and washing steps were carried out with exactly the same conditions, as presented above.

Concerning the elution step, the columns are disconnected and only the first one containing the treated resin is eluted, whereas the second one is kept for a re-use and for an eventual Tc reprocessing by pyrolysis. A suitably pure Tc and U stream resulted from the experiment.

Solid phase synthesis

Steam reforming of pertechnetate in the presence of carbon yielded Tc metal at 700°C under Ar or N_2. Alloy samples were prepared by grinding Tc and Zr metal in different ratios, from 25% to 75% Tc. Cylindrical pellets were obtained by pressing the powder and arc melting to produce the alloys. After arc melting, samples were analyzed by X-ray diffraction and optical microscopy. The alloy phases included hexagonal (α-phase) and cubic (β-phase) Zr phases. There is a diffraction peak that does not correspond to referenced Tc or Zr phases (α-Zr, β-Zr, Tc metal, Tc_2Zr, Tc_6Zr, ZrO_2 or TcO_2). Those peaks were fitted using a theoretical phase derived from the structure of Nb_3Te_7. This result which reveals a new Tc-Zr phase (Zr_3Tc_7), should be taken with prudence and further analysis by microprobe analysis will be done in order to confirm this hypothesis.

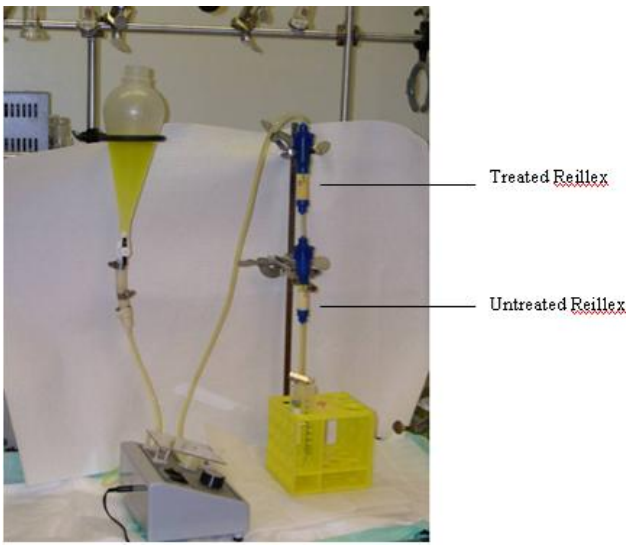

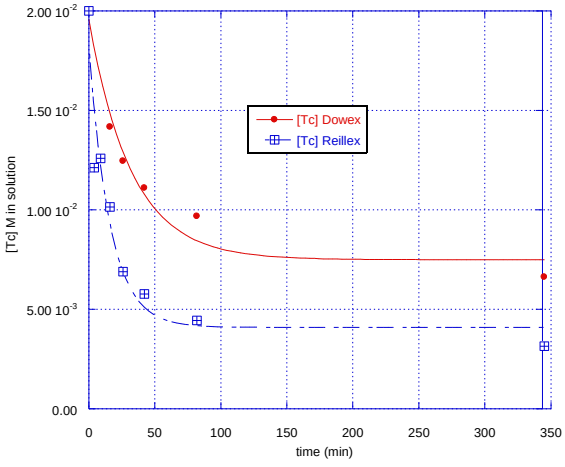

4/2/2012 6:21:21 PM

Separation process with two columns

Kinetics of TcO4- removal from solution with initial [TcO4-]=0.02 M by Dowex Marathon and Reillex resins

Tc/Zr sample before and after arc melting

Task 34 Solution-Based Synthesis of Nitride Fuels – Dr. Ken Czerwinski, Dr. Tyler Sullens

Background

Nitride fuels have appropriate properties for advanced fuels, including high thermal conductivity, thermal stability, solid-state solubility of actinides, fissile metal density, and suitable neutronic properties. The presence of oxide and carbide impurities that occur during the current nitride fuel synthesis limits their utility in advanced fuel cycles. The presence of these impurities can lead to the formation of phases with different properties from the bulk material, including the formation of secondary phases. Even a small amount of oxygen in the nitride fuel can reduce thermal conductivity by 10%. This limits the ability to fully develop nitride fuels for advanced reactors. To avoid the entrainment of carbides and oxides in the final actinide nitride product, a non-aqueous, carbon free solution phase route is proposed and investigated in this project.

A drawback of nitride fuels involves their synthesis. For nitride fuels, the current synthetic route is carbothermic reduction from the oxide to the nitride, which is based on solid phase reactions involving a stepwise process from the metal oxide, to the carbide, and finally the nitride. This high temperature, solid-phase approach is plagued by impurities in the final nitride product and difficulties in the synthesis and fabrication steps. A direct solution-based synthesis would eliminate, or at least minimize, the impurities and other synthetic problems. The proposed solution route to nitride would also have the added benefit of providing several adjustable parameters that would allow control of the properties of the final solid product.

Research Objectives and Methods:

The objective of this project is to develop solution phase synthetic routes for actinide nitrides for use in nuclear fuels. In the 1970s, a synthesis for actinide nitrides was proposed based on the reaction of plutonium triiodide (PuI_3) and uranium tetraiodide (UI_4) with sodium metal in liquid ammonia giving PuN and UN, respectively, as the reaction products. The synthetic chemistry of trivalent actinide complexes was advanced greatly with the discovery at Los Alamos National Laboratory (LANL) of efficient routes to soluble iodide starting materials of the type AnI_3L_4, where An is uranium, neptunium, or plutonium, and L is tetrahydofuran (thf), pyridine, dimethylsulfoxide, etc.

$$An + 1.5\ I_2 + xs\ L \rightarrow AnI_3L_4$$

PuI_3 is soluble in ammonia, presumably as the ammonia adduct $PuI_3(NH_3)_4$. More recent efforts by ANL and LANL collaborators have investigated amido reactions with actinides to produce $An(NR_2)_3$ complexes,

where An = U, Np, Pu:

$$AnI_3(solv)_4 + 3\ NaNR_2 \rightarrow An(NR_2)_3 + NaI + solv$$

These results suggest that the amido complexes could provide a non-aqueous solution method for the synthesis of nitrides. The resulting sodium iodide is readily soluble in liquid ammonia, making separation of these products possible. From these results, a plausible route for the synthesis of nitride fuels is:

$$An + 1.5\ I_2 \rightarrow AnI_3(NH_3)_4 \rightarrow An(NH_2)_3 \rightarrow AnN$$

where An is uranium, neptunium, plutonium or americium. To achieve the solution synthesis of actinide nitrides the fundamental chemical coordination and speciation involved in the above reaction will be examined. The non-aqueous synthetic route, based on amido chemistry, potentially provides property control over the nitride product. The resulting nitride product should be free of the impurities inherent in the carbothermic reduction technique.

The experiments are being performed by a joint research team from UNLV, LANL, and Argonne National Laboratory (ANL), with actinide experiments performed at each laboratory. This project maintains special emphasis on student participation in the project research with all team members collaborating in the educational efforts. The young researchers from UNLV have the opportunity to perform research at ANL and LANL, helping train the next generation of radiochemists and actinide scientists with experience in DOE laboratories. The synthesis of nitride fuels through this method is complementary to the ongoing carbothermic reduction syntheses being performed within the UNLV Radiochemistry program. The ANL and LANL participants are experts in synthetic actinide chemistry, including non-aqueous chemistry and materials science.

The experimental methods for the synthesis of the amido actinide species relies upon the use of inert atmosphere and elevated pressure. These conditions can be reached with the use of Schlenk lines, pressure vessels, and glove boxes. A combination of these techniques is being utilized in the project. Characterization of the resulting amido species will primarily utilize X-ray diffraction UNLV, ANL, and LANL partnership.

Single crystal X-ray diffraction will be used for examination of final and intermediate products at the atomic level for the determination of molecular structure, atomic interaction and spacing, crystal structure, speciation, and elemental oxidation state. X-ray Powder Diffraction, high resolution Transmission Electron Microscopy in combination with Energy Dispersive X-ray Analysis, Parallel-collection Electron Energy-Loss Spectroscopy, Electron-beam Microprobe Analysis and Scanning Electron Microscopy are currently in use at UNLV and will also be used to evaluate the actinide nitrides. For complete product characterization, X-ray Absorption Fine-structure Spectroscopy will also be used for analysis. Thermal analyses (Thermogravimetric Analyzer, Differential Thermal Analyzer, and Differential Scanning Calorimetry) of the final products will also be performed at UNLV.

Research Accomplishments:

The preliminary studies into the synthesis of actinide nitride fuels through a low temperature, liquid ammonia based synthesis route have been conducted on the uranium containing system, and there is good indication for the success of synthesizing uranium(III) nitride. The dissolution of iodine in ammonia is a rapid process, resulting in a pale green solution, which does not result in any observable oxidation of iodine. The cannula transfer of dissolved iodine into the reaction vessel containing U metal has been conducted with little to no residual iodine remaining in the original flask. The metal being used for these reactions has a noticeable brown/black oxide coating that prevents the formation of $UI_3(NH_3)_x$.

Stirring of U metal fragments with dissolved iodine in ammonia for 24 hours revealed a thickening of the oxide coating, which presumably is a result of O_2 or H_2O contamination in the solvent. Procedures for cleaning the metal prior to the reaction are under development. Two measures are being taken in order to use the most purified solvent possible; the highest grade ammonia available is being obtained and several

procedures are being developed to dry and deoxygenate the solvent. These actions should allow the reaction to proceed without formation of the boundary oxide layer between the two reactants.

One of the original synthetic routes devised for the synthesis of U(III)N involved the entire reaction taking place in liquid ammonia. Several experimental reactions were conducted in an attempt to synthesize the $UI_3(NH_3)_x$ and $U(NH_2)_3(NH_3)_x$ precursors of U(III)N. Each attempt involved cleaning of the uranium metal to remove the oxide coating of the metal reagent with 3 washes of concentrated nitric acid, each followed by a rinse with liquid ammonia. Success of this cleaning procedure was varied, with a majority of cleaned metal oxidizing rapidly once in contact with the liquid ammonia, despite the precautions taken to eliminate oxygen contamination in the reaction flasks. Due to the continual presence of oxide coating of the uranium metal, it was decided to alter the proposed synthetic route to utilize the synthesis of the $UI_3(THF)_4$ precursor, as described in *Inorganic Chemistry*. This involves the purification of THF through distillation, cleaning of the metal uranium, and slow reaction of U and I_2. Equipment to perform this synthesis was not available for immediate use, but all necessary glassware was purchased.

It was discovered that the uranium metal turnings being used for the synthesis had a possibility of containing niobium as well. Waste solutions were analyzed by ICP-AES, and no niobium was identified. Other reaction waste solutions were also analyzed in order to determine the reactivity of uranium in the liquid ammonia solution. These analyses determined that only a minimal amount of uranium became dissolved, indicating that either there was little reactivity in the liquid ammonia or the reaction was only taking place on the surface of the metal. Neither of these possibilities is desirable, therefore the synthetic route involving THF was selected to avoid these outcomes.

Single crystal and powder diffractometers are necessary instruments for the determination of the intermediate and final products.

<u>Other progress:</u>

- Reaction of UCl_4 + 4 $NaNH_3$ in liquid ammonia was performed. $UI_3(THF)_4$ + 3 $NaNH_2$ in liquid ammonia was performed. The samples were treated and processed.
- Samples were prepared for EA Modeling reactions and crystals were obtained. Modeling reactions were extended to scorpionates. This represents a new synthetic route actinide nitride. Initial characterization indicated other products are present.
- UN was obtained from UI_3 and Li_3N direct reaction and was characterized.
- Metallocenes were synthesized from starting materials. Reaction and monitoring of these metallocenes with amide salts was conducted.
- Liquid ammonia reaction between uranium (III) iodide and sodium amide yielded a new product with indications of being a UN pre-cursor. The product was characterized by XAFS

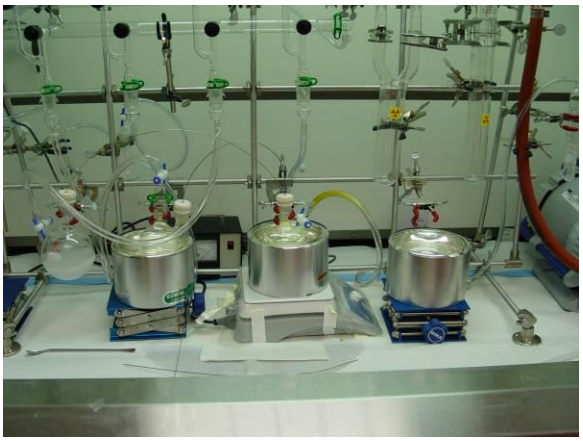

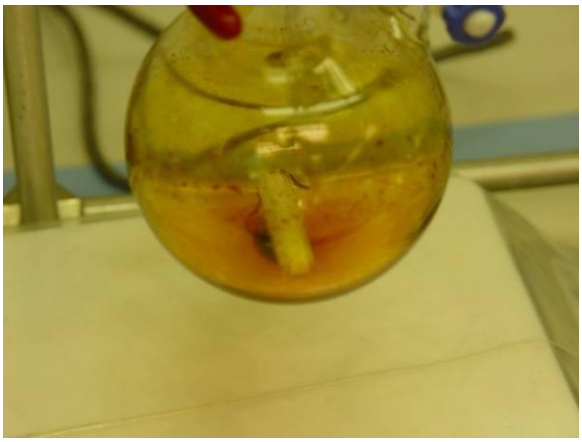

A depiction of dissolved iodine reacting with uranium metal after the liquid ammonia solvent has evaporated.

A depiction of the Schlenk line experimental set-up for the generation and storage of liquid ammonia, solvent transfer for the dissolution of iodine, and the cannula transfer of solution for reaction with uranium.

Task 35 Criticality Studies for UREX Processes

– Dr. Denis Beller, Dr. Charlotta Sanders

Background

The completion of criticality experiments for mixtures of transuranic actinides (TRU; includes neptunium, plutonium, americium, and curium) that will be created during the separation of used nuclear fuel may be a requirement in order to construct prototype plants for the Global Nuclear Energy Partnership (GNEP). In this program and the Advanced Fuel Cycle Research and Development (AFC R&D) program that supports it, economic and environmental methods are being developed to reduce the impact of waste from commercial nuclear fuel cycles.

Recycling of used fuel by chemically separating it into U, fission products, and TRU would be the first step in this new fuel cycle. Proposed mixtures and concentrations of TRU covering a wide range of conditions must be examined theoretically and experimentally to demonstrate criticality safety in advance of construction of a processing facility. Theoretical studies may be limited because of insufficient nuclear data for the rarer isotopes of Np, Pu, Am, and Cm. These data limitations include reaction cross sections in some energy regimes, thermal feedback coefficients, and delayed neutron fractions.

Research Objectives and Methods:

The completion of criticality experiments for mixtures of transuranic actinides that will be created during the separation of used nuclear fuel may be a requirement to construct prototype plants such as the Engineering-Scale Demonstration (ESD) and the Advanced Fuel Cycle Facility (AFCF) for the Global Nuclear Energy Partnership (GNEP).

GNEP is a program to develop a worldwide consensus to enable the expanded use of economical, environmentally-friendly nuclear energy to meet growing electricity demand. In this program and the Advanced Fuel Cycle R&D program that supports it, participants are developing economic and environmental methods to reduce the impact of waste from commercial nuclear fuel cycles. Recycling of used fuel by chemically separating it into uranium, fission products, and transuranic actinides would be the first step in this new fuel cycle. Proposed mixtures and concentrations of TRU covering a wide range of conditions must be examined theoretically and experimentally to demonstrate criticality safety in advance of construction of a processing facility. Theoretical studies may be limited because of insufficient nuclear data for the rarer isotopes of plutonium, americium, curium, and neptunium. These data limitations include reaction cross sections in some energy regimes, thermal feedback coefficients, and delayed neutron fractions (b).

In collaboration between UNLV, Los Alamos National Laboratory (LANL), Argonne National Laboratory (ANL), and Oak Ridge National Laboratory (ORNL), criticality studies will be conducted to support the development of future fuel cycle facilities.

The first step in determining requirements for criticality studies is an examination of past experiments and criticality and sensitivity studies, as well as available databases. Further sensitivity studies will determine what kinds of experiments should be performed to ensure criticality safety in advanced processes. This information can then be used to formulate an optimum set of experiments that can be analyzed in advance using state-of-the-art radiation transport codes. As these facilities and experiments will include complex geometries, a Monte Carlo N-Particle (MCNP) transport code will be used in these sensitivity, scoping, and design studies.

The work may also require generation of new cross section libraries and thermal scattering coefficient

databases. Future criticality studies may include cross section sensitivity studies and design of critical experiments including dilute mixtures of Pu, mixed higher actinides in solution, and fuels.

Research Accomplishments:

Progress implementing NJOY for cross section processing continued with the assistance of LANL and ORNL specialists. NJOY was successfully implemented and is now used to produce temperature-broadened point-wise cross section libraries from eight isotopes of higher actinides for sensitivity studies. Benchmarking of libraries and criticality studies is underway; a benchmark analysis of the Jezebel critical assembly with two temperature-broadened libraries was completed to validate variational and criticality methods.

Processing cross-sections in NJOY99.259 was completed and a review of criticality benchmark experiments was initiated for establishing the range of applicability of physical and spectral parameters. Modeling of criticality sensitivity testing with minor actinides in the UNM AGN-201 reactor continued. A review of criticality safety benchmark experiments was completed for the established range of applicability of physical and spectral parameters and reactivity sensitivity studies began on higher actinides. Fast spectrum reactivity sensitivity studies were completed on eight higher actinide isotopes at six different temperatures. Void and replacement reactivity changes were calculated with three fast benchmark experiments.

The SHEBA liquid-core critical assembly was modeled in preparation for sensitivity studies. Reactivity sensitivity studies of the SHEBA liquid-core critical assembly was completed and modeling detectors for determining ability to measure reactivity changes was initiated. A californium source was added opposite a neutron detector to model neutron transport through the liquid-core SHEBA for reactivity sensitivity studies.

Other Accomplishments

Dr. Charlotta Sanders joined the UNLV research faculty and this project as a co-investigator. Her expertise is in radiation transport, criticality, and shielding analyses, with substantial experience with investigations related to used nuclear fuel. She is advising students and developing new research projects for continuation of MPAC research.

Funding was approved for a contract with Professor Robert Busch of the University of New Mexico (UNM) to investigate the use of UNM's AGN-201 reactor for criticality sensitivity experiments with higher actinides. A MCNP model of AGN-201 reactor was obtained from UNM, some programming errors were corrected, and successful criticality runs were conducted in preparation for sensitivity studies.

These studies have begun by modeling small quantities of higher actinides in the reactor hole to determine reactivity sensitivity for potential experiments. Using this funding to prepare for future work, UNLV and UNM conducted a Reactor Experimentation Laboratory Course at UNM using the AGN 201M reactor. In addition, a research proposal was submitted to DOE/NE for collaboration with UNM and Georgia Tech for criticality studies using the UNM AGN reactor.

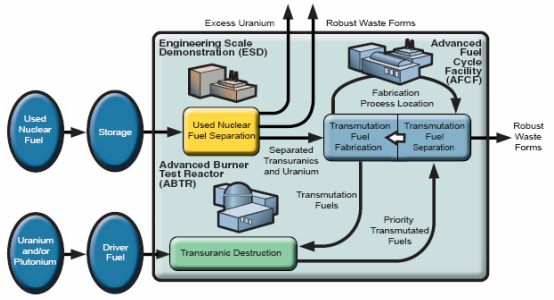

The Global Nuclear Energy Partnership research facilities

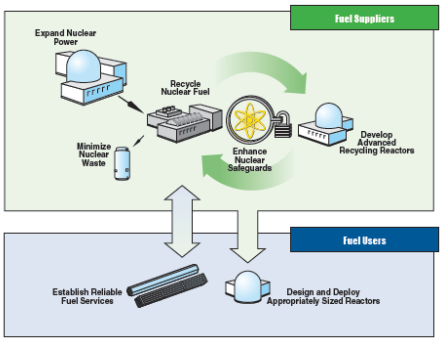

The Global Nuclear Energy Partnership (GNEP) structure.

Task
36 Evaluation of Cs/Sr Waste Form for Long Term Storage and Disposal – Dr. Gary Cerefice, Dr. Longzhou Ma

Background

In order to maximize the utilization of the proposed repository facility, the short-term decay heat generated by high-level waste must be removed from the waste stream. The proposed waste management baseline strategy for the GNEP program calls for the separation of cesium and strontium from used nuclear fuel in order to minimize the short-term heat loading in the repository facility. The separated waste stream will be converted to an aluminosilicate waste form, stored for decay (approximately 300 years), then managed as low-level radioactive waste.

The goal of this project is to examine two potential concerns regarding the long-term performance of a proposed cesium/strontium waste form. To facilitate long-term storage, up to 300 years, the disposal containers will need to be able to survive for the entire storage interval. The first aspect of the project will explore the potential interaction of the aluminosilicate waste form with the storage canister materials to determine if there is any corrosion or chemical interaction concerns for the storage of the materials.

At the end of the storage interval, most of the ^{137}Cs in the waste form will have decayed to its daughter, ^{137}Ba. While this decay provides a significant reduction in the decay heat generated by the waste form, it poses a new concern. Barium is hazardous, and is identified by the U.S. Environmental Protection Agency (EPA) as a hazardous constituent under the Resource Conservation and Recovery Act (RCRA). To dispose of any material containing a RCRA-identified constituent, the material must be demonstrated to be durable enough to prevent the release of the hazardous component or must be treated as hazardous waste. For the Cs/Sr waste stream, failure to contain the barium within the waste form would require disposal as a mixed waste stream, greatly increasing the disposal costs. Understanding the potential impacts of radioactive damage, high storage temperatures, and the crystallographic impacts of the decay transmutation itself on the performance of the waste form 300 years from now poses a significant challenge.

Research Objectives and Methods:

The goal of this task is to develop, characterize, and optimize the proposed aluminosilicate waste form for a separated cesium and strontium waste stream. The research effort at UNLV will be divided into two subtasks:

- Materials compatibility, and
- Waste form optimization and performance.

The materials compatibility subtask will examine the potential for chemical interactions between the waste form material and proposed structural materials for the disposal container (carbon steel, stainless steel, etc.). The waste form performance task will examine the leach resistance of the waste form, with particular attention to barium retention.

The research objectives of this project are:

- To characterize the Cs/Sr-loaded aluminosilicate waste form ceramic,
- To examine the impact of fabrication process parameters on the product waste form,
- To evaluation the potential for chemical interactions between the waste form and container material, and
- To examine the degradation and alteration behavior of the waste form

Research Accomplishments:

To optimize the Cs/Sr waste form, the impact of fabrication process parameters on the final product had to be evaluated. Initial experiments examined the impact of sintering temperatures on the waste form. Thermogravimetric analysis (TGA) identified the temperatures where sorbed and interstitial water is driven from the waste former matrix, as well as the temperatures where the bentonite waste former material undergoes a phase transition to a glass, establishing an upper temperature limit for the fabrication of the waste form. The impact of sintering time and temperature on the waste form and on the starting materials was examined by X-ray Diffraction (XRD) analysis. Significant differences in the crystallinity as well as phase composition of the Cs/Sr-loaded waste form were observed from increasing the sintering temperature from 800 °C to 1000 °C, with additional changes observed when the sintering time at temperature was increased to over 20 hours. Characterization of the product waste forms, including identification of all the composite phases, will continue through the end of the project.

Characterization of the product morphology by scanning electron microscopy showed that the current batch processing method (in which the bentonite clay is loaded with Cs and Sr in solution, dried, then sintered) yields a highly porous material with a sponge-like morphology. Coupled with the results of the TGA analysis, this is likely due to the release of interstitial or matrix water during the early stages of the sintering step. Electron microprobe analysis (EMPA) showed a uniform distribution of Cs, Sr, and Ba throughout the sample matrix, at least at the micron scale.

Further analysis by transmission electron microscopy (TEM) indicated, however, that the waste stream components are actually segregated into discrete phases, and that these discrete, sub-micron particles are distributed throughout the matrix. Initial characterization has identified separate Sr- and Ba-containing aluminosilicate phases in the host matrix. The Cs-bearing phase (or phases) in the matrix have not been identified and confirmed at this time.

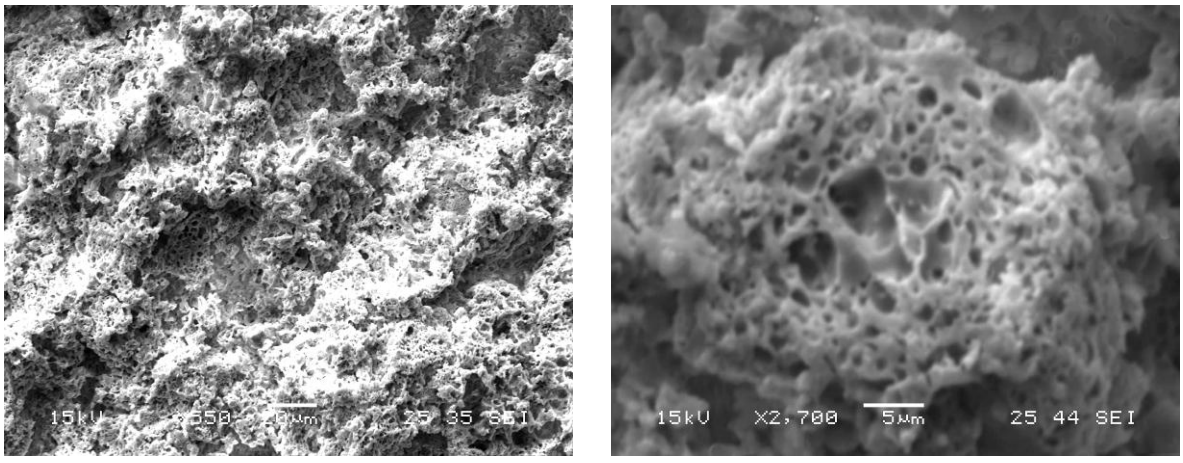

Cs/Sr/Ba-loaded waste form matrix at 550X (a) and 2700X (b) magnification.

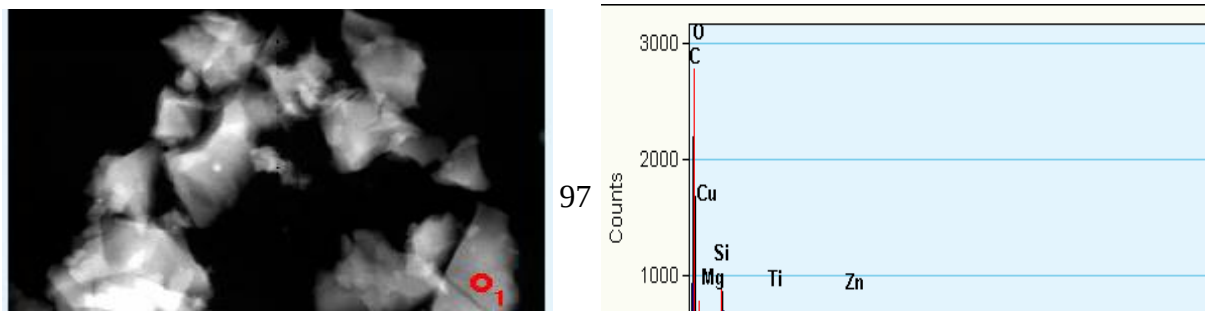

Task 37 Thermal Transient Flow Rate Sensor for High Temperature Liquid Metal Cooled Nuclear Reactor – Dr. Yingtao Jiang, Dr. Jian Ma

Background

In nuclear power plants and accelerator driven systems (ADS) for nuclear waste treatment, it is important to monitor the coolant flow rate in the reactor core and pipeline. In such a strong irradiation, high pressure, and temperature environment, the existing flow measurement techniques (such as Electromagnetic flow meters, Ultrasonic flow meters, Turbine flow meters, etc.) are not accurate and reliable.

The measurement of flow rates (mass flow rates or volume flow rate) plays a notable role in monitoring and controlling the experimental conditions. The bulk flow rates can be obtained through direct methods, which measure the amount of discharged fluids over a period of time. Alternatively, flow rates can also be obtained using indirect methods. For example, they can be derived through the measurement of fluid velocities. So far, the velocities have been found in strong correlation with signals of pressure, temperature, optical wave, ultrasonic wave, etc. based on diverse physical principles. Note that with some exceptions, the flow rate measurement systems require calibration or empirical corrections, especially after long term operation. In the application of liquid metal coolant flow rate measurement, the high temperature, pressure, and corrosion environment limit most flow meter devices from being used in long term and maintenance-free operation.

As the temperature measurement technique is well developed for high temperature applications, one flow rate measurement technique is proposed based on the correlated thermal signals. This way, the measurement errors due to long term corrosion will be easily counteracted using this proposed method. Correlated thermal signals are measured to deduce the flow velocity.

Research Objectives and Methods:

An alternative flow rate measurement technique has been proposed for this task based on correlated thermal signals obtained from a pair of temperature sensors placed a certain distance apart along the flow. A widely used cross-correlation algorithm, however, suffers from the ambiguity in reading of measurements. To alleviate this problem, a new algorithm is introduced to further improve the accuracy in the transit time estimation using an adaptive inverse system model at a higher cost of computation. When real-time computation is a concern, a second algorithm is proposed based on an adaptive filtering approach which makes a sound trade-off between accuracy and computation cost. This algorithm incurs less processing time than the first proposed algorithm with higher accuracy than the two aforementioned conventional algorithms. These algorithms were evaluated with experiments in a water-based testing loop.

This idea is based on the transit time estimation, using a pair of thermocouples along the flow to provide the temperature readings at two locations along the flow. It is safe to assume that there is a negligibly small change in the characteristics of flow structures, provided the sensors are within certain distances. In the

illustrated case (above), the upstream thermocouple records a flow signature *L/V* seconds earlier than the downstream one, where *L* is the distance between the two sensors and *V* is the flow velocity. By comparing the signals from the two thermocouples, the time delay, *t*, can be determined and thus the velocity can be given as follows:

$$V = L/t$$

Methods

The transition time can be obtained using two techniques: cross-correlation-function- or transfer-function-based methods. The first technique, which uses the maximum value of the cross correlation function (CCF) of a measured signal, has two main problems: (i) the obtained peak is too wide, having a negative impact on the result accuracy and (ii) besides the main peak, there can be other undesirable peaks. To alleviate this problem, the transfer function estimation approach was recently proposed. This approach tends to give a narrower peak to get the transit time. A new algorithm was introduced to further improve the accuracy in the transit time estimation using an adaptive inverse system model at a higher cost of computation. When real-time computation and measurement is a concern, a second algorithm is proposed based on an adaptive filtering approach. This algorithm incurs less processing time than the first algorithm, with higher accuracy than the two aforementioned conventional algorithms.

Objectives

This project focuses on experimental investigation of a correlation velocity measurement technique by analyzing the temperature fluctuations naturally existing in turbulent flows. Thermocouple temperature sensors are employed in the experiments to obtain local temperature fluctuations. The objectives of the proposed research are as follows:

- To design and construct a correlation velocity measurement device that utilizes the thermocouple temperature sensors to obtain temperature information;
- To develop a data processing scheme and to implement the scheme to build a LabVIEW-based data acquisition system;
- To test the correlation velocity measurement technique in a thermal-hydraulic experimental test facility (water-based), and to compare the results with those obtained from other commercial flow meters;
- To test the measurement device in the UNLV TC-1 loop test section;
- To suggest any improvements for the measurement technique based on the experimental results; and,
- To develop circuit boards for signal conditioning, signal processing, and system integration.

Research Accomplishments:

The flow velocity of liquid metal coolant, e.g., lead bismuth eutectic (LBE) can be determined through the measurements of temperature fluctuation recorded by a pair of temperature sensors placed a certain distance apart along the flow. Traditionally, this was done using a cross-correlation algorithm to estimate the transit time of the coolant, and thus its velocity. This widely used cross-correlation algorithm, however, suffers from the ambiguity in reading of measurements. To alleviate this problem, the transfer function estimation approach was recently proposed and tends to give more accurate results. Both algorithms have been coded and compared with two algorithms developed by the principal investigators and the students.

A new algorithm has been introduced which can further improve the accuracy in the transit time estimation using an adaptive inverse system model at a little higher cost of computation. When real-time computation is a concern, a second algorithm is proposed based on an adaptive filtering approach which makes a sound trade-off between accuracy and computation cost. This algorithm incurs less processing time than the first proposed algorithm with higher accuracy than the two aforementioned conventional algorithms. A test rig has been built to test the proposed algorithms.

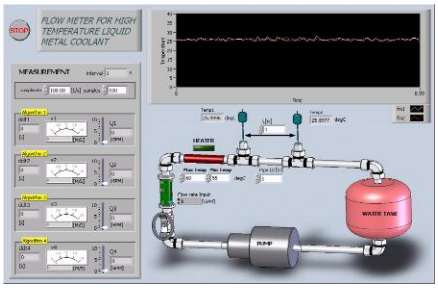

The console of the data acquisition system program in LabView.

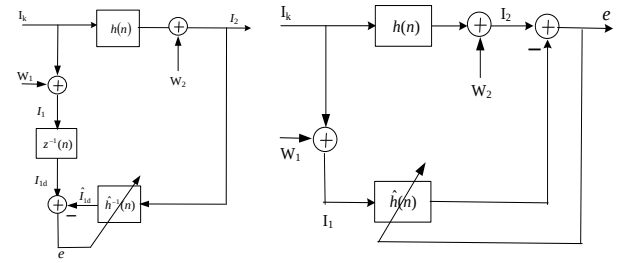

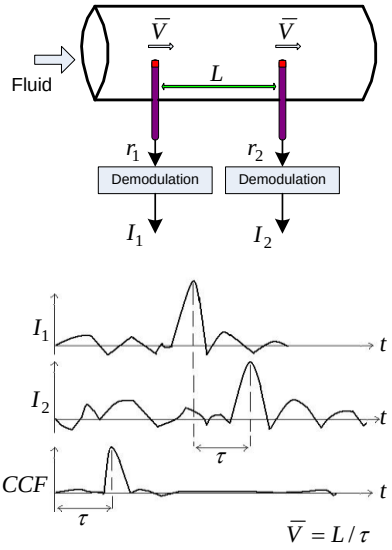

Time Transit Configuration.

Task 38 f-Element Electrochemistry in RTIL Solutions: Electrochemical Separation of Lanthanides and Actinides – Dr. David Hatchett, Dr. Ken Czerwinski

Background

Electrochemical methods can be used to effectively separate actinide and lanthanide species from complex mixtures. This is based on the unique electrochemical properties of each specific target species. In studies it has been found that, with the exception of Ce, aqueous solutions provide unsuitable electrochemical windows to effectively evaluate the thermodynamic properties that are useful for chemical separations. Therefore, a more novel approach was examined which eliminated the aqueous solution with a room temperature ionic liquid (RTIL) solution. RTIL solutions do not suffer from the side reactions that are prominent in aqueous environments. In addition, the potential window is much larger for the RTIL solutions. They are a new starting point for the electrochemical separation of individual species from a mixture.

The ultimate goal is to fully characterize the oxidation/reduction of f-elements in RTILs to establish the baseline thermodynamic and kinetic data for these systems. The data will be used to critically evaluate the ability to use electrochemical methods for controlled, potential mediated, separation of f-elements by electroplating on electrodes surfaces. Factors that will influence the ability to measure the redox processes

in f-elements in RTIL solutions and electroplating on electrode surfaces include the structure, solubility, and stability of the target species in these solutions.

Research Objectives and Methods:

The objective of this project is to use electrochemical techniques to develop a thermodynamic understanding of actinide and lanthanide species in RTIL solutions, and to use this data to effectively separate species with very similar chemical properties. In consultation with a U.S. Department of Energy national program collaborator, electrochemical methods and materials will be evaluated and used to exploit the thermodynamic differences between similar chemical species enhancing the ability to selectively target and sequester individual species from mixtures. This project is in its first year and has successfully completed Phase 1. This research allows for expansion into Phases 2 and 3 for the next year.

Research Accomplishments:

The proposed research included the extraction, speciation, and interfacial electrochemical measurement of actinide and lanthanide species in RTIL. The potential mediated electrochemical properties of lanthanide and actinide complexes in RTIL solutions have been evaluated the relevant results can broken into the following categories:

1. Electrochemistry of Lanthanides in RTIL Solutions
2. Direct Dissolution and Electrochemistry of UO_2CO_3 and U_3O_8
3. General RTIL Characterization

The formation of lanthanide and actinide complexes are based on the principal that the neutral species must be extracted to minimize crossover contamination. The complex would be extracted into the RTIL directly without TBP. This process may enhance the extraction of the f-element relative to the TBP/n-dodecane system based on incorporation of the common ion into the complex and diluent. The complexes can also be formed directly in RTIL.

Electrochemistry of Lanthanides in RTIL Solutions

We have synthesized the cation, $[Me_3N^nBu]Br$.

We have synthesized a new batch of ionic liquid, $[Me_3N^nBu][TFSI]$.

- We performed the synthesis of Ag(TFSI) for complexation studies.
- We performed the synthesis of $Sm(TFSI)_2$/$Sm(TFSI)_3$.
- We examined the extraction of $Sm(TFSI)_x$ into RTIL solutions.
- We examined the electrochemical signature of extracted $Sm(TFSI)_x$ in RTIL
- We electrochemically deposited Sm(0) using $Sm(TFSI)_3$ from aqueous solution.
- We performed SEM and TEM on the Sm deposits at UC Santa Barbara.
- We evaluated crystal diffraction patters and determined that the Sm complex with TFSI was contaminated with sulfate crystals.

- $SmTFSI_3$ was successfully synthesized using Sm_2O_3 and HTFSI as the starting materials. The resulting purified complex was a clear oily solution that contained crystals suitable for XRD analysis.

- Electrochemical deposition of U metal from UI_3, $UTFSI_3$, and UCl_4 in RTIL was achieved for all three starting materials.

- The electrochemical deposition of common lanthanides and actinides from RTIL solution can also be envisioned based on the following reduction potentials: Pu^{3+} (-2.228 V), Am^{2+} (-2.097 V), Am^{3+} (-2.245 V), Cm^{3+} (-2.237 V), and U^{3+} (-1.997 V). The reduction of any of these species would occur well within the negative potential limit for the RTIL at platinum (-2.8 V), gold (-2.4 V), and glassy carbon electrode (-3.6 V vs. Ag/AgCl) in the RTIL ($[MeBu_3N^+][TFSI]$) solution.

- We have successfully prepared the $UO_2(TFSI)_2$, $Sm(TFSI)_3$, $U(TFSI)_3$, and the $U(TFSI)_4$ complexes using the methods defined in Scheme 1. The individual complexes have also been extracted and directly dissolved into RTIL ($[MeBu_3N^+][TFSI^-]$). The electrochemical properties of $UO_2(TFSI)_2$ have been evaluated and the potential-dependent deposition of UO_2(s) has been achieved.

- The electrochemical deposition of common lanthanides and actinides from RTIL solution canalso be envisioned based on the following reduction potentials: Pu3+ (-2.228 V), Am2+ (-2.097 V), Am3+ (-2.245 V), Cm3+ (-2.237 V), and U3+ (-1.997 V). The reduction of any of these species would occur well within the negative potential limit for the RTIL at platinum (-2.8 V), gold (-2.4 V), and glassy carbon electrode (-3.6 V vs. Ag/AgCl) in the

- The electrodeposition of Sm and U metal have also been achieved from RTIL solutions using the $Sm(TFSI)_3$, $U(TFSI)_3$, and $U(TFSI)_4$ complexes prepared using the synthesis described in scheme1. We successfully demonstrated the extraction of $Sm(TFSI)_3$ from water and Sm(0) on gold for the electrochemical deposition of extracted $Sm(TFSI)_3$ from aqueous solution in RTIL.

- The direct dissolution of Ce, Sm, and Eu was achieved into RTIL consistent with methods currently used for aqueous dissolution processes.

- The influence of temperature on the electrochemical response of lanthanide, Ce, and Ferrocene in $[Me_3NBu][TFSI]$ was evaluated as a function of scan rate.

- The electrochemistry of Ce in RTIL was examined as a function of increasing temperature to determine if kinetically limited electrochemical processes can be resolved.

- A temperature study examining the electrochemical reduction of $Ce(TFSI)_3$ and deposition of Ce metal from RTIL was conducted at elevated temperatures (24, 45, 60, 75, 90 °C).

- UV-Vis was performed on the 10 mM direct dissolution $Ce(TFSI)_3$ into $Me_3NBuTFSI$ (from $Ce_2(CO_3)_3$ with HTFSI) sample along with comparison samples of $Me_3NBuTFSI$, HTFSI in $Me_3NBuTFSI$ background, similar concentration of $Ce_2(CO_3)_3$ with HTFSI in water, HTFSI in water background, and water.

- UV-Vis was performed on the 4.05 mM direct dissolution $Sm(TFSI)_3$ into $Me_3NBuTFSI$ from the $Sm_2(CO_3)_3$ with HTFSI sample along with comparison samples of $Me_3NBuTFSI$, HTFSI in $Me_3NBuTFSI$ background, similar concentration of $Sm_2(CO_3)_3$ with HTFSI in water, HTFSI in water background, and water. Previous $Sm(TFSI)_3$ that was first synthesized in water and crystalized then added to $Me_3NBuTFSI$, and two samples of $Sm(TFSI)_3$ in water were also examined.

Direct Dissolution and Electrochemistry of UO_2CO_3 and U_3O_8

We have continued to evaluate the solubility of UO_2^{2+} in RTIL

- We studied the electrochemical deposition of UO2(s) using linear scan voltammetry. We were successful in the deposition.

- We continued the studies of the electrochemical deposition of UO2(s) using linear scan voltammetry.

- We have successfully synthesized and characterized UO_2TFSI_2 using UCl_4 in aqueous solution.

    - While we have synthesized UO_2TFSI_2 in water, our initial target was $UTFSI_4$. Given the fact that UCl_4 so easily hydrolyzes, this may be a difficult route in aqueous solution. We are currently trying to obtain crystal structures from XRD data to confirm the chemical species. However, both the electrochemistry as well as the UV-Vis spectrum indicates that it is UO_2.
- We also replicated electrochemistry on uranium extraction samples using both cyclic and square wave voltammetry.

- We initiated the synthesis of both UO_2 and Sm TFSI complexes with pure TFSI without any detectable sulfate.
- Recrystallized the $U(TFSI)_4$ complex in THF solution is directly soluble in RTIL

- Examined the electrochemical properties of $U(TFSI)_4$ recrystallized in THF and performed scan rate studies and electrochemical deposition.

- Synthesized a new batch of $U(TFSI)_4$ in THF.

- We have purified $U(TFSI)_4$ using a rotavap was at 180 C for 24 hours to volatilize the Iodine from the RTIL solution.

- We conducted a solubility experiment with the UO_2CO_3 system with the addition of TFSI acid. After only 8 hours of Argon bubbling, a solubility of approximately 14mM was obtained. This is a vast improvement in both time and maximum solubility of the previous setup where no acid was added.

- A new purification method was attempted with the $UTFSI_4$ system to allow for heating without addition of RTIL. The goal is to obtain pure crystals for characterization using XRD.

- Electrochemical characterization of the UO_2CO_3 system with acid did not change the electrochemistry appreciably with deposition of UO_2 (s) visible within minutes.

- A new synthesis route was attempted with the $UTFSI_4$ system by starting with the HTFSI acid and UCl_4 in Acetone solvent. Resulting solution was initially yellow, followed by orange at 4 hours, followed by red at 24 hours. After removal of acetone solvent, product was a dark red oil.

- $UTFSI_3$ was synthesized using UI_3 and HTFSI as the starting materials and the $UTFSI_3$ complex was analyzed by IR and UV-Vis spectroscopy in the synthesis solution and in the RTIL solution.

- Made ICPMS standards for Uranium and Silver. Verified by running calibration. Obtained greater then 99.0% calibration curve accuracy.

- Attempted to purify $UTFSI_4$ product. Added small excess of UCl_4, but quantity available was limited. Added I_2 to obtain AgI precipitate. ICPMS revealed complete removal of Silver

- Added silver-free $UTFSI_4$ in THF to RTIL and removed excess THF using the rotovap

- We have synthesized UO_2TFSI_2 single crystals for XRD analysis.

- We have initiated UO_2TFSI_2 extraction from the aqueous layer using RTIL.
-
- We have begun to evaluate the cyclic voltammetry of soluble species in RTIL from ^{233}U based UO_2CO_3
-

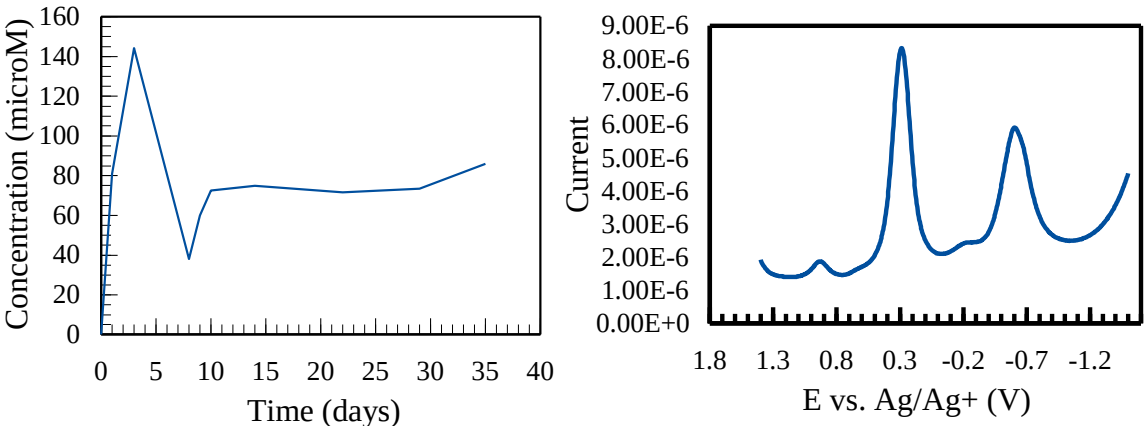

Solubility of UO_2CO_3 in a room temperature ionic liquid solution (left). Square wave voltammetry of UO_2CO_3 in room temperature ionic liquid after 24 hours (right).

- We completed the uranyl carbonate solubility/speciation experiment (sample collection).
- We obtained IR spectra for samples from the uranyl carbonate experiment
- We ran linear scan voltammetry on samples from uranyl carbonate experiment in for the cathodic region.

These studies demonstrate that RTIL solutions can be used to effectively probe the oxidation/reduction of f-element species and complexes. In addition the potential mediated deposition of f-elements is demonstrated indicating the controlled separation of chemical species is thermodynamically feasible. The deposition of UO_2(s) is initiated at ~-2.0 V vs. Ag/AgCl in the RTIL solution. The reduction of UO_2(s) to U(s) should occur at -2.443 V in aqueous solution. The initial reduction occurs at more thermodynamically favorable potentials (~0.44 V). However, the deposit composition is complicated because the sample was exposed to air before SEM measurement with a final product of UO_2(s) obtained based on EDX verification. Additional studies are required in inert environments to ensure the deposit is not influenced by air exposure.

The deposition of U at room temperature from ionic liquid had not been achieved previously. However we successfully deposited U metal on Au electrodes using $U(TFSI)_3$ and $U(TFSI)_4$ prepared using the defined synthetic methods from scheme 1. To date we have not examined the selective deposition of Lanthanides followed by Actinides as a method of separation. However, now that deposition potential are know for the RTIL solutions it is a logical progression to try to selectively electrodeposit the lanthanides in one step followed by U deposition in the second. Figure 3 provides the voltammetric response of an Au electrode for the deposition of U from RTIL and an SEM image of U deposits for clarity.

- $UO_2(TFSI)_2$ synthesis and characterization was initiated in an attempt to isolate crystals of the species for further analysis

- U_3O_8 Dissolution into RTIL was conducted using minimum concentrations of acid and ozone. Two additional measurements were conducted for verification of the processes.

- The U_3O_8 dissolution was verified spectroscopically with the characteristic uranyl peaks observed between 400-450 nm.

- The synthesis of $UO_2(TFSI)_2$ has continued and the crystallization was initiated using the pH of the solution to mediate the process.

- UV-Vis characterization of the $UO_2(TFSI)_2$ was completed with broad absorbance between 400 and 500 with lower definition of intrinsic peaks observed for aqueous uranyl carbonate.

- $U(TFSI)_3$ dissolution and cyclic voltammetry is being conducted. Specifically $U(TFSI)_3$ (0.0177 g) was transferred into a new cell with RTIL and cyclic voltammetry was then performed on the sample (1.9 to -2.8 V) using an Au disc working electrode and Pt counter electrode for 200, 100, 50, 25, and 10 mV/s so scan rate dependence could be investigated

- U_3O_8 synthesis was conducted. Uranyl nitrate was dissolved in water and precipitated out with ammonium hydroxide, removed from the centrifuge tube, placed into a ceramic vessel and heated in an oven at 100°C for 19 hours with U_3O_8 confirmed using the C2mm phase by TOPAS.

- The original U_3O_8 RTIL dissolution solution (2.01 mM U_3O_8 dissolved into $Me_3NBuTFSI$) was used in the newly designed e-chem cell for electro-depositing and electrochemical deposition was initiated.

- Dissolution was started with a control sample: 0.0338 g U_3O_8 (w/^{223}U) was placed in 20 mL of $Me_3NBuTFSI$. No HTFSI was added. Ozonation without acid produced only a 9% dissolution concentration. Increases were achieved with the addition of HTFSI.

- Deposition of UO_2(s) on stainless steel and Au electrodes was achieved used the direct dissolution of U_3O_8 in RTIL.

<u>General RTIL Characterization:</u>

- We ran backgrounds for new ionic liquid including CV, SW, and LSC.

- We ran EELS on the electrochemically deposited uranium on our electrode and unable to locate the uranium species.

- We electrodeposited a Uranium sample onto a gold sheet electrode for EXAFS analysis.

- Deposited UO_2 onto a gold electrode from RTIL solutions for surface analysis of the deposit.

- We electrodeposited Samarium from both aqueous and RTIL solutions.

- Performed SEM (including EDS) on gold electrode surface after electrochemical deposition studies.

- Performed in-depth voltammetry. Cyclic at 10,20,30,40,50,60,70,80,90, and 100 mV/s and attempted electrochemical deposition

- Performed Laser ablation gold electrode surface, No Uranium was located. Results indicate that iodine is now problematic.

- We have obtained X-Ray crystallography data on recrystallized $Sm(TFSI)_3$ and we are currently analyzing.

- We have electrochemically evaluated the RTIL solution containing $U(TFSI)_4$ with electrochemical deposition.

- We purified and obtained UV/Vis, IR Spectra for $UTFSI_4$.

- AgTFSI and $Sm(TFSI)_3$ were synthesized and purification using two different routes was started.

- The newly purified $UTFSI_4$ product was characterized using FTIR and UVVIS for comparison to other purification methods.

- $SmTFSI_3$ purification was performed using excess I_2 in the same manner as the $UTFSI_4$ to obtain pure crystals for XRD characterization.

- $SmTFSI_3$ was successfully characterized by single crystal XRD.

- The new $SmTFSI_3$ complex was added into aqueous solution and measured for Sm content by ICPMS analysis. The Resulting solution was divided into sections, one portion was isolated for aqueous electrochemistry, and a second portion was extracted into an RTIL solution.

- Both the new $SmTFSI_3$ and the $UTFSI_4$ complexes were analyzed by IR and UV-Vis spectroscopy in the synthesis solution and in RTIL solution.

- Metal deposits from electrochemistry were analyzed using SEM and the coupled EDS technique verifying the deposition uranium metal with no oxygen on the electrode surface.

- The metal deposit from the $UTFSI_3$ system was analyzed using powder XRD with preliminary results indicates alpha uranium metal deposition.

- We have prepared and packed XAFS samples for analysis including $SmTFSI_3$ in RTIL, $SmTFSI_3$ solid, $UTFSI_4$ in RTIL, and Uranium solid deposit.

- We performed laser ablation analysis of uranyl deposit on the glassy carbon electrode obtaining both measurements for the electrode and background.

- We electrochemically deposited uranyl onto gold electrodes from RTIL solution.

- Performed UV/Vis measurements on diluted uranyl solutions from the solubility experiments to ensure absorbance values were less than 1.

- Karl-Fischer titrations were performed on a RTIL samples the water content was determined for pristine RTIL and RTIL/HTFSI solutions.

- Karl-Fischer titrations were performed on RTIL samples after the direct dissolution of lanthanides and U_3O_8.

- The redox properties of ferrocene were examined to determine the working reference electrode potential relative to more common reference electrodes including NHE and Ag/AgCl.

$$UCl_6 + 5\ Ag(NTf_2) \longrightarrow U(NTf2)_6 + 6AgCl\ (s)$$

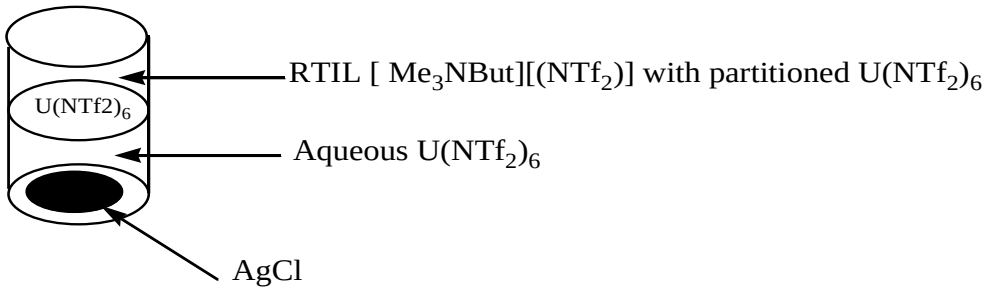

Schematic of experimental set-up for precipitation/complexation using $Ag(NTf_2)$.

Task 39 Knowledge-based Information Resource Management System for Materials of Sodium-Cooled Fast Reactor – Dr. Sean Hseih

Background

In the development of advanced fast reactors, materials and coolant/material interactions pose a critical barrier for higher temperature and longer core life designs. For sodium-cooled fast reactors (SFRs) such as the Experimental Breeder Reactors in Idaho and the Fast Flux Test Facility in Hanford, experience has shown that qualified structural materials and fuel cladding severely limits the IR economic performance.

Liquid sodium has been selected as the primary coolant candidate for the Advanced Burner Reactor (ABR) of the Global Nuclear Partnership (GNEP). Materials improvement has been identified as a major thrust to improve fast reactor economics. Researchers from universities, national laboratories, and related industrial participants have been continuously generating data and knowledge about materials and their interactions with coolants for the past few decades. Considering cost and time, the paradigm of designing and implementing a successful advanced nuclear system can be shifted and updated via the integration of information and internet technologies. Such efforts can be better visualized by implementing collective (centralized or distributed) data storages to serve the community with organized material data sets. Material property data provided by MatWeb.com and the ongoing development of a web-based material handbook for the Generation IV (GEN IV) advanced reactors are a few examples.

From a system design perspective, SFRs proposed in the GEN IV system have been significantly developed. Major activities defined in the current SFR research and development (R&D) plan can be summarized as the following:

- Ensuring that the needs and goals of the program are followed by the GEN IV International Forum (GIF) countries,

- Documenting and sharing the R&D progress and accomplishments, and
- Integrating relevant activities from GIF SFR R&D with GNEP.

All of these activities follow the path of data generation, analysis, knowledge discovery and, finally, decision making and implementation.

Research Objectives and Methods:

This project proposes to create a modularized web-based information system with models to systematically catalog and analyze existing data, and guide the new development and testing to acquire new data. Technically speaking, information retrieval and knowledge discovery tools will be implemented for researchers with both information lookup options from material databases and technology/development gap analysis from intelligent agent and reporting components. The goal of the system is not only to provide another database, but to also create a distributable and expandable, platform-free, location-free online system for research institutes and industrial partners. Such knowledge discovery and data mining processes generally include data integration, preparation and transformation, data mining and evaluation, and data visualization. Parallel to the development of these front-end analysis tools, web-based data updating and portal administration interfaces will also be designed and developed. Data collection will start during the early stage of the project due to its time consuming nature. The research objectives have been further divided into seven parts, described below:

To effectively identify research gaps. Past research on liquid metals need to be initially collected and documented.
To conduct requirement analysis on stakeholder identification, data-structure definition and analysis tool definition.
To design the multi-tier application architecture based on the requirement analysis. Two data sources, configuration settings and application contents, are stored in an XML (eXtensible Markup Language) file and Microsoft (MS) SQL Server database, respectively.
To develop the online system prototype to include database development, portal functionality development and portal presentation development.
To implement the web-based resource management system that integrates web portal programming and web server hardware configuration. A Windows-based resource management system will be designated as a web server while database servers can be located onsite with the web server, or at various locations depending on the accessibility of data sources.
To conduct system testing, debugging and refinement after the system is initially implemented.
To instruct graduate students and publish results related to information retrieval, and material search algorithm development.

Research Accomplishments:

The final project scope of the "Material Information System for Design, Analysis and Reporting" (MISDAR) was developed in
collaborators from LANL. Identified functionalities of the MISDAR are:

- Data manipulation (DM) with data uploading/updating/validation capabilities,
- Information search and analysis (ISA) with advanced search engine and organization algorithms
- System design (SD) with flexible data search engine and analysis tools
- Knowledge reporting (KR) with on-demand reporting tools.

Although the MISDAR is designed to document sodium-related data and information, the "Handbook on Lead-bismuth Eutectic Alloy and Lead Properties, Materials Compatibility, Thermal-hydraulics and Technologies (2007 Edition)," by the OECD/NEA Nuclear Science Committee, was initially used as a baseline reference and guideline on data classification, analysis, and presentation. The system under development will initially include thermo-physical and electrical properties, materials and testing issues,

thermal-hydraulics and system technologies, existing test facilities, safety guidelines and open issues and perspectives. Unlike the linear chapter arrangement seen in the paper material handbooks, the material properties and design objects of interest will be effectively presented through a sequence of search results, summary tables, and charts with reference hyperlinks.

The functional structures with the associated priority for the MISDAR implementation are: Portal Management (high), Portal Presentation (high), Data Manipulation (high), Knowledge Reporting (high), Information Search and Analysis (medium), and System Design (low).

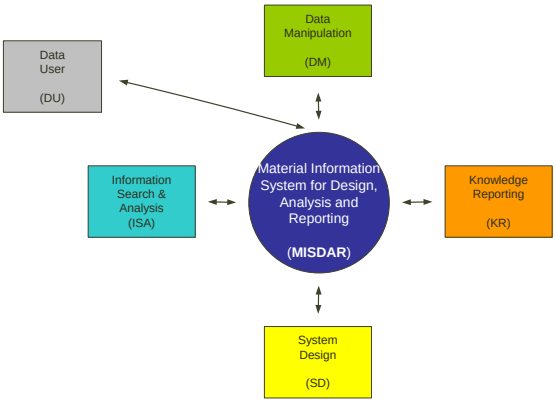

Main data flow diagram for the Material Information System for Design, Analysis and Reporting (MISDAR).

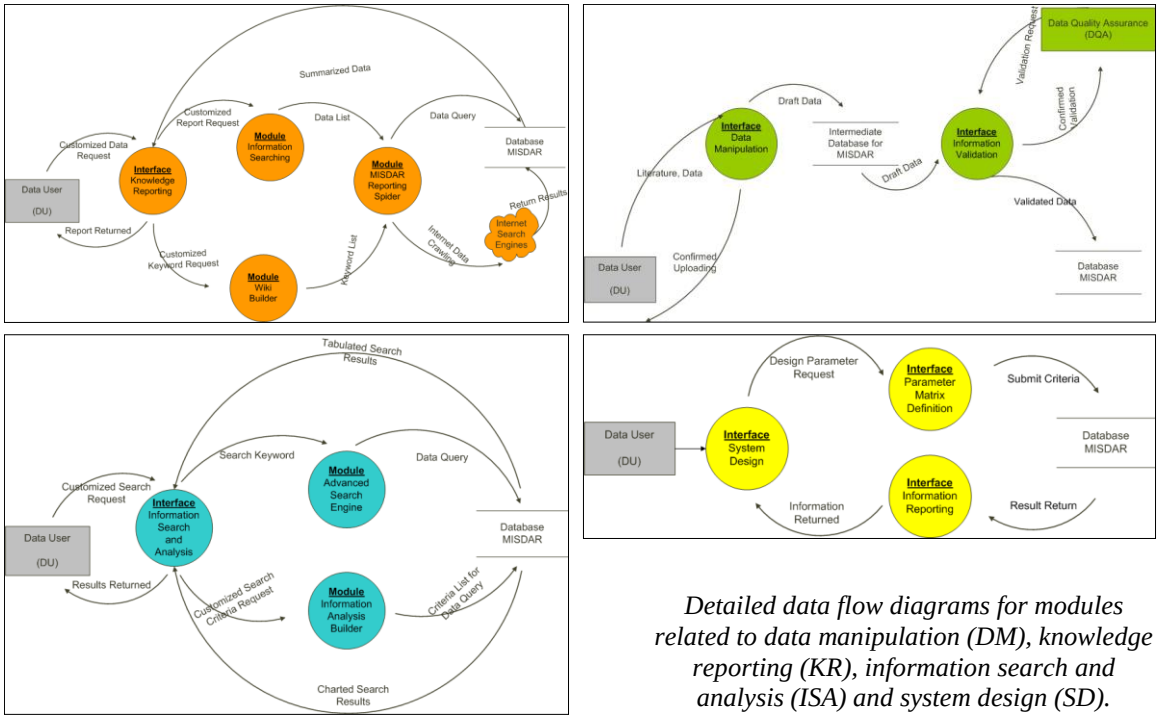

Detailed data flow diagrams for modules related to data manipulation (DM), knowledge reporting (KR), information search and analysis (ISA) and system design (SD).

Task 40 Evaluation of Fundamental Radionuclide Extraction Data for UREX – Dr. Ken Czerwinski

Background

The speciation of technetium and actinides in advanced solvent extraction systems is the basis for their manipulation in separations. The ability to understand and predict radionuclide speciation is paramount to successful modeling of proposed separation systems. This project will examine the speciation of radionuclides in different stages of the uranium extraction (UREX) separation scheme, providing data useful to modeling. The areas to be examined include the speciation of uranium and plutonium with tributylphosphate and the kinetics and thermodynamics of lanthanides and actinides in the TALSPEAK (Trivalent actinide lanthanide separation by phosphorous reagent extraction from aqueous complexes) system. The complexation constants of uranium and plutoniumu with tributylphosphate (TBP) will be evaluated. In the TALSPEAK system, studies will elucidate the difference in complexation kinetics for the lanthanides and actinides. Computational studies based on density functional theory will be performed for both systems.

Research Objectives and Methods:

Tributylphosphate-Based Extractions

The extraction of tetravalent Pu in nitric acid solution by TBP is well known and has been the basis of Pu purification for a number of decades. However, the data needed for detailed modeling of Pu extraction is not available for all conditions of concern to the Advanced Fuel Cycle Initiative.

Understanding the role of nitrate in plutonium speciation is important for determining the necessary data for plutonium extraction modeling. Data indicates the dinitrate complex of plutonium is strong and may account for difficulties in modeling plutonium extraction under some nitrate conditions. The formation of hydrolysis products may also form an extractable species that will need to be included in modeling. In the UREX process, acetohydroxamic acid (AHA, see figure below) is expected to be used. For the separation of Pu in a solvent extraction system using acetohydroxamic acid, it is necessary to determine the complexation kinetics and thermodynamics. In addition, since plutonium is a redox sensitive element, the change in speciation due to oxidation-reduction reactions upon complexation needs to be evaluated. This project will experimentally evaluate the fundamental speciation of plutonium and uranium in the TBP-dodecane-nitric acid system, with the main emphasis on nitrate speciation and subsequent third phase formation at high nitric and metal ion conditions. Experiments on the AHA systems will be conducted in collaboration with Argonne National Laboratory (ANL) with input from the U.S. Department of Energy Separations Working Group. For this project the focus will be on the evaluation on U and Pu complexation constants with TPB.

Lanthanide-Actinide Separations

The separation of trivalent lanthanides from trivalent actinides, and americium from curium, has been identified as a topic for investigations by the Global Nuclear Energy Partnership (GNEP). These separations are based on slight differences in ionic radii, small variations in Lewis acidity between the lanthanides and actinides, and redox state speciation.

Numerous ligands have been examined for actinide and lanthanide separations, some of which are the basis of separation schemes. In this work efforts will focus on the TALSPEAK process through the determination of thermodynamic and kinetic data necessary for separation modeling. The TALSPEAK conditions include an aqueous phase with 1 M lactic acid and 0.1 M diethylenetriaminepentaacetic acid (DTPA). In the original work, the lanthanides are extracted from the aqueous phase at pH 3 with an organic phase of 0.3 M Bis(2-ethylhexyl)phosphoric acid (HDEHP). The actinides americium and curium are then extracted into 0.3 M HDEHP at pH 1.5. The actinides can be removed from the organic phase with dilute mineral acid. Recent GNEP related results have focused on evaluating kinetic and thermodynamic parameters for the extraction of actinides and lanthanides in the TALSPEAK process. While complexation data is available for the interaction of americium and curium with some ligands used

in the TALSPEAK process, further efforts are necessary to complete the appropriate dataset for modeling separations in AMUSE (Argonne Model for Universal Solvent Extraction). Acquiring the necessary kinetic and thermodynamic data for AMUSE modeling of lanthanide and actinide extractions will be an important element of this project.

Evaluation of Chemical Thermodynamic and Kinetic Data

The goal of our plutonium and uranium speciation studies will be to obtain data for modeling the behavior of the actinides under a range of extraction conditions, including acid concentration, metal ion concentration, and temperature. Speciation calculations can be performed if the stability and solubility constants for the chemical species formed under the examined conditions are known. If conditions under which precipitation of the actinide occurs, solubility studies of the precipitated species will be included. A general chemical reaction is described as:

$$aM^{z+} + bL^{x-} \Leftrightarrow M_aL_b{}^{(az-bx)}$$

for complexation where M is the metal ion and L is a ligand. In the case of the extraction system under investigation, two ligands may be considered, namely nitrate and TBP. The kinetics of the reaction can be measured to establish conditions needed for equilibrium. For the extraction system under study the kinetics are expected to be rapid. However, kinetic evaluation of third phase formation may be needed.

Enthalpy and entropy will be investigated by evaluating the stability constant as a function of temperature. For a system with different species, if the stability constants are known, then all the species can be calculated at any given pH. The thermodynamic data can also easily be incorporated into existing codes such as AMUSE or the geochemical code CHESS.

Computational studies

Density functional theory (DFT) calculations will be performed to evaluate the electronic structure of the radionuclide species in the extraction system. Initial DFT calculations on the actinides have been performed using an all electron relativistic calculation rather than a relativistic effective core potential. The DFT calculations will provide a means to compare experimental spectroscopy data that investigates structure and electron transitions, providing a basis for examining and comparing the role of 5f electron mechanisms involved in the crucial species in separation systems.

Research Accomplishments:

- Extractions were performed at constant ionic strength. Aqueous solutions contained HNO_3, $UO_2(NO_3)_2$, $LiNO_3$, and the ionic strength was adjusted using $NaClO_4$. The organic phase consisted of pre-equilibrated 30% TBP/dodecane. It was mixed for 2 minutes, centrifuged, and separated for analysis. Diluted samples were analyzed by IC and ICP-AES.
- Four sets of extractions were performed for determining Eu-DTPA complexation constant for TALSPEAK separations studies. In the aqueous phase, DTPA varied from $1x10^{-7}$ to $5x10^{-7}$ M, ionic strength was 0.1M, pH of 3.60, and trace amount of ^{152}Eu. In the organic phase, $2x10^{-4}$ M HDEHP in dodecane pre-equilibrated three times. Analysis was performed on organic and aqueous phases by Liquid Scintillation Counting. The pH was measured in the aqueous phase after equilibration. The electrode was calibrated and adjustments were made in order to determine H^+ concentration.
- A slug flow problem was identified that affected UV-Vis spectra. The physical positions of the instrumentation was changed to alleviate issue.
- Steady-state conditions were successfully demonstrated in the contactors with a non-radioactive feed solution (after repairing leaks and checking flow rates via mass balances and flow meters). The radioactive feed solution used after this steady state was achieved, and the data acquired shows hot feed growing in as cold feed is pushed out.

- DFT calculations were performed of the possible equilibrium structures of the $UO_2^{2+}/NO_3^-/H_2O$ system for various concentrations of NO_3^- with determination of the corresponding molecular orbital energy levels and population analysis.

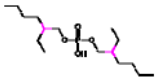	Bis(2-ethylhexyl)phosphoric acid (HDEHP) for TALSPEAK
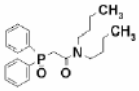	Diphenyl-N,N-dibutylcarbamoyl phosphine oxide (CMPO) for TRUEX
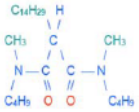	N,N'-dimethyl-N,N'-dibutyl-2-tetradecyl-malonamide (DMDBTDMA) for DIAMEX
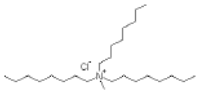	Quaternary ammonium salts (Aliquat 336)
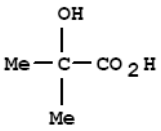	α–hydroxyisobutyrate

Examples of ligands for actinide and lanthanide separations

TBP-HNO_3-Np^{4+} third phase appearance

Task 41 Implementation of Uncertainty Propagation in TRITON/KENO – Dr. Charlotta Sanders, Dr. Denis Beller

Background

Monte Carlo methods are beginning to be used for three-dimensional fuel depletion analyses to compute various quantities of interest, including isotopic compositions of used nuclear fuel. The TRITON control module, available in the SCALE 5.1 code system, can perform three-dimensional (3-D) depletion calculations using either the KENO V.a or KENO-VI Monte Carlo transport codes, as well as the two-dimensional (2-D) NEWT discrete ordinates code. To overcome problems such as spatially non-uniform neutron flux and non-uniform statistical uncertainties in computed reaction rates and to improve the fidelity of calculations using Monte Carlo methods, uncertainty propagation is needed for depletion calculations.

Research Objectives and Methods:

To enhance and expand the proper/informed use of Monte Carlo methods for 3-D depletion analyses, statistical uncertainty propagation will be developed and implemented in the TRITON/KENO sequence of SCALE. In particular, work will focus on development and implementation of an approach to determine the uncertainty in isotopic predictions based on the compound effects of multiple calculations (depletion time steps) with stochastic uncertainties in the spatial fluxes in each time step. Subsequently, an evaluation of the statistical uncertainties for an actual commercial used fuel sample will be performed to verify the implementation and develop a better understanding of the importance of statistical uncertainties in the prediction of isotopic compositions.

Research Accomplishments:

This project was initiated in collaboration with Oak Ridge National Laboratory. The first step was initial acquisition of the TRITON/KENO code system from ORNL and identification of a test problem for evaluating the code. An initial test problem was identified and modeled in TRITON and KENO.

Studies of the Pressurized Water Reactor Rim Effect were used to verify the TRITON code implementation. Examination of uncertainty propagation will follow verification and benchmarking studies.

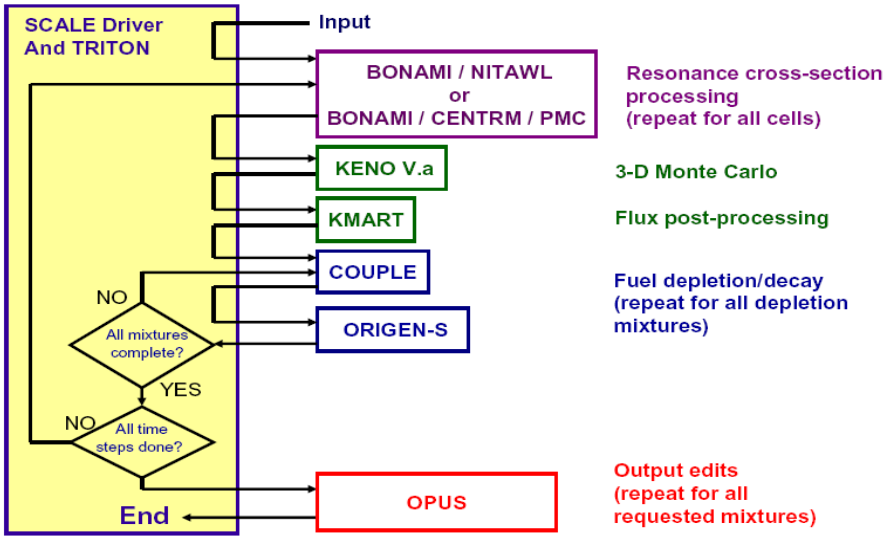

Flowchart of TRITON-K-5 Sequence (photo from the Nuclear Science and Technology Division, Oak Ridge National Laboratory).

Task 42 Monaco/MAVRIC Evaluation for Facility Shielding and Dose Rate Analysis – Dr. Charlotta Sanders, Dr. Denis Beller

Background

The dimensions and the large amount of shielding required for Global Nuclear Energy Partnership (GNEP) facilities, advanced radiation shielding, and dose computation techniques are beyond today's capabilities and will certainly be required. With the Generation IV Nuclear Energy System Initiative, it will become increasingly important to be able to accurately model advanced Boiling Water Reactor and Pressurized Water Reactor facilities, and to calculate dose rates at all locations within a containment (e.g., resulting from radiations from the reactor as well as the from the primary coolant loop) and adjoining structures (e.g., from the spent fuel pool).

In complex geometry problems, Monte Carlo methods are often used to compute fluxes or dose rates over large areas using mesh tallies. For problems that demand that the uncertainty in each mesh cell be less than some set maximum, computation time is controlled by the cell with the largest uncertainty. This issue becomes quite troublesome in deep-penetration problems, and advanced variance reduction techniques are required to obtain reasonable uncertainties over large areas. To overcome this issue, Oak Ridge National Laboratory (ORNL) has developed a new sequence, MAVRIC, which will be available with the release of SCALE 6. In this sequence, a methodology called Consistent Adjoint-Driven Importance Sampling (CADIS) has been incorporated for effective variance reduction. This was developed to quickly and automatically determine the biased source distribution and weight windows over a rectangular mesh and a given energy group structure. The method first determines the approximate adjoint particle flux, usually using a discrete ordinates code. The source for this calculation is the detector energy-group response for the process of interest (e.g., dose rate) at the location(s) of interest. The resulting adjoint flux at each location and energy is equated to the importance of particles and is combined with the source distribution to generate the biased source and weight window values that control particle populations at all locations. Very recently, a variation of the CADIS methodology, referred to as the Forward-Weighted CADIS (FW-CADIS) method has been developed, implemented in MAVRIC, and demonstrated for optimization of dose maps.

Research Objectives and Methods:

The MAVRIC sequence is being evaluated along with the Monte Carlo engine MONACO to investigate its effectiveness and usefulness in facility shielding and dose rate analyses. A previously MCNP-evaluated cask array from the Yucca Mountain Project's proposed aging pad and/or buffer area design will be utilized for evaluation and benchmarking purposes. In addition, dose mapping will be performed inside the surface facilities utilizing a transportation cask to evaluate the effectiveness of the code systems. The ability to calculate doses in deep-penetration problems will also be evaluated.

Research Accomplishments:

The project was initiated in collaboration with ORNL. The first step was initial acquisition of the MONACO/MAVRIC code system from ORNL and identification of a cask array configuration for evaluating the code. 3-D importance/tally mesh was optimized for neutron-photon transport simulation of a single used fuel aging cask. This configuration was modeled in MAVRIC and the model was transmitted to ORNL for review. In addition, inputs were established for a variety of 4x4 cask arrays to match cask storage configurations anticipated at the Yucca Mountain Project. Analyses for the 4x4 aging cask arrays were optimized with respect to dose analysis in between and far from the casks. In addition, the practicality of analyzing a 12 x (4x4) aging cask array is being evaluated with respect to memory limitations.

Other progress:

- Previously encountered memory issues with the SCALE/MONACO/MAVRIC code were resolved by ORNL.
- Dose assessment of a single aging cask was completed. The data indicates excellent agreement to

previous data obtained analyzing the same geometry with the MCNP code.

- Complex cask geometry incorporating air vents has been evaluated. As anticipated, the dose rate profile around the cask is slightly different when compared to a simple geometry, and higher dose rates are observed close to the air vents just outside the cask.
- Neutron-neutron and neutron-photon source-response analysis is being examined to determine if it significantly alters the results for much quicker photon-photon analysis.

Task 43 Standardization of Reference Materials for Environmental Monitoring and Safeguards – Dr. Ralph Sudowe

Background

The complete dissolution and subsequent radiochemical analysis of a soil sample allows for the determination of the total amount of radionuclides that the sample contains. On the other hand it gives only very limited information about the bioavailability of the radionuclides present. The later is however of great importance for assessing the risk that is associated with the presence of these radionuclides in the environment. By treating the soil sample with a series of increasingly more aggressive chemicals it is possible to determine under which conditions the radioactive material might become mobile and enter the surrounding environment. This technique is called sequential extraction. The goal of this project is to develop a robust and standardized sequential extraction protocol that can be applied to a variety of samples. Two different reference materials, ocean sediment and lake sediment, are used to optimize the protocol. This project is conducted in collaboration with the National Institute for Standards and Technology (NIST) in Gaithersburg, VA. This project engaged one Ph.D. student during the reporting period.

Accomplishments of the Research

The complete dissolution and subsequent radiochemical analysis of a soil sample allows for the determination of the total amount of radionuclides that the sample contains. On the other hand it gives only very limited information about the bioavailability of the radionuclides present. The later is however of great importance for assessing the risk that is associated with the presence of these radionuclides in the environment. By treating the soil sample with a series of increasingly more aggressive chemicals it is possible to determine under which conditions the radioactive material might become mobile and enter the surrounding environment. This technique is called sequential extraction. The goal of this research is to optimize a sequential extraction procedure for maximum dissolution of actinide elements thorium, uranium, plutonium and americium. Stable trace metals will be evaluated for phase selectivity as well as modeling of important groups of environmental contaminants. A sequential extraction procedure developed at the National Institute of Standards and Technology (NIST) for freshwater lake sediment will be optimized for additional actinide elements as well as trace elements. In addition, this research will evaluate the selectivity and recovery of each step of the fractionation procedure by adding solid matrix spikes to the sediment. The spikes will consist of a well characterized soil phase comparable to the fraction of interest spiked with a known amount of radioisotope. By examining the metal recovery of phases to which the solid matrix spikes have been added, one can achieve a better understanding of the quantification of the losses by re-adsorption in each fraction.

As a first step in this research, a procedure was developed for the sequential extraction based on a 2009 paper by I. Outola et. al. This procedure was then checked for problems and questionable steps by applying it to standard reference material IAEA 375 as sediment sample. The leachates were analyzed for trace elements by ICP-AES. On this initial sample no analysis for actinide elements was performed because it was necessary to first develop a procedure based on extraction chromatography for the necessary separations. The work of Outola et al. employed ion exchange as a separation technique.

A literature search was performed to assist with the selection of a suitable separation procedure for uranium, plutonium, thorium and americium in a soil sample using extraction chromatography. The method selected was based on a 2006 paper by S.L. Maxwell et al. Since the extraction chromatography method had not been used with the various reagents used in the sequential extraction procedure, experiments were then run to examine any losses in recovery when these two methods were run in tandem. Table 1 shows the maximum concentration of the reagents used during the sequential extraction procedure as well as the operationally defined target phase.

Fraction	Target Phase	Reagent	Max. Concentration
I	Exchangeables	$MgCl_2$	1 M
II	Carbonates	NH_4Ac in 25% HAc	2 M
III	Fe/Mn Oxides	$NH_2OH{\cdot}HCl$ in 25% HAc	0.1 M
IV	Organic	30% H_2O_2 in 0.05 M HNO_3	30 wt %
V	Residual	HNO_3	16 M

Table 1. Maximum concentrations of sequential extraction reagents used in Outola et al. procedure.

A single isotope study was designed and performed to examine the behavior of each actinide element throughout the extraction chromatography procedure. Tracers were run through the extraction chromatography procedure and eluates were collected for each step of the procedure. This allowed for analysis of total recovery as well as the determination of column breakthrough. The tracers used included ^{243}Am, ^{230}Th, and ^{242}Pu. Each experiment was conducted in triplicate to improve statistical accuracy.

In addition the effect of the reagents utilized for the sequential extraction on the performance of the extraction chromatography procedure was investigated. A blank sample as well as samples with reagents from fractions I-V of the sequential extraction procedure were prepared in triplicate for the study using tracers of ^{229}Th, ^{232}U, ^{242}Pu and ^{243}Am. The samples were prepared for alpha spectroscopy and counted for one week.

As an alternative to the Maxwell procedure a recently published separation method by Thakur et al. is also being investigated. The procedure involves an anion exchange column (AG 1-X8) to first separate Am/U from Th/Pu. Thorium and plutonium are then eluted from the anion exchange column and prepared for alpha spectroscopy by CeF3 microprecipitation. Uranium is then separated from americium using UTEVA. Americium is then further purified using TRU and TEVA resins. Uranium and americium samples will also be prepared for alpha spectroscopy using CeF_3 microprecipitation. This part of the research was conducted by a summer student from the Nuclear Fuel Cycle Summer School sponsored by the Department of Energy.

Presentations, Papers, Publications

1. Faye, S.A., Georgetown, B.A., Sudowe, R., *Evaluation of sequential extraction reagent effects on extraction chromatography resins*, Presentation at the 2011 ANS Student Conference, Atlanta, GA, SA , April 14-17, 2011.
2. Faye, S.A., Georgetown, B.A., Sudowe, R., *Evaluation of matrix effects of sequential extraction solutions on extraction chromatography resins*, Presentation at the Radionuclide Speciation Workshop at the 56th Annual Radiobioassay and Radiochemical Measurements Conference, Richland, WA, USA, October 25-28, 2010.

Names of Students who were Engaged in the Research

Sherry Faye (Ph.D. Radiochemistry)

Task 44 Development of Rapid Chemical Separations for the Study of Short-Lived Isotopes – Dr. Ralph Sudowe

Background

The goal of this project is the development of chemical separation systems that can be used for the study and measurement of short-lived isotopes, in particular the heavier actinide and transactinide elements. The work focuses on the use of extraction chromatography as a separation technique due to its high potential for automation of the developed procedure. This project supported on Ph.D. student during the reporting period.

Accomplishments of the Research

The goal of this research is to perform systematic studies on different extraction chromatographic resins that can be applied to the chemical characterization of elements 104 and 105, Rf and Db, respectively. DGA and the crown ether based Pb and Sr resins are extraction chromatographic resins that are commercially available from Eichrom Technologies, Inc. In addition to these three commercially available resins additional crown ether based resins were be made in-house and investigated. The extractant molecule used for the in-house made resins were be dicyclohexano-18-crown-6 and dibenzo-18-crown-6. In order for these resins to be effective in assessing the role of relativistic effects in the chemical behavior of Rf and Db, they must exhibit different extraction behavior for the lighter homologs and pseudo-homologs. Two types of chemistry set-ups can be envisioned for the use of Eichrom's DGA resin, either as a separation step for nuclides embedded in a catcher block based or for chemistry experiments performed behind a gas-filled physical pre-separator. In the case of the crown ether based resin the chemistry must be done behind a gas-filled pre-separator.

Eichrom's Sr and Pb resin have been investigated for use in the chemical characterization of Rf. The initial results indicated that these resins may be suited for use with on-line studies. However upon further investigation using dynamic column studies, these resins do not appear to provide adequate separation of Hf and Zr, as Hf elutes in both the Hf and Zr fractions. Based on these results, the initial Hf elution volume, 3mL, was increased to 5mL, in hopes of achieving an improved separation of Hf and Zr. The results show that increasing the elution volume for the Hf fraction effects the separation of Hf and Zr very little. Previous liquid-liquid studies conducted by Sudowe et al. showed better separation of Hf and Zr at lower concentrations of HCl, therefore the elution of Hf on dynamic columns using 7,8, and 9M HCl was investigated for both of Eichrom's resins. Based on the experimental results these systems do not show promise in unambiguously determining the chemical properties of Rf.

Previous work by Sudowe et al. illustrated that dicyclohexano-18-crown-6 (DC18C6) and dibenzo-18-crown-6 (DB18C6) shows promise for the chemical characterization of Rf in liquid-liquid extraction systems. However it is difficult to automate the liquid-liquid extraction system studied due to the high concentrations of hydrochloric acid involved. It would therefore be benefical to extend these studies to systems based on the utilization of extraction chromatographic resins. Resins were prepared analogous to the method used by Horwitz et al. for the Sr-Spec column material. A 10mL solution of 0.75M or 0.35M crown ether (DC18C6 and DB18C6 respectively) was prepared with either 1-octanol or dichloromethane. Dry Amberchrom resin was weighed out to give a mass crown to mass Amberchrom ratio of about 5. The dry resin was slurried in methanol until completely wet, before addition of the crown ether solution. Methanol was removed under vacuum (360 torr) at 40 ºC to yield the desired coated resin. Each resin was dried overnight in an oven at 40 ºC to ensure all methanol had been removed.

Resins containing 0.75M dicyclohexano-18-crown-6 synthesized with dichloromethane, 1-octanol or 1-dodecanol were investigated to determine the effect the solvent had on separations of Zr and Hf. Batch study results indicated there was little difference in uptake of Zr and Hf on the resins synthesized with different solvents. There was an indication that the best potential for separation on a dynamic column would be from a load solution of concentrated HCl and elution of Hf in 10 to 11M HCl, as this was where the highest separation factors of Zr and Hf occurred. However, the results of Sudowe and co-workers showed the best separation of Zr and Hf to occur between 7 and 8M HCl. Based on the results of the batch studies and the results of Sudowe et. al. the elution behavior of Hf at 7, 8, 10 and 11M HCl was investigated, while Zr elution off the column was investigated at 3M HCl. It was expected, from batch studies that Hf would elute from the columns first, followed by Zr. The elution profiles for Hf were

investigated at 7, 8, 10 and 11M HCl, while Zr was eluted from the column with 3M HCl. It was determined that none of the resin showed sufficient separation of Zr and Hf to be used to assess the chemical behavior of Rf compared to its lighter homologs.

Three resins containing 0.75M di-t-butylcyclohexano-18crown-6, 0.75M dicyclohexano-18-crown-6 and 0.75M dibenzo-18-crown-6 have been investigated to determine the influence the functional group has on the separation of Zr and Hf. Based on the batch study results the best potential for separation on a dynamic column was with a load solution of 11M or concentrated HCl and elution of Hf in 10 to 11M HCl, as this is where the highest separation factors of Zr and Hf occurred. However, the results of Sudowe and co-workers showed the best separation of Zr and Hf to occur between 7 and 8M HCl. Based on the results of the batch studies and the results of Sudowe et. al. the elution behavior of Hf at 7, 8, 9 and 10M HCl from a load solution of 11M HCl was investigated for Eichrom's Pb resin and elution behavior of Hf at 7, 8, 10 and 11M HCl from a load solution of concentrated HCl was investigated for the in-house synthesized resins. Zr elution off the columns was investigated at 3M HCl. It was expected, from batch studies that Hf would elute from the columns first, followed by Zr. The elution profiles for Hf were investigated at 7, 8, 9 and 10M HCl for Eichrom's Pb resin and at 7, 8, 10 and 11M HCl for the in-house resin, while Zr was eluted from the column with 3M HCl. It was determined that none of the resin showed sufficient separation of Zr and Hf to be used to assess the chemical behavior of Rf compared to its lighter homologs.

Two resins containing 0.75M di-t-butylcyclohexano-18crown-6 at concentrations of 0.75 and 1.0M have been investigated to determine the influence of extractant concentration on the separation of Zr and Hf. Based on the batch study results the best potential for separation on a dynamic column was from a load solution of 11M and elution of Hf in 10 M HCl, as this is where the highest separation factors of Zr and Hf occurred. Zr elution off the columns was investigated at 3M HCl. It was expected, from batch studies that Zr and Hf would have higher retention on Eichrom's Sr resin and eluted at higher volumes. It was also expected that Hf would elute from the columns first, followed by Zr. The elution profiles for Hf were investigated at 10M HCl, while Zr was eluted from the column with 3M HCl. It was determined that neither of the resin showed sufficient separation of Zr and Hf to be used to assess the chemical behavior of Rf compared to its lighter homologs.

Presentations, Papers, Publications

Bennett, M.E., Despotopulos, J.D., Henderson, R.A., Shaughnessy, D.A., Sudowe, R., *Extraction chromatographic studies of Rf homologs using crown ether based resins*, Presentation at the 2011 ANS Annual Meeting, Hollywood, FL, USA, June 26-30, 2011

Oganessian, Yu.Ts., Abdullin, F.Sh., Bailey, P.D., Benker, D.E., Bennett, M.E., Dmitriev, S.N., Ezold, J.G., Hamilton, J.H., Henderson, R.A., Itkis, M.G., Lobanov, Yu.V., Mezentsev, A.N., Moody, K.J., Nelson, S.L., Polyakov, A.N., Porter, C.E., Ramayya, AV., Riley, F.D., Roberto, J.B., Ryabinin, M.A., Rykaczewski, K.P., Sagaidak, R.N., Shaughnessy, D.A., Shirokovsky, I.V., Stoyer, M.A., Subbotin, V.G., Sudowe, R., Sukhov, A.M., Tsyganov, Yu.S., Utyonkov, V.K., Voinov, A.A., Vostokin, G.K., Wilk, P.A., *Synthesis of a new element with atomic number Z = 117*, Presentation at the 241st ACS National Meeting & Exposition, Anaheim, CA, USA, March 27-31, 2011

Bennett, M.E., Despotopulos, J.D., Henderson, R.A., Shaughnessy, D.A., Sudowe, R., *Extraction chromatographic studies of Rf homologs using crown ether based resins*, Presentation at the 241st ACS National Meeting & Exposition, Anaheim, CA, USA, March 27-31, 2011

Bennett, M.E., Despotopulos, J.D., Henderson, R.A., Shaughnessy, D.A., Sudowe, R., *Extraction chromatographic studies of Rf homologs with Eichrom's Pb and Sr resins*, Presentation at the 9th Workshop on Recoil Separator for Superheavy Element Chemistry, Darmstadt, Germany, November 18, 2010

Names of Students who were Engaged in the Research

Megan Bennett (Ph.D. Radiochemistry, graduated Spring 2011)
John Despotopulos (Ph.D. Radiochemistry)
1. -13, 2009

Task 45 Advanced Mass Spectroscopy Techniques for Materials Accountancy – Dr. Gary Cerefice

PI: Gary Cerefice, Asst. Professor (Health Physics, Radiochemistry)
Co-PI: Ken Czerwinksi, Professor (Chemistry, Radiochemistry)
Student: Keri Campbell, Radiochemistry Ph.D. Program

Project Summary:

Modern safeguards practices for a fuel recycling facility, such as the Rokkasho facility in Japan, require that hundreds of process samples be collected daily for destructive analysis (DA) to measure plutonium content and isotopics. Current practice for DA is based on chemical separation of the plutonium followed by high-precision mass spectroscopy (or other techniques) to measure plutonium content and isotope ratios. Due to the time required to process these samples prior to analysis, these measurements can often result in days (or weeks) delay in reporting the mass balance for the facility. For solid matrices, such as Mixed Oxide fuel (MOx), the process becomes even more time intensive as the samples must first be dissolved prior to conditioning and analysis.

The goal of this project is to develop and optimize advanced mass spectroscopy techniques for the analysis of both process solution and fuel matrix samples. Dynamic reaction cell inductively coupled plasma mass spectroscopy (DRC-ICP-MS) techniques have the potential to allow the separation of plutonium from its isobaric interferences as part of the analytical method, eliminating the need for chemical separation prior to analysis. Laser ablation mass spectroscopy (LA-ICP-MS) replaces the traditional solution sample introduction system with a laser ablation system, allowing the direct analysis of solid matrices and eliminating the need for sample dissolution for safeguards or quality assurance measurements in fuel matrices. Methods for the analysis of process stream samples and fuel products will be developed and compared with traditional safeguards and quality control destructive analysis procedures to evaluate the relative processing time, method detection limits, and method uncertainties to support the potential deployment of these techniques as part of a next-generation recycling facility.

Highlights

- (U/Zr)O2 matrix "standards" were synthesized across the full range of U:Zr ratios. Characterization of these standard samples is underway.

- LA-ICP-MS methodology was modified to incorporate correction factors for ionization potential, determined from solution standards of the elements in the sample matrix. Resulting method showed significantly better performance in determining U:Zr ratio in most samples.

Project Overview

There has been a revival of interest in the use of MOX (Mixed Oxide Fuel) which contains more than one oxide of fissile material as a potential fuel for generation IV reactors. There has been previous work done concerning the addition of an inert oxide, most commonly zirconia (ZrO_2), because of the expected enhancement in chemical stability and radiation resistance [1]. The addition of zirconia into mixed oxide and Th-U fuels has been shown to increase the durability of the fuel and the bonding between the phases [2]. Inert fuel matrices have the advantage of burning Pu and other transuranic elements from the fuel cycle without the production of other actinide elements which is desirable for proliferation acts. Of the possible materials for use in an inert matrix, ZrO_2 has been examined. The inclusion of ZrO_2 is expected to increase chemical stability and radiation resistance [1]. The natural analogue of zirconia, baddeleyite ($(Zr,M)O_2$), where M is a tetravalent ion such as hafnium), contains up to 3000 ppm uranium or thorium [1]. This supports the durability of inert matrix fuels using ZrO_2 in reactor conditions and repository conditions. Fuels intended for use must be assayed, whether destructive or non-destructive, for safeguard purposes. This is to ensure accountability of material and that the composition is desired. This is an issue in regards to

1. Gong W.L. et al., (2000) *Zirconia Ceramics for Excess Weapons Plutonium Waste*. Journal of Nuclear Materials, 277: 239-249
2. De Lima N.B., K. Imakuma, (1985) *X-ray Diffraction Study of the Formation of Solid-Solutions in Urania-Thoria Prepared by Aqueous Chemical Processes*. Journal of Nuclear Materials, 135: 215-221.

ZrO_2 which necessitates the use of potentially hazardous reagents such as hydrofluoric acid for dissolution in destructive assay [3].
The application of laser ablation-inductively coupled plasma mass spectrometry (LA-ICP-MS) to determine isotope ratio measurements grants superior technology for direct solid sampling in analytical chemistry. The advantages of this technique include reduced risk of contamination by direct sample analysis, no chemical dissolution necessary, and determination of spatial distributions of elemental compositions [4].
LA-ICP-MS is desirable for measuring uranium-zirconium oxides due to the difficulties in dissolving $Zr0_2$, which necessitates the use of potentially hazardous reagents such as hydrofluoric acid [3]. Dissolution procedures for uranium and zirconium oxides are often tedious and require lengthy periods of time for complete dissolution, which is problematic when trying to determine an accurate ratio of Zr: U in a given sample.
LA-ICP-MS has several limitations that can inhibit the utilization of this technique for many samples. A major limitation is elemental fractionation which is the non-sample related variation of the analyte response during the ablation process. Ablation is affected by the laser wavelength, which can vary from 157 to 1064 nm [5]. Shorter laser wavelengths produce higher ablation rates and result in lower elemental fractionation. Preferential vaporization of elements from the sample (in this case uranium) and the possibility of the composition altering during transport can lead to deviations in sample conditions [4]. The large particulates can undergo incomplete vaporization in the ICP and contributes to the elemental fractionation [4]. A second limitation of this technique is transportation efficiency, which relies on the volume of the ablation cell, flow rate of inert gas, and length of transport tube [6]. Particles of various sizes are generated during the ablation process and depending on the range of the particle sizes can decrease the transport efficiency.
Phase explosion is a process that occurs when a sample is rapidly heated beyond its normal boiling point and becomes a meta-stable liquid near its critical state. A dramatic change in the crater depth at different irradiances is an indication of phase explosion [4]. Other sample removal processes include desorption and thermal evaporation [7]. Once phase explosion occurs, a considerable increase in the quantity of mass removed is observed.
It is difficult to calibrate the LA-ICP-MS to determine elemental concentrations in solid samples. Calibration in general requires matrix-matched standards [4] and there is no universal method for calibrating solids. Three general calibration strategies are used for calibrating solid samples: external calibration using a solid reference standard, calibration using solutions, and external calibration to a solid reference standard in combination with internal standardization [4]. In this experiment, different methods of calibration were examined using both solids and solutions.

Results To-Date

Evaluation of Hydride Formation for Dissolved Samples
The formation of molecular plasma species, in particular hydride species, is known to occur in inductively coupled plasma (ICP) sample introductions systems. This can be problematic in determining small quantities of ^{239}Pu in large quantities of ^{238}U. The literature values reported for the $^{238}UH+/^{238}U$ ratio range from $1.2x10^{-4}$ to $5.0x10^{-6}$ [8]. The goal of this subtask was to quantify the formation of uranium hydrides from a dissolved sample matrix. The impact of instrument parameters on the hydride formation will be

3. Kohl, F., N. Jakubowski, N., Brandt, R., Pilger, C., and J.A.C. Broekaert. (1997) *New strategies for Trace Analyses of ZrO2, SiC and Al2O3 Ceramic Powders.* Fresenius J. Anal. Chem. 359 4-5:317-325.
4. Mokgalaka, N.S., and J.L Gardea-Torresdey. (2006) *Laser Ablation Inductively Coupled Plasma Mass Spectrometry: Principles and Applications.* Appl. Spectros., 41: 131-150
5. Alexander, M.L., Smith, M.R., Hartman, J.S., Mendoza, A., and Koppenaal, D.W. (1998) *Laser ablation ICP-MS*. Appl. Surf. Sci., 127–129: 255–261
6. Arrowsmith, P. and Hughes, S.K. (1988) *Entrainment and transport of laser ablated plumes for subsequent elemental analysis*. Appl. Spectros., 42 (7): 1231–1239.
7. Mao, X.L., Borisov, O.V., and Russo, R.E. (1998) *Enhancements in laser ablation ICP-AES based on laser properties and ambient environment*. Spectrochim. ActaB, 53: 731–739.
8. Vais, V., Chunsheng, L., Cornett, J., *Preventing uranium hydride formation in standard uranium samples for determination of 239Pu by ICP-MS*. J. Anal. At. Spectrom., 2004, 19, 1281-1283.

examined, and the results used to optimize an analytical method for minimizing hydride formation and its impact on ^{239}Pu measurement in a uranium-bearing sample.
A stock solution of uranium was prepared from a 1000 ppm standard solution of uranium in 2% HNO_3 (High Purity Standards cat# 100064-1) was volumetrically diluted in 2% HNO_3 stock solution. To determine the impact of uranium concentration on hydride formation, samples were prepared with a uranium concentration between 1 to 100 ppb for analysis. Both the 238 and 239 mass numbers were evaluated.
During this quarter the quantification of the hydride formation from 1-100 parts per billion of $^{238}Uranium$. The system was optimized both in hardware and software to determine the settings that would result in the lowest hydride formation. The instrument parameters were established using the Perkin-Elmer specified calibration solution (a multiple isotope calibration standard developed by the instrument vendor). The parameters used are shown in table T1. Data analysis was done using the vendor software for the system, which provides three options for signal processing: quantitative, spectral peak processing, and signal profile processing [9].

Table T1: Operating Parameters for ELAN DRC II mass spectrometer

Nebulizer gas flow rate	1.02 L min^{-1}
Auxiliary gas flow rate	1.2 L min^{-1}
Plasma gas flow rate	15 L min^{-1}
Lens Voltage	6 V
Quadrupole rod offset	0 V
RF Power	1100 W
Number of Sweeps	20
Number of Replicates	7
Dead Time	55 ns

The data consists of a series of intensity data points plotted against time. The intensity versus time signal profile is processed to generate a final intensity value that is representative of the peak. The signal profile processing uses a Savitzky-Golay moving point average over the readings. The processed data is presented in figure F1 along with the raw data for comparison (no processing).

9. ELAN Version 3.3 Software Guide, PerkinElmerSCIEX, 2004.

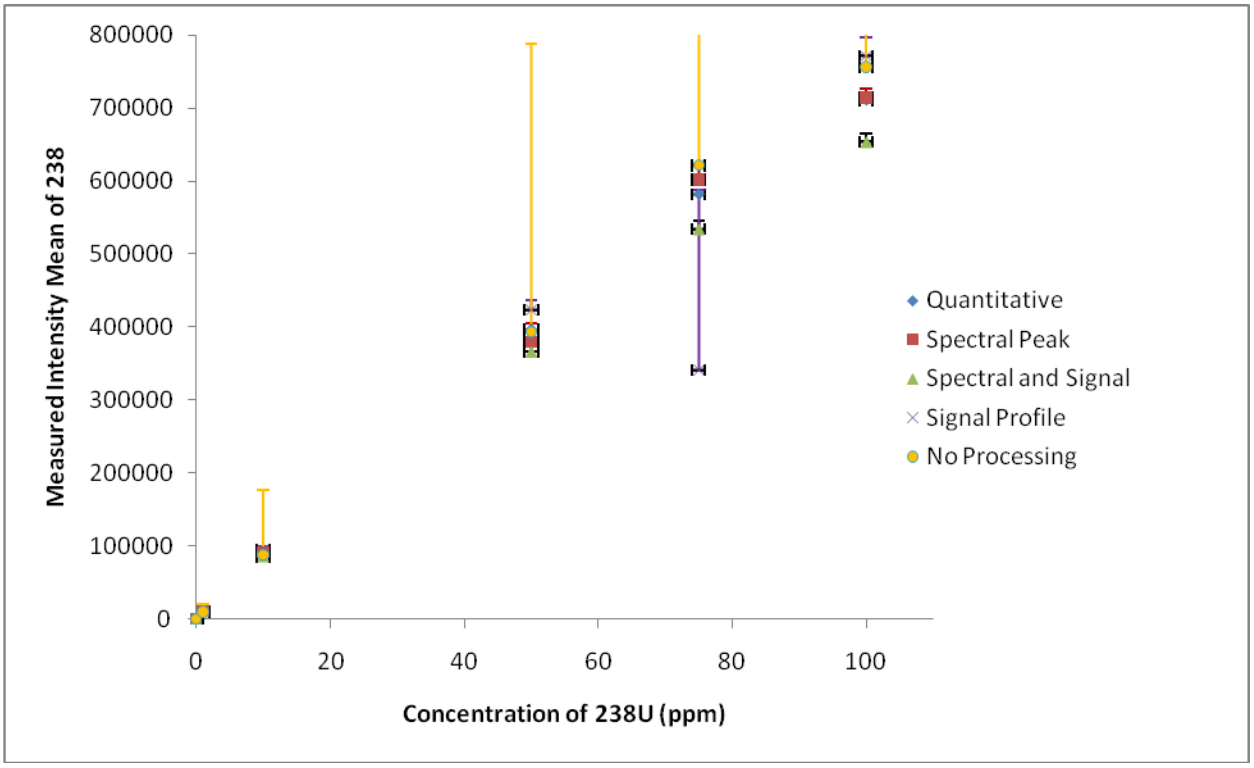

Figure F1: Comparison of calibration curves

Using only the raw data (no processing) results in significant uncertainty in the measurements as compared to the processed data. While it does produce the best correlation (table T2), it is not significantly better than the processed data.

Table T2: Correlation Coefficients for calibration curves in Figure F1

Processing Parameters	**Correlation Coefficient**
No Processing	0.9966
Quantitative	0.9956
Spectral and Signal	0.9955
Spectral Peak	0.9942
Signal Profile	0.9010

The Quantitative analysis method performed the same as the combination of spectral peak processing and signal profile processing except for the standard deviation of mass 239 (figure F3). The Quantitative analysis method was an order of magnitude higher than the combination processing in all channels monitored (234-239). This adds a higher uncertainty in the measurement of the hydride.
Although the Spectral peak processing parameter yielded one of the lowest correlation coefficient for the concentration of 238Uranium (table 2) is not desirable, the consistently low standard deviation of the 239 channel using this processing parameter is. Spectral peak processing has the stable counts per second in the 239 channel needed to simplify the correction for the hydride formation. This is necessary so the ^{239}Pu measurement has the least amount of interference.

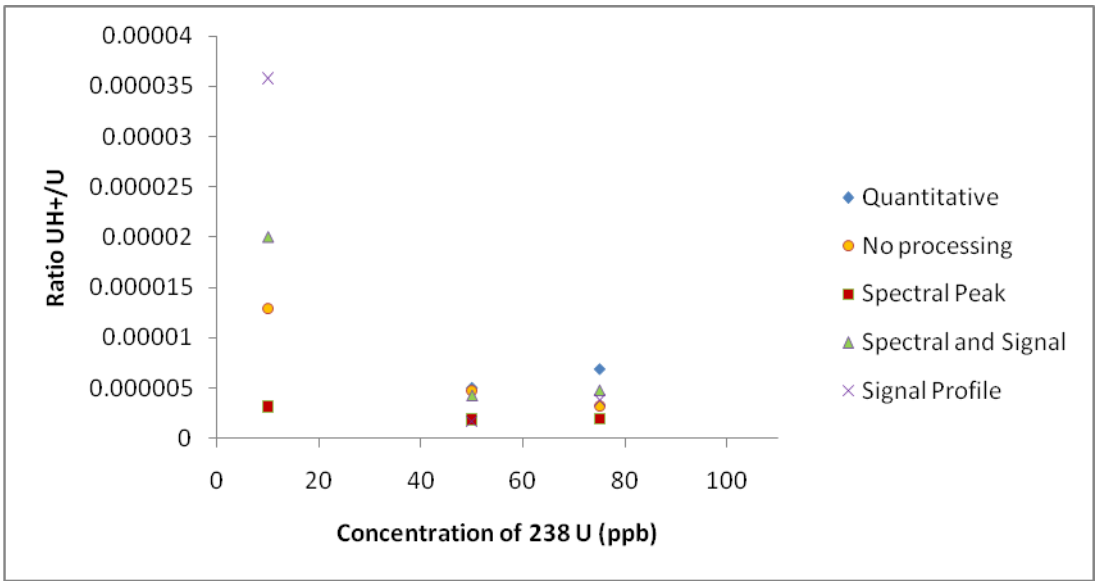

Figure F2: Comparison of processing parameters to determine hydride formation

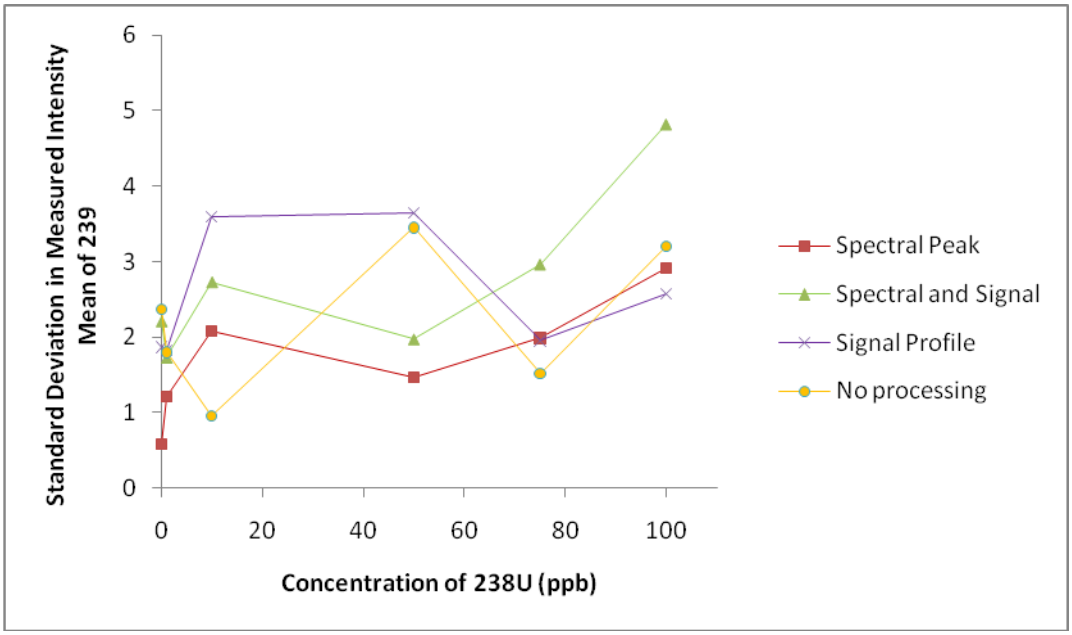

Figure F3: Comparison of standard deviation in 239 (hydride) measurements.

Quantitative Analysis standard deviation of 239 omitted for graphing purposes, values are an order of magnitude higher than above processing parameters.

Optimizing the system, the $^{238}UH+/^{238}U$ ratio obtained ranges from 5 E-06 to 3.5 E-05 for higher concentrations of ^{238}U (figure F2). The lower concentrations of ^{238}U produced higher values of the ratio, due to the variability of the 239 value is significant to the lower counts of the 238 channel. In conclusion, the spectral peak processing parameter is beneficial to the quadrupole ICP-MS method for data processing.

Method Development for Laser-Ablation Mass Spectroscopy

In order to develop and evaluate a laser ablation ICP-MS technique for the direct measurement of uranium, and eventually plutonium, in solid samples, a series of samples of varying uranium content were developed. Leveraging previous work on the characterization of urania/zirconia matrices (for inert matrix fuel applications), a uranium-zirconium matrix was selected for these experiments.

Sample Preparation and Characterization

Uranium-zirconium oxide pellets of differing ratios from 0-100% in intervals of 10% were prepared. The desired ratio of the metals were measured from metal nitrates and dissolved in water. The metals were then precipitated using a solution of concentrated ammonium hydroxide saturated with oxalic acid. The precipitate was dried in an oven overnight at 100°C and then calcined overnight at 450°C to remove oxalic acid. The precipitate was then ball milled for 5 minutes at 450 rpm and reduced in a tube furnace at 600°C with 5% hydrogen gas. Aluminum stearate binder (1% by weight) was added to the reduced precipitate and then pellets were pressed. The green pellets were then sintered in a tube furnace at 1700°C. After the pellets cooled, the mass and volume were determined for density measurements.

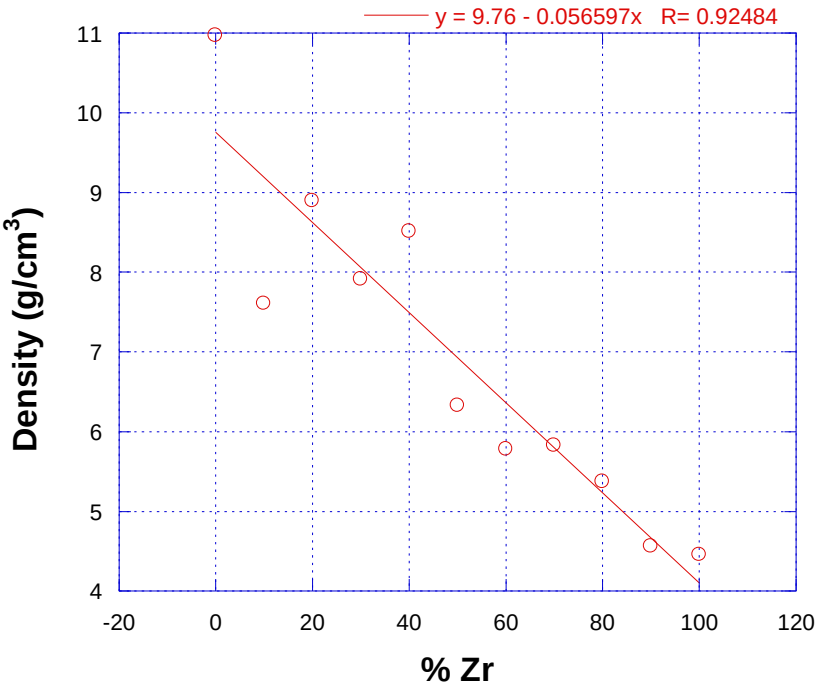

Figure F4: Density Change in Pellets Over Range Tested

In order to confirm pellet preparation was sufficient to produce pellets in thermal equilibrium XRD measurements were conducted. Table T3 shows the results of this experiment (labeled Experimental) compared to literature results of phase diagrams. There are discrepancies in the literature for the phase boundaries as shown. Comparing the patterns with the published patterns by Piluso, et. al. [10], the 80, 60, 50 and 40% uranium pellets appear to have reached thermal equilibrium. Comparison to the published patterns by Kinoshita, et. al. [11], suggests that the 70, 50, 40 and 30% uranium pellets are also in thermal equilibrium. However, comparison of the observed patterns with the literature values does indicate that the 90, 20 and 10% uranium pellets did not reach thermal equilibrium during sintering. Additional sintering time at 1700 ^{0} C should allow these systems to reach thermal equilibrium; however, further studies are necessary to determine the exact amount of time to achieve thermal equilibrium.

10. Piluso, P. et al., (2005) *The UO_2-ZrO_2 System at High Temperature (T>2000 K): Importance of the Meta-Stable Phases Under Severe Accident Conditions.* Journal of Nuclear Materials, 344: 259-264.
11. Kinoshita, H. et al., (2004) *Stability Evaluation of Fluorite Structure Phases in ZrO2-MO2 (M = Th, U, Pu, Ce) Systems by Thermodynamic Modeling.* Journal of Alloys and Compounds, 370: 25-30.

Table T3: XRD Results of Lattice Structures with Published Results from References 7 and 8.

%U	Experimental	Reference 7	Reference 8
90	T/C	C	C
80	C	C	T/C
70	T/C	C	T/C
60	C	C	T/C
50	T/C	T/C	T/C
40	T/C	T/C	T/C
30	T/C	T	T/C
20	T/C	T	T
10	M/C	T	T

T: Tetrahedral, C: Cubic, M: Monoclinic

LA-ICP-MS Method Development

A Nd:YAG ultraviolet laser system at 266 nm (LSX-500, CETAC, Omaha, NE) was used to generate pulses of < 6 nsec duration, >9 mJ energy and 20-Hz repetition rate. The laser radiation was focused onto the surface of the pellet positioned inside a cylindrical ablation cell (V = 110 cm^3). Aerosols were released under argon atmosphere at 0.4 $Lmin^{-1}$. Table T4 contains all the relevant experimental parameters used throughout this study. The composition of transported aerosol particles were determined with a quadrupole ICP-MS (ELAN DRC II, Perkin-Elmer). Signals were acquired over a period of 90 seconds. Each pellet was ablated in the same position 5 times in 100 pulse intervals. The m/z monitored in this experiment was 90 and 238.

Table T4: LA and ICP-MS conditions

ICP-MS	
Scan Mode	Peak Processing
Plasma Power	1200 W
Nebulizer Gas (Ar)	0.4 $Lmin^{-1}$
Sweeps	10 per reading
Readings	200-240
Dwell Time	10 ms
Laser Ablation	
Wavelength	266 nm
Energy Level	100%
Pulse energy	20 Hz
Spot Size	25 µm
Time	5 s

The raw data was first normalized for time of integration because the width of peak generated varies with the change in elemental oxide ratio. This can be attributed to the differences in matrices resulting in different transportation efficiencies. The isotopic abundance of ^{90}Zr is 51.45%, in order to account for this the data for ^{90}Zr was divided by 0.5145 as an isotopic correction. Since the uranium used in this experiment was depleted, it is unnecessary to correct for isotopic abundance as depleted uranium often is 99.7% or more ^{238}U.

The 100% UO_2 and ZrO_2 pellets were used as solid reference standards to take into account the differences in elemental properties, matrices, ablation efficiency (effects of LA), plasma and detector interactions (effects of ICP-MS). Once the time and isotope corrections were made the counts (U_x or Zr_x, where x represents the percentage of that element in the pellet) of each pellet were divided by the corresponding counts of the 100% pellets (U_{100} = 2013125 with RSD of 8.6% or Zr_{100} = 141501.8 with RSD of 32.5%) resulting in the corrected data graphed in Figure F5.

$$U_{corr} = \frac{U_x}{U_{100}} \qquad Zr_{corr} = \frac{Zr_x}{Zr_{100}}$$

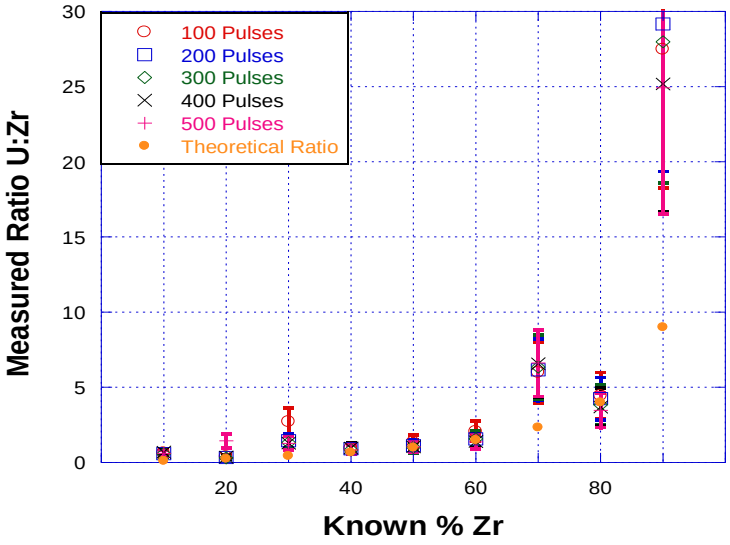

Figure F5: Comparison of the Determined Ratio of Zr:U Using Solid Correction factor and the Theoretical Ratio.

For each depth of 100 pulses, the ratio closely matches for all the replicates except the first run, the average ratio and RSD for each pellet is listed in Table T5. For each pellet the theoretical ratio is within the measured ratio's uncertainty, except for the 70% and 90% zirconium pellets. These outliers will need to be evaluated further to understand the discrepancy. To take into account the fact that the first 100 pulses are outliers a second correction was made using 200-500 pulses of the 100% pellets as the correction factor. U_{100} was found to be 2051690 with RSD of 8.4% and Zr_{100} was found to be 108661.8 with RSD of 2.6% resulting in the corrected data graphed in Figure F5. Comparing the corrected ratio values of figure F5 and F6 we find the ratios in figure F5 to be slightly higher and the standard deviation of the ratio to be significantly lower. This is due to the high standard deviation of the 100% Zirconium pellet when factoring all of the pulses which has a %RSD of 32.5%.

	Solid Reference			Solution Reference			Solid Reference 200-500 Pulses		
% Zr	Average Zr:U	□	%RSD	Average Zr:U	□	%RSD	Average Zr:U	□	%RSD
10	0.618	0.040	6.4	0.053	0.003	6.4	0.820	0.053	6.4
20	0.562	0.490	87.2	0.048	0.042	87.2	0.746	0.650	87.2
30	1.598	0.620	38.8	0.123	0.053	38.8	2.120	0.823	38.8
40	0.905	0.054	5.9	0.077	0.005	5.9	1.202	0.071	5.9
50	1.111	0.137	12.3	0.095	0.012	12.3	1.475	0.181	12.3
60	1.592	0.274	17.2	0.136	0.023	17.2	2.113	0.364	17.2
70	6.339	0.269	4.2	0.542	0.023	4.2	8.410	0.356	4.2
80	3.941	0.404	10.3	0.337	0.035	10.3	5.230	0.536	10.3
90	27.762	2.793	10.1	2.303	0.157	6.8	36.840	3.706	10.1

Table T5: Ratios and Statistics for Solid and Solution Standard References in Depth Comparison

A second standard reference set was prepared using solutions uranium and zirconium and analyzed using only the ICP-MS. The 100% uranium and zirconium solutions contained concentrations of 100 ppb each and the mole ratios of the solutions were used as the correction factor. The zirconium counts were corrected for isotopic abundance and the ratio of U: Zr was found to be 1.2159 with RSD of 2.8%. Using this ratio the zirconium counts of the pellets that have been normalized by time and isotopic abundance were then multiplied by the U: Zr ratio of the solution. The final corrected counts for Zirconium were then divided by the time normalized uranium counts to determine the ratio graphed in Figure F5. This correction accounts for differences in elemental properties in the plasma and detector of the ICP-MS.

$$Zr_{corr} = Zr_x * (U_{sol} / Zr_{sol})$$

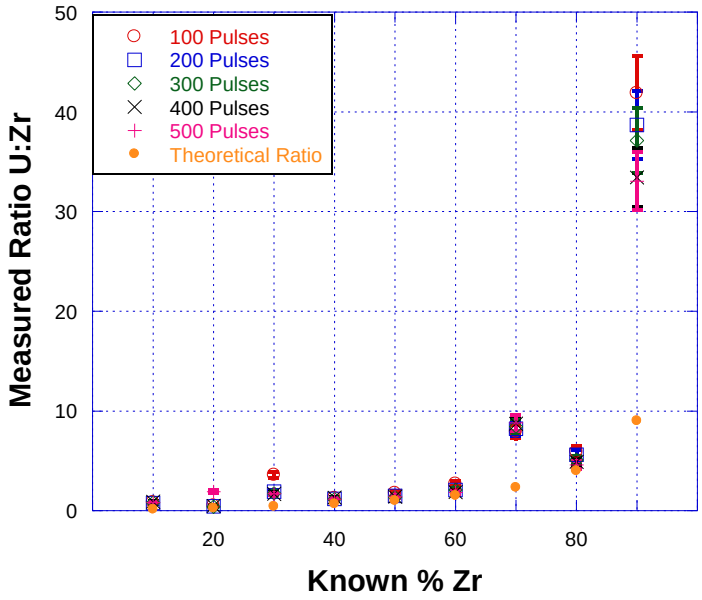

Figure F6: Comparison of the Determined Ratio of Zr:U Using Solid Correction factor of 200-500 Pulses and the Theoretical Ratio.

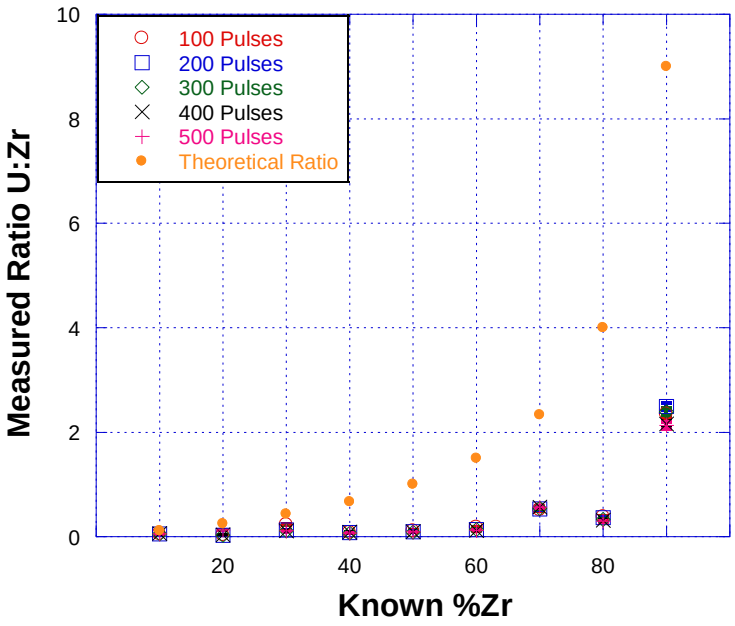

Figure F7: Comparison of the Determined Ratio of Zr:U Using Solution Correction factor and the Theoretical Ratio.

The overall shape of the experimental curve matches the solid corrected data (Figure 1) except the solution data is shifted below the theoretical curve for the ratio. This shift shows that the ablation efficiency must be considered when using LA-ICP-MS and a solution correction is not sufficient to correct for the limitations mentioned in the introduction. Table T5 shows the average ratio and %RSD for each pellet.
In Figure F7, the measured density of the pellets varies significantly within the ratios tested, with R= 0.914. Pellets with 0-40% zirconium fall within 7.5-10.97 gcm^{-3} and pellets with 50-100% zirconium are grouped between 4.5-6.5 gcm^{-3}. The effects of density on the ablation efficiency will be investigated further to determine if a correction factor is needed.
Evaluation of Ablation Crater by Optical Microscopy
Using a Leica DM2500P microscope the grain size and crater diameter of each pellet was measured. Overall the average grain size is consistent between pellets, but the crater diameter significantly changes throughout the pellet series. The grain size was calculated by measuring and averaging five grain diameters and calculating the area assuming circle geometry. The crater diameter varied from 64.214 -290.865 µm. Using the crater diameter to find the surface area of ablation and dividing by the average grain size for the pellet the average grains ablated per area was calculated and graphed in figure F8. The amount of grains ablated varies from 16 to 529. This significant difference can be explained by phase explosion where a significant quantity of mass is removed from the sample. Comparing the pellets in figures F9 and F10 it is apparent that the pellets with more uranium undergo phase explosion while the Zirconium-rich pellets do not. This difference can be explained by the change in density between the pellets, but will need to be verified in further studies using SEM imaging to measure the depth of the craters.

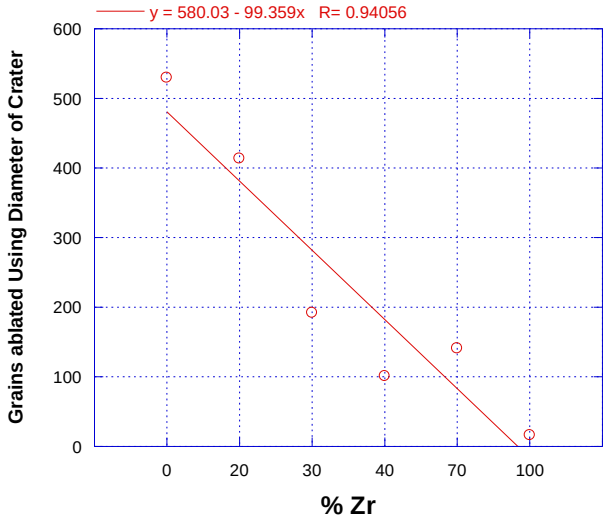

Figure F8: Grains Ablated Using Diameter of Crater (Depth is not Factored in) vs %Zr

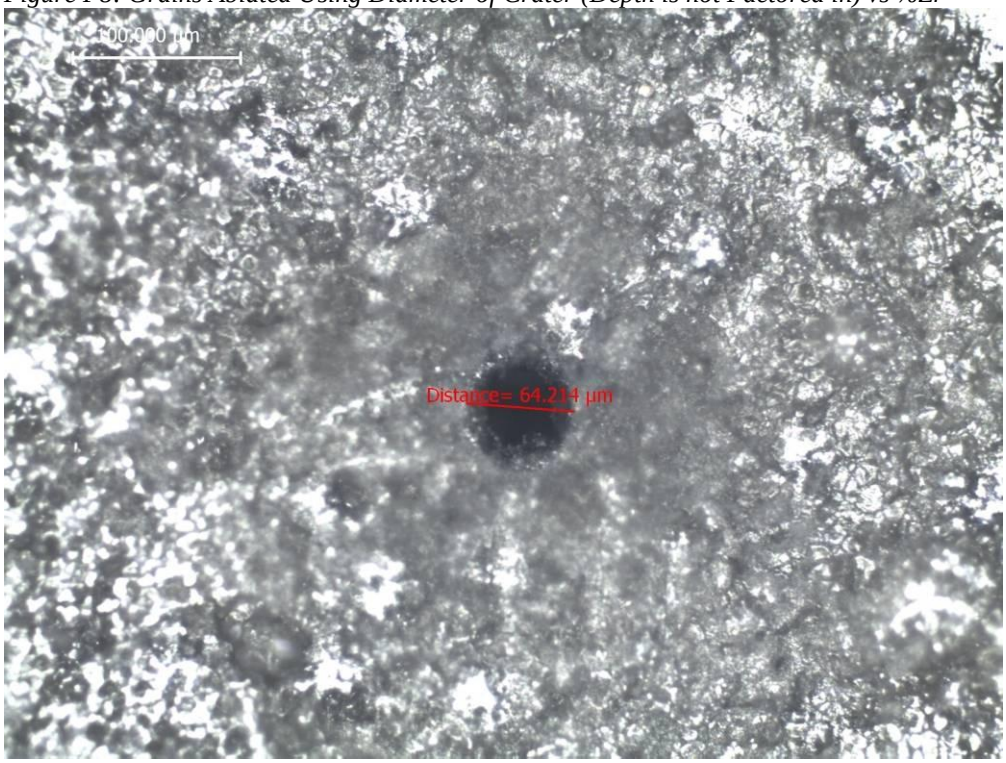

Figure F9: Crater Diameter of 100 % Zr Pellet

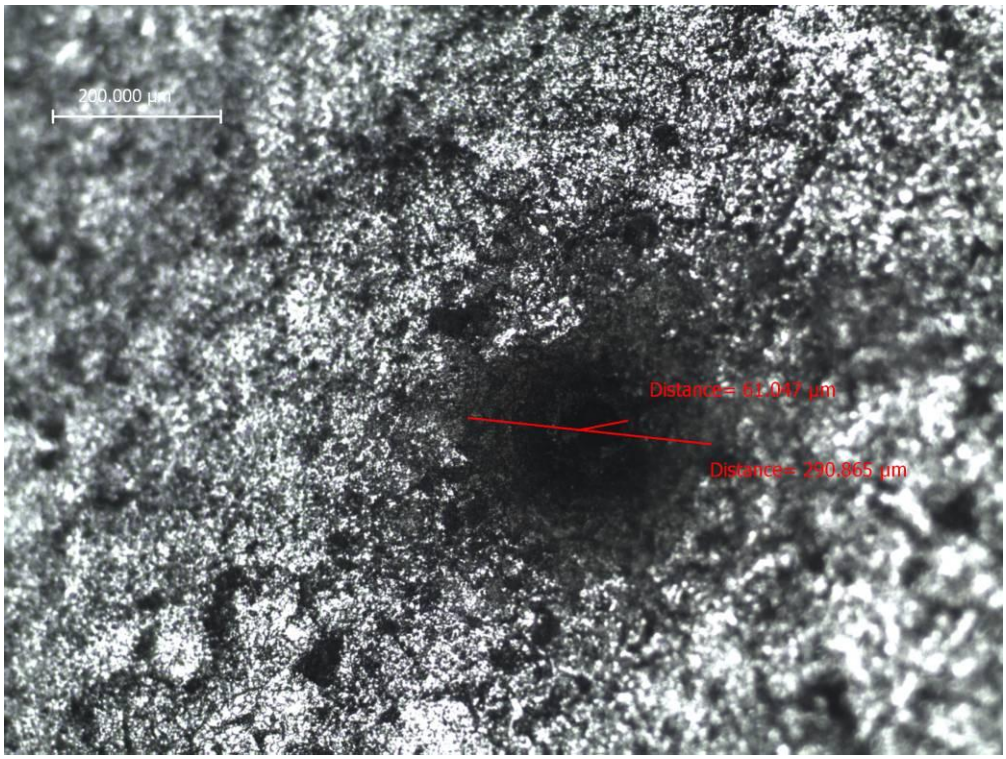

Figure F10: Crater Diameter of 100% Uranium Pellet

Evaluation of Ablation Crater by Scanning Electron Microscopy (SEM)
To determine the volume sampled during the ablation process, a SEM was used to measure the crater dimensions. The radiuses of the craters were measured in the standard way. In order to measure the depth of the crater it was assumed that at the distance of the stage to the electron beam source the beams would be parallel. The SEM model used has ability to tilt the stage to a desired angle. For these measurements the stage was tilted to 20°. Once the stage was tilted, the beam was then focused to the bottom of the crater. Once the bottom of the crater was in focus the length of the leg of the right triangle labeled b (shown in figure F11) was measured. Using trigonometry the hypotenuse a was then calculated. [a = b/sin(20°)].

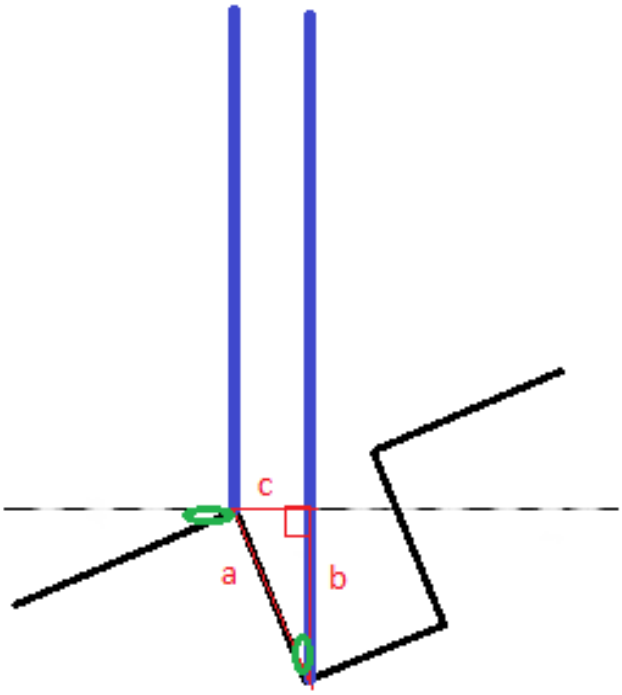

Figure F11: Method for measuring depth of craters on SEM. Blue lines indicate electron beam, Dotted line: plane of stage, Green circles: 20° angle.

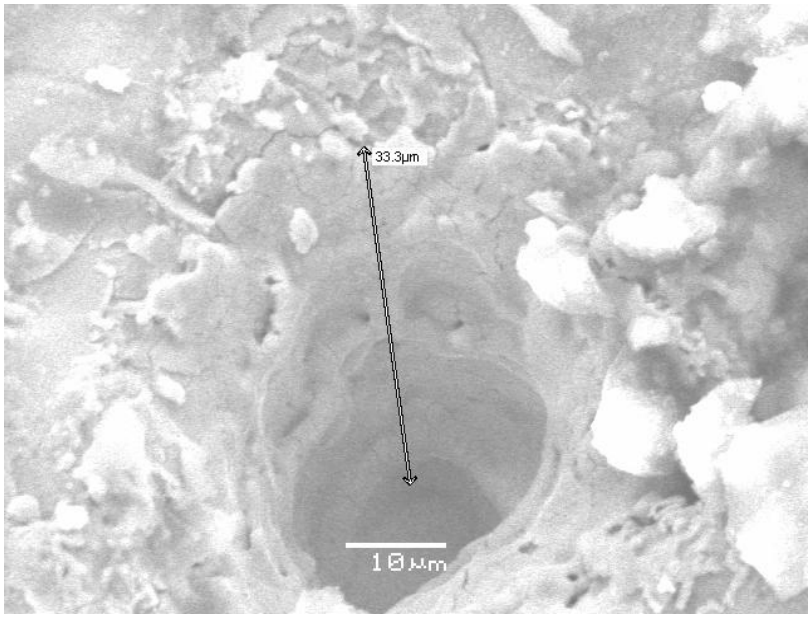

Figure F12: SEM Image of 90% U Pellet

As shown in figure F12, the craters were not perfectly cylindrical. In order to account for this, the craters were assumed to be between a cone and a cylinder. The errors shown in figure F13 accounts for this where the extremes are a volume calculation of a cone and a cylinder and the value is the average of the two.

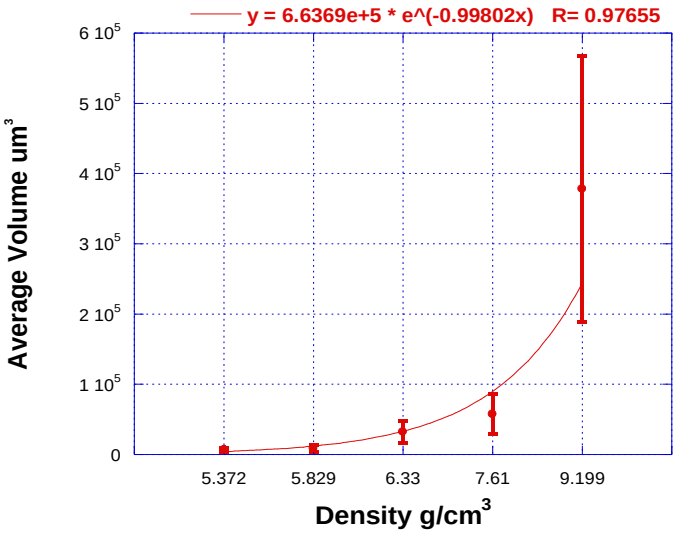

Figure F13: SEM Data Volume of Ablated Material

By plotting the volume of the craters as a function of density measurements (see figure F4) the volume ablated is found to increase exponentially as the Uranium concentration increases. This is evidence of phase explosion at the higher concentrations of Uranium. An interesting note is the debris found around the craters (see figure F12) this is evidence that some of the material was incompletely vaporized which leads to fractionation. This is found in all of the pellets measured. Figure F4 does not include all of the pellets in the series. Some of the pellets measured were not carbon coated properly leading to charging when trying to measure the craters. Charging occurs when the sample is absorbing the electrons resulting in poor resolution in the image. Other pellets were mounted on the wrong side where the crater was inaccessible. Further studies would be needed to measure all of the pellets properly.

Observations To-Date

In conclusion, the solid internal standard reference was able to verify the correct ratio for the pellets with the exception of 70% and 90% zirconium. Portions of the precipitate were set aside of each ratio during each step of the pellet making process. These portions will be dissolved and analyzed on the ICP-MS to determine if the ablation measurements are a true representation of the whole pellet. This dissolution will enable confirmation of the 70% and 90% zirconium ratios using the correction factor determined for these pellets. The solution standard reference was significantly lower than the correct ratio for zirconium pellets above 40%. This difference shows that the ablation efficiency must be considered when using LA-ICP-MS and a solution correction is not sufficient to correct for the overall limitations of this technique. Future work includes an investigation into pellet ablation using helium as the carrier gas. In existing literature, researchers have reported lower RSD compared to using argon as the carrier gas [4]. Further characterization of the ablated samples is necessary to determine sample volume more accurately, as well as to investigate the samples to determine if any chemical or phase changes have occurred in the ablated zone.

REFERENCES

[1]. Gong W.L. et al., (2000) *Zirconia Ceramics for Excess Weapons Plutonium Waste*. Journal of Nuclear Materials, 277: 239-249

[2]. De Lima N.B., K. Imakuma, (1985) *X-ray Diffraction Study of the Formation of Solid-Solutions in Urania-Thoria Prepared by Aqueous Chemical Processes*. Journal of Nuclear Materials, 135: 215-221.

[3]. Kohl, F., N. Jakubowski, N., Brandt, R., Pilger, C., and J.A.C. Broekaert. (1997) *New strategies for Trace Analyses of ZrO2, SiC and Al2O3 Ceramic Powders.* Fresenius J. Anal. Chem. 359 4-5:317-325.

[4]. Mokgalaka, N.S., and J.L Gardea-Torresdey. (2006) *Laser Ablation Inductively Coupled Plasma Mass Spectrometry: Principles and Applications.* Appl. Spectros., 41: 131-150

[5]. Alexander, M.L., Smith, M.R., Hartman, J.S., Mendoza, A., and Koppenaal, D.W. (1998) *Laser ablation ICP-MS*. Appl. Surf. Sci., 127–129: 255–261

[6]. Arrowsmith, P. and Hughes, S.K. (1988) *Entrainment and transport of laser ablated plumes for subsequent elemental analysis*. Appl. Spectros., 42 (7): 1231–1239.

[7]. Mao, X.L., Borisov, O.V., and Russo, R.E. (1998) *Enhancements in laser ablation ICP-AES based on laser properties and ambient environment*. Spectrochim. ActaB, 53: 731–739.

[8]. Vais, V., Chunsheng, L., Cornett, J., *Preventing uranium hydride formation in standard uranium samples for determination of 239Pu by ICP-MS.* J. Anal. At. Spectrom., 2004, 19, 1281-1283.

[9] ELAN Version 3.3 Software Guide, PerkinElmerSCIEX, 2004.

[10]. Piluso, P. et al., (2005) *The UO_2-ZrO_2 System at High Temperature (T>2000 K): Importance of the Meta-Stable Phases Under Severe Accident Conditions.* Journal of Nuclear Materials, 344: 259-264.

[11]. Kinoshita, H. et al., (2004) *Stability Evaluation of Fluorite Structure Phases in ZrO2-MO2 (M = Th, U, Pu, Ce) Systems by Thermodynamic Modeling.* Journal of Alloys and Compounds, 370: 25-30.